INVESTIGATING THE CATALYTIC AND REGULATORY MECHANISMS OF DIHYDRODIPICOLINATE SYNTHASE.

A thesis submitted in partial fulfilment of the requirements for the degree of

Doctor of Philosophy in Biochemistry

at the

University of Canterbury

by

Renwick C J Dobson

2003

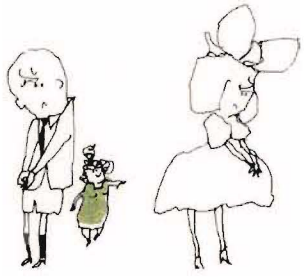

Able but unwilling molecules

The enzyme performs its duty

Willing and able molecule

Acknowledgements.

No thesis is the work of just one person and this is no exception. Many people have contributed over the years and for this I warmly thank them. Firstly, thanks to my supervisors, Juliet, Jack, and John, for their guidance, advice, and patience. Special and sincere thanks to Juliet for her unerring enthusiasm, support, friendship, great parties, and cultivating a fantastic lab environment so all can flourish. Very special thanks to Mum, Dad, Gar, Rohan, and the kids. My love and thanks to Emma for her support (mostly emotional) and putting up with the years of study. To Mike and Miller for their friendship, on-tour shenanigans, and camaraderie about the lab. To Laurence, Susie and Hugo for general mischief. Thanks to Jen for teaching me the use of en and em dashes, how to canulate, and to speak proper Australian. To Jackie for excellent advice and kicking my ass when required. Thanks to past students Grant, Liz, Sarah, Paula "I love Brad Pitt" Brown, and Russell. To the person, who shall not be named, for their tasteful pole dancing to the music of George Thorogood—the memory shall haunt me till the day I die. To the rest of the Gerrard group—it was a pleasure and an honour.

Much of this work was accomplished in other labs: the Morris organic chemistry lab; the Mahanty genetics lab; the Heinemann molecular biology lab; and the Hajdu crystallography lab. Firstly, thanks to those in Jonathans organic lab for teaching me what to do when I smell almonds or lose a crystal of OsO_4 on the lab floor. Thanks to those in the genetics and molecular biology labs for explaining the virtues sterile technique and other strange goings on. Special thanks to Janos, Karin, Anka, Remko, Al, Inga, Jenny, and the rest of the Uppsala crew for making life in Sweden so enjoyable (and that X-ray stuff).

Thanks to Matt for photo stuff and Ashley for statistical advice. Finally, thanks to the Randy Walrus for inspiring me to continue with biology and your sincere enthusiasm for scientific endeavour.

Table of Contents.

List of Abbreviations.

α	ratio of *V* and *V'*
A	alanine
A	substrate A
ΔA_{340}	change in absorbance at 340 nm
amp^r	gene conferring ampicillin resistance
Ar	aryl
(*R*/*S*)-ASA	racemic mixture of aspartate β-semialdehyde
(*S*)-ASA	(*S*)-asparate β-semialdehyde
ATP	adenosine-5'-triphosphate
B	substrate B
bd	broad doublet
BOC	*tert*-butoxycarbonyl
bp	base pairs
BSA	bovine serum albumin
°C	degrees Celsius
cm	centimetre
d	doublet
δ	chemical shift in parts per million downfield from tetramethylsilane
Da	Daltons
DAP	*meso*-diaminopimelate
*dap*A	gene encoding dihydrodipicolinate synthase
*dap*B	gene encoding dihydrodipicolinate reductase
DCM	dichloromethane
DEAE	diethylaminoethyl
DHDPR	dihydrodipicolinate reductase
DHDPS	dihydrodipicolinate synthase
DIBAL	Diisobutylaluminium hydride
DNA	deoxyribonucleic acid
ddNTP	2',3' dideoxynucleic acid triphosphate
dH_2O	distilled/de-ionised water
ddH_2O	double distilled water
DMF	dimethylformamide
dt	doublet of triplets
ε	extinction coefficient
E. coli	*Escherichia coli*
ESMS	electrospray mass spectrometry
EDTA	ethylenediaminetetraacetic acid
F	phenylalanine
FAB	fast atom bombardment
g	gram
g	gravities
G	glycine
H	histidine
HEPES	*N*-2-hydroxyethylpiperazine-*N'*-2-ethane sulphonic acid
HIC	hydrophobic interaction chromatography

HTPA	(4*S*)-4-hydroxy-2,3,4,5-tetrahydro-(2*S*)-dipicolinate
hr	hour
I	isoleucine
I	inhibitor
[I]	inhibitor concentration
IC_{50}	inhibitor concentration giving 50% inhibition
IPTG	isopropyl β-D-thiogalactopyranoside
IR	infra-red
J	coupling constant
K	lysine
kb	kilobase
k_{cat}	catalytic constant
kDa	kilodalton
K_i	inhibition constant
K_m	michaelis-menton constant
lac	operon encoding β-galactosidase
L	litre
LB	Luria-Bertani broth
μg	microgram
μL	microlitre
M	moles per litre
M_r	relative molecular mass
m/z	mass to charge ratio
min	minute
mg	milligram
mL	millilitre
mp	melting point
MS	mass spectrum
Ng	nanograms
nm	nanometers
N	asparagine
NMR	nuclear magnetic resonance
NAD^+	nicotamide adenine dinucleotide
NADH	nicotamide adenine dinucleotide, reduced form
$NADP^+$	nicotamide adenine dinucleotide phosphate
NADPH	nicotamide adenine dinucleotide phosphate, reduced form
NAL	*N*-acetyl neuraminate lyase
Ori	origin of replication
P	proline
PAGE	polyacrylamide gel electrophoresis
PCR	polymerase chain reaction
PDB	Protein Data Bank
pJG001	Bluescript plasmid containing the *dap*A gene encoding DHDPS
pJK001	Bluescript plasmid containing the *dap*B gene encoding DHDPR
ppm	parts per million
Q	glutamine
R	arginine
*rec*A	gene encoding for the RecA protein
rpm	revolutions per min

r.m.s.d.	root mean square deviation
RNase	ribonuclease
r.t.	room temperature
S	serine
S	substrate
[S]	substrate concentration
SDS	sodium dodecyl sulphate
T	threonine
TAE	tris-acetyl EDTA electrophoresis buffer
TEMED	tetramethylethylenediamine
tet^r	tetracycline resistance gene
TFA	trifluoroacetic acid
THF	tetrahydrofuran
TLC	thin layer chromatography
TMS	tetramethylsilane
Tris.HCl	tris(hydroxymethyl)methylamine
UV	ultraviolet
V	valine
V	maximum rate of reaction
V'	maximum rate of reaction in the presence of saturating inhibitor
X-gal	5-bromo-4-chloro-3-indolyl-β-δ-glactosidase
Y	tyrosine

Abstract.

Dihydrodipicolinate synthase (DHDPS, E.C. 4.2.1.52) catalyses the branchpoint reaction of lysine biosynthesis in plants and microbes—the condensation of (*S*)-aspartate-β-semialdehyde ((*S*)-ASA) and pyruvate.

In an attempt to better understand the reaction catalysed by DHDPS, the wild-type enzyme was over-expressed and, following purification, kinetically characterised using a coupled assay. The kinetic mechanism was of the ping-pong type and the kinetic parameters obtained were consistent with other literature values. An improved synthesis of (*S*)-ASA was successfully achieved in three steps with an overall yield of 94%; this represents a significant advance over previously published routes to (*S*)-ASA. There are literature reports that high levels of (*S*)-ASA inhibit DHDPS, whilst others have not observed this phenomenon. It is shown unequivocally that this difference can be attributed to the different methods of preparing (*S*)-ASA used by each researcher: DHDPS is not inhibited by (*S*)-ASA, rather, the inhibition is due to an, as yet, unidentified inhibitor in the preparations of the substrate generated by ozonolysis.

Others have published the crystal structure of wild-type DHDPS to 2.5–Å. They have hypothesized that the catalytic mechanism of the enzyme involves a catalytic triad of amino acid residues, Y133, T44, and Y107 that provides a proton-relay to transport protons within the active site and from the active site to solvent. Additionally, R138 has been implicated in (*S*)-ASA binding. These hypotheses were tested using site-directed mutagenesis to produce five mutant enzymes: DHDPS-Y133F, DHDPS-T44S, DHDPS-R138H, DHDPS-T44V, and DHDPS-Y107F. Each of these mutants had reduced catalytic activity, consistent with the catalytic triad hypothesis. DHDPS-R138H showed an increased K_{mASA}, consistent with its role in (*S*)-ASA binding. The crystal structures of DHDPS-Y133F, DHDPS-T44V, DHDPS-Y107F were determined to at least 2.35–Å resolution and compared to the wild-type structure. All mutant enzymes crystallised into the same space group as the wild-type and only minor differences in structure were observed. These results suggest that the catalytic triad is indeed in operation in wild-type DHDPS.

The mechanism of lysine inhibition in DHDPS appears complex but two hypotheses were previously suggested. These were that lysine affects the proton-relay and/or the flexibility of R138 to inhibit DHDPS catalysis. The mutants generated above were used to test these hypothesises. DHDPS-Y133F, DHDPS-T44V, and DHDPS-R138H showed less sensitivity to lysine inhibition compared to the wild-type, while DHDPS-T44S and DHDPS-Y107F showed identical behaviour to the wild-type. The results showed that some mutations in the proton-relay attenuated lysine inhibition so lysine may operate, at least in part, *via* this motif. That DHDPS-R138H also showed decreased sensitivity to lysine suggests that this residue also has some role in lysine inhibition. However, the crystal structure of DHDPS-T44V with bound lysine showed that the flexibility of R138 had increased, in contrast to the situation of the wild-type. To reconcile these results, a new mechanism of inhibition is proposed involving a hitherto undocumented channel of well-defined water molecules.

Chapter One.

Introduction.

This thesis examines an enzyme in plant and bacterial lysine biosynthesis, dihydrodipicolinate synthase (DHDPS), which catalyses the first committed step in the diaminopimelate pathway leading to lysine and is itself regulated by lysine. The catalytic and regulatory mechanisms of dihydrodipicolinate synthase are investigated using a combination of experimental approaches such as site-directed mutagenesis, steady-state kinetics, and X-ray crystallography.

1.1 Background.

The early studies by Work in the 1950's led to the discovery of *meso*-diaminopimelate (DAP) in the acid hydrolysates of *Corynebacterium diphthariae*,[1] and subsequently in *Mycobacterium tuberculosis*.[2] Understanding its biosynthesis and cellular role inspired further research, from which a description of bacterial lysine biosynthesis was elucidated.

Lysine is an essential amino acid and is a member of the aspartate family of amino acids that also includes methionine, threonine, and isoleucine.[3] Evolution has restricted the synthesis of the aspartate-derived amino acids to plants, fungi, and bacteria; hence amino acids derived from aspartate are essential dietary components for animals. As such, this pathway has become the focus for two avenues of research.[4] Firstly, lysine is the limiting amino acid in many cereals, so an understanding of lysine biosynthesis may lead to more nutritious crops in the future. Secondly, inhibitors of lysine biosynthesis have the potential to be antibacterial and/or herbicidal agents. Since lysine is an essential amino acid, inhibitors of lysine biosynthesis could be selectively toxic to plants and microorganisms but not to animals.[5, 6]

1.1.1 Antibiotics and herbicides.

It has been postulated that inhibitors of the lysine biosynthetic pathway may represent a new class of antimicrobial and herbicidal agents.[3] Specific inhibitors of this pathway are likely

to be of low toxicity because mammals lack lysine biosynthesis.[3] Interestingly, lysine biosynthesis *via* the DAP pathway appears not to be a target for naturally occurring compounds and, as such, natural resistance mechanisms may be absent.[3] There are currently no commercial drugs available that use inhibition of lysine biosynthesis as a strategy despite substantial research.[3]

In 1956, Cummins and Harris[7] demonstrated that *meso*-diaminopimelate, the direct precursor to lysine, was a component of bacterial cell wall peptidoglycan (Figure 1.1). The peptidoglycan layer of the bacterial cell wall is a thick rigid layer found in both Gram-positive and Gram-negative cells and is a macromolecule with an interesting chemical structure. It is a heteropolymer with a backbone consisting of alternating *N*-acetylmuramic acid (MurNAc) and *N*-acetylglucosamine (GluNAc) sugar residues cross-linked with peptide side chains.[8, 9] The peptide side chain consists of (*S*)-alanine, (*R*)-alanine, (*R*)-glutamic acid, and (*S*)-lysine (or sometimes DAP). Chains of peptidoglycan subunits are joined by cross-links between the peptide side chains, whereby an amide bond is formed between the carboxyl group of a terminal (*R*)-alanine and the ε-amino group of (*S*)-lysine or DAP. Formation of the cross-links enables the cell wall to be resistant to lysis by intracellular osmotic pressure,[10] and it is by inhibiting the cross-linking process that the β-lactam and vancomycin families of antibiotics exert their biological activities.

Figure 1.1 *Structure of peptidoglycan layer of Gram-negative bacteria.*

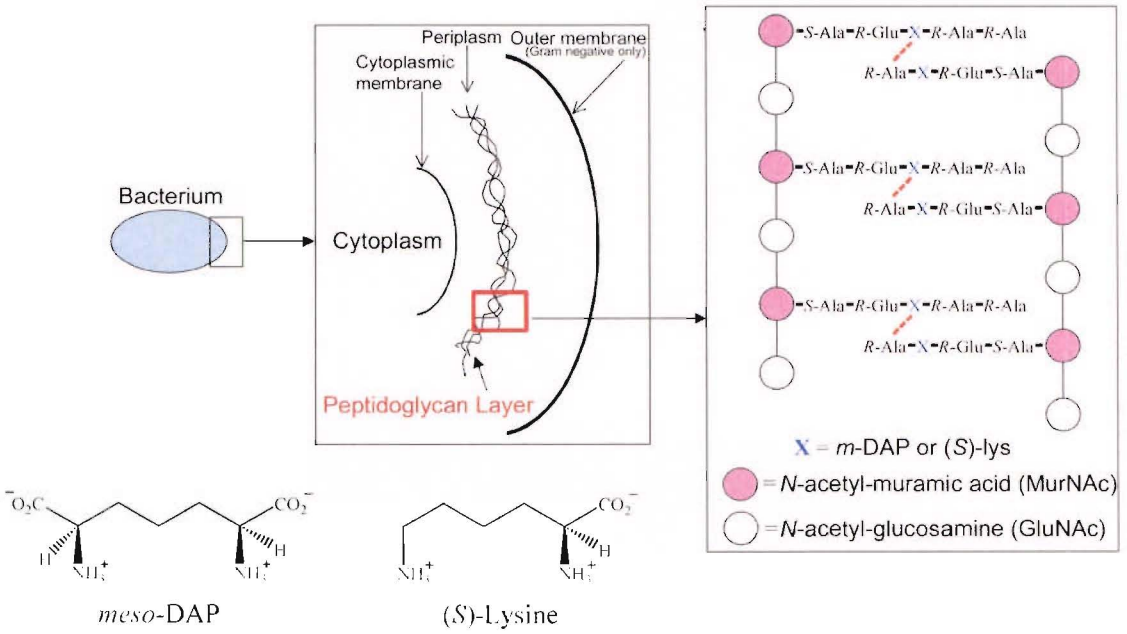

1.1.2 Nutrition.

Humans and other animals must obtain a number of amino acids from their diet because they cannot synthesise all 20 protein amino acids.[11] However, from the viewpoint of animal and human nutrition, many crop plants contain relatively low levels of these essential amino acids and in particular lysine and threonine; increasing the amino acid composition will, therefore, enhance the nutritional value of the plant products.[12, 13] Towards this end, the regulation of lysine metabolism in plants and bacteria has been studied extensively at the biochemical and genetic levels in an effort to boost lysine levels.[14-24]

In order to increase the free lysine concentration in plants, some workers have manipulated the regulatory properties of the enzymes involved in its biosynthesis. (*S*)-Lysine biosynthesis is regulated primarily by aspartate kinase and dihydrodipicolinate (DHDPS). To enhance lysine production, the enzymes need to be altered so that catalytic activity is increased or the enzyme is less sensitive to feedback inhibition by the end-products. Ghislain *et al.*[20] have shown that modification of enzymes in lysine biosynthesis can lead to overproduction of lysine: through selection of enzymes that lack feedback inhibition, the total lysine content has been increased in plants such as tobacco,[21] soybean,[23] canola,[25] and barley.[26]

Another strategy is to engineer lysine rich proteins and express them in plants. Keeler *et al.*[11] have designed a gene, expressed in tobacco seeds, that encodes for a protein containing 30% lysine and 20% methionine, which resulted in a significant increase in the lysine content. This approach is entirely complementary to the manipulation of enzymes in amino acid biosynthesis for the enhancement of necessary amino acids.

1.2 The aspartic acid family of amino acids.

As the name suggests, the aspartate family of amino acids is synthesised from (*S*)-aspartate, itself derived from oxaloacetate from the citric acid cycle (Figure 1.2). Initially, aspartokinase phosphorylates (*S*)-aspartate to give (*S*)-β-aspartyl phosphate, before being reduced in an NADPH-dependent reaction to (*S*)-aspartate-β-semialdehyde ((*S*)-ASA) by aspartate-β-semialdehyde dehydrogenase.[27] This is the branch point for the biosynthesis of the four aspartate-derived amino acids.[27] (*S*)-ASA either enters the DAP

pathway to produce (*S*)-lysine, or is reduced by homoserine dehydrogenase to give (*S*)-homoserine, the precursor to (*S*)-methionine, (*S*)-threonine, and (*S*)-isoleucine.[3, 27]

Figure 1.2 *Biosynthesis of the aspartate family of amino acids.*

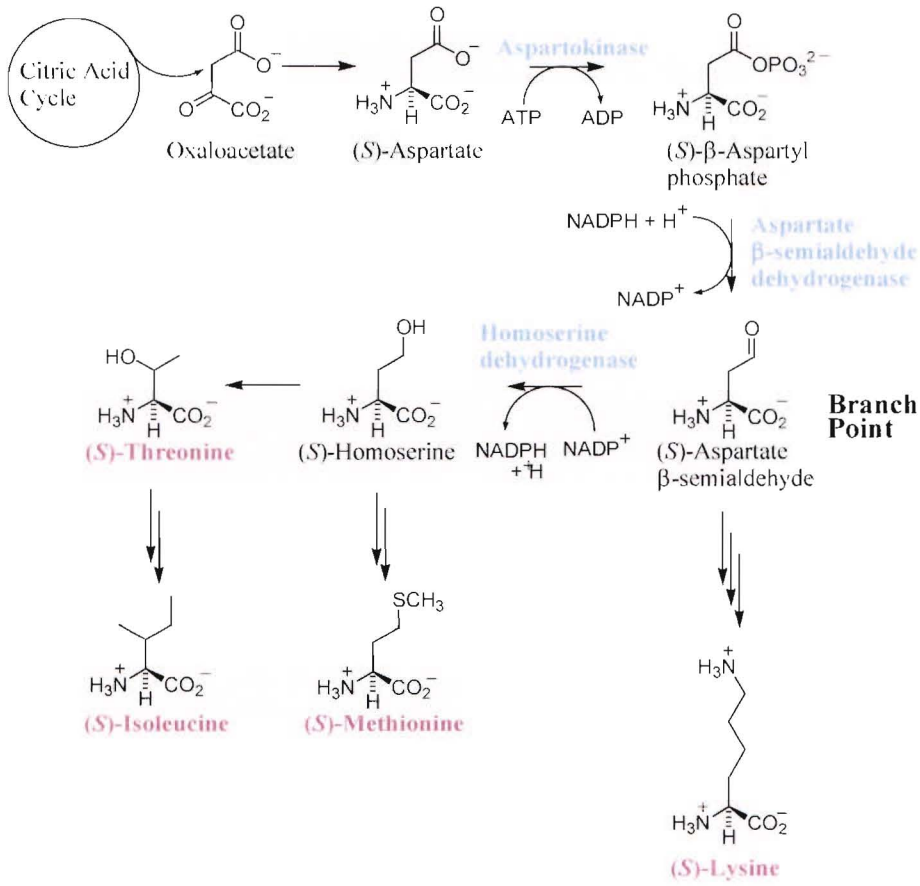

1.3 The diaminopimelate (DAP) pathway leading to lysine.

Since the discovery of diaminopimelate by Work,[1] two distinct pathways for lysine biosynthesis have been described. Fungi and euglenoids produce lysine by a pathway that originates with 2-oxoglutarate and acetyl-CoA. Here the key intermediates are saccharopine and aminoadipidic acid and the pathway is commonly referred to as the aminoadipidic pathway.[28, 29] Plants and bacteria, on the other hand, produce lysine *via* the DAP pathway (Figure 1.3). This route begins with the condensation of pyruvate and (*S*)-ASA to form (4*S*)-hydroxy-2,3,4,5-tetrahydro-(2*S*)-dipicolinate (HTPA) and is catalysed by the enzyme DHDPS. Six further enzyme-catalysed reactions afford the biosynthesis of

(*S*)-lysine. It is the DAP pathway, and in particular the enzyme DHDPS, on which the work described in this thesis focuses.

Figure 1.3 *The three known variants of the diaminopimelate pathway.*[30]

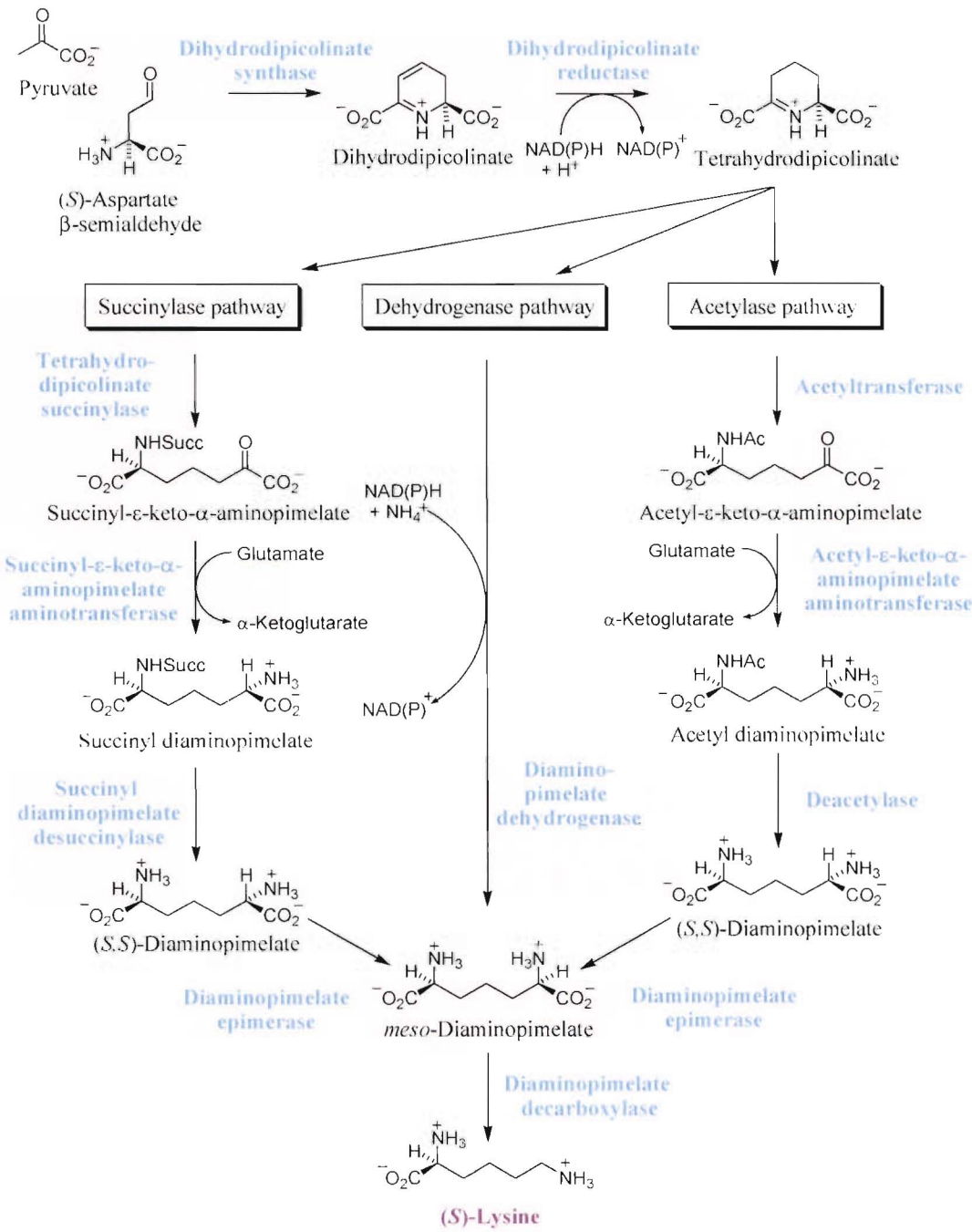

The DAP pathway has three variants that differ after the formation of tetrahydrodipicolinate (Figure 1.3). They have been identified in various bacterial species:[30, 31] one in which succinylated intermediates are used, the succinylase variant;[32] a second in which acetylated intermediates are used, the acetylase variant;[33] and a third in which tetrahydrodipicolinate is converted by a dehydrogenase to DAP in a single step.

(1) Succinylase pathway.

The succinylase pathway appears the most common route and is used by *E. coli*.[32] Tetrahydrodipicolinate is ring opened *via* an *N*-succinylation of the α-amino group by succinyl-CoA, a reaction catalysed by tetrahydrodipicolinate succinylase, to form succinyl-ε-keto-α-aminopimelate.[34] Ketopimelate undergoes transamination by a pyridoxal phosphate (PLP) dependent aminotransferase, using glutamate as the amino donor by the enzyme succinyl-ε-keto-α-aminopimelate aminotransferase to yield succinyl diaminopimelate.[35] Succinyl diaminopimelate is deprotected (desuccinylation) to form (*S*,*S*)-diaminopimelate[36] by the enzyme succinyl diaminopimelate desuccinylase. Diaminopimelate epimerase then catalyses the epimerisation of (*S*,*S*)-diaminopimelate to form *meso*-diaminopimelate,[37] which is decarboxylated to yield (*S*)-lysine by diaminopimelate decarboxylase.[38]

(2) Acetylase pathway.

An alternative pathway, termed the acetylase pathway, involves *N*-acetylated intermediates instead of *N*-succinylated intermediates.[33] The reaction proceeds through an identical series of steps to the succinylase pathway and, like the dehydrogenase pathway below, is extremely limited in its bacterial distribution, but has been described in some *Bacillus* species.[39]

(3) Dehydrogenase pathway

The dehydrogenase pathway is the most direct route to lysine. The intermediate tetrahydrodipicolinate, a precursor of all three pathways, is converted in a single step to *meso*-diaminopimelate. This is an NADPH dependent reaction catalysed by diaminopimelate dehydrogenases. *Meso*-diaminopimelate is then decarboxylated to yield lysine as in the pathways 1 and 2. Diaminopimelate dehydrogenase has been identified in

Corynebacterium glutamicum, *Bacillus sphaericus*, and *Pseudomonas* and *Brevibacterium* species.[27, 31]

Intriguingly, some bacterial species apparently utilise more than one pathway. For example, the industrially important lysine producing bacterium, *Corynebacterium glutamicum*, uses both the succinylase and the dehydrogenase pathways.[27] The presence of multiple biosynthetic pathways may signify the importance of (*S*)-lysine and DAP in bacterial survival.

1.4 Previous work on dihydrodipicolinate synthase (DHDPS).

The chemistry that DHDPS catalyses is deceptively simple, but has interesting features *in vivo*, and has proved challenging to perform *in vitro*.[6, 40-42] Strikingly, the biologically relevant form of both substrate and product molecules is still unresolved. Also unresolved is the mechanism by which DHDPS is feedback inhibited by lysine; this is a major focus of the work herein and is introduced in section 1.5 and discussed in more detail in Chapter six. DHDPS has been classified as a type I aldolase, by the method of Grazi *et al.*,[43] meaning that its reaction is catalysed through a Schiff base intermediate.[44, 45] For almost 40 years, DHDPS from various sources have been studied in terms of structure, function, and genetics but there have been few fundamental advances since the seminal early papers.[19, 46]

1.4.1 Genetics.

For *E. coli*, the *dap*A locus, which encodes for DHDPS, was mapped to 53 minutes on the *E. coli* chromosome,[47] cloned,[48] and sequenced.[47] The *dap*A gene has also been cloned and sequenced from a number of other plant and bacterial species (Table 1.1).

Table 1.1 *Examples of cloned and sequenced* dap*A genes from various sources.*

Bacteria	Plants
Escherichia coli[47]	*Arabidopsis thaliana*[49]
Corynebacterium glutamicum[29, 50]	*Poplus deltoids × trichocarpa*[49]
Bacillus subtilis[51]	*Triticum aestivum*[52]
Sinorhizobium meliloti[53]	*Glycine max cv.*[54]
	Nicotiana sylvestris[20]
	Zea mays[55]
	Nicotiana tabacum[20]
	Glycine max[54]

1.4.2 Enzymology.

DHDPS has been purified from a number of plant[20, 56-58] and bacterial[19, 59-62] species. Early gel filtration experiments suggested that in solution DHDPS from *E. coli* was a homotetramer with a molecular mass of 134 kDa.[46] The published *E. coli dap*A sequence predicted a polypeptide of 292 amino acid residues, which corresponds to a monomeric molecular mass of 31372 Da.[47] However, electrospray mass spectrometry gave a molecular mass of 31272 Da.[60] and this difference was attributed to errors in the published amino acid sequence—later to be confirmed by X-ray crystallography.[45, 63, 64] Thus far, all characterised DHDPS enzymes are reported to be tetrameric, with one exception: gel filtration experiments suggested that DHDPS isolated from *Pisum sativum* was trimeric.[58]

Kinetic studies of DHDPS.

Once purified, DHDPS from various sources has been studied kinetically and in all cases the kinetic mechanism appears to be of the compulsory ordered substituted type* (Figure 1.4). This mechanism is called the "ping-pong" mechanism, the substituted enzyme mechanism, or the double displacement mechanism. There are several lines of evidence that lead to this conclusion: (1) steady-state data collected with respect to each substrate show a set of parallel lines in the reciprocal plots;[19, 44, 59] (2) the covalent intermediate can be identified

* This means the reaction requires the substrates to bind in a given order, proceeds through a covalent substrate-enzyme intermediate, and has two substrates and two products.[44]

independently and in the absence of the other substrate (in this case by the reduction of the enzyme-pyruvate complex with $NaBH_4$,[19] which can be observed by mass spectrometry[60] or in X-ray crystal structures[45]—see section 1.4.3); (3) product analogues show the predicted types of inhibition with respect to the substrates;[44] and (4) the reaction appears to show predicted substrate inhibition with respect to the second substrate, (*S*)-ASA.[44†]

Figure 1.4 *Scheme showing the kinetic mechanism of DHDPS. This was modified from Karsten.[44] In this scheme E refers to the unligated enzyme form and F to the substituted form. Pyr is pyruvate, (S)-ASA is aspartate semialdehyde, and HTPA is (4S)-4-hydroxy-2,3,4,5-tetrahydro-(2S)-dipicolinate.*

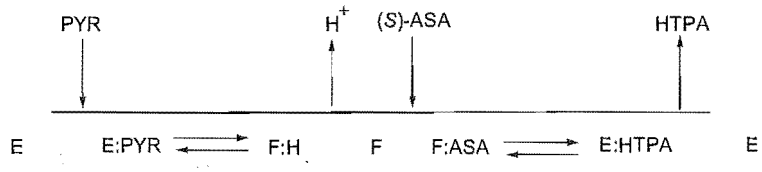

The published Michaelis-Menten constants (K_m) from a variety of sources range between 0.19–11 mM for pyruvate and 0.11–5.1 mM for (*S*)-ASA (Table 1.2). DHDPS from other bacterial sources, except from sporulating bacteria, have K_{mASA} values much larger than those determined for the *E. coli* enzyme. In comparison, various plant sources are reported to have K_{mASA} values similar to that calculated for *E. coli*. This suggests a similar binding affinity between DHDPS from plants and the *E. coli* enzyme for the substrate (*S*)-ASA. For DHDPS from bacterial sources, the Michaelis-Menten constants with respect to pyruvate range approximately 10-fold or larger. In contrast, DHDPS from a range plant sources show similar $K_{mPyruvate}$ values, although they are still larger than DHDPS obtained from *E. coli*. DHDPS from *E. coli* also appears to show high specificity for each substrate; as yet, no alternative substrate has been found, although some obvious candidates, such as oxaloacetate, succinic semialdehyde, and glutamic semialdehyde, have been explored.[19]

† Substrate inhibition is predicted if DHDPS is able to bind the second substrate ((*S*)-ASA), without first binding the initial substrate (pyruvate), to form a "dead-end" complex.[65]

Table 1.2 *Kinetic constants of DHDPS from various sources.*

Organism	$K_{m\ Pyruvate}$ (mM)	$K_{m\ ASA}$ (mM)
Bacteria		
Escherichia coli[44]	0.19	0.12
Corynebacterium glutamicum[66]	6.2	–
Bacillus subtilis[62]	1.07	3.13
Bacillus licheniformis[67]	5.3	2.6
Bacillus sphericus[68]	9	5.1
Sporulating Bacteria		
Bacillus megaterium[69]	0.5	0.46
Plants		
Zea mays[55]	2.1	0.6
Pisum sativum[58]	1.7	0.4
Triticum aestivium[70]	11.8	0.8
Spinacia oleracea[56]	1.4	–

1.4.3 Structural studies of DHDPS.

General structural features.

The solid state structures of DHDPS isolated form *E. coli* and *N. sylvestris* have been determined by X-ray crystallography to a resolution beyond 2.5–Å.[45, 63, 64] These studies confirmed the homotetrameric structure of *E. coli* DHDPS, revealing a dimer of dimers (Figure 1.5).

Each monomer is composed of two domains. In *E. coli*, the amino-terminal domain consists of residues 1–224 that form a parallel $(\beta/\alpha)_8$-barrel homologous to that of triose phosphate isomerase (TIM).[64] The carboxyl-terminal domain consists of residues 224–292, forming three α-helices;[64] this domain has no known role. The β-barrel comprises a hydrophobic core formed by an irregular layer of mainly hydrophobic residues. The catalytic site, as defined by the position of K161, is located at the C-terminus end of the β-barrel lying in a 10–Å deep by 30–Å long cleft. This is a similar active site structure to 3-dehydroquinase

and another class I aldolase, *N*-acetyl neuraminate lyase, both of which are mechanistically related to DHDPS.[71]

Figure 1.5 *The tetrameric structure of E. coli DHDPS. The monomers are labelled **A**, **B**, **C**, and **D**. **A/D** and **B/C** associate tightly to form dimers, which loosely associate to form the tetrameric structure of wild-type DHDPS. β-Sheets are coloured blue, α-helices are detailed in red and yellow, and the turns grey. This image was generated using MolMol[72] and the coordinates of DHDPS (1DHP from the Protein Data Bank).*

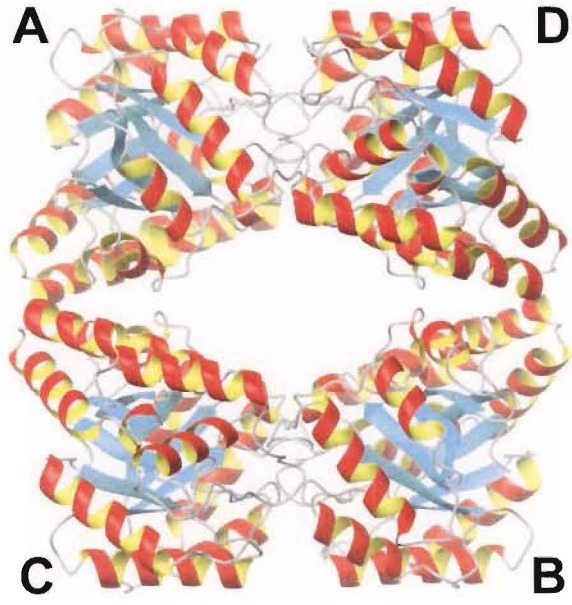

Many residues at the tight interface between the monomers, including tyrosine residues 106 and 107, are conserved in all DHDPS sequences.[45, 63] In both *N. sylvestris* and *E. coli*, the side chains of tyrosine 106 and 107 of each monomer interdigitate, resulting in a hydrophobic, sandwich-like stacking of their aromatic rings.[64] This forms a tight association between the two monomers, resulting in 12.4% burial of the total surface area of each monomer, almost blocking the N-terminus end of the active site. Intriguingly, Y107 lies in the forbidden region of the Ramachandran plot, suggesting a role in catalysis or feedback regulation.[45] The lysine-binding site is also formed at the monomer-monomer interface.

In contrast to the tight association between the monomers, the dimers associate loosely to form the tetrameric wild-type enzyme. As seen in Figure 1.5, these contacts occur between

monomers A/D and monomers B/C *via* three α-helices. It is interesting to note that Mirwaldt *et al.*[64] reported that just three residues from each monomer make contact between the dimers. However, re-examination of the structure published by Mirwaldt *et al.*,[64] suggests that other contacts might also be important (*pers. comm.* Mike Griffin). Nevertheless, this association is rather weak and less than 5% of the total surface area of each monomer is reported to be buried in the loose dimer interface.[45, 64] In contrast, the *N. sylvestris* isoenzyme structure shows significantly more contacts at the dimer-dimer interface. Here the tetrameric structure is arranged differently with sixteen contact residues observed in each monomer participating in the interdimer connections.[45]

Sequence alignment and related enzymes.

A high level of similarity exists at the amino acid level between DHDPS sequenced from different species. For example, *E. coli* DHDPS shows 30% identity to wheat,[52] 35% identity to *N. sylvestris,*[63] and 33% identity to *Brevibacterium lactofermentum.*[73] The level of sequence homology within plants is higher. For example, there is 87% identity between the wheat and maize genes.[54]

The tertiary scaffold of DHDPS is shared by a number of other enzymes that catalyse quite different chemistry.[74] This group is known as the $(\beta/\alpha)_8$-family of proteins whose members include triosephosphate isomerase. The family has been split into subfamilies based on sequence alignment, structure, and function.[75] The subfamily that includes DHDPS also includes: *N*-acetyl neuraminate lyase (NAL), which is involved in the regulation of sialic acid concentration; *trans-o*-hydroxybenzylidenepyruvate hydratase-aldolase, involved in naphthalene degradation; D-4-deoxy-5-oxoglucarate dehydratase, involved in glucarate metabolism; and MosA, which is thought to catalyse the addition of a methyl group to *scyllo*-insoamine.[74] These enzymes catalyse different chemistry but do so through a Schiff base intermediate. Furthermore, Joerger *et al.*[76] have illustrated how close a relationship there is within the sub-family by demonstrating that NAL will catalyse the aldol condensation of (*S*)-ASA and pyruvate—the same reaction as DHDPS—although at a reduced rate. They further demonstrated this relationship by making NAL mutants that increased the DHDPS activity in NAL, although not to the levels of wild-type DHDPS.

Alignment of DHDPS sequences with those in the NAL-subfamily reveal residues important for the enzymes tertiary structure, active site, or lysine-binding site. Some workers suggest

that certain residues can be grouped according to their conservation within the NAL-subfamily:[74]

i The first is a highly conserved group within the family. These include Y133 (*E. coli* DHDPS numbering) thought to be a proton donor/acceptor, K161, which forms the Schiff base, and the conserved motif GxxGE that binds a substrate carboxyl group. These elements are assumed to have similar roles throughout the family of residues.

ii A second group that is conserved within a given enzyme from different sources, and is presumed to be linked to the different substrate binding requirements of each enzyme. For DHDPS these would include R138, implicated in binding the carboxyl of (*S*)-ASA, and D187 and D188, which are thought to bind the amino group of (*S*)-ASA. Y106 and Y107 are also conserved in all DHDPS isoenzymes,[45] although their role is elusive.

1.4.4 Reaction mechanism mediated by DHDPS.

The proposed mechanism is shown in Figure 1.6 and can be divided into three consecutive steps. Schiff base formation with pyruvate followed by aldol reaction of (*S*)-ASA and finally transimination and cyclisation with simultaneous dissociation of HTPA.[45] Discussed here is the mechanism, as accepted at the outset of this work, and an introduction to the principle amino acid residues of DHDPS thought to be necessary for catalysis.

Figure 1.6 *Reaction mechanism at the active site (green) of DHDPS proposed at the outset of this work. Adapted from Blickling et al.*[45]

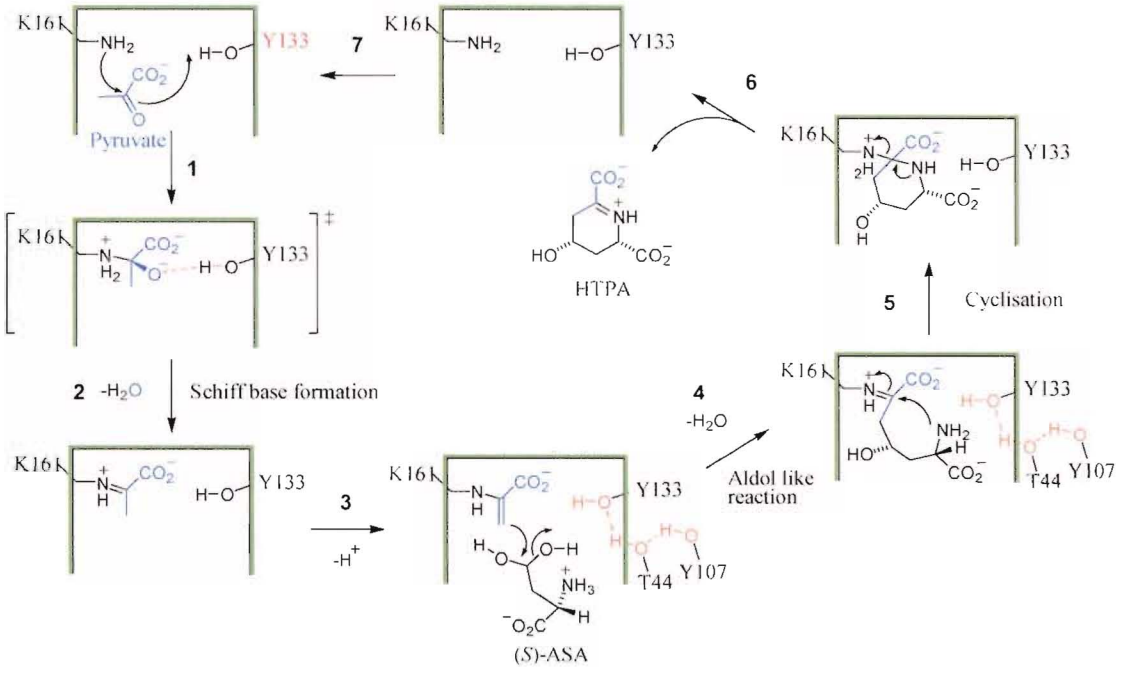

Schiff base formation.

Pyruvate forms a Schiff base with the ε-amino group of a highly conserved lysine residue (K161) in the active site of the enzyme (steps 1 and 2 of Figure 1.6). The hydroxyl of Y133 is proposed to act as a proton donor/acceptor. Potentially, the aldehyde form of (*S*)-ASA, the second substrate of DHDPS, could also form a Schiff base with this K161. However, the observation that DHDPS is inactivated by $NaBH_4$ reduction only in the presence of pyruvate suggests that only pyruvate can form the Schiff base (Figure 1.7).[19] The imine with pyruvate that is formed by $NaBH_4$ reduction has been observed by electrospray mass spectrometry.[59, 60]

Figure 1.7 *Sodium borohydride trapping of the Schiff base.*[19]

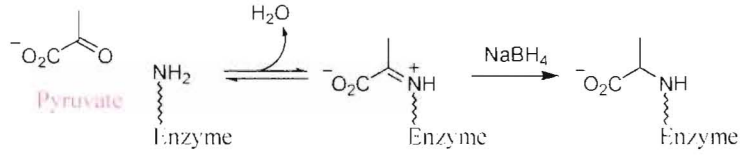

Aldol reaction.

The next step in the DHDPS reaction mechanism is the binding of (*S*)-ASA (Figure 1.6: step 3) followed by aldol condensation (Figure 1.6: step 4). In solution, (*S*)-ASA can exist as a number of species (Figure 1.8). Although (*S*)-ASA is usually referred to as the aldehyde in the literature, the biologically relevant species is still under debate.[42, 44, 45] It has been estimated that the proportion of hydrate (*S*)-ASA in solution at pH 7.5 is as high as 85%.[77] Karsten reports that succinic semialdehyde, an analogue of (*S*)-ASA, is a potent competitive inhibitor of DHDPS with respect to (*S*)-ASA.[44] A study of succinic semialdehyde derivatives concluded that the acyclic form was a very minor component of an equilibrium, which favours the cyclic lactol. Using ^{1}H NMR techniques, Coulter failed to detect the lactol species of (*S*)-ASA in solution under physiological conditions.[42] Blickling *et al.*[45] note that G186 and R248 are well placed in the active site to coordinate the hydroxyl groups of the hydrate, suggesting that the hydrate form of (*S*)-ASA is the biologically relevant form.

The enamine, which is formed from the Schiff base with pyruvate (Figure 1.6: step 3), acts as a nucleophile in the condensation reaction (Figure 1.6: step 4). Assuming that the hydrate of (*S*)-ASA is the relevant species, Y133 is in position to protonate one of the hydroxyls while G186 is in position to coordinate the other hydroxyl. It has been suggested that a catalytic triad, involving Y133, T44, and Y107, is involved in stabilising the tyrosine anion *via* a proton-relay to bulk solvent.[45]

Figure 1.8 *Solution structure of (S)-ASA.*

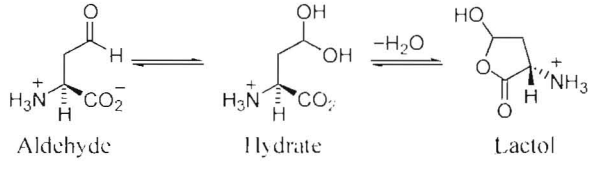

(*S*)-Aspartate β-semialdehyde

Cyclisation and product release.

Nucleophilic attack by the amine results in cyclisation (Figure 1.6: step 5), the last step before the release of HTPA and the binding of pyruvate (Figure 1.6: steps 6 and 7). Here also Y133 is proposed to play a role, as its hydroxyl is in a position to coordinate the attacking amine. There has been some speculation as to what the product of the catalysed

reaction might be. Originally, dihydrodipicolinate, was thought to be the product.[19] However, there are also other cyclic possibilities, as well as an open chain isomer, and a hydroxyl compound (Figure 1.9). Using ^{13}C and ^{1}H NMR spectrometry, Blickling *et al.*[45] showed that the product of DHDPS catalysis was a cyclic imine and that elimination of H_2O had not occurred, suggesting that HTPA undergoes a non-enzymatic dehydration reaction to give dihydrodipicolinate. However, there remains some debate due to the relatively basic conditions used in the experiment, which may influence dehydration and account for the accumulation of the hydroxyl intermediate.[3]

Figure 1.9 *Possible products of the DHDPS reaction.*

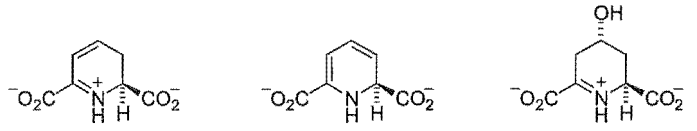

2,3-Dihydrodipicolinate 1,2-Dihydrodipicolinate 4-Hydroxy-2,3,4,5-tetrahydrodipicolinate

DHDPR, the next enzyme in the pathway, reduces the unstable heterocycle to tetrahydrodipicolinate with the subsequent oxidation of NAD(P)H; this provides an interesting means for assaying DHDPS.[19] The X-ray crystal structure of *E. coli* DHDPR,[31] mechanistic studies,[78, 79] and electrospray mass spectrometry[80] have helped enhance our knowledge of the DHDPR reaction mechanism.

1.5 Control of lysine biosynthesis in bacteria and higher plants.

In the aspartate family of amino acids, lysine biosynthesis appears to be controlled at two points (Figure 1.10). The first is the feedback inhibition of one isozyme of aspartate kinase by lysine. Bacteria encode three isozymes of aspartate kinase (AK): a lysine sensitive variant (AK3); a threonine sensitive aspartate kinase-homoserine dehydrogenase bi-functional variant (AK-HD1), which is also gene regulated by threonine and isoleucine; and an aspartate kinase-homoserine dehydrogenase bi-functional enzyme (AK-HD2), which is similar to AK-HD1 except that methionine regulates its expression.[27] In contrast, plants appear to have only two isozyme forms of AK; a lysine sensitive form and a threonine sensitive bi-functional homoserine dehydrogenase form.[81]

The second control point is DHDPS. In plants, two lines of evidence suggest that DHDPS is the rate-limiting step. Firstly, DHDPS has greater sensitivity to lysine (K_i = 5–50 μM) in comparison to AK (K_i = 200–600 μM),[17, 82] and secondly, expression of lysine-insensitive AK in plants results in the accumulation of threonine, not lysine, whereas expression of lysine-insensitive DHDPS results in the accumulation of lysine.[17, 81]

1.5.1 Regulation of DHDPS by (S)-lysine.

As the committed step in lysine biosynthesis, DHDPS is the key point in regulation of the pathway and it undergoes allosteric feedback regulation by the pathway's end product, (*S*)-lysine. The precise mechanism by which lysine exerts regulatory control over DHDPS is unclear, although kinetic and structural studies support the proposal that lysine is an allosteric inhibitor.[18, 19, 45, 59, 63, 70] While enzymes from different sources show varied degrees of lysine inhibition, random mutagenesis and sequence alignment suggest this is due to alterations in the lysine-binding site and that the mechanism of inhibition is similar. In plants, DHDPS is 20–100 fold more sensitive to lysine inhibition than bacterial enzymes, such as *E. coli*.[17] Plant DHDPS is thought to catalyse the rate limiting step in lysine biosynthesis while aspartate kinase, the first enzyme in the aspartate pathway, plays a secondary role. In contrast, lysine biosynthesis in *E. coli* is controlled by aspartate kinase, while DHDPS plays a secondary role.

Unlike other enzymes in the DAP pathway, expression of the gene encoding DHDPS is not regulated in *E. coli*.[83] However, an interesting question is whether DHDPS in this organism might be post-translationally regulated by the chaperone GroE. DHDPS was the first enzyme to be associated with both GroE and cell growth *in vivo* when it was shown that *E. coli* bacteria lysed if defective in GroE because of a lack of diaminopimelate.[84] Lysis could be briefly overcome by the increased expression of DHDPS, presumably because of slightly increased levels of diaminopimelate. Some evidence also suggests that the regulation of yeast AK by threonine may not be by simple enzyme-substrate interactions but require the chaperone FKBP12.[85] The exact nature of the relationship between DHDPS and GroE is yet to be elucidated.[81]

Figure 1.10 *Control of the diaminopimelate pathway.*[4] *(–) refers to inhibition by lysine of DHDPS and aspartokinase*

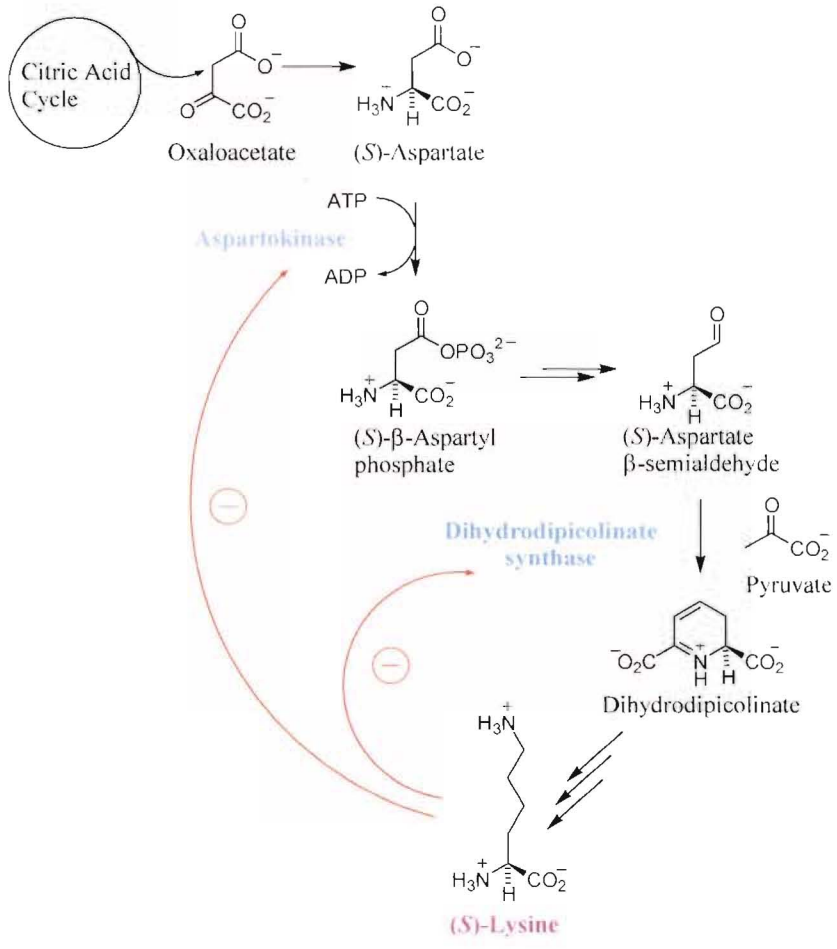

Some have tried to increase cellular lysine concentrations by transforming plants with lysine insensitive varieties of DHDPS. For example, the *E. coli dap*A gene, which encodes a DHDPS enzyme that is relatively insensitive to feedback inhibition, has been expressed in many plants: tobacco,[21] soybean,[23] canola,[25] and barley.[26] This resulted in an increase in lysine content but has highlighted the importance of lysine catabolism in the generation of lysine rich plants. Another strategy is to introduce mutations into the plant DHDPS gene that renders it less sensitive to lysine inhibition. This has been done with the use of agents that mimic lysine inhibition followed by mutagenesis and the selection of plants with high free lysine concentrations.[86] Many of the lysine-accumulating mutants, however, showed unusual phenotypes.[87] Not surprisingly, the mutations where characterised to the

lysine-binding region of DHDPS and presumably cause insensitivity by blocking lysine binding.

Depending on their regulatory properties with respect to lysine, isozymes of DHDPS can be grouped into three classes:[88]

i Plant enzymes which are strongly inhibited by lysine IC_{50} = 0.01–0.05 mM; *T. aestivium*,[70] *Daucus carota sativa*,[89] *S. oleracea*,[56] *N. sylvestris*,[90] *Z. mays*,[55] *P. sativum*.[58]

ii Enzymes from gram negative bacteria such as *E. coli*,[19] *B. sphaericus*,[68] and *Methanobacterium thermoautotrophicum*,[91] which are only weakly inhibited with an IC_{50} between 0.25 and 1.0 mM.

iii DHDPS from Gram positive bacterial that appear not to be inhibited by lysine at all (IC_{50} > 10 mM). For example, little or no feedback inhibition by lysine was observed for DHDPS from bacteria such as *B. licheniformis*,[18] *B. megaterium*,[69] *B. subtilis*,[62] *C. glutamicum*,[50] *Bacillus cereus*,[92] and *B. lactofermentum*.[93]

1.6 Conclusions; aims of this project.

It is clear that the mechanisms of catalysis and regulation in DHDPS have not been resolved. However, the crystal structure of *E. coli* DHDPS has been determined by X-ray crystallography[45] and others have hypothesized that an essential motif of DHDPS, a catalytic triad of amino acid residues, provides a mechanism to transport protons to and from the active site to bulk solvent.[45]

The primary aim of this study was to understand the catalytic mechanism of *E. coli* enzyme DHDPS. Following this, an understanding of its regulatory mechanisms was sought. To achieve these goals, mutants were designed and created to test the role of the proton-relay in both the kinetic and regulatory mechanism of DHDPS. Their kinetic properties were compared to the wild-type and X-ray crystallography was used to examine changes in the structure induced by the mutations. Finally, the behaviour of the mutants with respect to lysine was investigated and compared to the wild-type.

1.7 References.

1. Work, E. (1950). A new naturally occurring amino acid. *Nature*, **165**, 74-75.
2. Work, E. (1951). Isolation of α-ε-diaminopimelic acid from *Corynebacterium diphtheriae* and *Mycobacterium tuberculoses*. *Biochemistry Journal*, **49**, 17-23.
3. Cox, R., Sutherland, A. & Vederas, J. (2000). Bacterial diaminopimelate metabolism as a target for antibiotic design. *Bioorganic and Medicinal Chemistry*, **8**, 843-871.
4. Viola, R. E. (2001). The central enzymes of the aspartate family of amino acid biosynthesis. *Accounts of Chemical Research*, **34**, 339-349.
5. Cox, R. (1996). The DAP pathway to lysine as a target for antimicrobial agents. *Natural Products Reports*, **13**, 29-43.
6. Coulter, C. V., Gerrard, J. A., Kraunsoe, J. A. E. & Pratt, A. J. (1999). *Escherichia coli* dihydrodipicolinate synthase and dihydrodipicolinate reductase: kinetic and inhibition studies of two putative herbicide targets. *Pesticide Science*, **55**, 887-895.
7. Cummins, C. S. & Harris, H. (1956). The chemical composition of the cell wall in some Gram-positive bacteria and its possible value as a taxonomic character. *Journal of General Microbiology*,**14** , 583-600.
8. Prescott, L. M., Harley, J. P. & Klein, D. A. (1996). Microbiology 2nd edit., pp. 325. W. C. Brown Publishers, London.
9. Bugg, T. D. & Walsh, C. T. (1992). Intracellular steps of bacterial cell wall peptidoglycan biosynthesis: enzymology, antibiotics, and antibiotic resistance. *Natural Products Reports*, **9**, 199-215.
10. Cox, R., Sherwin, W., Lam, L. & Vederas, J. (1996). Synthesis and evaluation of novel substrates and inhibitors of *N*-succinyl-L,L-diaminopimelate aminotransferase (DAP-AT) from *E. coli*. *Journal of the American Chemical Society*, **188**, 7449-7460.
11. Keeler, S. J., Maloney, C. L., Webber, P. Y., Patterson, C., Hirata, L. T., Falco, S. C. & Rice, J. A. (1997). Expression of *de novo* high-lysine α-helical coiled-coil proteins may significantly increase the accumulated levels of lysine in mature seeds of transgenic tobacco plants. *Plant Molecular Biology*, **34**, 15-29.

12. Bright, S. W. J. & Shewry, P. R. (1983). Improvement of protein quality in cereals. *CRC Critical Reviews Plant Science*, **1**, 49-93.

13. Bittle, D., Shaver, J., Somers, D. & Gengenbach, B. (1996). Lysine accumulation in maize cell cultures transformed with a lysine-insensitive form of maize dihydrodipicolinate synthase. *Theoretical and Applied Genetics*, **92**, 70-77.

14. Azevedo, R. (2002). Analysis of the aspartic acid metabolic pathway using mutant genes. *Amino Acids*, **22**, 217-230.

15. Azevedo, R., Arruda, P., Turner, W. & Lea, P. (1997). The biosynthesis and metabolism of the aspartate derived amino acids in higher plants. *Phytochemistry*, **46**, 395-419.

16. Amir, R. & Galili, G. (1999). Regulation of lysine and threonine metabolism in plants. *Genetic Engineering*, **21**, 57-77.

17. Galili, G. (1995). Regulation of lysine and threonine synthesis. *Plant Cell*, **7**, 899-906.

18. Stahly, D. (1969). Dihydrodipicolinate synthase of *Bacillus licheniformis*. *Biochimica et Biophysica Acta*, **191**, 439-451.

19. Yugari, Y. & Gilvarg, C. (1965). The condensation step in diaminopimelate synthesis. *Journal of Biological Chemistry*, **240**, 4710-4716.

20. Ghislain, M., Frankard, V. & Jacobs, M. (1995). A dinucleotide mutation in dihydrodipicolinate synthase of *Nicotiana sylvestris* leads to lysine overproduction. *Plant Journal*, **8**, 733-743.

21. Kwon, T., Sasahara, T. & Abe, T. (1995). Lysine accumulation in transgenic tobacco expressing dihydrodipicolinate synthase of *Escherichia coli*. *Journal of Plant Physiology*, **146**, 615-621.

22. Miflin, B., Napier, J. & Shewry, P. (1999). Improving plant product quality. *Nature Biotechnology*, **17**, 13-14.

23. Silk, G. & Matthews, B. (1997). Soybean *dapA* mutations encoding lysine-insensitive dihydrodipicolinate synthase. *Plant Molecular Biology*, **33**, 931-933.

24. Shaver, J., Brittel, D., Sellner, J., Frisch, D., Somers, D. & Gengenbach, B. (1996). Single-amino acid substitutions eliminate lysine inhibition of maize dihydrodipicolinate synthase. *Proceedings of the National Academy of Sciences of the United States of America*, **93**, 1962-1966.

25. Falco, S., Guida, T., Locke, M., Mauvais, J., Sanders, C., Ward, R. & Webber, P. (1995). Transgenic canola and soybean seeds with increased lysine. *Biotechnology (NY)*, **13**, 577-582.

26. Brinch-Pedersen, H., Galili, G., Knudsen, S. & Holm, P. (1996). Engineering of the aspartate family biosynthetic pathway in barley (*Hordeum vulgare L.*) by transformation with heterologous genes encoding feed-back-insensitive aspartate kinase and dihydrodipicolinate synthase. *Plant Microbiology and Biology*, **32**, 611-620.

27. Scapin, G. & Blanchard, J. (1998). Enzymology of bacterial lysine biosynthesis. *Advances in Enzymology and Related Areas of Molecular Biology*, **72**, 279-297.

28. Girodeau, J. M., Agouridas, G., Masson, M., Pineau, R. & Le Goffic, F. (1986). The lysine pathway as a target for a new generation of synthetic antibacterial antibiotics? *Journal of Medicinal Chemistry*,**29** , 1023-1030.

29. Bonnassie, S., Oreglia, J. & Sicard, A. (1990). Nucleotide sequence of the *dapA* gene from *Corynebacterium glutamicum. Nucleic Acids Resarch*, **18**, 6421.

30. Pavelka, M., Weisbrod, T. & Jacobs, W. (1997). Cloning of the *dapB* gene, encoding dihydrodipicolinate reductase, from *Mycobacterium tuberculosis. Journal of Bacteriology*, **179**, 2777-2782.

31. Scapin, G., Blanchard, J. S. & Sacchettini, J. C. (1995). Three-dimensional structure of *Escherichia coli* dihydrodipicolinate reductase. *Biochemistry*, **34**, 3502-3512.

32. Kindler, S. & Gilvarg, C. (1960). *N*-Succinyl-L-α, ε-diaminopimelic acid deacylase. *Journal of Biological Chemistry*, **235**, 3532-3535.

33. Sundharadas, G. & Gilvarg, C. (1967). Biosynthesis of α,ε-diaminopimelic acid in *Bacillus megaterium. Journal of Biological Chemistry*, **242**, 3983-3988.

34. Simms, S. A., Voiges, W. H. & Sahm, H. (1984). Purification and characterization of succinyl-CoA: tetrahydrodipicolinate *N*-succinyltransferase from *Escherichia coli*. *Journal of Biological Chemistry*, **259**, 2734-2741.

35. Peterkofsy, B. & Gilvarg, C. (1961). *N*-succinyl-L-diaminopimelic-glutamic transaminase. *Journal of Biological Chemistry*, **242**, 3983-3984.

36. Lin, Y., Myhrman, R., Schrag, M. L. & Gelb, M. H. (1988). Bacterial *N*-succinyl-L-diaminopimelic acid desuccinylase. *Journal of Biological Chemistry*, **263**, 1622-1627.

37. Wiseman, J. S. & Nicholos, J. S. (1984). Purification and properties of diaminopimelic acid epimerase from *Escherichia coli*. *Journal of Biological Chemistry*,**259** , 8907-8914.

38. White, P. J. & Kelly, B. (1965). Purification and properties of diaminopimelate decarboxylase from *Escherichia coli*. *Biochemical Journal*, **96**, 75-84.

39. Weinberger, S. & Gilvarg, C. (1970). Bacterial distribution of the use of succinyl and acetyl blocking groups in diaminopimelic acid biosynthesis. *Journal of Bacteriology*, **101**, 323-324.

40. Roberts, S. J., Morris, J. C., Dobson, R. C. J. & Gerrard, J. A. (2003). The preparation of (*S*)-aspartate semi-aldehyde appropriate for use in biochemical studies. *Bioorganic and Medicinal Chemistry Letters*, **13**, 265-267.

41. Tudor, D. W., Lewis, T. & Robins, D. J. (1993). Synthesis of the trifluoroacetate salt of aspartic acid β-semialdehyde, an intermediate in the biosynthesis of L-lysine, L-threonine, and L-methionine. *Synthesis*, **11**, 1061-1062.

42. Coulter, C. V., Gerrard, J. A., Kraunsoe, J. A. E. & Pratt, A. J. (1996). *(S)*-Aspartate semi-aldehyde: synthetic and structural studies. *Tetrahedron*, **52**, 7127-7136.

43. Grazi, E., Cheng, T. & Horecker, B. L. (1962). Formation of a stable aldolase-dihydroxyacetone phosphate complex. *Biochemical and Biophysical Research Communications*, **7**, 250-253.

44. Karsten, W. E. (1997). Dihydrodipicolinate synthase from *Escherichia coli*: pH dependent changes in the kinetic mechanism and kinetic mechanism of allosteric inhibition by L-lysine. *Biochemistry*,**36** , 1730-1739.

45. Blickling, S., Renner, C., Laber, B., Pohlenz, H., Holak, T. A. & Huber, R. (1997). Reaction mechanism of *Escherichia coli* dihydrodipicolinate synthase investigated by X-ray crystallography and NMR spectroscopy. *Biochemistry*, **36**, 24-33.

46. Shedlarski, J. G. & Gilvarg, C. (1970). The pyruvate-aspartic semialdehyde condensing enzyme of *Escherichia coli*. *Journal of Biological Chemistry*, **245**, 1362-1373.

47. Richaud, F., Richaud, C., Ratet, P. & Patte, J. (1986). Chromosomal location and nucleotide sequence of the *Escherichia coli dapA* gene. *Journal of Bacteriology*, **166**, 297-300.

48. Richaud, F., Richaud, C., Haziza, C. & Patte, J. (1981). Isolement et purification de genes d'*Escherichia coli* K12 impliques dans la biosynthese de la lysine. *Comptes Rendus de l'Acadedmie des Sciences. La vie des Sciences*, **293**, 507-512.

49. Vauterin, M. & Jacobs, M. (1994). Isolation of a poplar and an *Aribidopsis* dihydrodipicolinate synthase cDNA clone. *Plant Molecular Biology*, **25**, 545-550.

50. Cremer, J., Eggeling, L. & Sahm, H. (1990). Cloning the *dapA dapB* cluster of the lysine-secreting bacterium *Corynebacterium glutamicum*. *Molecular General Genetics*, **229**, 478-480.

51. Chent, N., Jiang, S., Klein, D. A. & Paulus, H. (1993). Organization and nucleotide sequence of the *Bacillus subtilis* diaminopimelate operon, a cluster of genes encoding the first three enzymes of diaminopimelate synthesis and dipicolinate synthase. *Journal of Biological Chemistry*, **268**, 9448-9465.

52. Kaneko, T., Hashimoto, T., Kumpaisal, R. & Yamada, Y. (1990). Molecular cloning of wheat dihydrodipicolinate synthase. *Journal of Biological Chemistry*, **265**, 17451-17455.

53. Garcia-Rodriguez, F. M., Zekri, S. & Toro, N. (2000). Characterization of the *Sinorhizobium meliloti* genes encoding a functional dihydrodipicolinate synthase (*dapA*) and dihydrodipicolinate reductase (*dapB*). *Archives of Microbiology*, **173**, 438-444.

54. Silk, G. W., Matthews, B. F., Somers, D. a. & Gengenbach, B. G. (1994). Cloning and expression of the soybean *dapA* gene encoding dihydrodipicolinate synthase. *Plant Molecular Biology*, **26**, 989-993.

55. Frisch, D. A., Gengenbach, B. G., Tommey, A. M., Sellner, J. M., Somers, D. A. & Myers, D. E. (1991). Isolation and characterization of dihydrodipicolinate synthase from maize. *Plant Physiology*, **96**, 444-452.

56. Wallsgrove, R. M. & Mazelis, M. (1981). Spinach leaf dihydrodipicolinate synthase: partial purification and characterization. *Biochemistry*, **20**, 2651-2655.

57. Kumpaisal, R., Hashimoto, T. & Yamada, Y. (1987). Purification and characterization of dihydrodipicolinate synthase from wheat suspension cultures. *Plant Physiology*, **85**, 145-151.

58. Dereppe, C., Bold, G., Ghisalba, O., Ebert, E. & Hans-Peter, S. (1992). Purification and characterization of dihydrodipicolinate synthase from pea. *Plant Physiology*, **98**, 813-821.

59. Laber, B., Gomis-Ruth, F., Romao, M. & Huber, R. (1992). *Escherichia coli* dihydrodipicolinate synthase. Identification of the active site and crystallization. *Biochemical Journal*, **288**, 691-695.

60. Borthwick, E. B., Connel, S. J., Tudor, D. W., Robins, D. J., Shneier, A., Abell, C. & Coggins, J. R. (1995). *Escherichia coli* dihydrodipicolinate synthase: characterisation of the imine intermediate and the product of bromopyruvate treatment by electrospray mass spectrometry. *Biochemical Journal*, **305**, 521-524.

61. Eggeling, L., Oberle, S. & Sahm, H. (1998). Improved L-lysine yield with *Corynebacterium glutamicum*: use of *dapA* resulting in increased flux combined with growth limitation. *Applied Microbiology and Biotechnology*, **49**, 24-30.

62. Yamakura, F., Ikeda, Y., Kimura, K. & Sasakawa, T. (1974). Partial purification and some properties of pyruvate-aspartic semialdehyde condensing enzyme from sporulating *Bacillus subtilis*. *Journal of Biochemistry*,**76** , 611-621.

63. Blickling, S., Beisel, H., Bozic, D., Knablein, J., Laber, B. & Huber, R. (1998). Structure of dihydrodipicolinate synthase of *Nicotiana sylvestris* reveals novel quaternary structure. *Journal of Molecular Biology*, **274**, 608-621.

64. Mirwaldt, C., Korndorfer, I. & Huber, R. (1995). The crystal structure of dihydrodipicolinate synthase from *Escherichia coli* at 2.5 Å resolution. *Journal of Molecular Biology*, **246**, 227-239.

65. Cornish-Bowden, A. (1999). *Fundamentals of enzyme kinetics*. 2nd edit., Portland Press Ltd, London.

66. Eggeling, L. (1994). Biology of L-lysine overproduction by *Corynebacterium glutamicum*. *Amino Acids*, **6**, 261-272.

67. Halling, S. M. & Stahly, D. P. (1976). Dihydrodipicolinate acid synthase of *Bacillus licheniformis*. Quaternary structure, kinetics, and stability in the presence of sodium chloride substrates. *Biochimica et Biophysica Acta*, **452**, 580-596.

68. Bartlett, A. & White, P. (1986). Regulation of the enzymes of lysine biosynthesis in *Brevibacterium lactofermentum* NCTC 9602 during vegetative growth. *Journal of General Microbiology*, **132**, 3169-3177.

69. Webster, F. & Lechowich, R. (1970). Partial purification and characterization of dihydrodipicolinate synthase from sporulating *Bacillus megaterium*. *Journal of Bacteriology*, **101**, 118-126.

70. Kumpaisal, R., Hashimoto, T. & Yamada, Y. (1989). Inactivation of wheat dihydrodipicolinate synthase by 3-bromopyruvate. *Agricultural and Biological Chemistry*,**53** , 355-359.

71. Gourley, D. G., Shrive, A. K., Polikarpov, I., Krell, T., Coggins, J. R., Hawkins, A. R., Isaacs, N. W. & Sawyer, L. (1999). The two types of 3-dehydroquinase have distinct structures but catalyze the same overall reaction. *Nature Structural Biology*, **6**, 521-525.

72. Koradi, R., Billeter, M. & Wüthrich, K. (1996). MOLMOL: a program for display and analysis of macromolecular structures. *Journal of Molecular Graphics*, **14**, 51-55.

73. Pisabarro, A., Malumbres, M., Mateos, L. A., Oguiza, J. F. & Martin, J. F. (1993). A cluster of three genes (*dapA*, *orf2*, and *dapB*) of *Brevibacterium lactofermentum* encodes dihydrodipicolinate synthase, dihydrodipicolinate reductase, and a third polypeptide of unknown function. *Journal of Bacteriology*, **175**, 2743-2749.

74. Lawrence, M., Barbosa, J., Smith, B., Hall, N., Pilling, A., Ooi, H. & Marcuccio, S. (1997). Structure and mechanism of a sub-family of enzymes related to *N*-acetylneuraminate lyase. *Journal of Molecular Biology*, **266**, 381-399.

75. Farber, G. & Pesko, G. (1990). The evolution of α/β-barrel enzymes. *Trends in Biochemical Sciences*,**5** , 228-234.

76. Joerger, A. C., Mayer, S. & Fersht, A. (2003). Mimicking natural evolution *in vitro*: an *N*-acetylneuraminate lyase mutant with an increased dihydrodipicolinate synthase activity. *Proceedings of the National Academy of Sciences of the United States of America*, **100**, 5694-5699.

77. Shames, S. & Wedler, F. (1984). Homoserine kinase of *Escherichia coli*: kinetic mechanism and inhibition by L-aspartate semialdehyde. *Archives of Biochemistry and Biophysics*, **235**, 359-370.

78. Reddy, S., Sacchettini, J. & Blanchard, J. (1995). Expression, purification, and characterization of *Escherichia coli* dihydrodipicolinate reductase. *Biochemistry*, **34**, 3492-3501.

79. Reddy, S., Scapin, G. & Blanchard, J. (1996). Interaction of pyridine nucleotide substrates with *Escherichia coli* dihydrodipicolinate reductase: thermodynamic and structural analysis of binary complexes. *Biochemistry*, **35**, 13924-13302.

80. Wang, F., Blanchard, J. & Tang, X. (1997). Hydrogen exchange/electrospray ionization mass spectrometry studies of substrate and inhibitor binding and conformational changes of *Escherichia coli* dihydrodipicolinate reductase. *Biochemistry*, **36**, 3755-3759.

81. Galili, G. (2002). New insights into the regulation and functional significance of lysine metabolism in plants. *Annual Review of Plant Biology*, **53**, 27-43.

82. Karchi, H., Miron, D., Ben-Yaacov, S. & Galili, G. (1995). The lysine-dependent stimulation of lysine catabolism in tobacco seed requires calcium and protein phosphorylation. *Plant Cell*, 7, 1963-1970.

83. Bouvier, E., Richaud, C., Richaud, F., Patte, J. & Stragier, P. (1984). Nucleotide sequence and expression of *Escherichia coli dapB* gene. *Journal of Biological Chemistry*,**258** , 14829-14834.

84. Mclennan, N. & Masters, M. (1998). GroE is vital for cell wall synthesis. *Nature*, **392**, 139.

85. Alarcon, C. M. & Heitman, J. (1997). FKBP12 physically and functionally interacts with aspartokinase in *Saccharomyces cerevisiae.M olecular and Cellular Biology*, **17**, 5968-5975.

86. Frankard, V., Ghislian, M. & Jacobs, M. (1992). Two feedback-insensitive enzymes of the aspartate pathway in *Nicotiana sylvestris*. *Plant Physiology*, **99**, 1285-1293.

87. Azevedo, R. & Lea, P. J. (2001). Lysine metabolism in higher plants. *Amino Acids*, **20**, 261-279.

88. Blickling, S. & Knablein, J. (1997). Feedback inhibition of dihydrodipicolinate synthase enzymes by L-lysine. *Biological Chemistry*, **378**, 207-210.

89. Mathews, B. & Widholm, J. (1978). Regulation of lysine and threonine synthesis in carrot cell suspension cultures and whole carrot roots. *Planta*, **141**, 315-321.

90. Ghislain, M., Frankard, V. & Jacobs, M. (1990). Dihydrodipicolinate synthase of *Nicotiana sylvestris*,a chloroplast-localized enzyme of the lysine pathway. *Planta*, **180**, 480-486.

91. Bakhiet, N., Forney, F., Stahly, D. & Daniels, L. (1984). Lysine biosynthesis in *Methanobacterium thermoautotropicum* is by the diaminopimelic acid pathway. *Current Microbiology*,**10** , 195-198.

92. Hoganson, D. & Stahly, D. (1975). Regulation of dihydrodipicolinate synthase during growth and sporulation of *Bacillus cereus*. *Journal of Bacteriology*, **124**, 1344-1350.

93. Tosaka, O. & Takinami, K. (1978). Pathway and regulation of lysine biosynthesis in *Brevibacterium lactofermentum*. *Agricultural Biological Chemistry*, **42**, 95-100.

Chapter Two.

Enzyme purification and a new synthesis of (*S*)-ASA.

2.1 Introduction.

Both DHDPS and DHDPR occur early in the DAP biosynthetic pathway and are common to all forms of bacteria. In order to examine the properties of DHDPS biochemically, a sufficient quantity of purified enzyme was required. Furthermore, the assay used to collect the initial rate data for DHDPS required DHDPR as a coupling enzyme, so a large amount of this enzyme, in a purified form, was also essential. The genes encoding for *E. coli* DHDPS (*dap*A) and DHDPR (*dap*B) were each available on multi-copy plasmids, thus providing a ready source of each enzyme. With the plasmids in hand, and adapting reported purification methods for DHDPS and DHDPR, we hoped to isolate and purify milligram quantities of each.

As described in Chapter one, DHDPS catalyses the condensation of (*S*)-ASA and pyruvate to form an unstable heterocyclic product. For detailed kinetic analysis, pure (*S*)-ASA and pyruvate were thus required. Pyruvate is available commercially as a white crystalline solid and is stable for many months at 4°C. While the literature reports several syntheses of (*S*)-ASA, all are laborious or produce impure product. Some effort was therefore invested to improve the synthesis of this substrate.

The first part of this chapter deals with the isolation and purification of both DHDPS and DHDPR enzymes. The second part discusses a newly developed synthetic route to (*S*)-ASA, which was accomplished in collaboration with Sarah Roberts.

2.2 Part A: Purification of DHDPS and DHDPR

In order to study the properties of *E. coli* DHDPS and DHDPR, large quantities of purified enzyme were required. The *E. coli dap*A and *dap*B genes were previously cloned into pBluescript (a high copy number plasmid) by Gerrard[1] to give pJG001::*dap*A, and Kraunsoe[2] to give pJK001::*dap*B. These high copy number plasmids had been introduced into *E. coli* XL-Blue using the calcium chloride method whereby successful transformants were identified by the conferred ampicillin resistance.[3, 4] These strains provide a simple and convenient means for over-expression of both enzymes, generating several hundred-fold increases in enzyme expression, since transcription of DHDPS from this plasmid is constitutive.

2.2.1 Plasmid extraction and restriction digests.

Before purifying either enzyme, the integrity of the pJG001 and pJK001 plasmids was routinely confirmed by restriction analysis. The standard methods for plasmid preparation were used to isolate pJG001 and pJK001.[5] Following restriction digestion and DNA gel electrophoresis, the predicted restriction patterns for pJG001 and pJK001 were seen (Figure 2.1). When subjected to digestion by *Eco*RI (a restriction enzyme with only one cutting site in the multi-cloning site of pBluescript) pJG001 produced a single linear DNA fragment (4100 bp), which corresponded to the complete pJG001 plasmid (Figure 2.1: lane 6). The cloned *dap*A gene was excised from pJG001 if digested with *Eco*RI and *Hin*dIII, resulting in two linear fragments corresponding to the pBluescript vector (3000 bp) and the *dap*A insert (1100 bp) (Figure 2.1: lane 7).

Like pJG001, pJK001 showed a single band (5300 bp) on an agarose gel following digestion with *Eco*RI (Figure 2.1: lane 1). Two linear fragments, corresponding to the pBluescript vector (3000 bp) and the *dap*B fragment (2300 bp) were observed, when pJK001 was subjected to a double enzyme digest with *Hin*dIII and *Eco*RI (Figure 2.1: lane 4). Once the plasmid integrity was confirmed, over-expression and purification ensued.

Figure 2.1 *Typical example of an agarose gel showing DNA restriction fragments of pJG001 and pJK001.*

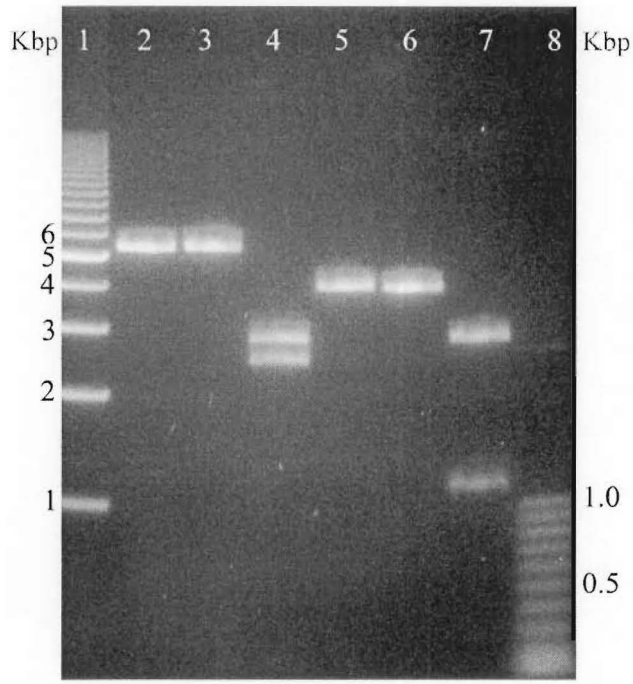

pJK001: 1, 1 kb ladder; **2**, pJK001 single digest (*Hin*dIII) 5300 bp linear fragment; **3**, pJK001 single digest (*Eco*R1); **4**, pJK001 double digest (*Hin*dIII and *Eco*RI) 3000 bp and 2300 bp linear fragments.

pJG001: 5, pJG001 single digest (*Hin*dIII) 4100 bp linear fragment; **6**, pJG001 single digest (*Eco*R1) 4100 bp linear fragment; **7**, pJG001 double digest (*Hin*dIII and *Eco*RI) 3000 bp and 1100 bp linear fragments; **8**, 100 bp ladder.

2.2.2 Over-expression and purification of DHDPS

DHDPS was purified from *E. coli* XL-1 Blue (pJG001) based on the methods originally reported by Mirwaldt *et al.*[6] with some modifications. Purification steps were monitored by the detection of DHDPS activity using the qualitative *o*-aminobenzaldehyde assay.[4, 7] This assay is simple, rapid, and sensitive to very low levels of DHDPS activity, and is therefore ideal for qualitative measurements to monitor for the presence of the enzyme.

E. coli cells that contained pJG001 were incubated overnight, harvested by centrifugation, and resuspended in buffer. Previous workers have used freeze-thaw cycles to gently disrupt the cells, but in this study, greater yields were achieved by ultrasonication without a significant loss in specific activity. Thus, ultrasonication was used to isolate the cell extract.[4] After centrifugation, the pellet was discarded and the supernatant containing the crude extract was collected.

The relatively high thermostability of DHDPS enabled a heat shock step to be incorporated into the procedure. This step removed nearly two thirds of the soluble protein, yet retained nearly 100% activity. Following heat shock, the sample was loaded onto a Q-Sepharose column in order to separate DHDPS from other contaminating enzymes. The proteins were eluted with a sodium chloride gradient (0–1 M) and any fractions displaying activity in the *o*-aminobenzaldehyde assay were pooled. DHDPS from the pooled fractions was further purified based on surface hydrophobicity, using a Phenyl-Sepharose column. Fractions were eluted with a ammonium sulphate gradient (0.5–0 M) and those that gave a positive result, when tested for DHDPS activity by the *o*-aminobenzaldehyde assay, were pooled and dialysed overnight. If necessary, the sample was concentrated using 10000 MW spin filters, without any loss of activity. Following purification, SDS-PAGE analysis revealed a 31 kDa band, corresponding to DHDPS, as the predominant protein component (Figure 2.2; lane 6).

As judged by the coupled assay, DHDPS was purified 5.8 fold from the crude extract and to a specific activity of 1.8 units mg^{-1} (where 1 unit is defined as the consumption of 1 μmol NADPH s^{-1}) (Table 2.1). This is a substantial improvement on previously reported values for specific activity of 0.47 units mg^{-1} [(4)] and 0.87 units mg^{-1},[(8)] both of which were determined using the quantitative coupled assay. The increase in specific activity associated with the increase in purity of the DHDPS during the purification protocol is shown in Table 2.1.

Figure 2.2 *Typical SDS-PAGE comparison of sample solutions after each DHDPS purification step.*

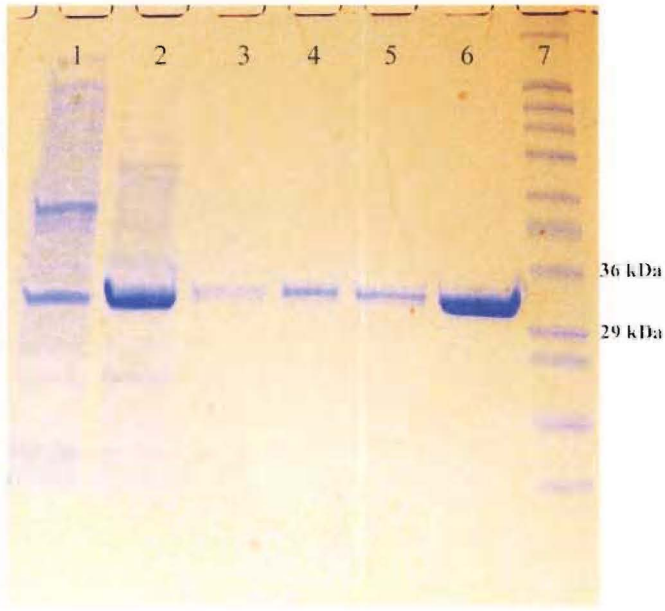

Lanes: 1, crude cell extract after freeze thaw and ultrasonication; 2, heat shock for 2 min at 70°C; 3, Q-Sepharose ion exchange; 4, dialysis; 5, Phenyl-Sepharose hydrophobic interaction chromatography; 6, concentration with spin filter; 7, Sigmamarker, wide molecular weight range of the bands (from top) 205, 116, 97, 84, 66, 55, 45, 36, 29, 24, 20, 10.2 and 6.5 kDa.

Table 2.1 *Typical purification of wild-type DHDPS from* E. coli *XL-1 Blue (pJG001). From 21g wet cell weight (5 L of culture)*

	Protein[a] (mg)	Total activity[b] (units[c])	Specific activity (units mg^{-1})	Yield (%)	Degree of purification (fold)
Crude	2883	898	0.31		
Heat shock	1083	896	0.83	100	2.7
Q-Sepharose	440	687	1.6	77	5.0
Phenyl-Sepharose	193	351	1.8	39	5.8

[a] Protein concentrations were determined using the Bradford assay.[12]
[b] Activity was determined using the quantitative coupled assay.
[c] 1 unit is defined as the consumption of 1 μmol NADPH s^{-1}.

2.2.3 *Over-expression of the* dap*B gene and purification of DHDPR*

Purification of DHDPR was based on the methods of Reddy *et al.*,[9] who produced DHDPR suitable for crystallisation.[10] The method was both simple and efficient, providing enzyme of purity appropriate for kinetic studies.

After incubation overnight, *E. coli* XL-1 Blue (pJK001) cells were harvested by centrifugation then washed and resuspended in buffer. Ultrasonication was used to disrupt the cell wall, releasing DHDPR.

DHDPR also displays an unusual heat tolerance, as shown by Farkas and Gilvarg.[11] Heat shock treatment of the crude preparation at 70°C for two minutes resulted in no significant loss of DHDPR activity, as shown by the purification table (Table 2.2). This step is thought to destroy any contaminating NADPH-utilising enzymes that might interfere with the coupled assay and is carried out early in the purification scheme. Following both ultrasonication and heat shock treatment, the predominant protein in the crude extract was DHDPR, the monomer being visible as a band of molecular weight 29 kDa after SDS-PAGE and staining with Coomassie Brilliant Blue (Figure 2.3: lane 2).

Table 2.2 *Typical data for the purification of DHDPR.*

	Protein[a] (mg)	Total activity[b] (units[c])	Specific activity (units mg^{-1})	Yield (%)	Degree of Purification (fold)
Crude	1024	13.4	0.013		
Heat Shock	140	13.3	0.095	99	7
Q-Sepharose	54	12.5	0.23	94	18
Hi-Trap Blue	8	12.3	1.5	92	118

[a] Protein concentrations determined using the Bradford assay.[12]
[b] Activity determined using the quantitative coupled assay for DHDPR activity
[c] 1 unit is defined as the consumption of 1 μmol NADPH s^{-1}.

The extract was subjected to charge-based purification using a Q-Sepharose anion exchange chromatography column. Fractions were eluted in a sodium chloride gradient and assayed for DHDPR activity using the qualitative coupled assay. Following dialysis, the active

fractions were purified and concentrated further by affinity chromatography using a Hi-Trap Blue nucleotide exchange column. The fractions were again eluted in a sodium chloride gradient and assayed for DHDPR activity using the qualitative coupled assay. The Hi-Trap Blue column preferentially binds NAD(P)H-utilising enzymes and therefore introduces a very specific and selective step for the purification of DHDPR. Those fractions that showed activity were pooled and the final product, after dialysis, displayed a specific activity of 1.5 units mg^{-1}. This is consistent with the previously reported value of 2.25 units mg^{-1},[4] but of lower purity than produced by Reddy,[9] probably because size exclusion was not used as a strategy. Nevertheless, DHDPR was purified to homogeneity as judged by SDS-PAGE (Figure 2.3: lane 6), which shows a single band (29 kDa) with an electrophoretic mobility corresponding to a protein monomer of DHDPR. Moreover, that DHDPR did not utilise NADPH when in the presence pyruvate and ASA, unless DHDPS was added, confirms that it was free of any contaminating wild-type DHDPS; this was a prerequisite that was required for accurate initial rate determinations of DHDPS and its mutants. As with DHDPS, the increase in purity was reflected in an increase in the specific activity of the enzyme (Table 2.2).

Figure 2.3 *Typical SDS-PAGE comparison of sample solutions after each DHDPR purification step.*

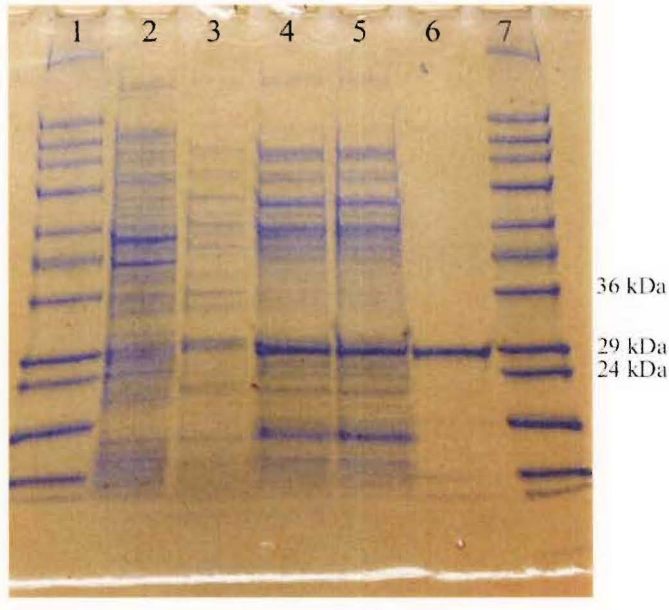

Lanes: **1**, Sigmamarker, wide molecular weight range of the bands (from top) 205, 116, 97, 84, 66, 55, 45, 36, 29, 24, 20, 10.2 and 6.5 kDa; **2**, crude cell extract after freeze thaw and ultrasonication; **3**, heat shock for 2 min at 70°C; **4**, Q-Sepharose ion exchange; **5**, dialysis; **6**, Hi-Trap Blue column; 7, Sigmamarker.

2.3 Part B: Synthesis of aspartate β-semialdehyde ((*S*)-ASA).

In this thesis, three methods were used to synthesise (*S*)-ASA. Since the aim of this project involved kinetic analysis of DHDPS and its mutants, (*S*)-ASA free of contaminates was required. For the purpose of initial rate collection, unless explicitly stated, we used (*S*)-ASA manufactured by the method of Coulter *et al.*[3] or by our published method,[13] which was completed in collaboration with Sarah Roberts.

Enantiomerically pure (*S*)-ASA and its derivatives are increasingly important synthetic intermediates, as the aldehyde moiety of (*S*)-ASA can be functionalised to yield more complex structures. The potential to access a variety of polyfunctional non-proteinogenic and unnatural amino acids using (*S*)-ASA and its derivatives has already been demonstrated.[14, 15] (*S*)-ASA manipulation has also proved to be important in the synthesis of pharmaceuticals, aroma and flavour chemicals, pesticides and herbicides, dyes, and pigments.[16]

At the outset of this work, there were three reported methods for (*S*)-ASA synthesis that were used in the kinetic studies of DHDPS and DHDPR.[3, 17, 18] The modern methods were derived from the original procedure of Black and Wright,[17] which involves the direct ozonolysis of (*S*)-allylglycine (Figure 2.4). Tudor *et al.*[18] investigated the ozonolysis of protected derivatives of (*S*)-allylglycine. Removal of the protecting groups with TFA affords (*S*)-ASA as a hydrate of trifluoroacetate salt, which can be stored as a stable solid for many months at 0°C. While other methods that yield free or diprotected (*S*)-ASA have been reported in the literature, they are often complex multi-step procedures and/or are low yielding reactions.[3] This complexity is brought about by the fact that (*S*)-ASA is difficult to synthesise and characterise since, like many amino aldehydes, it has a marked tendency to polymerise and is only stable in aqueous strong acid solutions.[16, 18, 19] Reported here, and published elsewhere,[13] is a new synthetic route to (*S*)-ASA.

2.3.1 Ozonolysis of allyl glycine

In the first reported synthesis of (*S*)-ASA, the aldehyde moiety was obtained by oxidative cleavage of the double bond of (*S*)-allylglycine by ozonolysis.[17] The reaction was carried out in a 1 M aqueous hydrochloric acid solution at 0°C, with ozone bubbled through the

solution (Figure 2.4). The reported yield of the desired product was 90–100% and was determined by an enzymatic assay following the conversion of (*S*)-ASA into homoserine by homoserine dehydrogenase (Figure 2.4).[17] (*S*)-ASA produced by ozonolysis has variable purity as described by Coulter *et al.*,[3] Gerrard,[1] and Tudor *et al.*[18] This is due to the fact that the reaction generates a complex mixture of products including ASA, aspartic acid and formic acid.[18, 19] In the hands of Coulter *et al.*[3] and Gerrard[1], (*S*)-ASA generated by ozonolysis proved difficult to purify, largely due to its instability, and had to be kept in cold acid solutions. Given these problems, ozonolysis was deemed to be unsuitable for the production of (*S*)-ASA for kinetic analysis. This assumption is examined further in Chapter three. However, it must be noted that ozonolysis is still commonly used today for kinetic studies of DHDPS and DHDPR.[9, 20]

Figure 2.4 *Ozonolysis of allyl glycine. Determining the (S)-ASA concentration by the method of Black and Wright.*[17]

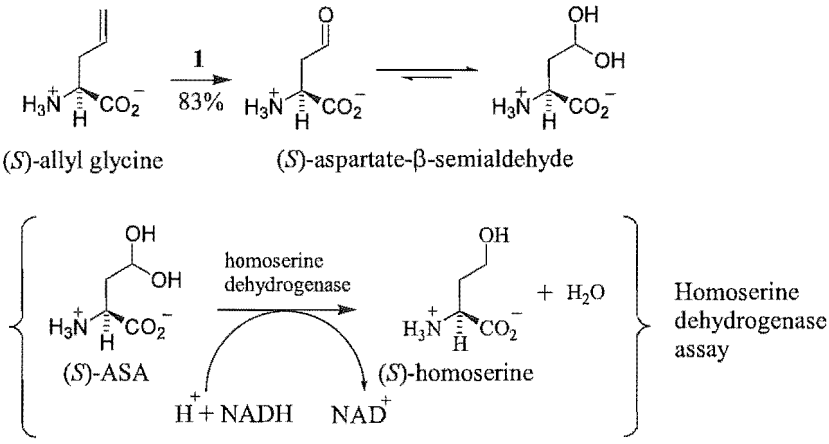

Reaction conditions: **1** ozone, 1 M HCl.

Initial work used ozonolysis in order to verify its unsuitability in the production of (*S*)-ASA (see Chapter three). The method used was that of Black and Wright,[17] although the ineffective purification step was omitted. In our hands, the reaction yield was 83% as judged by assay with DHDPS. This is in contrast to a 90–100% yield reported by Black and Wright,[17] as measured by the homoserine dehydrogenase assay outlined in Figure 2.4. When analysed by ^{1}H NMR, the sample gave a complicated spectrum, consistent with the formation of a mixture of compounds, one of which corresponded to (*S*)-ASA.

2.3.2 *A route to (S)-ASA via the Lemieux-Johnson reaction*

As an alternative to ozonolysis, Gerrard[1] developed a new method, based upon that of Tudor *et al.*,[18] whereby allylglycine was first protected, but the oxidation of *N*-BOC-α-diphenylmethyl allylglycine was accomplished using catalytic amounts of osmium tetroxide with sodium periodate (Lemieux-Johnson reaction) (Figure 2.5).

Figure 2.5 *Synthesis of (S)-ASA via the Lemieux-Johnson reaction.*

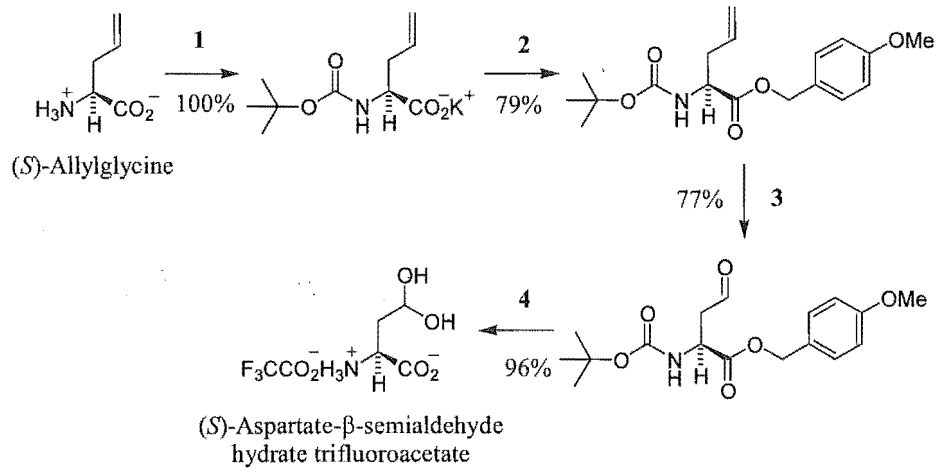

Reaction conditions: **1** di-*tert*-butylpyrocarbonate, dioxane, $KHCO_3$; **2** *p*-methoxybenzyl chloride, DMF; **3** OsO_4, $NaIO_4$; **4** CF_3CO_2H, DCM.

Osmium tetroxide reacts with various double bonds to form a cyclic osmate (VI) diester, which can then be hydrolysed to a diol. Sodium periodate efficiently cleaves the 1,2-diol bond to give a carbonyl compound as the final product (Figure 2.5: step 3).[21] The reaction is rapid, clean (has few side reactions), and specific because the carbonyl compound generated is inert towards further oxidation under the reaction conditions. The combination of osmium tetroxide hydroxylation of an alkene and periodate cleavage of a 1,2-glycol permits the use of relatively small amounts of this very expensive and poisonous hydroxylating agent. Periodate oxidises osmium (when in its lower valence forms) to the tetroxide, thus regenerating the hydroxylating agent.[21]

The osmium tetroxide technique is advantageous because oxidation does not proceed beyond the aldehyde oxidation state, thus affording the same product, but eliminating many of the side products produced by the ozonolysis reaction.[3, 18] Furthermore, the starting material

can be easily separated from the product by column chromatography, increasing the overall conversion.

(*S*)-Allylglycine was *N*-protected as a *tert*-butyl carbonate in quantitative yield using the reagent di-*tert*-butylpyrocarbonate (BOC) under basic conditions. The reaction was performed in dioxane in the presence of $KHCO_3$ at room temperature. The product obtained was a white powder.

The carboxyl group was then protected as a *p*-methoxybenzyl ester, *via* reaction of the potassium salt of (*S*)-BOC-allylglycine with a slight excess of *p*-methoxybenzyl chloride in DMF. Purification by column chromatography provided the desired material as a yellow oil in 79% yield.

The alkene moiety of the diprotected allylglycine was oxidised at room temperature using catalytic osmium tetroxide and three equivalents of sodium periodate to give the desired aldehyde in 77% yield, following purification by column chromatography. The major impurity of this reaction was unreacted starting material, which could be recovered.

The final step was deprotection of (*S*)-*N*-*tert*-butoxycarbonylaspartate-β-semialdehyde *p*-methoxybenzyl ester by stirring in trifluoroacetic acid dissolved in dry dichloromethane (DCM). (*S*)-ASA was isolated as the hydrated trifluoroacetate salt, in 96% yield and the ^1H NMR data are consistent with the product existing predominantly as the hydrate. The material was stable for many months if kept in a desiccator at –20°C. (*S*)-ASA was isolated in 59% overall yield from (*S*)-allylglycine. This is an improvement on the reported value of 43% overall yield obtained from Tudor *et al.*[18] and 42% by Coulter.[19] However, the purity of the (*S*)-ASA seemed to vary considerably; this compromised its suitability for kinetic studies.

2.3.3 Alternative synthetic routes to (S)-ASA.

Due to the high cost of allylglycine, either racemic or enantiopure, an alternative synthetic route to (*S*)-ASA was investigated. It was envisaged that (*S*)-ASA could be obtained from selectively protected aspartic acid (*pers. comm.* Dr. J. Morris). Aldehydes can, in theory, be obtained from aspartic acid by a selective reduction of the side chain, after the α-carbonyl

group of aspartic acid has been protected and the side chain activated to facilitate facile reduction (Figure 2.6).[16]

Figure 2.6 *Proposed synthesis of (S)-ASA from protected aspartic acid.*[16]

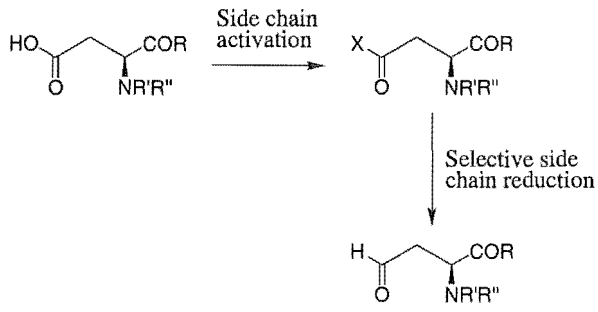

As (*S*)-ASA is only stable in acidic solutions,[18] the groups used to protect aspartic acid need to be acid labile. Accordingly, the ideal protected form of aspartic acid is *N*-BOC-α-*tert*-butyl aspartate and fortunately, it was commercially available and is considerably cheaper than (*S*)-allylglycine.

Two literature procedures were investigated to activate the diprotected aspartic acid side chain. The first method was to generate a Weinreb amide[22] and the second, to generate the thioester.[23] Following either activation, a selective reduction could take place to generate the aldehyde functional group as reported by Wernic *et al.*,[22] or Bergmeier *et al.*[23] Removal of the protecting groups with TFA would then generate the hydrated trifluoroacetate salt of (*S*)-ASA.[18]

Weinreb amide activation.

With the selectively protected amino acid in hand, side chain activation by conversion to the Weinreb amide was carried out following a procedure by Wernic *et al.*[22] (Figure 2.7). α-*tert* Butyl (*S*)-*N*-*tert*-butoxycarbonyl aspartate was converted to the corresponding *N*-methoxy-*N*-methylamide (Weinreb amide) in a reaction involving (benzotriazol-1-yloxy)-tris(dimethyl-amino)phosphonium hexafluorophosphate (BOP.PF_6), triethylamine and *N,O*-dimethylhydroxylamine hydrochloride in excellent yield (86%). The resulting product was reduced with diisobutyl aluminium hydride to give the aldehyde in quantitative yield, which required no further purification. The method of Tudor *et al.*[18] was used to deprotect

the aldehyde by stirring in trifluoroacetic acid and dry dichloromethane (DCM). The (*S*)-ASA was isolated as the hydrated trifluoroacetate salt, a pale yellow solid in 96% yield.

Figure 2.7 *Synthesis of (S)-ASA* via *Weinreb amide side chain activation.*[22]

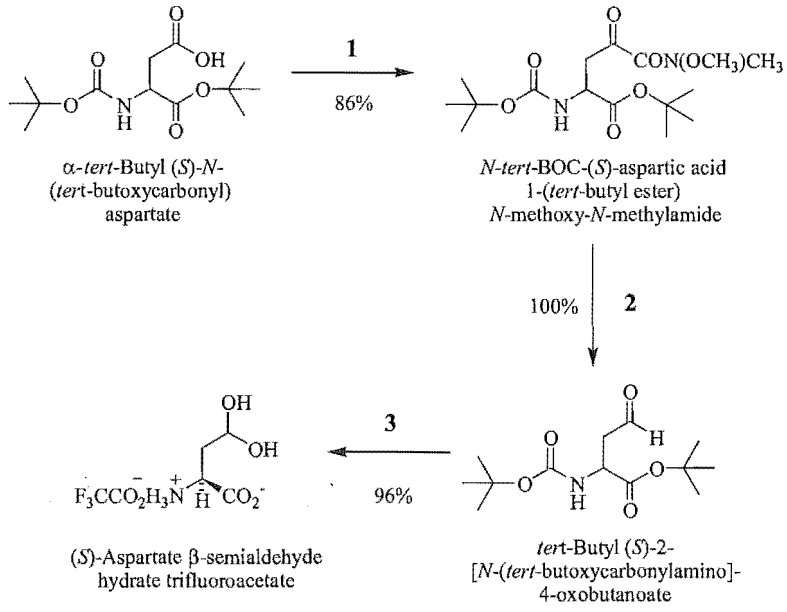

Reaction conditions: **1**, Et_3N, $BOP.PF_6$; **2**, DIBAL, THF, -70°C; **3**, CF_3CO_2H, DCM

This procedure provided a more efficient method for obtaining (*S*)-ASA than the reduction of diprotected (*S*)-allyglycine by osmium tetroxide or by ozonolysis. The overall yield of the reaction was also significantly improved (94%) from the diprotected aldehyde compared to other literature procedures that are currently used to synthesis (*S*)-ASA for kinetic studies.[3, 18] The above procedure is three steps to the pure aldehyde, eliminating the need to use the very expensive and poisonous dihydroxylating agent osmium tetroxide. Another promising feature was that it required only one purification step. The purity of the (*S*)-ASA generated was also of a very high standard (96–99%) as checked by the coupled assay of DHDPS and DHDPR.

2.4 Summary.

In order to kinetically assess DHDPS, large quantities of DHDPS and DHDPR were required in a purified form. Both enzymes, DHDPS and DHDPR, were over-expressed in *E. coli* and purified for use in enzyme kinetic studies. DHDPS was purified to a specific activity of

1.8 units mg^{-1} while DHDPR was purified to a specific activity of 1.5 units mg^{-1}.[¥] Both results are considerably higher than values obtained in the literature.

(*R,S*)-ASA was synthesised from diprotected (*R,S*)-allylglycine as described by Tudor *et al.*,[18] except periodate-osmium tetroxide was used as the oxidising agent rather than ozone.[19] The overall yield of the reaction was 59%, an increase on previously reported values of 42%[19] and 43%.[18]

In addition, an improved synthesis (*S*)-ASA was successfully achieved from *N-tert*-butoxycarbonyl-(*S*)-aspartic acid α-*tert*-butyl ester in three steps with an overall yield of 94%. This represents a significant advance over previously published routes to (*S*)-ASA and was the preferred synthetic route to (*S*)-ASA for further biochemical investigations.

2.5 References

1. Gerrard, J. A. (1992). Studies on dihydrodipicolinate synthase. D. Phil. thesis, Oxford University.

2. Kraunsoe, J. A. E. (1992). Studies in lysine biosynthesis. BSc. Hons. Part II, Corpus Christi College.

3. Coulter, C. V., Gerrard, J. A., Kraunsoe, J. A. E. & Pratt, A. J. (1996). *(S)*-Aspartate semi-aldehyde: synthetic and structural studies. *Tetrahedron*, **52**, 7127-7136.

4. Coulter, C. V., Gerrard, J. A., Kraunsoe, J. A. E. & Pratt, A. J. (1999). *Escherichia coli* dihydrodipicolinate synthase and dihydrodipicolinate reductase: kinetic and inhibition studies of two putative herbicide targets. *Pesticide Science*, **55**, 887-895.

5. Maniatis, T., Fritsch, E. & Sanbrook, J. (1990). *Molecular cloning: A laboratory Manual*. 2nd edit., Cold Spring Harbor Press, Cold Spring Harbor, New York.

6. Mirwaldt, C., Korndorfer, I. & Huber, R. (1995). The crystal structure of dihydrodipicolinate synthase from *Escherichia coli* at 2.5 Å resolution. *Journal of Molecular Biology*, **246**, 227-239.

¥ 1 unit is defined as the consumption of 1 μmol NADPH s^{-1}

7. Shedlarski, J. G. & Gilvarg, C. (1970). The pyruvate-aspartic semialdehyde condensing enzyme of *Escherichia coli*. *Journal of Biological Chemistry*, **245**, 1362-1373.

8. Borthwick, E. B., Connel, S. J., Tudor, D. W., Robins, D. J., Shneier, A., Abell, C. & Coggins, J. R. (1995). *Escherichia coli* dihydrodipicolinate synthase: characterisation of the imine intermediate and the product of bromopyruvate treatment by electrospray mass spectrometry. *Biochemical Journal*, **305**, 521-524.

9. Reddy, S., Sacchettini, J. & Blanchard, J. (1995). Expression, purification, and characterization of *Escherichia coli* dihydrodipicolinate reductase. *Biochemistry*, **34**, 3492-3501.

10. Scapin, G., Blanchard, J. S. & Sacchettini, J. C. (1995). Three-dimensional structure of *Escherichia coli* dihydrodipicolinate reductase. *Biochemistry*, **34**, 3502-3512.

11. Farkas, W. & Gilvarg, C. (1965). The reduction step in diaminopimelic acid biosynthesis. *Journal of Biological Chemistry*, **240**, 4717-4722.

12. Bradford, M. (1976). A rapid and sensitive method for the quantitation of microgram quantities of protein utilizing the principle of protein-dye binding. *Analytical Biochemistry*, **72**, 248-254.

13. Roberts, S. J., Morris, J. C., Dobson, R. C. J. & Gerrard, J. A. (2003). The preparation of (*S*)-aspartate semi-aldehyde appropriate for use in biochemical studies. *Bioorganic and Medicinal Chemistry Letters*, **13**, 265-267.

14. Baldwin, J. E. & Flinn, A. (1987). Use of L-aspartic acid β-semialdehyde in the synthesis of more complex non protein amino acids. *Tetrahedron Letters*, **28**, 3605-3608.

15. Lusch, H. & Uzar, H. C. (2000). New access to the synthetic building block L-aspartic acid β-semialdehyde *via* Grignard reaction. *Tetrahedron Asymmetry*, **11**, 4965-4973.

16. Meffre, P. (1999). Synthesis of optically active 2-amino-oxobutyric acid and N,O- derivatives. *Amino Acids*, **16**, 251-272.

17. Black, S. & Wright, N. G. (1954). Aspartic β-semialdehyde dehydrogenase and aspartic β-semialdehyde. *Journal of Biological Chemistry*, **213**, 39-50.

18. Tudor, D. W., Lewis, T. & Robins, D. J. (1993). Synthesis of the trifluoroacetate salt of aspartic acid β-semialdehyde, an intermediate in the biosynthesis of L-lysine, L-threonine, and L-methionine. *Synthesis*, **11**, 1061-1062.

19. Coulter, C. V. (1997). Studies in lysine biosynthesis. PhD thesis, University of Canterbury.

20. Karsten, W. E. (1997). Dihydrodipicolinate synthase from *Escherichia coli*: pH dependent changes in the kinetic mechanism and kinetic mechanism of allosteric inhibition by L-lysine. *Biochemistry*,**36** , 1730-1739.

21. Pappo, R., Allen, D. S., Lemieux, R. U. & Johnson, W. S. (1956). Osmium tetroxide-catalyzed periodate oxidation of olefinic bonds. *Journal of Organic Chemistry*,**21** , 478-479.

22. Wernic, D., Dimaio, J. & Adams, J. (1989). Enantiospecific synthesis of L-α-aminosuberic acid. Synthetic applications in preparation of atril natriuretic factor analogues. *Journal of Organic Chemistry*, **54**, 4224-4228.

23. Bergmeier, S., Cobas, A. & Rapoport, H. (1993). Chirospecific synthesis of (*1S,3R*)-1-amino-3-(hydroxymethyl)cyclopentane, precursor for carbocyclic nucleoside synthesis. Dieckmann cyclisation with an amino acid. *Journal of Organic Chemistry*,**58** , 2369-2376.

Chapter Three.

Kinetics of wild-type DHDPS.

3.1 Introduction.

The first requirement for the kinetic study of any enzyme is a suitable method for determining the initial rate of the reaction. This is achieved by measuring the change in concentration of substrates, or products, with respect to time. In order to assay wild-type DHDPS, which was purified in the last chapter (or the mutants generated in later chapters) a quantitative assay system was required. This assay had to be capable of accurately measuring the initial rate of the enzyme-catalysed reaction.

In the literature, there are three assays reported for the kinetic studies of DHDPS: the imidazole buffer assay, the *o*-aminobenzaldehyde assay, and the coupled assay. The simple and very sensitive *o*-aminobenzaldehyde assay[1] yields qualitative results, which were useful for following the purification steps of DHDPS, while both the coupled assay and the imidazole buffer assay have been used quantitatively.[1-4]

This chapter gives a kinetic description of wild-type DHDPS, yielding kinetic constants similar to those reported by others, and describes a previously unreported regulatory behaviour of DHDPS with respect to lysine inhibition. There has been some debate as to whether the source of substrate inhibition by (*S*)-ASA, reported by Karsten[5] and others,[4] is an artefact of the ozonolysis procedure used to synthesise (*S*)-ASA. Coulter *et al.*[6] did not find substrate inhibition with respect to (*S*)-ASA, synthesised *via* another route. Presented here are results that unequivocally resolve this question.

3.2 Assay systems used to collect initial rate data for DHDPS.

3.2.1 The o-aminobenzaldehyde assay.

Yugari and Gilvarg[1] observed that others had used *o*-aminobenzaldehyde to detect Δ^1-pyrroline and Δ^1-piperidine derivatives and this was used as the basis for the *o*-aminobenzaldehyde assay that they devised. The structure of (4*S*)-4-hydroxy-2,3,4,5-tetrahydro-(2*S*)-dipicolinic acid, the product of the reaction catalysed by DHDPS, is thought to lend itself to the formation of dihydroquinazolium salts that produce a characteristic purple colour. Addition of *o*-aminobenzaldehyde to a solution containing DHDPS in the presence of its substrates pyruvate and (*S*)-ASA, results in a yellow solution that develops a characteristic deep purple colour, which is enhanced by acid treatment. Thus, the basis of the *o*-aminobenzaldehyde assay is the increase in absorbance at 540 nm due to this complex formation of the enzymatic reaction product with *o*-aminobenzaldehyde.[1]

Several problems with the assay limit its effectiveness for quantitative work. For example, the exact chemical nature of the chromophore, as yet, is not determined, although suggestions have been made (Figure 3.1).[6, 7]

Figure 3.1 *Possible reaction of dihydrodipicolinate with o-aminobenzaldehyde to form the purple chromophore.*[6]

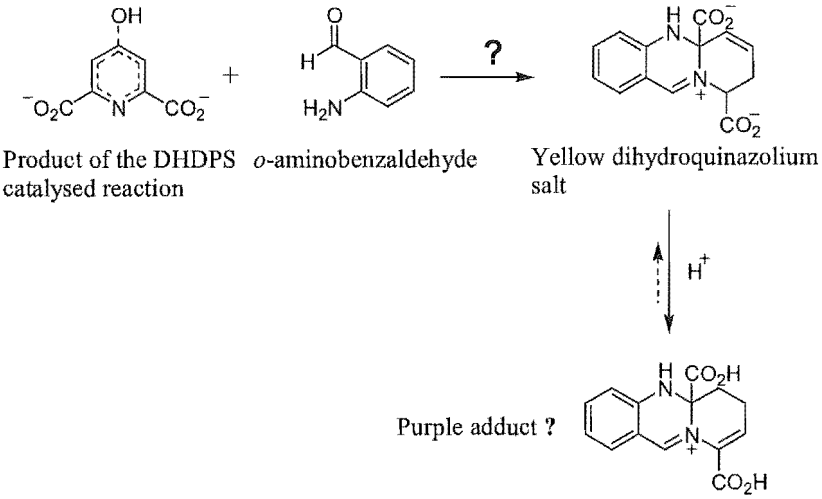

In order to use this assay to measure the initial rate of the enzyme-catalysed formation of the dihydrodipicolinate species, a key assumption is made, the rate of dihydrodipicolinate

formation, rather than the rate of complex formation, is rate limiting. Unfortunately, this assumption is not necessarily valid, given that a lag period of 10–20 minutes is observed before the absorbance at 540 nm increases. Nevertheless, it is an extremely useful qualitative tool and was the preferred method for monitoring DHDPS during the purification procedure, as it is both extremely substrate specific, and particularly sensitive in detecting low levels of DHDPS present in crude samples. The assay is also very simple to perform and can be scaled down to a 100 µl volume in a microtitre plate.

3.2.2 Imidazole buffer assay.

When DHDPS and its substrates, pyruvate and ASA, are placed in the presence of imidazole buffer, an absorption spectrum is obtained that has a peak at 270 nm and the rise in absorption at this wavelength is then monitored.[1] This assay is simple, but suffers similar problems to the *o*-aminobenzaldehyde assay system, in that the exact nature of the chromophore formed is unknown and that the reaction follows a lag phase before the absorbance at 270 nm increases. As such, this assay was unsuitable for generating detailed quantitative kinetic measurements, although it continues to be used by other workers,[3, 8, 9] since it is convenient and easy to perform.

3.2.3 The coupled assay.

A coupled assay is usually employed if the enzyme of interest is difficult to monitor, but the enzyme catalysing the transformation of the reaction product is relatively easy to monitor, for example, a change in UV absorption, such as the reduction or oxidation of a nicotinamide cofactor, or by a change in fluorescence.[10] Therefore, a coupled assay requires sufficient quantity of the second enzyme to ensure that the intermediate product reacts rapidly and does not accumulate. If the second enzyme is in excess, then the rate of the reaction will depend entirely on the rate of the first reaction. This is also the case for following the activity of the second enzyme: if the first enzyme is in excess, then the overall rate will now depend entirely on the rate of the second reaction.

The DHDPS-DHDPR coupled assay involves following the activity of DHDPS by monitoring the activity of the following enzyme DHDPR (Figure 3.2). DHDPR is an NADPH-dependent enzyme that reduces dihydrodipicolinate, presumed to form

non-enzymatically from (4*S*)-dihydroxy-2,3,4,5-tetrahydro-(2*S*)-dipicolinate (HTPA), the product of DHDPS. The oxidation of NADPH to $NADP^+$ by DHDPR is easily monitored:[1] NADPH has a strong absorbance at the range of 340 nm (extinction coefficient of 6220 M^{-1} cm^{-1}), while the oxidation product $NADP^+$ exhibits little absorbance at this wavelength and therefore, the rate of this reaction can be measured by the decrease in absorbance at 340 nm, which corresponds to the oxidation of NADPH (to $NADP^+$) by DHDPR. Hence such a coupled assay is extremely sensitive and convenient. The coupled assay is able to measure DHDPS kinetics if DHDPR was present in excess, since under these conditions the reaction catalysed by DHDPS becomes rate limiting.

Yugari and Gilvarg[1] originally devised the coupled assay, but after these initial reports the coupled assay was not widely used, perhaps due to a lack of availability of DHDPR. This situation has now changed, as new procedures have become available for obtaining sufficient quantities of both purified enzymes DHDPS and DHDPR.[5, 11, 12]

Figure 3.2 *The coupled assay utilising DHDPR.*

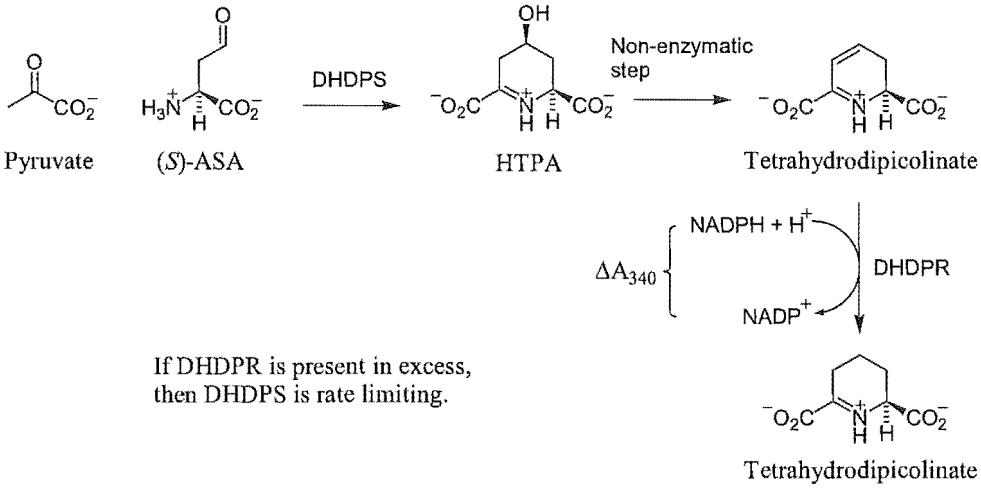

3.2.4 Modifications to the coupled assay.

The coupled assay was used to measure the kinetics of DHDPS and DHDPR, since plentiful supplies of purified DHDPS, DHDPR, and (*S*)-ASA were available. The assay was optimised to make it effective for the range of kinetic investigations under observation. The pH optimum for DHDPS is 8.4,[1] but it has been suggested that it is advantageous to run the assay at near physiological pH, to best mimic the true biological situation in the cell.[6] The original coupled assay measured DHDPS using Tris buffer at a near physiological pH of 7.4.[1]

However, due to the inadequate capacity of Tris to buffer at this pH, an alternative buffer was sought. At both pH 8.0 (close to the optimum pH for DHDPS[1]) and 7.2 (near physiological pH) the reaction proceeds in the forward direction. Pearce[13] showed that there was no significant difference between the kinetic parameters at pH 8.0 and 7.2 ($p(F)>0.10$). It was therefore decided to choose a buffer that had a buffering capacity around the optimum pH for DHDPS. HEPES buffer was chosen as it was found to buffer the assay adequately at pH 8.0 and consistent initial rates could be obtained; this allowed accurate K_m and k_{cat} values to be determined.

3.3 Steady state kinetics of *E. coli* DHDPS.

As outlined in Chapter one, a ping-pong kinetic mechanism has been proposed for DHDPS, based on the observation of initial velocity patterns that appear parallel.[3-5, 14] The ping-pong kinetic mechanism, also known as the substituted enzyme mechanism or the double displacement mechanism,[10] requires two stable enzyme forms with the presence of an irreversible step between the binding of the two substrates; this is typically release of the first product.[5]

Figure 3.3 *Schematic representation of the kinetic mechanism of* E. coli *DHDPS enzyme as proposed by Karsten.*[5] *The dead-end complex is generated when (S)-ASA binds the E enzyme form and blocks the binding of pyruvate (see section 3.4).*

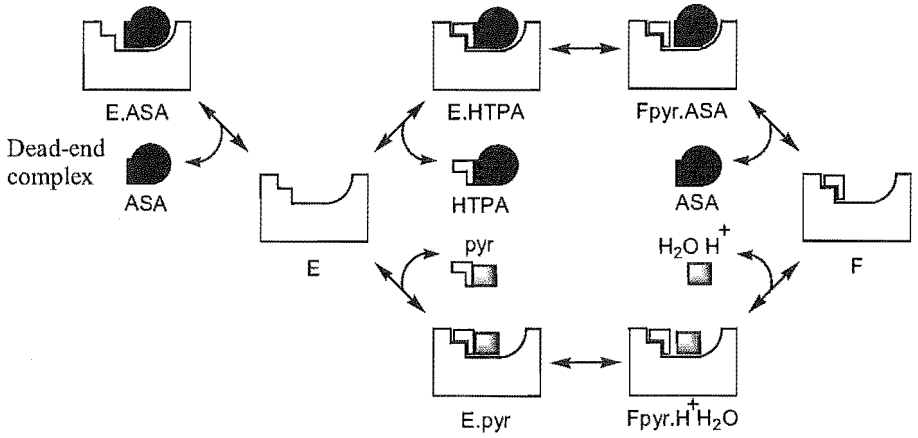

In this scheme, E refers to the unligated enzyme form, and F refers to the substituted (Schiff base) form. Pyr is pyruvate, ASA is aspartate β-semialdehyde, and HTPA is (4*S*)-hydroxy-2,3,4,5-tetrahydro-(2*S*)-dipicolinate.

In the case of DHDPS (Figure 1.4 and 3.3), this involves the binding of pyruvate to the free enzyme form (E), followed by the release of water, and enamine formation, which has been suggested to be irreversible.[5] (*S*)-ASA then binds to the stable substituted-enzyme form (F), followed by release of product and regeneration of the free enzyme form (E). Equation (**1**) is the steady state rate equation that describes the ping-pong mechanism and is shown below.

$$v = VAB / (K_{mB}A + K_{mA}B + AB) \qquad \text{Equation (1)}^{10}$$

Here V is the maximal velocity when both substrates are at saturating concentrations, K_{mA} and K_{mB} are the Michaelis-Menten constants for the two substrates, A and B are the substrate concentrations, and v is the initial velocity.[10]

Although these kinetic constants are analogous to those generated by a single substrate reaction, the K_m values in equation **1** cannot be reduced to K_s.[10] In this sense, analysis of the ping-pong mechanism, with respect to defining individual rate constants, is limited. Individual rate constants in the ping-pong model are defined as:

$$E + Pyr \underset{k_{-1}}{\overset{k_1}{\rightleftharpoons}} E.Pyr \xrightarrow{k_2} F + ASA \underset{k_{-3}}{\overset{k_3}{\rightleftharpoons}} F.ASA \xrightarrow{k_4} E + HTPA$$

However, because k_{cat}/K_{mA} and k_{cat}/K_{mB} do not share any rate constants for the individual steps in the reaction, the specificity constants for each substrate (k_{cat}/K_{mA} and k_{cat}/K_{mB}) are still informative.[10] A change in k_{cat}/K_{mA} must reflect a change in the first half reaction, and *vice versa* for k_{cat}/K_{mB} (k_{cat}/K_{mA} and k_{cat}/K_{mB} are defined in Equations **3** and **4** with respect to the scheme above).

$$k_{cat}/K_{mA} = k_1k_2 / k_{-1} + k_2 \qquad \text{Equation (3)}$$

$$k_{cat}/K_{mB} = k_3k_4 / k_{-3} + k_4 \qquad \text{Equation (4)}$$

Karsten[5] thoroughly investigated the kinetic mechanism of *E. coli* enzyme using initial velocity and dead-end inhibition kinetics.† He obtained parallel initial velocity patterns at pH 8 consistent with the ping-pong kinetic model, as had been previously shown by others.[3, 4, 14] He also reported that (*S*)-ASA displayed competitive substrate inhibition versus pyruvate, which is diagnostic for a ping-pong mechanism. Dead-end inhibition patterns obtained for the DHDPS reaction were also found to be consistent with a ping-pong mechanism.[5]

In order to determine the kinetic parameters of DHDPS, the initial rates with respect to varied (*S*)-ASA and pyruvate were measured using the coupled assay, where DHDPR was present in approximate 10-fold excess. Following Cornish-Bowden,[10] values of substrate ranged between 0.2 K_m and 10 K_m.[10] Thus, the concentration of (*S*)-ASA was varied between 0.04 and 1.5 mM, while the concentration of pyruvate was varied between 0.05 and 2.2 mM; these ranges were chosen from the K_m values determined by others. Initial rates were taken at least in duplicate and the results were analysed using the Enzfitter computer program (Biosoft, Cambridge) to determine the K_m and k_{cat} values using Equation **1**.

The Enzfitter program was also used to generate Lineweaver-Burk (1/Rate *vs.* 1/[Substrate]) and Eadie-Hofstee (Rate *vs.* Rate/[Substrate]) plots. The Lineweaver-Burk plot is good for initial analysis of kinetic data, and is by far the most widely used plot in enzyme kinetics. However, as the reaction rate decreases it often gives a misleading impression of experimental error. The Eadie-Hofstee plot is a more demanding treatment, since it enhances the effects of higher experimental error occurring at low reaction rates. This is due to the presence of rate (v) in both coordinates, and means that the errors affect both of them and cause deviations towards or away from the origin rather than parallel with the ordinate axis as with the Lineweaver-Burk plot. As a consequence, the Lineweaver-Burk plot tends to make good data look even better whereas the Eadie-Hofstee plot makes even good data look worse.[10] In any event, both plots were employed, but the Eadie-Hofstee plot was a better indicator of the quality of the data.

Included with the kinetic plots here, and in the following chapters, is a standardised residual plot, which was used to evaluate the quality of the data. The diagnostic value of a residual

† Dead-end inhibition is most useful for distinguishing between competing kinetic models because one can predict the inhibition pattern for both the ping-pong and tertiary-complex mechanisms.[10]

plot is discussed in detail by Cornish-Bowden.[10] The type of residual plot used here fits the percentage residual initial rate against the substrate concentration. This is most useful for finding trends in the data (often curved) that indicate whether an incorrect model has been fitted. It should also be noted that, when these residual plots are inspected, the points should be normally distributed around a mean of zero for the substrate concentration, but show less variation as the substrate concentration increases. This is because as the substrate concentration increases, and thus the reaction rate increases, a constant experimental error will lead to a reduced proportional error.[10]

The initial rate data obtained was fitted to a ping-pong Bi-Bi model using Enzfitter (Table 3.1). The data fitted the model well: there was a tight grouping of points about the lines of best fit for both the Lineweaver-Burk and Eadie-Hofstee plots, indicating that the data were of high quality and fitted the ping-pong equation. Enzfitter also generated the kinetic parameters for DHDPS—the K_{mPyr} was determined to be (0.23–0.29) mM (Figure 3.4) and the K_{mASA} was found to be (0.09–0.12) mM (Figure 3.5). The k_{cat} was found to be in a range of (117–131) s^{-1}.

Table 3.1 *Kinetic parameters for wild-type DHDPS.*

Parameter	Wild-type DHDPS[1]
k_{cat} (s^{-1})[2]	124 ± 6.8
K_{mPyr} (mM)	0.26 ± 0.03
K_{mASA} (mM)	0.11 ± 0.01
k_{cat}/K_{mPyr} (M^{-1} s^{-1})	$(4.8 \pm 0.6)\times10^{5}$
k_{cat}/K_{mASA} (M^{-1} s^{-1})	$(1.1 \pm 0.2)\times10^{6}$

[1] Protein concentrations were determined by the method of Bradford.[15]
[2] A statistical analysis for the fit to the ping-pong Bi-Bi model revealed $R^2 = 0.96$, and $p(F) < 0.01$.

These values are in reasonable agreement with those obtained from Karsten,[5] who reported a K_{mASA} of (0.07 ± 0.1) mM and a k_{cat} value of (188 ± 7) s^{-1}. Karsten's data were obtained under similar conditions to those used in the above assay.[5] Other values obtained in the literature using the coupled assay are also in good agreement, but it is important to note that data were fitted to a slightly different model (Michaelis-Menten model). Coulter[6] reports a K_{mASA} range of (0.1–0.14) mM at a pH of 7.2, Yugari and Gilvarg[1] found the K_{mASA} to be 0.13 mM at a pH of 7.4 while Pearce[13] reports a K_{mASA} range of (0.10–0.46) mM. All these values obtained by the coupled assay are notably lower than those obtained using the imidazole buffer assay. For example, Couper *et al.*,[8] reports the K_{mASA} to be 0.23 mM, while Laber *et al.*,[3] reports the K_{mASA} to be 0.55 mM. The difference in values obtained by the coupled assay and the imidazole buffer assay could be due to the shortcomings of the imidazole assay method; lags in the reaction time course and the uncharacterised reaction product do not allow the accurate acquisition of initial rate data.[5]

The K_{mPyr} value was also similar to those obtained from Karsten[5] who reports a K_{mPyr} of (0.17 ± 0.1) mM and to others using the coupled assay. Coulter[6] reports a K_{mPyr} in the range of (0.11–0.13) mM, while Yugari and Gilvarg[1] report a K_{mPyr} of 0.25 mM. K_{mPyr} values obtained using the imidazole buffer were once again higher than the values obtained in the coupled assay. For example, Laber *et al.*[3] report a K_{mPyr} of 0.57 mM. This difference between the coupled assay and the imidazole buffer assay further highlights the shortcomings of the imidazole assay.

Figure 3.4 *Kinetic plots of DHDPS with respect to pyruvate at different (S)-ASA concentrations.* ***A*** *is a direct plot,* ***B*** *is the Eadie-Hofstee plot,* ***C*** *is the Lineweaver-Burk plot, and* ***D*** *is a percentage residual plot of the data* ($100\times(v_{obs}-v_{cal})/v_{cal}$). *Enzfitter generated all plots after non-linear regression of the data against the ping-pong model. The* R^2 *0.96 and* $p(F)<0.01$.

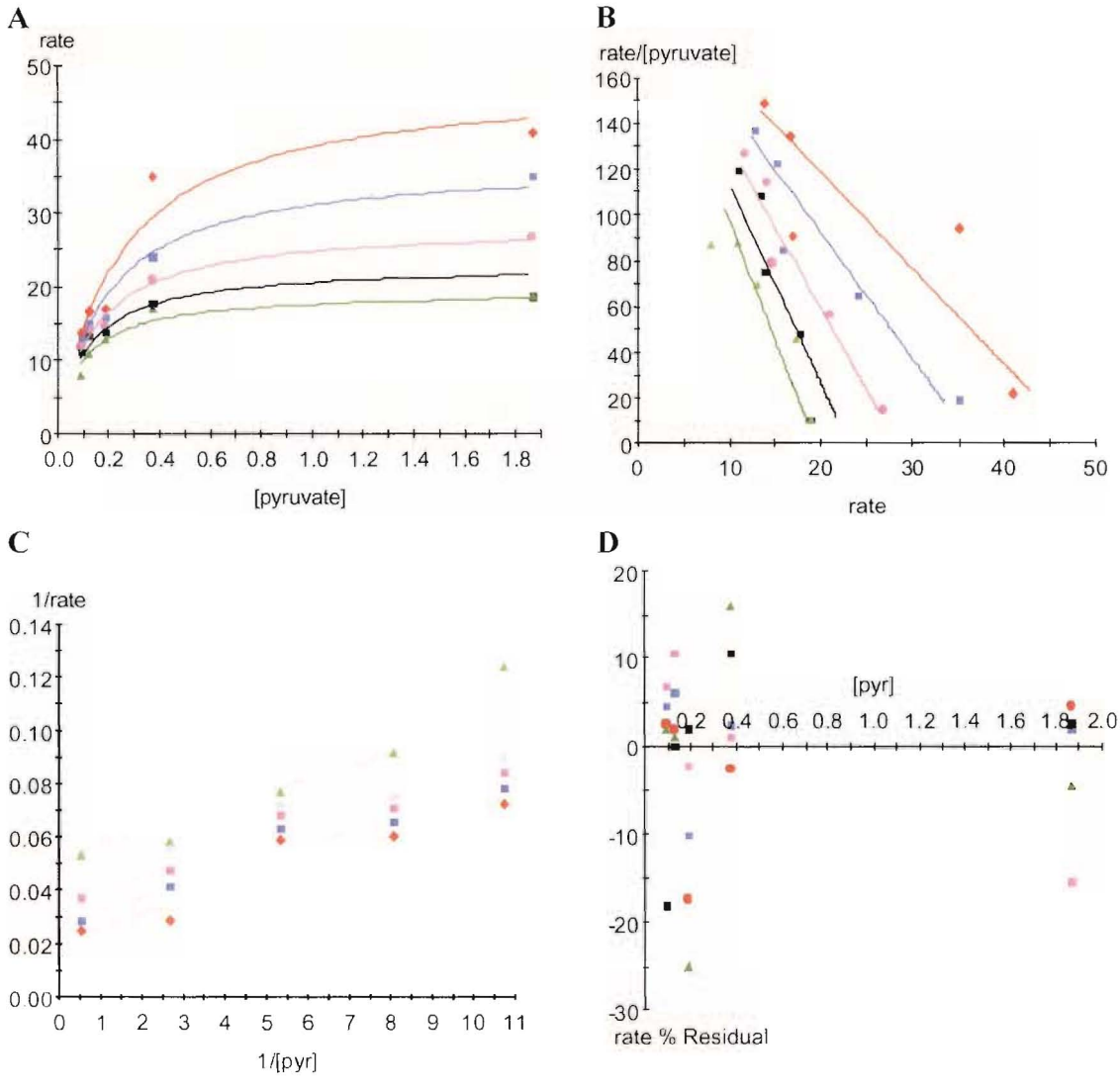

Figure 3.5 *Kinetic plots of DHDPS with respect to (S)-ASA at varying pyruvate concentrations.* ***A*** *is a direct plot,* ***B*** *is the Eadie-Hofstee plot,* ***C*** *is the Lineweaver-Burk plot, and* ***D*** *is a percentage residual plot of the data* ($100\times(v_{obs}-v_{cal})/v_{cal}$). *Enzfitter generated all plots after non-linear regression of the data against the ping-pong model. The* $R^2 = 0.96$ *and* $p(F)<0.01$.

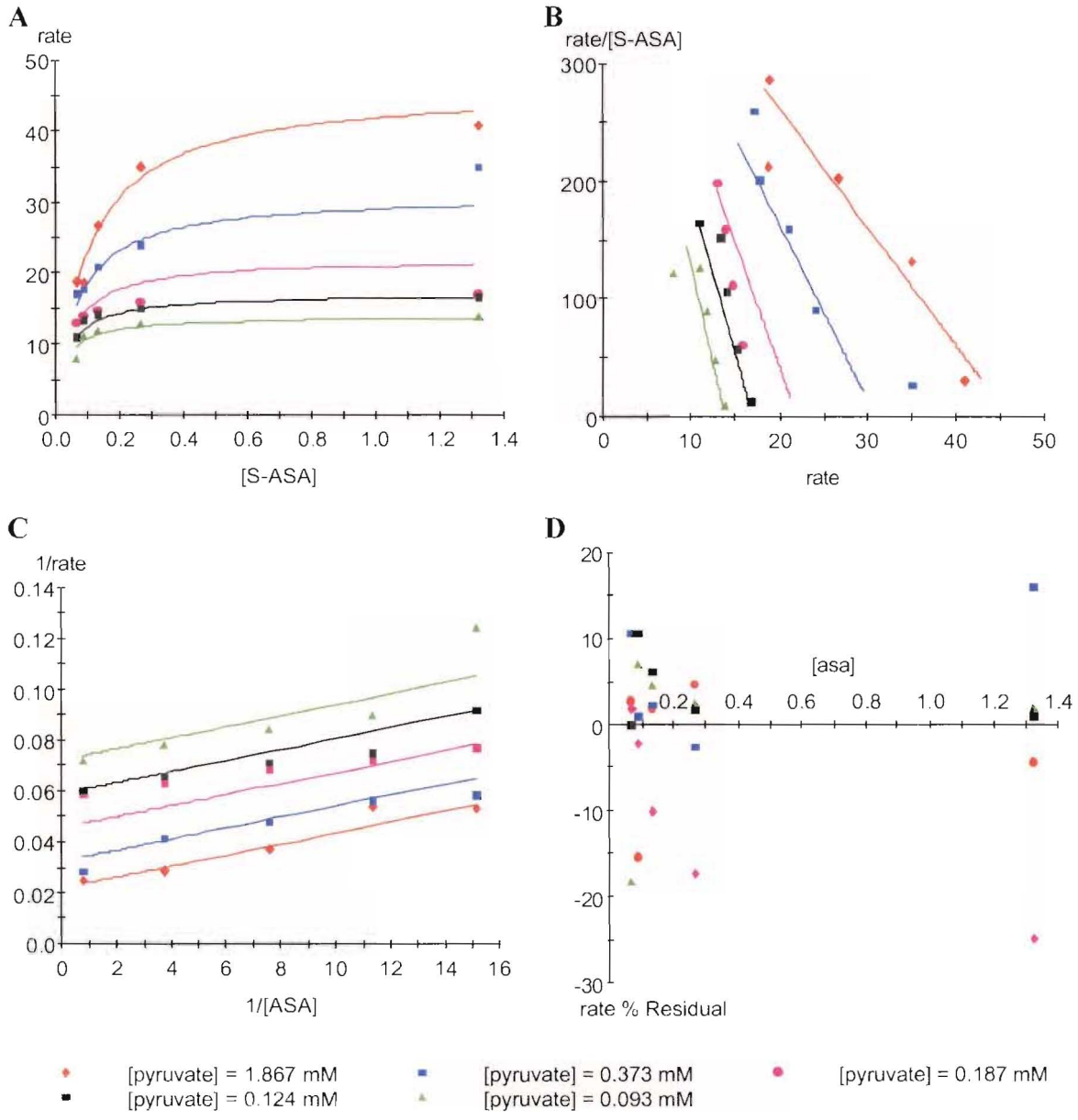

3.4 Is DHDPS inhibited by its substrate?

A number of conflicting reports have appeared in the literature concerning the K_m for each of the substrates, the nature of (*S*)-lysine inhibition, and the observation of substrate inhibition by (*S*)-ASA at high concentrations.

Stahly[16] first reported inhibition by (*S*)-ASA and suggested that it affected pyruvate binding, but not the maximal velocity. This was no surprise, because substrate inhibition is predicted by the ping-pong kinetic mechanism such that binding of (*S*)-ASA to the active site subsequently blocks access for pyruvate (Figure 3.3). Later studies have also reported (*S*)-ASA inhibition of DHDPS isolated from a variety of plant sources.[4, 17, 18] Given that different workers used different enzymes from different organisms, and different assays, it seemed that these discrepancies could arise from a variety of sources.

However, a recent report on the kinetics of the *E. coli* enzyme appears to show unambiguous substrate inhibition with respect to (*S*)-ASA.[5] This result contradicts the work in this laboratory where substrate inhibition has not been observed (Figure 3.5).[11, 19] In this work, and that of Coulter[11] and Karsten,[5] the *E. coli* enzyme and the coupled assay to DHDPR was employed. Thus, the difference in reported kinetic behaviour demanded a re-evaluation of the data. Karsten[5] synthesized (*S*)-ASA by ozonolysis, which is a complex reaction,[20] and we hypothesised that, given the quality of the (*S*)-ASA produced by the ozonolysis of allylglycine, substrate inhibition reported by Karsten[5] and others[4, 21] may be due to structural analogues in the (*S*)-ASA reaction mix that inhibit DHDPS.

The varying methods of (*S*)-ASA synthesis were discussed in detail in Chapter two. (*S*)-ASA is an elusive molecule, which for many years evaded rigorous chemical characterisation. Including that described in Chapter two, there are now four published syntheses of (*S*)-ASA that have been used for the analysis of DHDPS.[19, 22-24] The first and simplest (illustrated in Figure 2.4) involves the direct ozonolysis of allyl glycine, a product that is commercially available both as a pure enantiomer and in racemic form. In two separate experiments, we collected initial rate data for DHDPS, repeating the kinetic methods of Karsten using (*S*)-ASA prepared by the methods of Roberts *et al.*[19] and Black and Wright.[22]

3.4.1 Comparing the kinetics of DHDPS using alternate preparations of (S)-ASA.

The results of the experiment are presented in Table 3.2 and illustrated in Figure 3.6. There was a striking difference in the behaviour of DHDPS with respect to each preparation. At high (*S*)-ASA concentrations, DHDPS inhibition occurred when (*S*)-ASA prepared by ozonolysis was used, but not in the other preparation under identical conditions. Thus, inhibition is not caused by (*S*)-ASA itself. Our experiment, comparing alternative preparations of (*S*)-ASA, suggests that substrate inhibition is caused by an as yet unknown inhibitor and not by (*S*)-ASA, as concluded by Karsten.[5] It is clear that previous experiments documenting substrate inhibition[5] may result from artefacts associated with the ozonolysis preparation.

The data for (*S*)-ASA prepared by the methods of Coulter[11] or Roberts *et al.*[19] were fit to Equation **4**, which is the classical Michaelis-Menten equation that, in this instance, gives apparent values ($K_m^{(app)}$ and $V^{(app)}$) because the other substrate (pyruvate) is not at a saturating concentration. The data for (*S*)-ASA prepared by the methods of Black and Wright[11] were fit to Equation **5**[10]—the equation that describes substrate inhibition.[10]

$$v = V^{(app)}A / (K_m^{(app)} + A) \qquad \text{Equation (4)}$$

$$v = V^{(app)}A / (K_m^{(app)} + A + A^2 / K_i) \qquad \text{Equation (5)}$$

Table 3.2 *Kinetic constants for DHDPS using the alternate (S)-ASA preparations.*

ASA synthetic method.	$K_{mASA}^{(app)}$ (mM)	K_i (mM)	$V^{(app)}$ (μmol s^{-1} mg^{-1})
Black and Wright (Ozonolysis)	0.020 ± 0.007	1.1 ± 0.4	0.030 ± 0.003
Roberts *et al.* (Weinreb amide)	0.016 ± 0.002	–	0.027 ± 0.007

Kinetic constants were generated by the fit of data generated using alternative preparations of ASA. Data for ASA prepared *via* a Weinreb amide was fitted to equation (**4**). Data for ASA prepared by O_3 was fitted to equation (**5**). The R^2 values for the fits were 0.87 for the O_3 regression and 0.92 for Weinreb amide regression.

The apparent K_i for the inhibitor in the mix was (1.1 ± 0.4) mM, which is four times that reported by Karsten.[5] That inhibition was seen only at low pyruvate concentrations suggests the contaminant is competitive in nature with respect to pyruvate. Our experiment, comparing alternative preparations of (*S*)-ASA, supports the view that substrate inhibition observed by others is caused by an as yet unknown inhibitor and not by (*S*)-ASA, as

concluded by Karsten.[5] Clearly, the previous experiments documenting substrate inhibition may be artefactual.

Figure 3.6 *Kinetic plots illustrating the different behaviours of the two ASA preparations. **A** is a direct plot, **B** is the Eadie-Hofstee plot, **C** is the Lineweaver-Burk plot, and **D** is a percentage residual plot of the data ($100\times(v_{obs}-v_{cal})/v_{cal}$). Enzfitter generated all plots after non-linear regression of the data against the Equations **4** and **5**. ▲, data for ASA prepared by ozonolysis. —, Fit of the ozonolysis data using Equation **5**. ■, data for ASA prepared via the Weireb amide. , Fit of data using Equation **4**.*

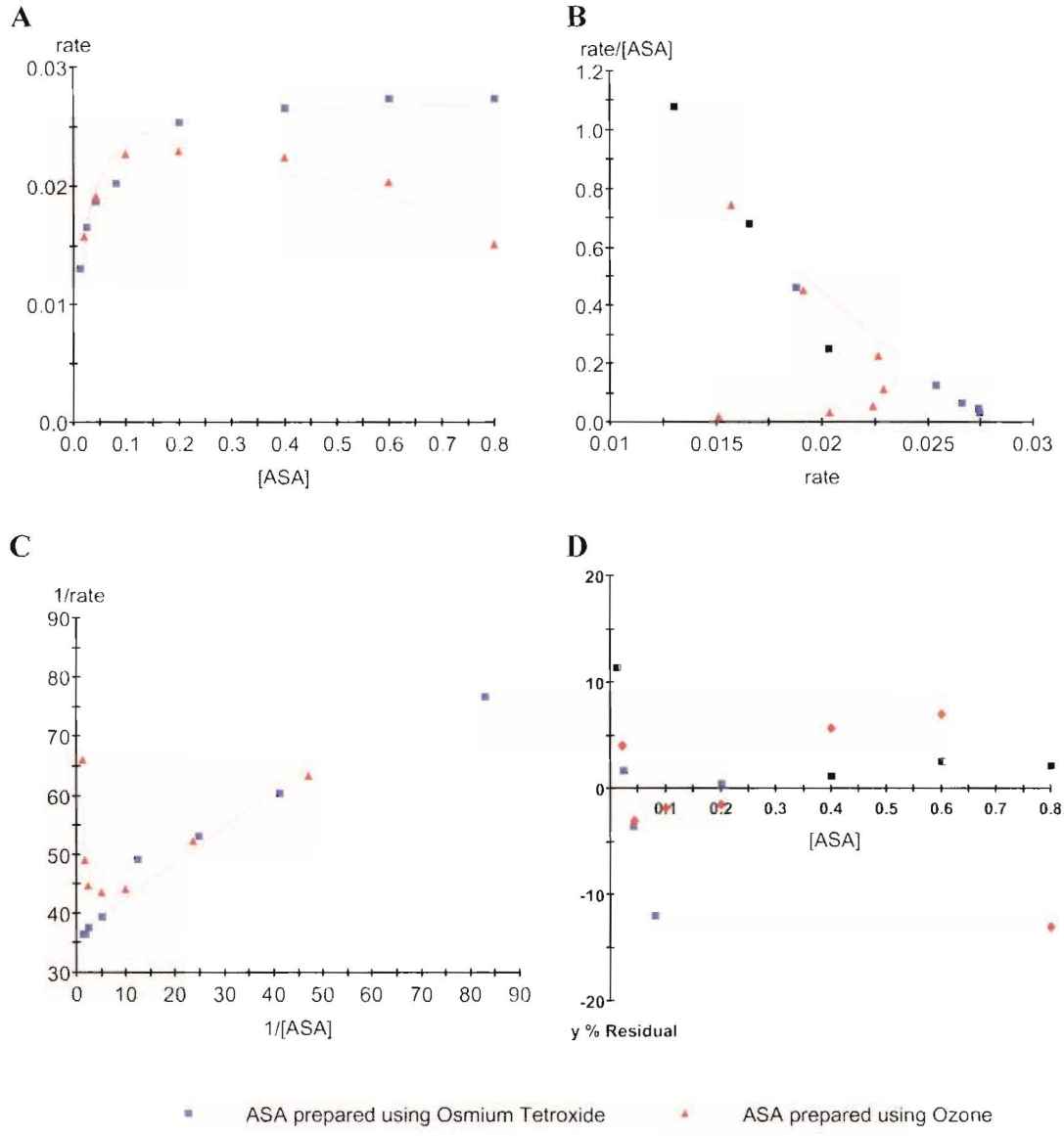

Although the kinetic model for a ping-pong mechanism predicts substrate inhibition when (*S*)-ASA is in high concentration relative to the pyruvate, its apparent absence does not preclude assignment of the ping-pong model. Kumpaisal *et al.*[4] originally assigned this kinetic mechanism based on initial velocity patterns that appear parallel and others also observed this result. The inhibition patterns of substrate and product analogues are also consistent with the ping-pong model.[5]

3.5 Feedback inhibition of lysine on *E. coli* DHDPS.

As described in Chapter one, DHDPS is a branch point enzyme in the synthesis of the aspartate family of amino acids. As the committed step in lysine biosynthesis, DHDPS is thought to be the key point in regulation of the pathway, because it undergoes allosteric feedback regulation by the pathway's end product, lysine. The precise mechanism by which lysine exerts regulatory control over DHDPS is unclear, although kinetic and structural studies support the proposal that lysine is an allosteric inhibitor.[1, 3, 9, 16, 25, 26]

DHDPS has been reported to show partial inhibition properties (approximately 80–90% inhibition) at high lysine concentrations.[3, 5] Karsten[5] has shown that Dixon plots (1/Rate *vs.* [Inhibitor]) asymptotically approach a finite initial rate, at saturating (*S*)-lysine concentrations, of about 10% that of the initial rate without (*S*)-lysine.

Initial rate data were collected at a range of inhibitor and substrate concentrations. Because there were three variables—(*S*)-lysine and two substrates—data was collected at varying concentrations of the inhibitor and one substrate, while the other substrate was keep at a sub-saturating level about its determined K_m, in accordance with Karsten.[5] Thus, only apparent K_m and V values could be determined. (*S*)-Lysine concentrations were varied between 0.1 and 5 mM. (*S*)-ASA concentrations ranged between 0.04 and 1.5 mM, and pyruvate concentrations ranged between 0.05 and 2.2 mM. The kinetic data were fitted to mathematical models using the Enzfitter computer program that simulated competitive, non-competitive, uncompetitive and mixed inhibition patterns to determine the best fit and inhibition constant K_i. Lineweaver-Burk and Eadie-Hoftsee plots were used to show the quality of the generated data.

Partial uncompetitive inhibition.

When an enzyme displays pure uncompetitive inhibition, the inhibitor binds only to the enzyme-substrate complex, affecting both the V and K_m values by decreasing them with increasing inhibitor concentrations.[10] Equation **6** is the steady-state expression that describes partial uncompetitive inhibition, illustrated in Figure 3.7.[27] Here the inhibitor constant $K_i = k_{-3}/k_3$, the apparent substrate binding constant $K_s = k_{-1}/k_1$, the maximal velocity in the absence of inhibitor $V = k[E]_T$, and the maximal velocity in the presence of a saturating inhibitor concentration $V' = k'[E]_T$. Thus, the ratio of V to V' reflects the degree of partial inhibition, which in Tables 3.4 and 3.5 is given the symbol α and expressed as a percentage. I represents the inhibitor concentration, and S the substrate concentration.

$$v = 1 / [1 / (V K_i + V' I)] [(I + K_i(1 + K_s / S)] \qquad \text{Equation } (\mathbf{6})^{27}$$

Figure 3.7 *Schematic representation of partial uncompetitive inhibition. E represents the enzyme, S the substrate, and I the inhibitor.*

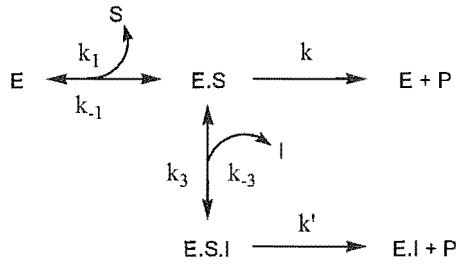

The inhibition of DHDPS by (*S*)-lysine with respect to pyruvate was determined to have partial uncompetitive inhibition and the K_i was found to be in a range of (0.19–0.25) mM (Table 3.4 and Figure 3.8). In addition, α was determined to be 7%, that is, the maximum rate of reaction at saturating (*S*)-lysine concentrations was 7% of that without (*S*)-lysine. Both results were in good agreement with Karsten[5] who reports uncompetitive inhibition with respect to pyruvate with a K_i value of (0.29 ± 0.04) mM.

Table 3.4 *The effect on wild-type DHDPS with varying lysine concentrations with respect to varying concentrations of pyruvate. (S)-ASA was held constant at 0.09 mM. The statistics for the fit to Equation* **6** *were* $R^2 = 0.98$ *and* $p(F) < 0.01$.

	Wild-type DHDPS
Inhibition Type	Uncompetitive
V^{app} (units mg^{-1})[1, 2]	43 ± 2
V'^{app} (units mg^{-1})	3 ± 0.7
α (%)[3]	7 ± 2
K_{mPyr}^{app} (mM)	0.33 ± 0.03
K_i (mM)	0.22 ± 0.03

[1] One unit is equal to 1 $\mu M_{NADPH}\, min^{-1}$.
[2] The protein concentration was determined using the method of Bradford.[15]
[3] α is defined as the ratio of V, the maximal velocity in the absence of inhibitor, and V', the maximal velocity at saturating inhibitor concentration.

Figure 3.8 *Kinetic plots of DHDPS with respect to pyruvate at different (S)-lysine concentrations.* ***A*** *is a direct plot,* ***B*** *is the Eadie-Hofstee plot,* ***C*** *is the Lineweaver-Burk plot, and* ***D*** *is a percentage residual plot of the data* $(100\times(v_{obs}-v_{cal})/v_{cal})$. *Enzfitter generated all plots after non-linear regression of the data against, partial uncompetitive inhibition, Equation* ***6***. *The* $R^2 = 0.98$ *and* $p(F)<0.01$.

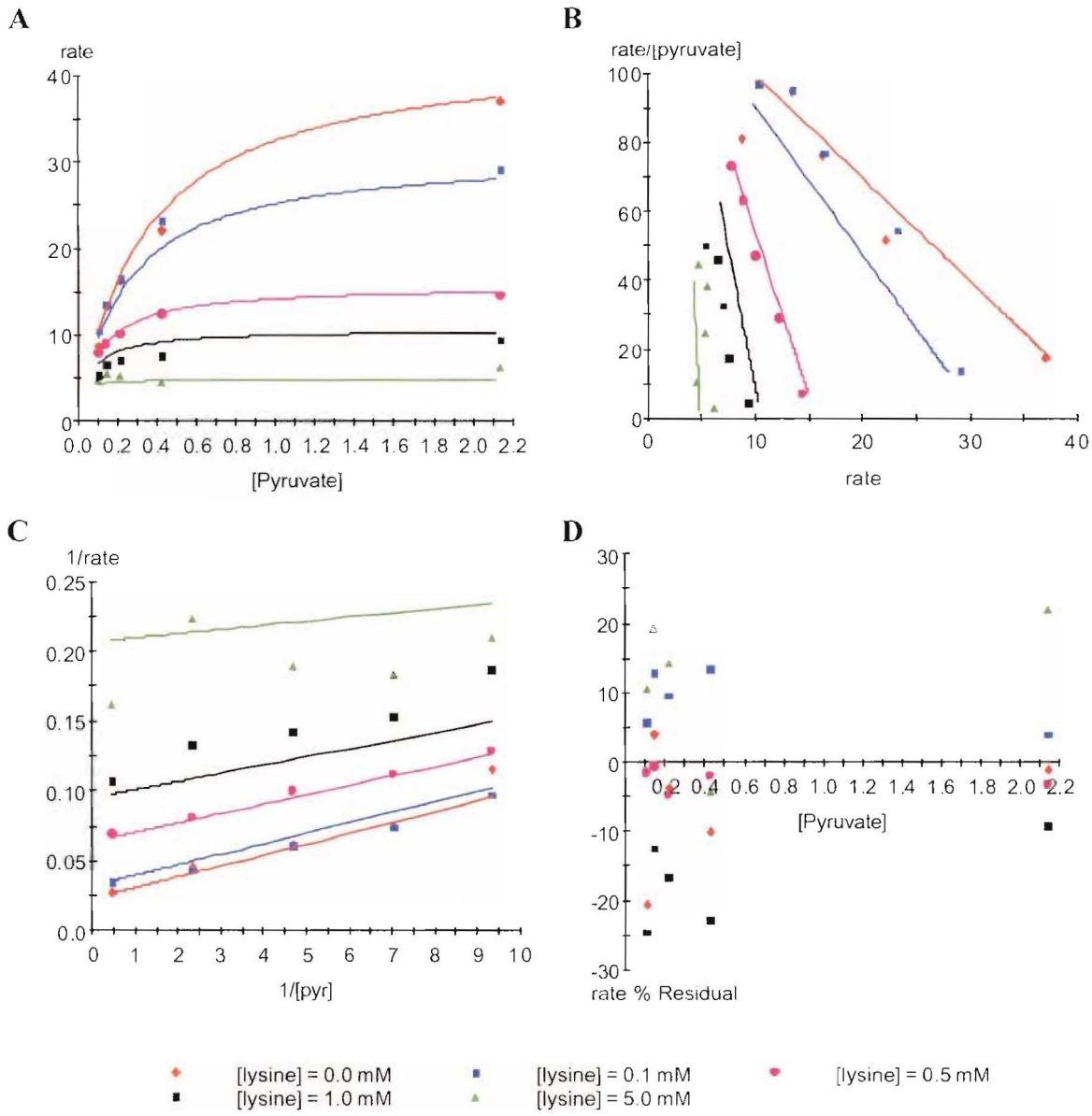

Partial non-competitive inhibition.

Pure non-competitive inhibition involves the inhibitor binding to a site on the enzyme away from the active site, altering catalysis but not substrate binding. As such, V is decreased and the K_m stays constant with increasing inhibitor concentration.[10] Partial non-competitive inhibition arises when either the inhibitor or the substrate bind to the enzyme independently, without affecting the binding of the other ligand. With respect to Figure 3.9, at saturating levels of inhibitor, E.S.I predominates, but the enzyme still functions, albeit at a decreased rate ($k > k'$). Equation **7** is the steady state-kinetic equation that describes partial non-competitive inhibition shown in Figure 3.9.[27] Here, the inhibitor constant $K_i = k_{-4}/k_4 = k_{-3}/k_3$, the apparent substrate binding constant $K_s = k_{-1}/k_1 = k_{-2}/k_2$, the maximal velocity in the absence of inhibitor $V = k[E]_T$, and the maximal velocity in the presence of a saturating inhibitor concentration $V' = k'[E]_T$. As discussed above, the ratio of V to V' reflects the degree of partial inhibition.

$$\upsilon = 1 / \{[(K_i + I)/(V' K_i + V I)][1+K_s / S]\} \qquad \text{Equation (7)}^{27}$$

Figure 3.9 *Schematic representation of non-competitive inhibition. E represents the enzyme, S the substrate, and I the inhibitor.*

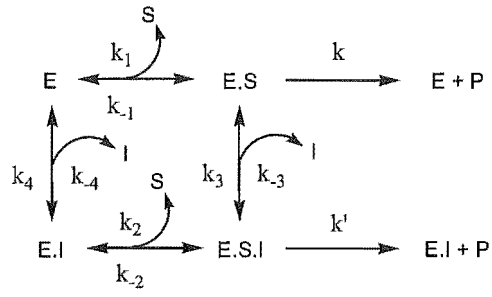

Inhibition of DHDPS by (*S*)-lysine with respect to (*S*)-ASA was shown to be consistent with partial non-competitive inhibition (Figure 3.10). The apparent K_i was found to be in a range of 0.28–0.38 mM and was determined to be 8%. Again these results were in good agreement with Karsten[5] who reports non-competitive inhibition with respect to (*S*)-ASA with a K_i value of (0.4 ± 0.01) mM.

Table 3.5 *The effect on wild-type DHDPS with varying lysine concentrations with respect to varying concentrations of pyruvate. The pyruvate concentration was held constant at 0.15 mM. The statistics for the fit were* $R^2 = 0.98$ *and* $p(F) < 0.01$.

	Wild-type DHDPS
Inhibition Type	Non-competitive
V^{app} (units mg^{-1})[1, 2]	30 ± 1
V'^{app} (units mg^{-1})	2.3 ± 0.9
α (%)[4]	8 ± 3
$K_{mPyr}{}^{app}$ (mM)	0.10 ± 0.01
K_i (mM)	0.33 ± 0.05

[1] One unit is equal to 1 μM_{NADPH} min^{-1}.
[2] The protein concentration was determined using the method of Bradford.[15]
[4] α is defined as the ratio of V, the maximal velocity in the absence of inhibitor, and V', the maximal velocity at saturating inhibitor concentration.

The molecular mechanism by which lysine exerts its regulatory effect on DHDPS is still a matter of controversy. Some results obtained for (*S*)-lysine inhibition, with respect to both (*S*)-ASA and pyruvate, agree with the inhibition properties determined above. Blickling *et al.*,[9] showed that lysine inhibits DHDPS uncompetitively with respect to pyruvate and non-competitively with respect to (*S*)-ASA. They also showed lysine inhibition to be cooperative. However, there has been some variation in the literature as to lysine inhibition models assigned to DHDPS with respect to each substrate. For example, Coulter[6] showed that *E. coli* DHDPS, with respect to both (*S*)-ASA and pyruvate, was of the uncompetitive type for (*S*)-lysine inhibition. Furthermore, (*S*)-Lysine was shown to be competitive with respect to (*S*)-ASA from wheat,[4] while maize DHDPS has been shown to be competitive with respect to pyruvate and mixed with respect to (*S*)-ASA.[28]

Figure 3.10 *Kinetic plots of DHDPS with respect to (S)-ASA at different (S)-lysine concentrations. Kinetic plots of DHDPS with respect to pyruvate at different (S)-ASA concentrations.* ***A*** *is a direct plot,* ***B*** *is the Eadie-Hofstee plot,* ***C*** *is the Lineweaver-Burk plot, and* ***D*** *is a percentage residual plot of the data* $(100\times(v_{obs}-v_{cal})/v_{cal})$. *Enzfitter generated all plots after non-linear regression of the data against Equation 7. The* $R^2 = 0.98$ *and* $p(F)<0.01$.

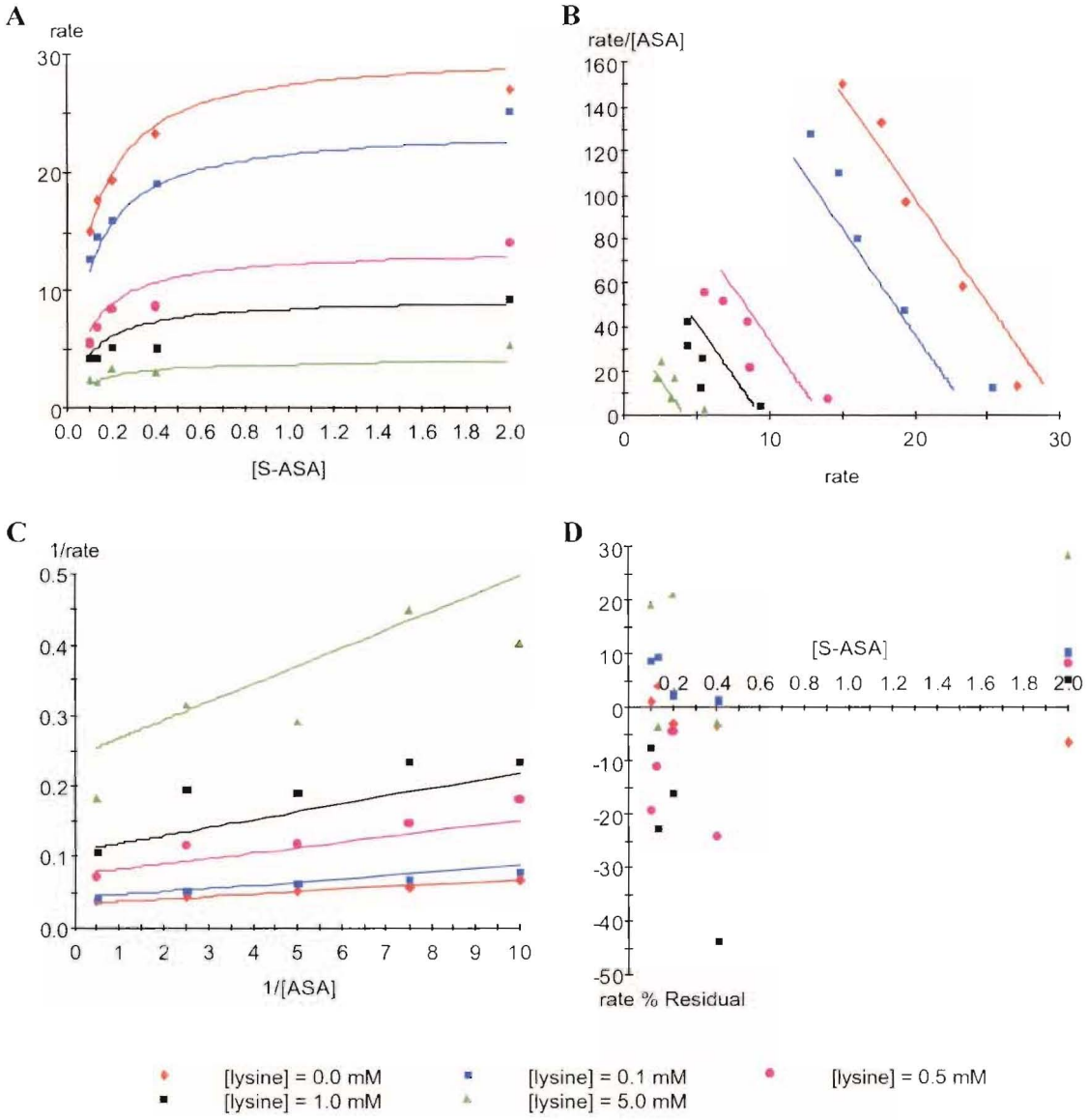

3.6 Summary

In this chapter, a preparation of pure DHDPS was kinetically characterised using the coupled assay. As reported by others, the kinetic mechanism was the ping-pong type. The parameters obtained are consistent with other literature values: DHDPS, at pH 8.0, had a K_m for (*S*)-ASA in the range of (0.07–0.08) mM, while for pyruvate, K_m was found in the range of (0.18–0.21) mM, and a k_{cat} of (118–131) s^{-1}.

There are various literature reports that suggest that high levels of (*S*)-ASA inhibit the enzyme, whilst others have not observed this phenomenon. It is shown unequivocally that this difference can be attributed to the different methods of preparing (*S*)-ASA used by each researcher. DHDPS is not inhibited by (*S*)-ASA; rather, the inhibition is due to an, as yet, unidentified inhibitor in preparations of the substrate generated by ozonolysis.

In addition, the inhibition patterns of DHDPS with respect to (*S*)-lysine were reassessed. With respect to pyruvate, DHDPS showed partial uncompetitive inhibition with a K_i in the range of (0.16–0.18) mM. With respect to (*S*)-ASA, DHDPS showed partial non-competitive inhibition with a K_i in the range of (0.25–0.38) mM. The pattern of lysine inhibition is consistent with the conclusion of Karsten that lysine can only bind the F enzyme form. The initial rate under saturating (*S*)-lysine conditions is estimated to be about 9% that of DHDPS in the absence of (*S*)-lysine.

3.7 References

1. Yugari, Y. & Gilvarg, C. (1965). The condensation step in diaminopimelate synthesis. *Journal of Biological Chemistry*, **240**, 4710-4716.

2. Shedlarski, J. G. & Gilvarg, C. (1970). The pyruvate-aspartic semialdehyde condensing enzyme of *Escherichia coli*. *Journal of Biological Chemistry*, **245**, 1362-1373.

3. Laber, B., Gomis-Ruth, F., Romao, M. & Huber, R. (1992). *Escherichia coli* dihydrodipicolinate synthase. Identification of the active site and crystallization. *Biochemical Journal*, **288**, 691-695.

4. Kumpaisal, R., Hashimoto, T. & Yamada, Y. (1987). Purification and characterization of dihydrodipicolinate synthase from wheat suspension cultures. *Plant Physiology*, **85**, 145-151.

5. Karsten, W. E. (1997). Dihydrodipicolinate synthase from *Escherichia coli*: pH dependent changes in the kinetic mechanism and kinetic mechanism of allosteric inhibition by L-lysine. *Biochemistry*,**36** , 1730-1739.

6. Coulter, C. V. (1997). Studies in lysine biosynthesis. PhD thesis, University of Canterbury.

7. Gerrard, J. A. (1992). Studies on dihydrodipicolinate synthase. D. Phil. thesis, Oxford University.

8. Couper, L., McKendrick, J. E. & Robins, D. J. (1994). Pyridine and piperidine derivatives as inhibitors of dihydrodipicolinic acid synthase, a key enzyme in the diaminopimelate pathway to L-lysine. *Bioorganic and Medicinal Chemistry Letters*, **4**, 2267-2272.

9. Blickling, S., Renner, C., Laber, B., Pohlenz, H., Holak, T. A. & Huber, R. (1997). Reaction mechanism of *Escherichia coli* dihydrodipicolinate synthase investigated by X-ray crystallography and NMR spectroscopy. *Biochemistry*, **36**, 24-33.

10. Cornish-Bowden, A. (1999). *Fundamentals of enzyme kinetics*. 2nd edit., Portland Press Ltd, London.

11. Coulter, C. V., Gerrard, J. A., Kraunsoe, J. A. E. & Pratt, A. J. (1999). *Escherichia coli* dihydrodipicolinate synthase and dihydrodipicolinate reductase: kinetic and inhibition studies of two putative herbicide targets. *Pesticide Science*, **55**, 887-895.

12. Paiva, A., Vanderwall, D., Blanchard, S., Kozarich, J., Williamson, J. & Kelly, T. (2001). Inhibitors of dihydrodipicolinate reductase, a key enzyme of the diaminopimelate pathway of *Mycobacterium tuberculosis*. *Biochimica et Biophysica Acta: Protein, Structure, and Molecular Enzymology*, **1545**, 67-77.

13. Pearce, F. G. (1999). Kinetic studies of dihydrodipicolinate synthase. B.Sc (Hons), University of Canterbury.

14. Dereppe, C., Bold, G., Ghisalba, O., Ebert, E. & Hans-Peter, S. (1992). Purification and characterization of dihydrodipicolinate synthase from pea. *Plant Physiology*, **98**, 813-821.

15. Bradford, M. (1976). A rapid and sensitive method for the quantitation of microgram quantities of protein utilizing the principle of protein-dye binding. *Analytical Biochemistry*, **72**, 248-254.

16. Stahly, D. (1969). Dihydrodipicolinate synthase of *Bacillus licheniformis*. *Biochimica et Biophysica Acta*, **191**, 439-451.

17. Mazelis, M., Whatley, F. & Whatley, J. (1997). The enzymology of lysine biosynthesis in higher plants. *FEBS Letters*, **84**, 236-240.

18. Wallsgrove, R. M. & Mazelis, M. (1981). Spinach leaf dihydrodipicolinate synthase: partial purification and characterization. *Biochemistry*, **20**, 2651-2655.

19. Roberts, S. J., Morris, J. C., Dobson, R. C. J. & Gerrard, J. A. (2003). The preparation of (*S*)-aspartate semi-aldehyde appropriate for use in biochemical studies. *Bioorganic and Medicinal Chemistry Letters*, **13**, 265-267.

20. March, J. (1992). *Advanced organic chemistry: reactions, mechanisms, and structure.* 4th edit., Wiley, New York.

21. Joerger, A. C., Mayer, S. & Fersht, A. (2003). Mimicking natural evolution *in vitro*: an *N*-acetylneuraminate lyase mutant with an increased dihydrodipicolinate synthase activity. *Proceedings of the National Academy of Sciences of the United States of America*, **100**, 5694-5699.

22. Black, S. & Wright, N. G. (1954). Aspartic β-semialdehyde dehydrogenase and aspartic β-semialdehyde. *Journal of Biological Chemistry*, **213**, 39-50.

23. Coulter, C. V., Gerrard, J. A., Kraunsoe, J. A. E. & Pratt, A. J. (1996). *(S)*-Aspartate semi-aldehyde: synthetic and structural studies. *Tetrahedron*, **52**, 7127-7136.

24. Tudor, D. W., Lewis, T. & Robins, D. J. (1993). Synthesis of the trifluoroacetate salt of aspartic acid β-semialdehyde, an intermediate in the biosynthesis of L-lysine, L-threonine, and L-methionine. *Synthesis*, **11**, 1061-1062.

25. Kumpaisal, R., Hashimoto, T. & Yamada, Y. (1989). Inactivation of wheat dihydrodipicolinate synthase by 3-bromopyruvate. *Agricultural and Biological Chemistry*,**53** , 355-359.

26. Blickling, S., Beisel, H., Bozic, D., Knablein, J., Laber, B. & Huber, R. (1998). Structure of dihydrodipicolinate synthase of *Nicotiana sylvestris* reveals novel quaternary structure. *Journal of Molecular Biology*, **274**, 608-621.

27. Keleti, T. (1986). *Basic enzyme kinetics*. 1st edit. Trans. Freidrich, P. & Kramer, M., Akademiai Kiado, Budapest.

28. Frisch, D. A., Gengenbach, B. G., Tommey, A. M., Sellner, J. M., Somers, D. A. & Myers, D. E. (1991). Isolation and characterization of dihydrodipicolinate synthase from maize. *Plant Physiology*, **96**, 444-452.

Chapter Four.

Investigating the mechanism of DHDPS using site-directed mutagenesis.

4.1 Introduction.

Site-directed mutagenesis is a powerful tool that has enabled the identification of residues important in enzyme catalysis and substrate binding.[1-3] The preceding chapters discussed the general procedures involved in purification and collection of initial rate data of wild-type DHDPS. This chapter focuses primarily on whether particular residues are necessary for catalysis as determined by the sensitivity of enzyme function following their mutation.

Mutants were designed to test the catalytic role of the putative active site residues, and to try to understand their role in the inhibition of DHDPS by lysine. To achieve this, residues were chosen that were considered important for both functions (Figure 4.1).[4] In particular, residues in the proposed catalytic triad (consisting of Y133, T44, and Y107) and the residue R138 were chosen: all are regarded as important for catalysis, either by directly assisting in the chemical mechanism or in the binding of substrate/s, and for lysine inhibition, as concluded by Blickling's.[4] The advent of site-specific mutagenesis has allowed us to test the role of these residues in a rational manner. The chosen mutations were structurally as conservative as possible in order to preserve the steric bulk of each residue and simultaneously disrupt the hydrogen-bonding network in the catalytic triad.

Y133 and Y107 were substituted with phenylalanine in order to disrupt the hydrogen-bonding network. For the same reason, T44 was changed to valine. For each of these mutations it was predicted that enzymatic function would be severely attenuated if the catalytic triad was necessary for enzyme function. In addition, T44 was exchanged for serine in order to examine the role of the methyl group of T44. To test whether R138 was involved in (*S*)-ASA binding, this residue was exchange for histidine.

The following sections detail the generation of the site-specific mutations, their expression and purification, and their kinetic characterisation in comparison with the wild-type presented in Chapter three.

Figure 4.1 *Proposed reaction mechanism of DHDPS.*[4] *See also Figure 1.6.*

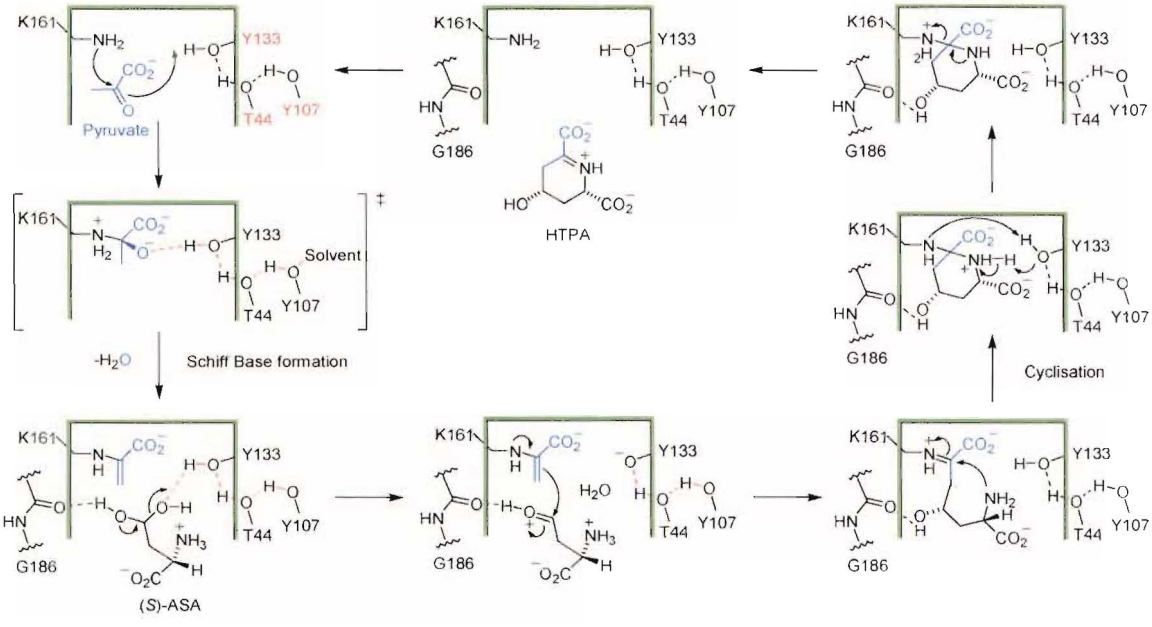

4.1.1 Site-directed mutagenesis.

PCR has made it possible to introduce deletion, insertion, and substitution mutations in a target DNA gene by simple and efficient procedures. The possible uses of mutagenesis are enormous, and the structure/function relationships of many proteins are currently being studied using these techniques. A novel method for mutagenesis has been described that uses a high fidelity thermostable DNA polymerase to generate copies of the plasmid by linear amplification, while incorporating the mutation of interest (deletion, base substitution or insertion). To introduce mutations in *dap*A, the Quikchange site-directed mutagenesis kit, based on the method of Kunkel,[5] was used.

Site-directed mutagenesis was accomplished in a number of steps, as summarised in Figure 4.2. The first step was the design of the primer that incorporated the desired codon change. Following this, the PCR reactions were set up. Conveniently, the Quikchange mutagenesis kit included controls that enabled the detection of various problems throughout the process. This was particularly useful in the PCR reaction where a control reaction (discussed below) allowed differentiation between problems in the reaction conditions and poor primer design. Following amplification, treatment with *Dpn*I endonuclease specifically degraded parental DNA since DNA isolated from most *E. coli* strains is dam-methylated and susceptible to *Dpn*I digestion, whereas the DNA from the PCR reaction is not. The remaining mutated DNA was then used to transform *E. coli*. The purported mutagenic efficiency for the entire process is greater than 80%.[6]

Figure 4.2 *Summary of the method used to introduce mutations into* dap*A*. *1, primers (red) were designed to incorporate the desired mutation. 2, During the PCR reaction, the primers anneal to the template DNA (black) and were amplified (red). 3. Following PCR, template DNA was digested by* Dpn*I resulting in nicked mutagenic DNA. 4, Transformation of* E. coli *XL-1 Blue repaired the nicks in the mutagenic plasmid.*

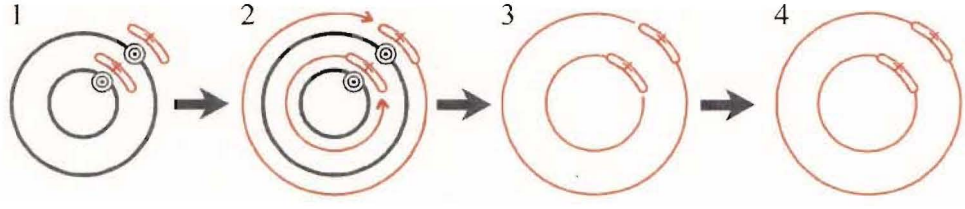

4.2 Results.

4.2.1 Introducing specific changes in dap*A*.

As described in Chapter two, the *E. coli* gene for DHDPS had previously been cloned into a pBluescript vector by Gerrard.[7] who had also determined the gene sequence. The primers were designed from this sequence information. Thus, the template plasmid was pJG001[8] and the primers used are shown in Table 4.1. Stratagene recommended that the primers meet the following conditions: they must contain the desired mutation and anneal to the

same sequence on opposite strands: contain a minimum GC content of 40%; should be 25–45 bases in length: have a melting temperature of 78°C or greater; have 10–15 bases each side of the mutation; terminate in one or more GC bases: and tertiary structures should be avoided.

Where possible, the primers had been designed such that successful mutation resulted in a new restriction site, allowing rapid confirmation of successful mutagenesis by inspection of the plasmid's restriction map, as discussed in Chapter seven.

Table 4.1 *Sequences of the primers used for site-directed mutagenesis. The exchanged nucleotides are shown in red and the codon is underlined. Italicised are the new restrictions for* Acy*1 and* Sca*1.* Ras*1 cuts the sequence GTAC in the wild-type but this is removed by the point mutation in pRD-R138H. Y107 and Y133 have no useful restriction changes.*

Primer name	Primer
Y133F#1	5'C CTG CCG CAA ATT CTG TTT AAT GTG CCG TCC CG3'
Y133F#2	5'CG GGA CGG CAC ATT AAA CAG AAT TTG CGG CAG G3'
T44V#1	5'CG ATC GTT TCT GTT *GGC GTC* ACT GGC GAG TCC GC3'
T44V#2	5'GC GGA CTC GCC AGT *GAC GCC* AAC AGA AAC GAT CG3'
T44S#1	5'CG ATC GTT TCT GTT GGC *AGT ACT* GGC GAG TCC GC3'
T44S#2	5'GC GGA CTC GCC *AGT ACT* GCC AAC AGA AAC GAT CG3'
Y107F#1	5'GC CTG ACG GTA ACC CCT TAC TTT AAT CGT CCG TCC C3'
Y107F#2	5'G GGA CGG ACG ATT AAA GTA AGG GGT TAC CGT CAG GC3'
R138H#1	5'CTG TAT AAT GTG CCG TCC CAT ACT GGC TGC GAT C3'
R138H#2	5'G ATC GCA GCC AGT ATG GGA CGG CAC ATT ATA CAG3'

Reactions were set up using a constant primer concentration with several template DNA concentrations to optimise for amplification. Initially, the amplification reactions failed, which after trials, was attributed to a high elongation temperature. Lowering this to 50°C presumably stabilised the template/primer binding step and resulted in amplification, which could be shown using gel electrophoresis (Figure 4.3). At this point the amplified reaction was subject to *Dpn*1 endonuclease digestion (incubation at 37°C for 2 hours) followed by transformation of *Epicurean coli* XL-1 Blue competent cells using the heat shock method.

To monitor problems in the transformation step, controls were also set up. These were the transformation of competent cells by pUC18 to test the viability of the competent cell, and the addition of water instead of DNA to ensure the antibiotic selection was effective. The transformation reactions were spread on X-gal/IPTG plates. The efficiency of transformation with pUC18 was high. Twenty potential mutants from each reaction were selected, restreaked, and stored as glycerol freezes at –80°C.

In order to diagnose potential problems in the PCR step, a control reaction was provided and run in parallel with the *dap*A mutagenesis reactions. This entailed mutation of pWhitescript, which has a point mutation in the β-galactosidase gene. If the PCR were successful, a stop codon at position nine in the amino acid sequence would be replaced for a glutamine codon. After transformation, growth of *E. coli* harbouring the mutated pWhitescript on X-gal/IPTG plates would produce blue colonies if the mutation reaction was successful. This is because a functional β-galactosidase gene would be expressed. The efficiency of the mutation process could be calculated by the proportion of blue/white colonies grown after transformation of *E. coli* XL-1 Blue. It was found that after PCR mutagenesis and transformation, 93% of the colonies with pWhitescript were blue, suggesting a similar proportion of colonies from the *dap*A reactions should also hold the desired nucleotide change. This meant that the potential mutants in *dap*A required screening to ensure the presence of the mutation. This was accomplished by restriction mapping and sequencing of the mutated *dap*A inserts.

Figure 4.3 *Agarose gel showing amplification of the plasmid DNA. Lanes 1 and 8 show a standard ladder with their size indicated at the left of lane 1 (Kb). Lanes 2–5 show amplification of pJG001 with primers incorporating the mutations T44V, T44S, Y107F, and Y133F respectively. Lanes 2–5 show a strong band at approximately 4.1 Kb—the same size as the template, pJG001. Lane 6 is the control reaction and confirms amplification (~4.5 Kb) of the pWhitescript plasmid as outlined in the experimental chapter. An equivalent volume of non-amplified pJG001 template DNA was added to lane 7.*

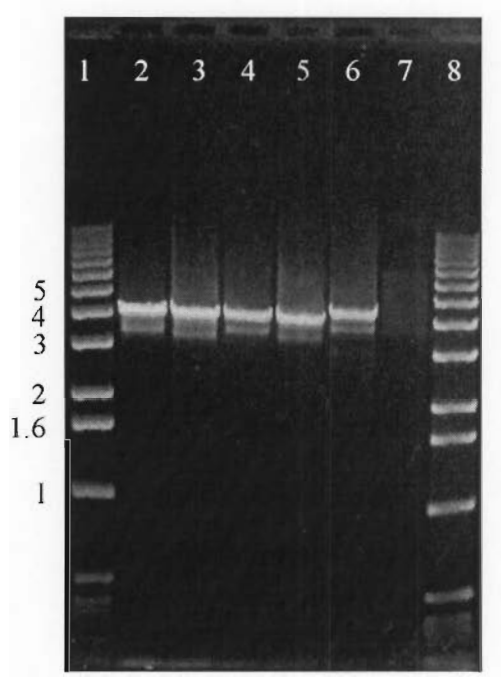

Figure 4.4 shows the restriction pattern of the plasmids pRD-T44V, pRD-T44S, and pRD-R138H when digested with diagnostic restriction enzymes to confirm the mutation. Examination of lanes 3 and 4 of Figure 4.4 **A**, illustrates the difference between pRD-T44V and pJG001 when cut by the restriction enzyme *Acy*I. Whereas pRD-T44V was cut twice, resulting in two linear bands, pJG001 was cut only once. The extra cutting site for *Acy*I confirmed the mutation is present in pRD-T44V. Comparing lanes 7 and 8 showed that the extra cutting site was situated in the *dap*A insert—the insert (1100 bp band shown in lane 5) was cut into two bands of 750 bp and 350 bp. The same analysis can be applied to pRD-T44S; *Sca*I cuts pRD-T44S twice (Figure 4.4 **B**: lane 2) but pJG001 only once (Figure 4.4 **B**: lane 3). In the case of pRD-R138H, the loss of a restriction site for *Rsa*I confirmed

the presence of the mutation. It can be seen in Figure 4.4 **C** that when pRD-R138H was cut with *Rsa*1, two bands, one at 300 bp and another at 1.7 Kb, were lost and a larger band at 2 Kb was gained (Figure 4.4 **C**: lane 2) compared with pJG001 (Figure 4.4 **C**: lane 3). However, not all of the designed mutations afforded a convenient new restriction site; the mutations Y107F and Y133F were confirmed by sequencing, along with the other mutations, using the T_7 and T_3 priming sites.

Figure 4.4 *Checking for the presence of the mutations by an altered restriction pattern. **A**, pRD-T44V. **B**, pRD-T44S. **C**, pRD-R138H.*

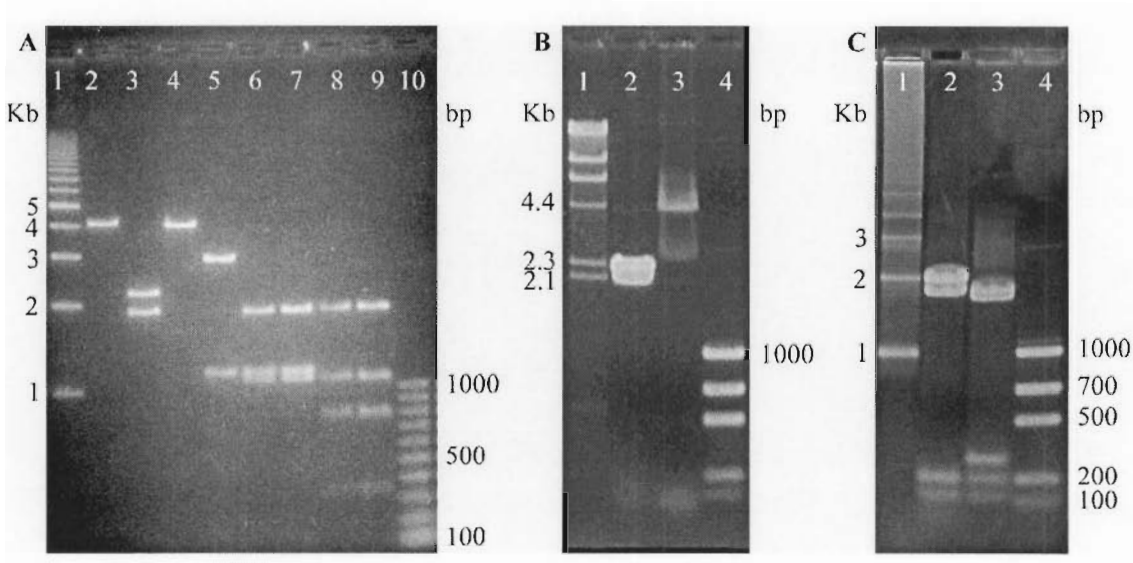

A: 1 Kb marker; 2, pRD-T44V/*Xho*I; 3, pRD-T44V/*Acy*I; 4, pJG001/*Acy*I; 5, pRD-T44V/*Xho*I/*Bam*HI; 6-7, pJG001/*Acy*I/*Xho*I/*Bam*HI; 8–9, pRD-T44V/*Acy*I/*Xho*I/*Bam*HI
B: 1, Lambda *Hin*dIII; 2, pRD-T44S/*Sca*I; 3, pJG001/*Sca*I; 4, 100 bp marker.
C: 1, 1 Kb marker; 2, pRD-R138H/*Rsa*I; 3, pJG001/*Rsa*I; 4, 100 bp marker.

4.2.2 Sequencing.

To confirm that the desired change had been made in *dap*A, and that the integrity of *dap*A was intact after mutagenesis, all the mutant plasmids were sequenced. Sequencing was performed by the Auckland Genomics Unit or the Waikato DNA Sequencing Facility using plasmid DNA prepared by methods, detailed in Chapter seven, which provided the very clean plasmid DNA required for long sequence reads. Typically, 800–1000 bp reads were achieved. It can be seen in Figure 4.5 that each sequence showed the predicted change in the electropherogram.

Figure 4.5 *Electropherograms comparing the sequences of wild-type DHDPS and its mutants. The wild-type sequences are: T44, Y107, Y133, and R138.*

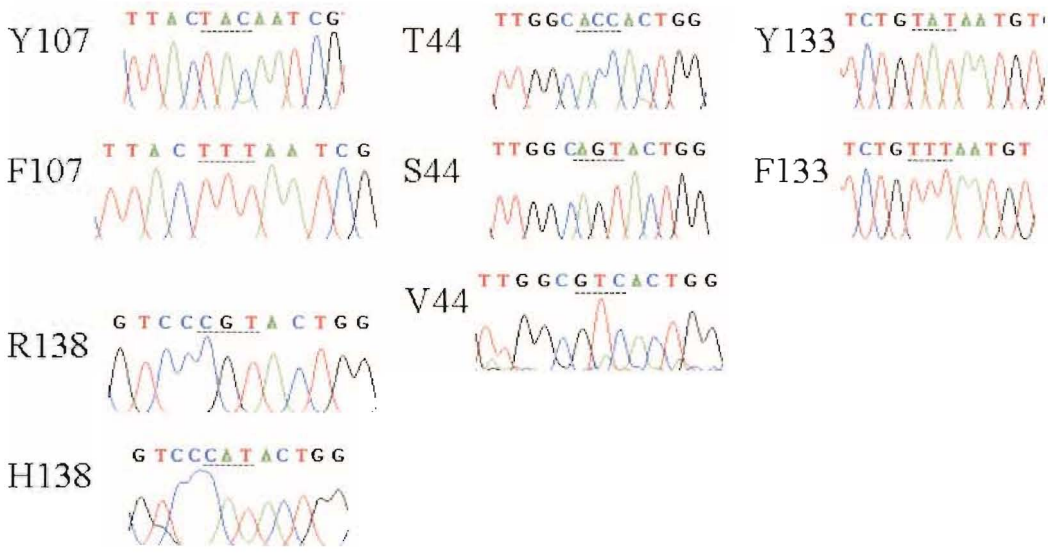

4.2.3 Over-expression and purification.

In order to kinetically characterise a mutant enzyme it is necessary to show that the wild-type enzyme, derived from the host chromosome, is not present, since its activity would also be detected in a biochemical assay. To this end, a strain of *E. coli* with a non-functional DHDPS gene (*dap*A$^-$) was acquired. This strain was known as *E. coli* AT997.[9, 10*] and had previously been used for the expression of various forms of plant DHDPS enzymes, including DHDPS mutants from the *A. thaliana*.[11]

---

* *E. coli* AT997 had been generated in experiments designed to elucidate the operon structure of the DAP and lysine biosynthetic pathways.[10] It had been proposed that the genes for lysine biosynthesis were organised in an operon structure like those for aromatic amino acid synthesis. Instead, the genes were found throughout the *E. coli* chromosome.[10] AT997 was originally characterised as a strain carrying mutations in the *dap*C gene, but was re-described as *dap*A$^-$ when it was shown that the *dap*A gene, if in trans, restored the ability AT997 to grow on media lacking DAP.[9]

AT997 was initially grown on LB supplemented with DAP and then prepared for –80°C storage. All cultures of *E. coli* AT997 were grown with controls that lacked DAP to test for contamination or *dap*A$^-$ reversion. AT997 would not grow on LB (or minimal media) unless DAP was present, or the strain was complemented with a plasmid-borne DHDPS gene. In order to further test the absence of any functional DHDPS, the cell lysate from AT997 was confirmed to exhibit no DHDPS activity as judged by both the coupled assay and the sensitive *o*-aminobenzaldehyde assay developed by Yugari and Gilvarg.[12] The cell lysate of *E. coli* XL-1 Blue, which holds a chromosomal copy of *dap*A, was used as a control—it showed a positive reaction for DHDPS activity.

As an added precaution, the creation of a *rec*A$^-$ strain of AT997 was undertaken to prevent homologous recombination between a plasmid-borne *dap*A mutant gene and the *E. coli* genome. Such an event could contaminate mutant lysates with wild-type enzyme. AT997 was rendered *rec*A$^-$ using P1 transduction[13] to replace the chromosomal *rec*A gene with a non-functional version containing an inserted tetracycline marker for convenient screening. The *rec*A$^-$ phenotype was confirmed by growth of AT997 on media with the DNA-alkylating agent MMS (0.125 mM) or a brief dose of UV irradiation immediately after spreading, conditions that differentiate between *rec*A$^-$ and *rec*A$^+$ strains;[14] bacteria that are *rec*A$^-$ fail to grow when exposed to these conditions (Figure 4.6). The new strain was renamed AT997r$^-$ and was grown and maintained on LB (or minimal media) in the presence of tetracycline only if the media was supplemented with DAP, allowing easy selection and confirmation of the *dap*A$^-$ phenotype.

Figure 4.6 *Following transduction, colonies were selected by growth on tetracycline and fifteen of these were stored at –80°C. They were then tested for recA and dapA function, as shown below. Each plate has five potential transductants and an isogenic* recA^+ *control,* E. coli *AT997. Plates 1 and 2 show that none could grow unless DAP was added while plates 3 and 4 show that none, apart from the* recA^+ *control, grew when exposed to UV irradiation or MMS.*

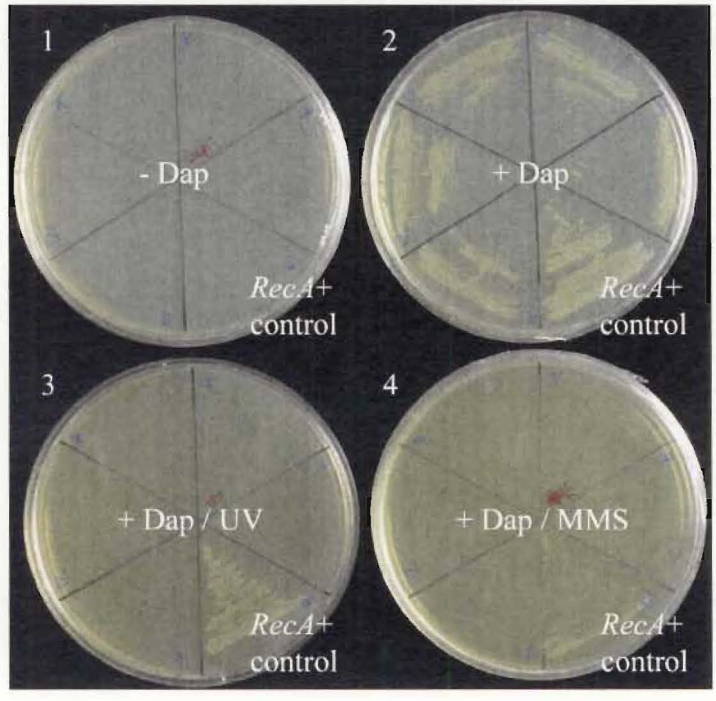

4.2.4 Transforming E. coli *AT997r⁻ with DHDPS mutant plasmids.*

After transforming AT997r⁻ with the generated mutant plasmids, the transformants were grown in the absence of DAP to assess their ability to complement the *dap*A⁻ phenotype, repeating the complementation experiment of Yeh *et al.*[9] The wild-type plasmid, pJG001, (control) and each mutant plasmid rescued AT997r⁻ when grown on LB agar media (Figure 4.7), suggesting that all mutant enzymes retained some DHDPS activity. A control transformation containing *E. coli* AT997r competent cells without DNA failed to grow on the same media (not shown).

Figure 4.7 *The designed mutations in DHDPS all complement the* dap*A strain AT997r . Bacteria were grown on LB agar media with and without DAP.*

4.2.5 Purification.

Transformation of AT997r⁻ by the mutated DHDPS plasmids provided a convenient source of mutated DHDPS without the risk of contamination by the wild-type enzyme. Following overnight incubation, *E. coli* cells, harbouring the mutated *dap*A plasmids, were harvested by centrifugation and washed with buffer. As with the wild type, the cells were lysed by sonication and the cell lysates showed sufficient activity that their presence could be detected using the *o*-aminobenzaldehyde assay, which facilitated further purification. There was some concern that the heat-shock step may not be feasible as the mutants could have been more sensitive to denaturation by heat treatment. Careful testing, however, showed that the mutants were stable at 70°C for two minutes. This suggested a similar thermostability to the wild-type in each case. As shown in Table 4.2, the heat-shock step

gave satisfactory results and typically removed over two thirds of the soluble protein in the crude lysates, with little loss in DHDPS activity. Interestingly, the heat-shock step sometimes resulted in an increase in total activity. This is likely due to the removal of inhibitors of DHDPS or other enzymes in the crude lysates that compete for the substrates of DHDPS in the assay.

Following heat-shock, ion-exchange (Q-Sepharose) and hydrophobic interaction chromatography (Phenyl-Sepharose) were successfully employed to purify the mutants to homogeneity. All of the mutant forms showed identical behaviour to that of the wild-type during these steps. Following the final step, the samples were dialysed overnight against buffer and the stored at –20°C. When analysed by SDS-PAGE, each enzyme showed a single band corresponding to the expected monomeric mass of approximately 31.2 kDa (Figure 4.8).

4.2.6 Mass spectrometry.

The mass of proteins can be accurately determined using modern mass spectrometry techniques. For investigating the mass of DHDPS and its mutants, liquid chromatography was used to purify the proteins prior to examination by electrospray mass spectrometry. This work was performed either by Jackie Healy (School of Biological Sciences, UC) or Bruce Clark (Department of Chemistry, UC). DHDPS was found typically to elute after 13 minutes in an acetonitrile/H_2O gradient run for 25 minutes on a C5 purification column. The purified protein was then injected into the mass spectrometer.

Table 4.2 *The purification of DHDPS mutants.*

	Protein[a] (mg)	Total activity[b] (units)	Specific activity (units mg^{-1})	Yield total (%)	Degree of purification (fold)
DHDPS-Y107F					
Crude	1182	18.2	0.015		
Heat shock	343	26.2	0.076	144	5.0
Q-Sepharose	180	33.4	0.186	184	12.1
Phenyl-Sepharose	78	21.1	0.272	116	17.6
DHDPS-T44V					
Crude	2114	0.37	0.00031		
Heat shock	342	0.35	0.00102	94	3.3
Q-Sepharose	126	0.33	0.00263	90	8.6
Phenyl-Sepharose	54	0.18	0.00336	24	15.8
DHDPS-T44S					
Crude	1259	24.3	0.019		
Heat shock	393	23.1	0.059	95	3.0
Q-Sepharose	143	19.7	0.13	78	6.9
Phenyl-Sepharose	87	15.7	0.18	65	9.4
Q-Sepharose	47	13.7	0.29	56	15.1
DHDPS-Y133F					
Crude	1355	0.6	0.00044		
Heat shock	385	0.43	0.0011	71	2.5
Ion-exchange	98	0.46	0.0047	77	10.7
Q-Sepharose	49	0.39	0.0079	65	18.0
DHDPS-R138H					
Crude	1943	0.016	0.000006		
Heat shock	593	0.046	0.000078	100	12.1
Q-Sepharose	376	0.048	0.00127	103	19.6
Phenyl-Sepharose	251	0.032	0.00129	70	19.9
Q-Sepharose	179	0.027	0.00152	59	23.4

[a] Protein concentrations were determined using the Bradford assay.[15]
[b] One unit of enzyme activity is equal to the consumption of 1 μmol_{NADPH} s^{-1}

Figure 4.8 *SDS-PAGE following the purification of the DHDPS mutant proteins.*

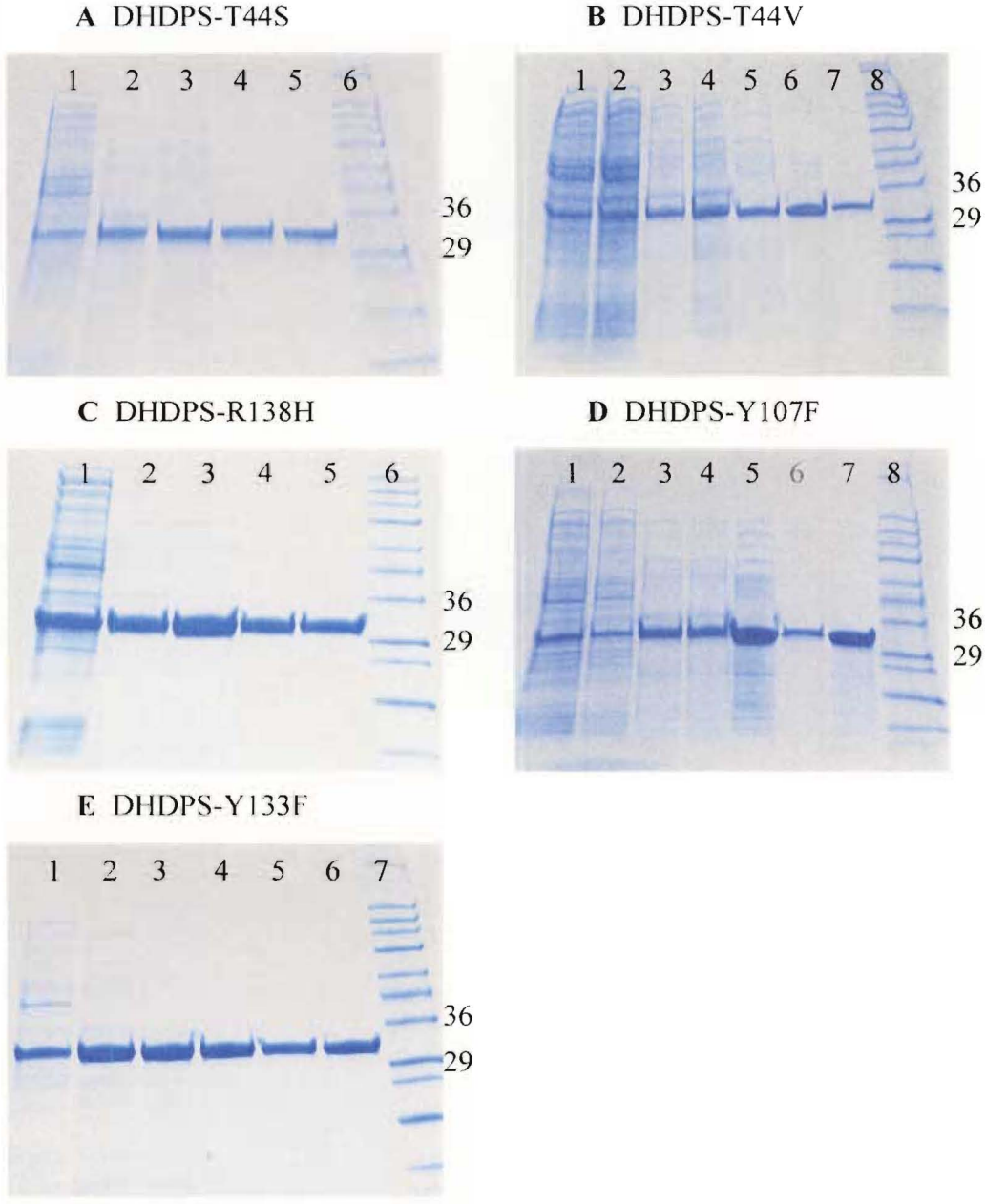

A **DHDPS-T44S** 1, crude cell extract; 2, heat-shock; 3, Q-Sepharose ion exchange; 4, Phenyl-Sepharose; 5, second Q-Sepharose ion exchange; 6, Sigmamarker, wide molecular weight range of the bands (from top) 205, 116, 97, 84, 66, 55, 45, **36**, **29**, 24, 20, 10.2 and 6.5 kDa.

B **DHDPS-T44V** 1 & 2, crude cell extract; 3 & 4, heat-shock; 5, Q-Sepharose ion exchange; 6, dialysis; 7, Phenyl-Sepharose; 8, Sigmamarker.

C **DHDPS-R138H** 1, crude cell extract; 2, heat-shock; 3, Q-Sepharose ion exchange; 4, Phenyl-Sepharose; 5, Q-Sepharose ion exchange; 6, Sigmamarker.

D **DHDPS-Y107F** 1 & 2, crude cell extract; 3 & 4, heat shock; 5, Q-Sepharose ion exchange; 6, dialysis; 7, Phenyl-Sepharose; 8, Sigmamarker

E **DHDPS-Y133F** 1, crude cell extract; 2 & 3, heat shock; 4, Q-Sepharose ion exchange; 5, dialysis; 6, Phenyl-Sepharose; 7, Sigmamarker

The molecular mass of wild-type DHDPS was determined to be 31272 ± 1 Da (Table 4.3), which was consistent with the predicted mass from the sequence including the changes at positions 207 and 224. Borthwick *et al.*[16] also observed a mass of 31272 Da and reported the mutation at position 224 while they were uncertain of the other change. Mirwaldt *et al.*[17] found two mutations in their structure that were also confirmed in our parent, and subsequent mutant clones, of DHDPS. These were an alanine at position 207 instead of a threonine and a glycine at position 224 instead of a glutamic acid. It is now confirmed to be a threonine to alanine change at position 207. These mutations appear not to affect the enzymes function as the kinetic properties of our wild-type clone are the same as those reported by others.[8, 12, 18] Indeed they may not represent mutations at all, but rather errors in the original published sequence.

Each enzyme, apart from DHDPS-Y107F, exhibited its predicted mass within error. DHDPS-Y133F showed a mass of 31258 ± 3 Da and DHDPS-T44V a mass of 31270 ± 1 Da. DHDPS-Y107F revealed two distinct masses, 31452 ± 0.8 and 31652 ± 0.8 Da (200 and 400 Da above the predicted mass), which contradicts the sequence data. Unfortunately, this result was not reproducible, and consistent data could not be obtained despite persistent attempts.

Table 4.3 *The mass of the wild-type enzyme and three mutants, as measured by electrospray mass spectrometry.*

	Observed Mass (Da)	**Predicted Mass** (Da)
DHDPS wild-type	31272 ± 1	31272
DHDPS-T44V	31270 ± 1	31270
DHDPS-Y133F	31258 ± 3	31256
DHDPS-R138H	31250 ± 6	31253

4.2.7 Kinetic comparison of the mutants with the native.

Following purification, the mutants were subject to kinetic analysis to determine any changes in their kinetic parameters—K_m, k_{cat}, and k_{cat}/K_m. The initial rate kinetics of the DHDPS mutants, with respect to pyruvate and (*S*)-ASA, were measured using the coupled assay with

DHDPR; this was present in excess, which was determined by observing that the a parallel reaction containing additional DHDPR had an identical initial rate. Care was taken to ensure that all substrates and enzymes were stable over the course of the assay (usually 1–2 minutes).

Are the mutant enzymes suitable for kinetic analysis?

Some enzymes are more stable at high rather than at low concentrations. An enzyme could, therefore, lose activity when diluted from a stable stock solution to a lower concentration, such as in a biochemical assay. This may lead to errors in the observed rate of enzyme activity, but more importantly, the type of behaviour displayed, such as distinguishing between mixed and competitive inhibition. Also, given that some enzymes are more stable as an enzyme-substrate complex rather than the corresponding free enzyme, loss of activity at low substrate concentrations could be due, at least in part, to the increased rate of enzyme inactivation. This is all the more important when considering that mutant enzymes may be less stable than their natural counterparts. Although stable at 70°C, it was necessary to show that the mutant enzymes were stable under the conditions of the assay. Fortunately, this could be easily tested using a method developed by Selwyn,[19] and each of the mutants appeared stable under the assay conditions (Appendix 1).

Kinetics.

Initial rate data were analysed using the Enzfitter programme available from Biosoft (Cambridge, UK). Data were fitted to the appropriate models as judged by the SIGMA value of the regression (defined by Cleland[20]) and the lowest standard error associated with the kinetic constants.[20] Where competing models indicated a similar or slightly lower SIGMA value, an F test was used to assess whether the change in the model fit was statistically significant. Initial velocity data for the wild-type and the mutant enzymes were fitted by the above criteria to the following kinetic models:

$$v = VAB / (K_{mB}A + K_{mA}B + AB) \qquad \text{Equation } (\mathbf{1})^{21}$$

$$v = VAB / (K_{mB}A[1 + A/K_{ia}] + K_{mA}B[1 + B/K_{ib}] + AB) \qquad \text{Equation } (\mathbf{8})^{22}$$

$$v = VAB / (K_{mB}A + K_{mA}B + AB + K_{sA}K_{mB}) \qquad \text{Equation } (\mathbf{9})^{21}$$

Equation **1** describes the ping-pong model. Equation **8** also describes the ping-pong model except here both substrates, A and B, inhibit the enzyme at high concentrations. Equation **9** describes the ternary-complex mechanism. V is the maximal velocity, K_{mA} and K_{mB} are the Michaelis-Menten constants for the two substrates, A and B are the substrate concentrations, and v is the initial velocity. K_{ia} is the dissociation constant for A binding to the F enzyme form and K_{ib} is the dissociation for B binding to the E enzyme form.[22] K_{sA},[†] which appears in Equation **9**, is the binding constant for substrate A to the E enzyme form.[21]

Data and model fits were plotted with Enzfitter. The usefulness of the different plots for assessing the data was discussed in Chapter three.

Y133F.

It was clear from the qualitative *o*-aminobenzaldehyde assay used during enzyme purification that the activity of DHDPS-Y133F was severely impaired with respect to wild-type DHDPS. Furthermore, preliminary determination of the Michaelis-Menten constants revealed that the K_{mPyr} was far greater than that observed for the wild-type. When a complete set of initial rate data was collected, it was evident that the classical ping-pong kinetic mechanism would not fit well because both substrates appeared to inhibit catalysis at high concentrations. The data did fit the ping-pong model with substrate inhibition, Equation **8** (Figures 4.9 and 4.10), better than Equation **1**, and gave the kinetic parameters shown in Table 4.4. The R^2 for the fit was 0.986 and the $p(F)<0.01$. The catalytic constant (k_{cat}) was found to be (0.70 ± 0.21) s^{-1}, less than 1% of the wild-type. The K_m values were both found to be greater than the wild-type: the K_{mPyr} was (35 ± 13) mM and the K_{mASA} was (2.7 ± 0.9) mM.

[†] Cleland[21] denotes this parameter, shown in the tertiary mechanism, Equation (**9**), as K_{iA}. Here it is changed to K_{sA} to avoid confusion with K_{ia} in Equation (**8**), which has an entirely different meaning.

Table 4.4 *Kinetic analysis of the mutants of DHDPS enzymes.*

	Wild-type [1]	Y133F	T44V	T44S [2]	Y107F
k_{cat} (s^{-1}) [3]	124 ± 6.8	0.70 ± 0.21	0.116 ± 0.005	10.4 ± 0.2	10.8 ± 0.2
Relative k_{cat} (%)	100	0.31	0.1	8.4	9.1
K_{mPyr} (mM)	0.26 ± 0.03	35 ± 13	0.08 ± 0.008	0.92 ± 0.04	0.16 ± 0.01
k_{cat}/K_{mPyr} ($M^{-1} s^{-1}$)	$(4.8 \pm 0.6) \times 10^5$	$(2.0 \pm 0.9) \times 10^1$	$(1.4 \pm 0.2) \times 10^3$	$(1.14 \pm 0.06) \times 10^4$	$(6.6 \pm 0.3) \times 10^4$
K_{mASA} (mM)	0.11 ± 0.01	2.7 ± 0.9	0.09 ± 0.01	0.129 ± 0.006	0.58 ± 0.03
k_{cat}/K_{mASA} ($M^{-1} s^{-1}$)	$(1.1 \pm 0.2) \times 10^6$	$(2.6 \pm 1.2) \times 10^2$	$(1.3 \pm 0.2) \times 10^3$	$(8.1 \pm 0.4) \times 10^4$	$(1.9 \pm 0.09) \times 10^4$
K_{ia} (mM)	–	41 ± 20	–	–	–
K_{ib} (mM)	–	6.3 ± 3.1	–	–	–
K_{sA} (mM)	–	–	–	0.11 ± 0.03	–

	R138H	
Varied substrate	Pyruvate	(*S*)-ASA
Constant substrate	(*S*)-ASA [4]	Pyruvate [5]
k_{cat}^{app} (s^{-1}) [3]	0.0198 ± 0.0007	0.090 ± 0.007
Relative k_{cat} (%)	0.02	0.07
K_{mPyr}^{app} (mM)	0.28 ± 0.04	–
K_{mASA}^{app} (mM)	–	37 ± 5
$k_{cat}^{app}/K_{mPyr}^{app}$ ($M^{-1} s^{-1}$)	70 ± 10	–
$k_{cat}^{app}/K_{mASA}^{app}$ ($M^{-1} s^{-1}$)	–	2.4 ± 0.6

[1] As determined in Chapter three.
[2] The tertiary substituted mechanism.
[3] The protein concentration was determined using the method of Bradford.
[4] The concentration of (*S*)-ASA was set at 11 mM—much less than the enzyme's K_{mASA}—primarily because of cost.
[5] The concentration of pyruvate was constant at 15 mM—close to saturating conditions.

Figure 4.9 *Kinetic analysis of DHDPS-Y133F with respect to pyruvate.* ***A*** *is a direct plot,* ***B*** *is the Eadie-Hofstee plot,* ***C*** *is the Lineweaver-Burk plot, and* ***D*** *is a percentage residual plot of the data* ($100\times(v_{obs}-v_{cal})/v_{cal}$). *Enzfitter generated all plots after non-linear regression of the data against the ping-pong model with substrate inhibition, Equation* ***8***. *The* $R^2 = 0.99$ *and* $p(F)<0.01$.

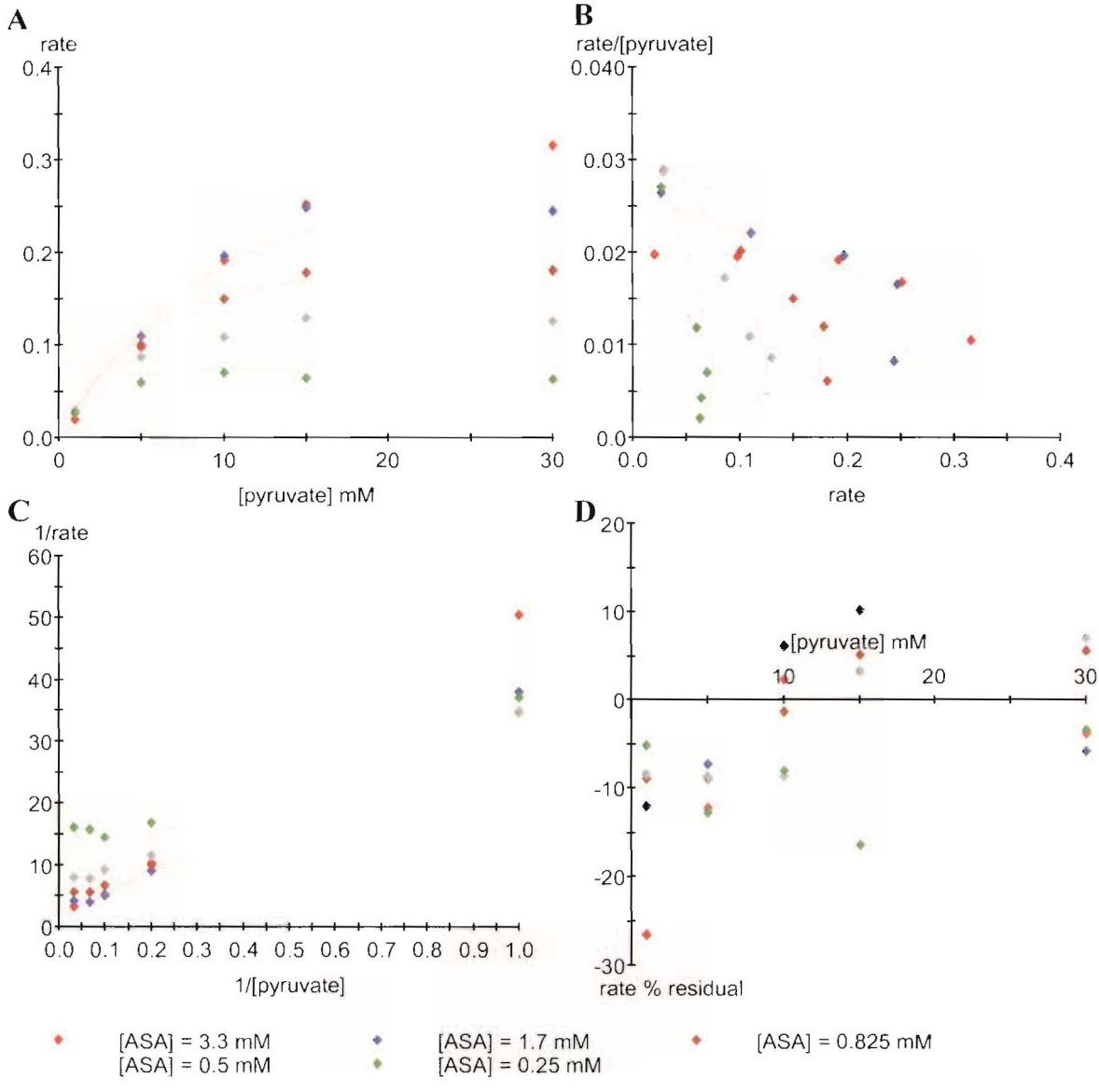

Figure 4.10 *Kinetic analysis of DHDPS-Y133F with respect to (S)-ASA.* ***A*** *is a direct plot,* ***B*** *is the Eadie-Hofstee plot,* ***C*** *is the Lineweaver-Burk plot, and* ***D*** *is a percentage residual plot of the data* ($100\times(v_{obs}-v_{cal})/v_{cal}$). *Enzfitter generated all plots after non-linear regression of the data against the ping-pong model with substrate inhibition, Equation* ***8***. *The* $R^2 = 0.99$ *and* $p(F)<0.01$.

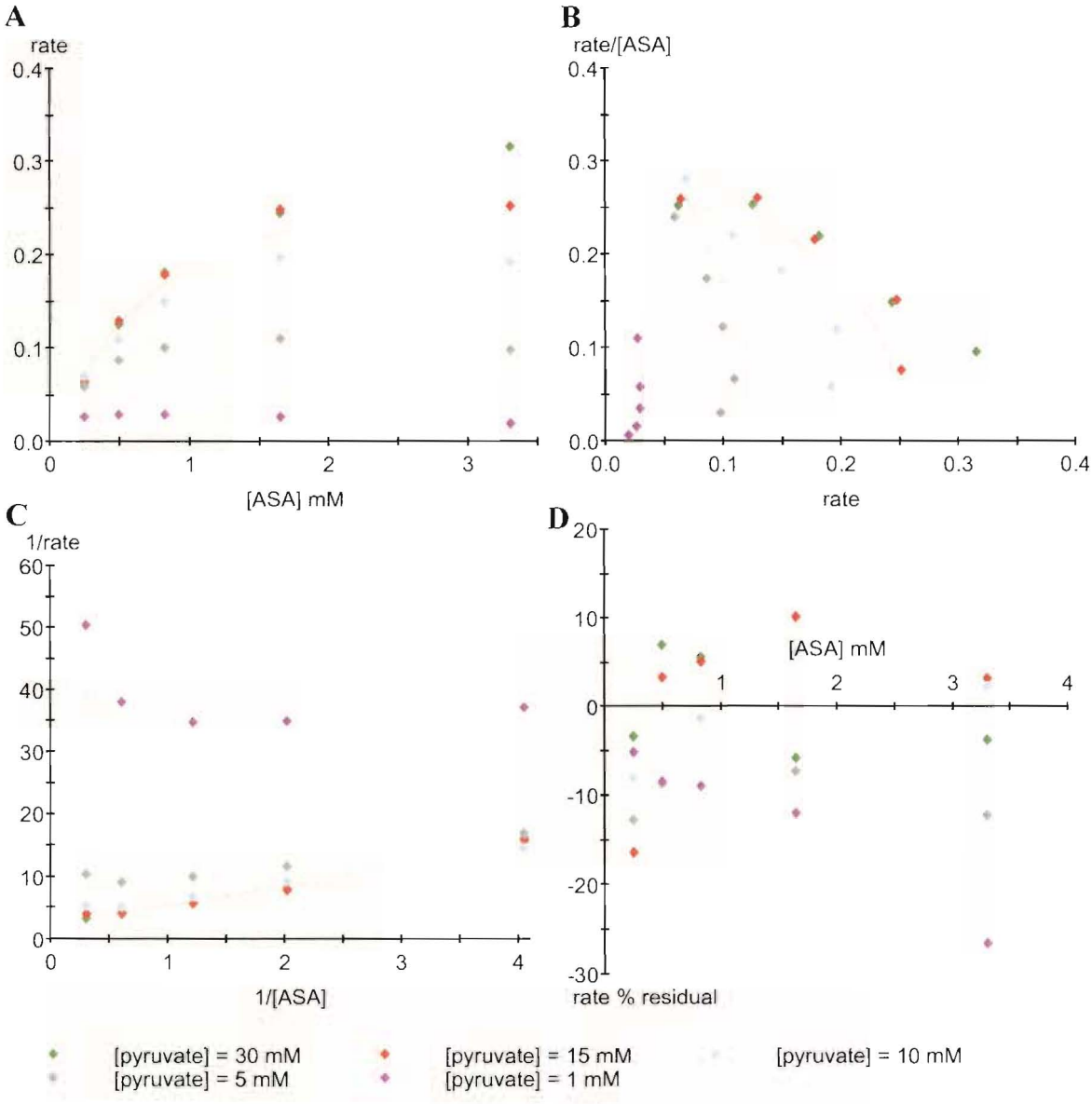

T44V.

Like DHDPS-Y133F, it was evident during the purification that DHDPS-T44V exhibited a severe loss of activity. When initial rate data were collected, they fitted well to the classical ping-pong model (Equation **1**), which can be seen in Figures 4.11 and 4.12. The k_{cat} was

found to (0.116 ± 0.005) s^{-1}—over 1000 times less active than the wild-type (Table 4.4). The K_{mPyr} was found to be significantly lower than the wild-type at (0.08 ± 0.008) mM while the K_{mASA} was (0.09 ± 0.01) mM, similar to wild-type DHDPS.

Figure 4.11 *Kinetic analysis of DHDPS-T44V with respect to pyruvate.* ***A*** *is a direct plot,* ***B*** *is the Eadie-Hofstee plot,* ***C*** *is the Lineweaver-Burk plot, and* ***D*** *is a percentage residual plot of the data* ($100\times(v_{obs}-v_{cal})/v_{cal}$). *Enzfitter generated all plots after non-linear regression of the data against the ping-pong model,* Equation ***1***. *The* $R^2 = 0.97$ *and* $p(F)<0.01$.

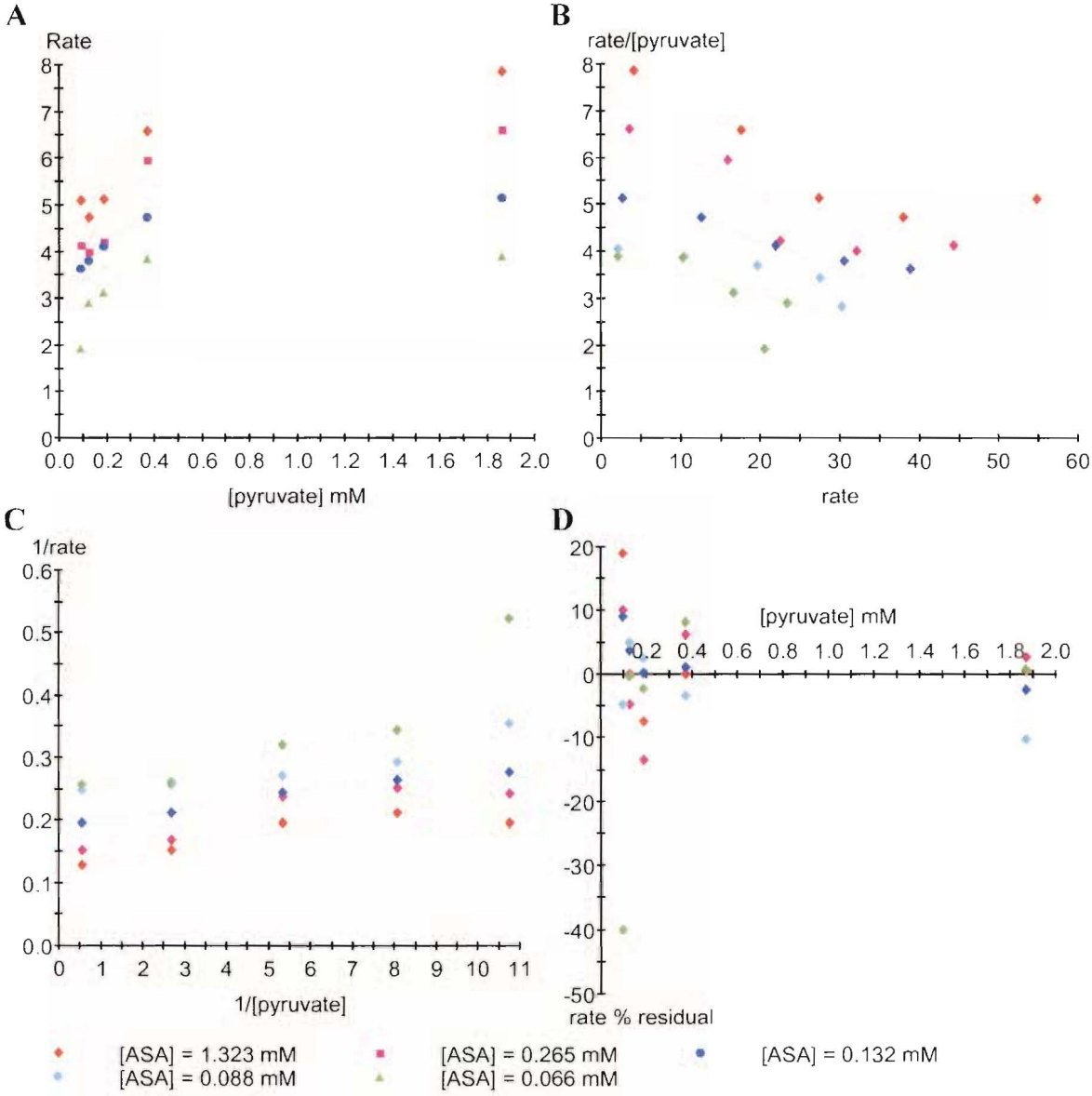

Figure 4.12 *Kinetic analysis of DHDPS-T44V with respect to (S)-ASA. **A** is a direct plot, **B** is the Eadie-Hofstee plot, **C** is the Lineweaver-Burk plot, and **D** is a percentage residual plot of the data ($100\times(v_{obs}-v_{cal})/v_{cal}$). Enzfitter generated all plots after non-linear regression of the data against the ping-pong model, Equation 1. The $R^2 = 0.97$ and $p(F)<0.01$.*

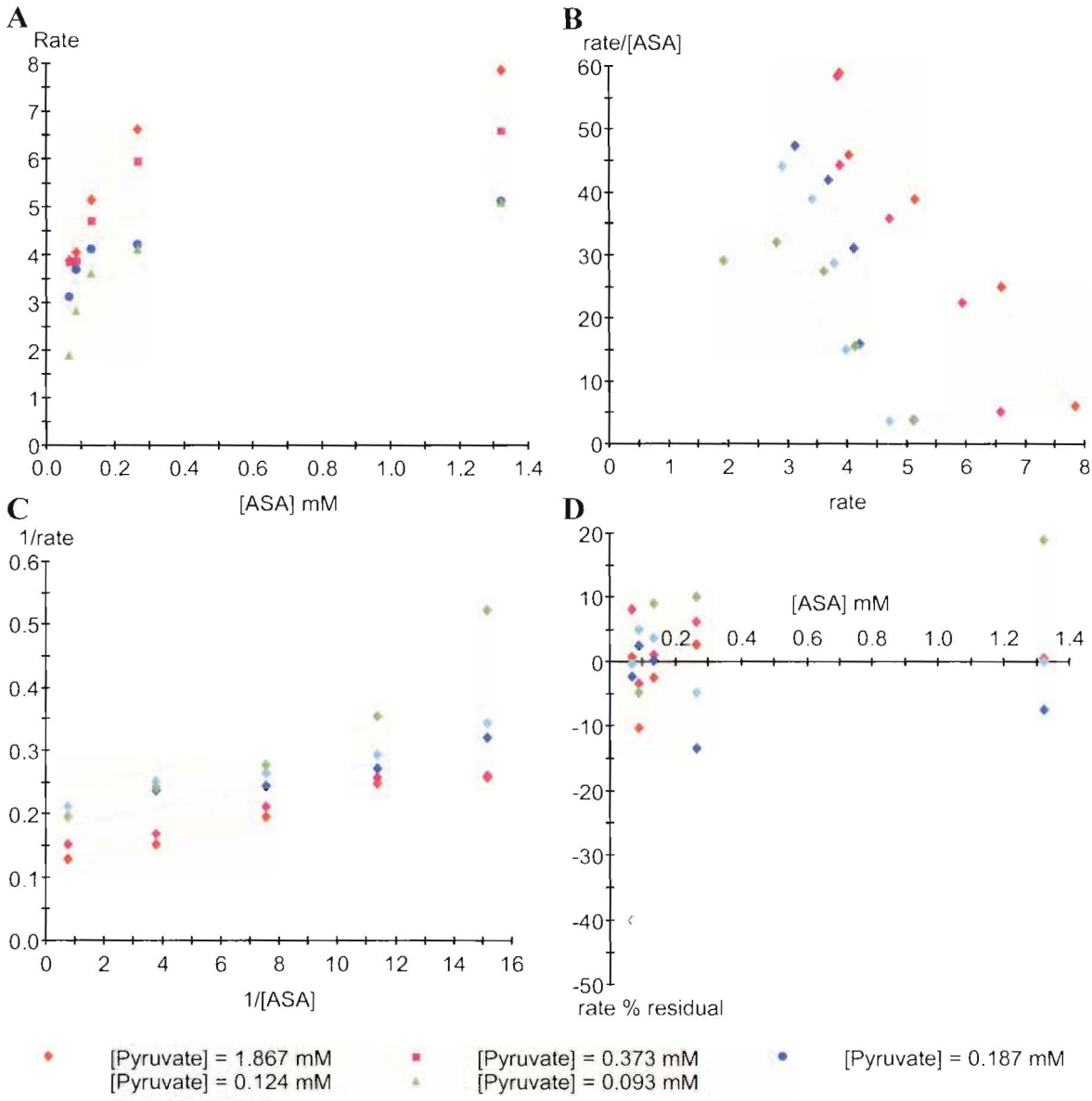

T44S.

Activity was partially restored when T44 was mutated to serine, although, remarkably, the kinetic mechanism now showed an intersecting type in the Lineweaver-Burk plot (Figures 4.13 **C** and 4.14 **C**). This was suggestive that the tertiary-complex mechanism (Equation **9**), rather than the ping-pong mechanism (Equation **1**),[21] was operating in DHDPS-T44S. The catalytic constant was (10.8 ± 0.2) s^{-1}, 10% that of the wild-type (Table 4.4). The K_{mPyr} was increased 4 fold (0.92 ± 0.04 mM) while the K_{mASA} was similar to the wild-type (0.129 ± 0.006 mM). Unlike the ping-pong model, the tertiary-complex model (Equation **9**) includes another parameter (K_{sA}) that directly reflects the binding constant of the first substrate to the enzyme form, in this case pyruvate.[‡] Thus the binding constant for pyruvate to enzyme was determined to be (0.11 ± 0.03) mM. The data and the kinetic fits are shown in Figures 4.13 and 4.14.

[‡] More correctly, K_{sA} is a measure of the dissociation constant of the E.A complex.

Figure 4.13 *Kinetic analysis of DHDPS-T44S with respect to pyruvate.* ***A*** *is a direct plot,* ***B*** *is the Eadie-Hofstee plot,* ***C*** *is the Lineweaver-Burk plot, and* ***D*** *is a percentage residual plot of the data* ($100\times(v_{obs}-v_{cal})/v_{cal}$). *Enzfitter generated all plots after non-linear regression of the data against the tertiary-complex model, Equation* ***9***. *The* $R^2 = 0.99$ *and* $p(F)<0.01$.

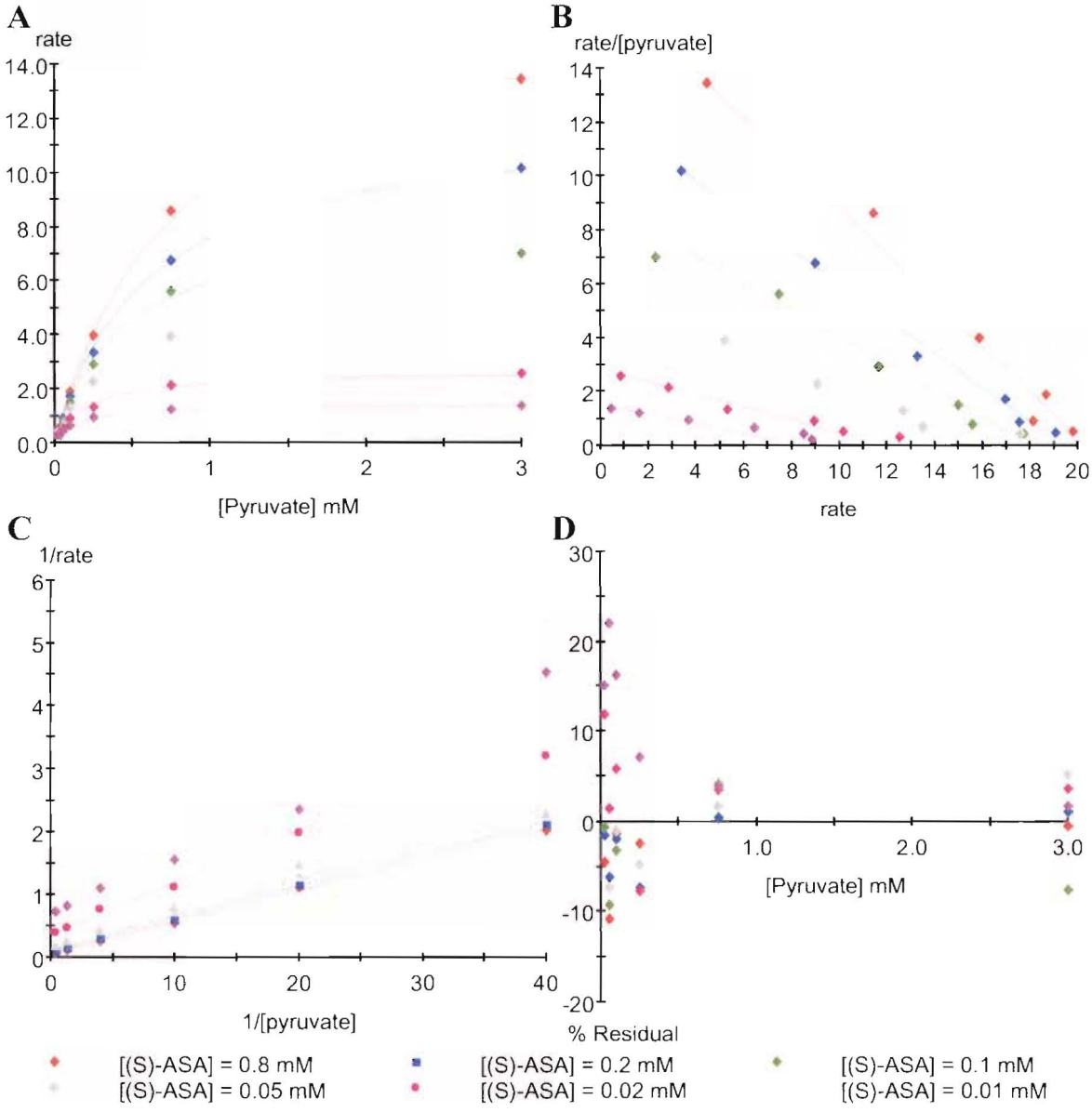

Figure 4.14 *Kinetic analysis of DHDPS-T44S with respect to (S)-ASA. **A** is a direct plot, **B** is the Eadie-Hofstee plot, **C** is the Lineweaver-Burk plot, and **D** is a percentage residual plot of the data ($100\times(v_{obs}-v_{cal})/v_{cal}$). Enzfitter generated all plots after non-linear regression of the data against the tertiary-complex model, Equation **9**. The $R^2 = 0.99$ and $p(F)<0.01$.*

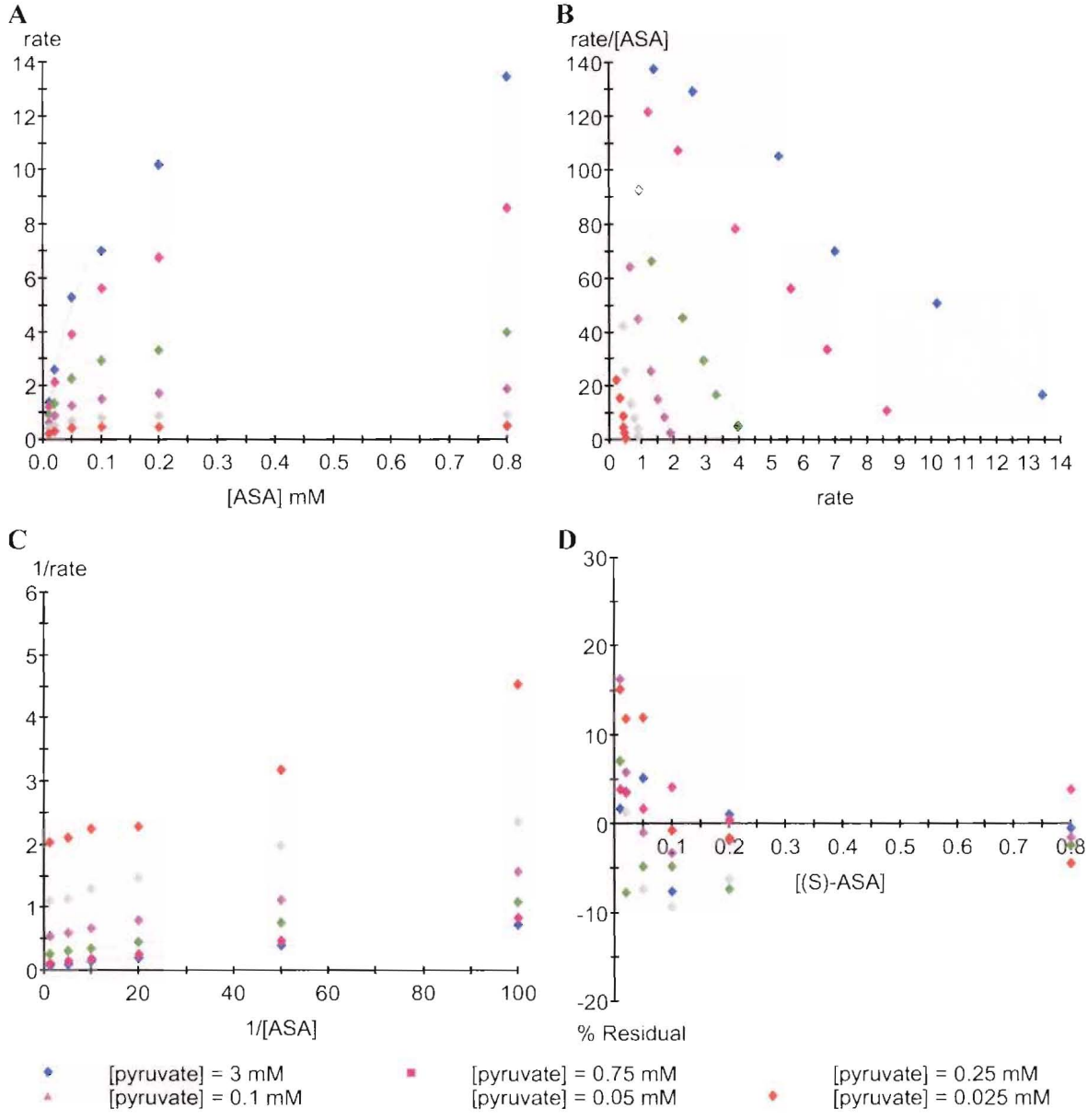

Y107F.

This residue was, perhaps, the most enigmatic of those mutated in this thesis. When mutated to phenylalanine, DHDPS-Y107F retained some activity with a k_{cat} of (10.8 ± 0.2)

s^{-1}, again about 10% that of the wild-type (Table 4.4). The Michaelis-Menten constants with respect to pyruvate and (*S*)-ASA were (0.16 ± 0.01) mM and (0.58 ± 0.03) mM respectively (Figures 4.15 and 4.16).

Figure 4.15 *Kinetic analysis of DHDPS-Y107F with respect to pyruvate. **A** is a direct plot, **B** is the Eadie-Hofstee plot, **C** is the Lineweaver-Burk plot, and **D** is a percentage residual plot of the data ($100\times(v_{obs}-v_{cal})/v_{cal}$). Enzfitter generated all plots after non-linear regression of the data against the ping-pong model, Equation **1**. The $R^2 = 0.99$ and $p(F)<0.01$.*

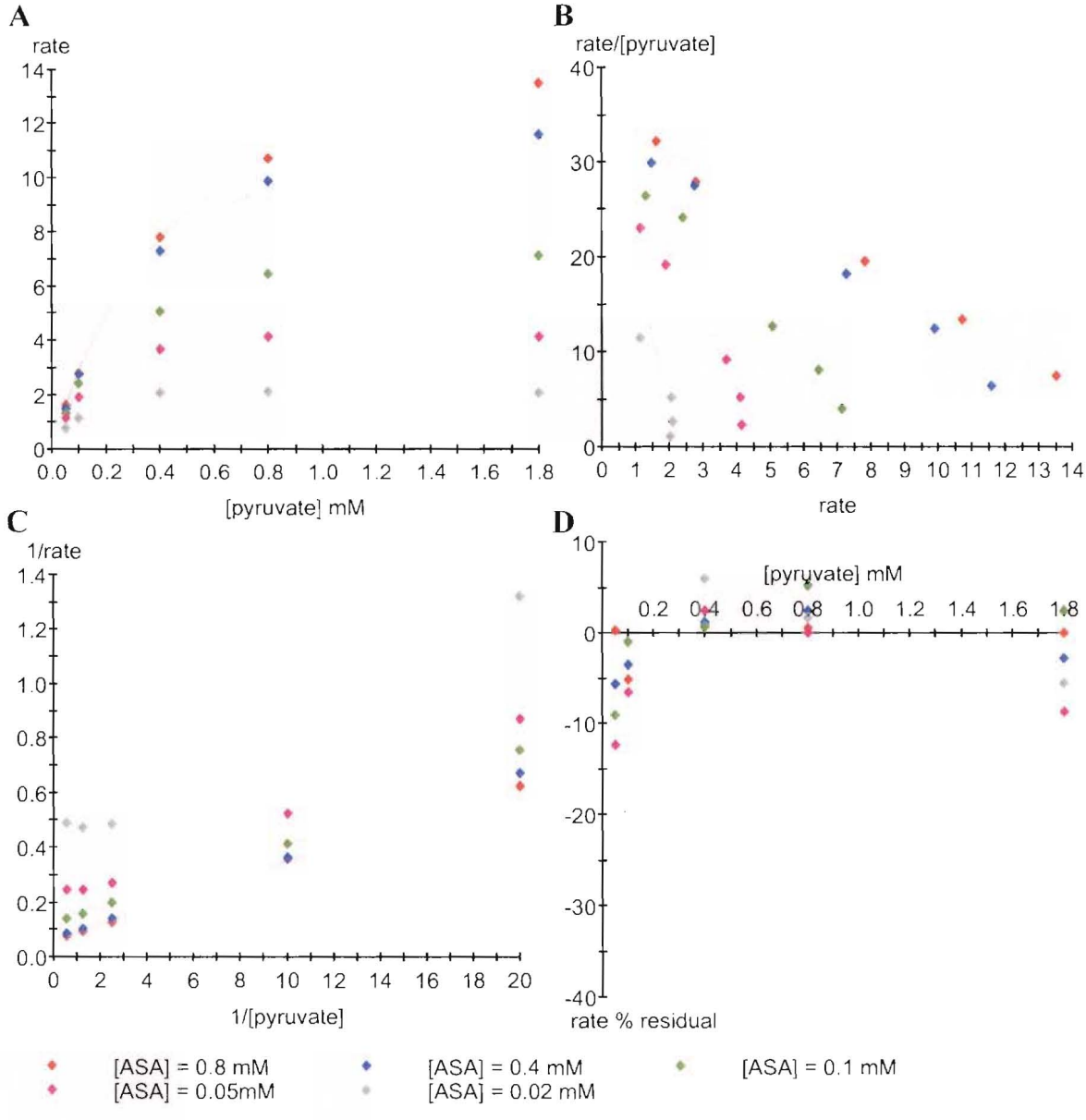

Figure 4.16 *Kinetic analysis of DHDPS-Y107F with respect to (S)-ASA.* ***A*** *is a direct plot,* ***B*** *is the Eadie-Hofstee plot,* ***C*** *is the Lineweaver-Burk plot, and* ***D*** *is a percentage residual plot of the data* ($100\times(v_{obs}-v_{cal})/v_{cal}$). *Enzfitter generated all plots after non-linear regression of the data against the ping-pong model, Equation* ***1***. *The* $R^2 = 0.99$ *and* $p(F)<0.01$.

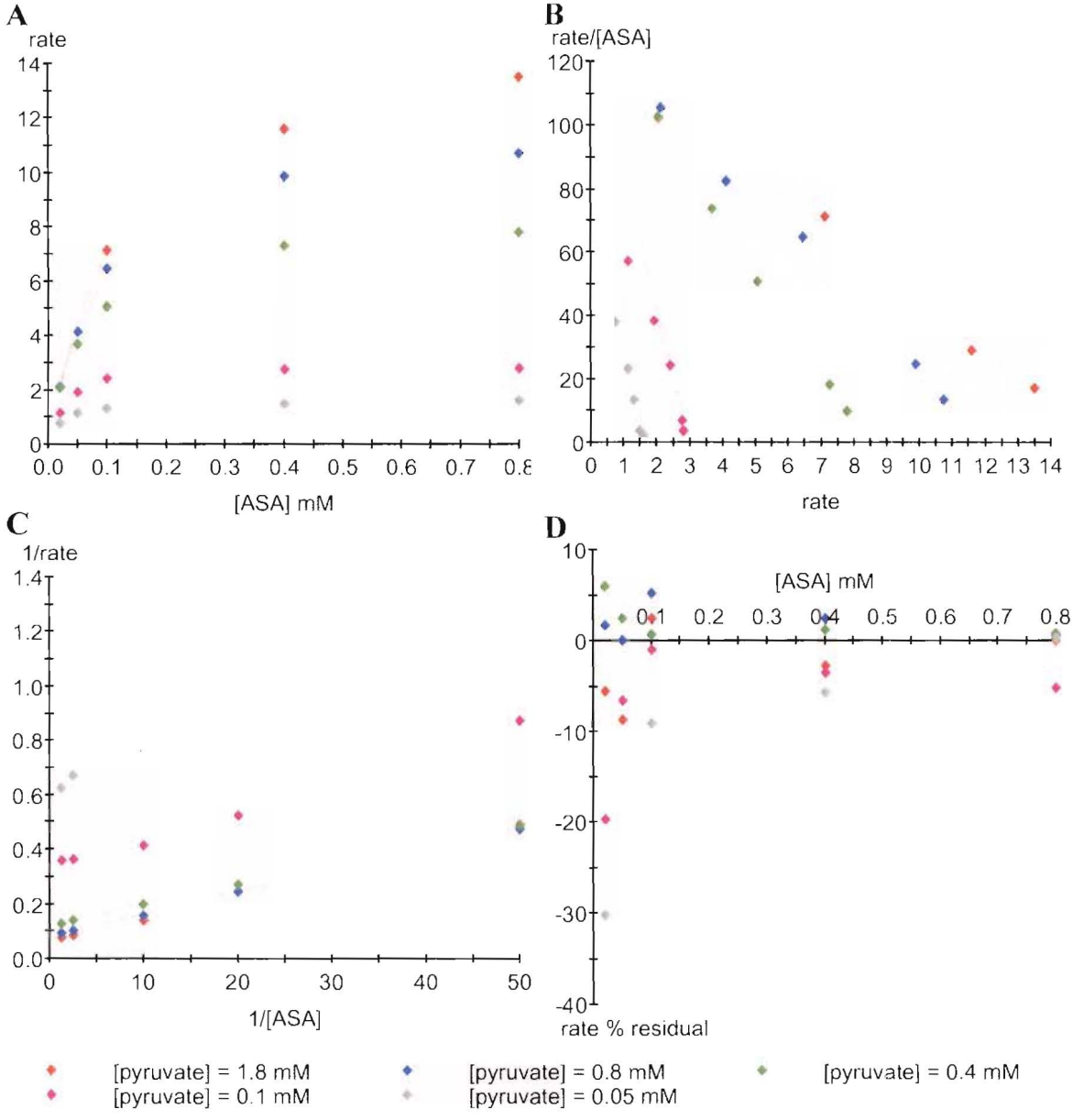

R138H.

The mutation of R138 to histidine proved more challenging because, as was evident during the purification, DHDPS-R138H was extremely inactive. A preliminary study to assess the effect of the mutation, and to test the feasibility of further kinetic study, revealed a K_{mASA} far greater than the wild-type. Given the cost and availability of (*S*)-ASA, the large amount of protein required, and the likelihood of imprecise data at low substrate concentrations, it was decided not to attempt the comprehensive kinetic analysis of the other mutants, but to compromise by simplifying Equation **1** to a pseudo single-substrate mechanism. This can be done if the second substrate is kept constant, so Equation **1** reduces to Equation **10** where V^{app} and $K_{mA}{}^{app}$ are the apparent maximal velocity and Michaelis-Menten parameters at the fixed concentration of the other substrate.[21] Equation **10** is identical to the Michaelis-Menten equation.

$$v = V^{app}A / (K_{mA}{}^{app} + A) \qquad \text{Equation (10)}$$

Despite this, meaningful results were obtained as seen in Table 4.4 and Figures 4.17 and 4.18.

The apparent k_{cat} was determined to be (0.02 ± 0.0007) s^{-1} when pyruvate was varied and (0.090 ± 0.007) s^{-1} when (*S*)-ASA was varied. When determining k_{cat} with respect to varying pyruvate, (*S*)-ASA was held constant at sub-saturating concentrations because of the cost and availability (*S*)-ASA. However, when determining k_{cat} with respect to varying (*S*)-ASA, the constant pyruvate concentration was approaching saturation so the calculated $k_{cat}{}^{app}$ approaches the true k_{cat}.[¥]

[¥] The true k_{cat} is defined when the other substrate is saturated while $k_{cat}{}^{app}$ is defined at a constant concentration of the second substrate.

Figure 4.17 *Kinetic analysis of DHDPS-R138H with respect to pyruvate. **A** is a direct plot, **B** is the Eadie-Hofstee plot, **C** is the Lineweaver-Burk plot, and **D** is a percentage residual plot of the data ($100 \times (v_{obs}-v_{cal})/v_{cal}$). Enzfitter generated all plots after non-linear regression of the data against the Michaelis-Menten model, Equation **10**. The $R^2 = 0.99$ and $p(F)<0.01$.*

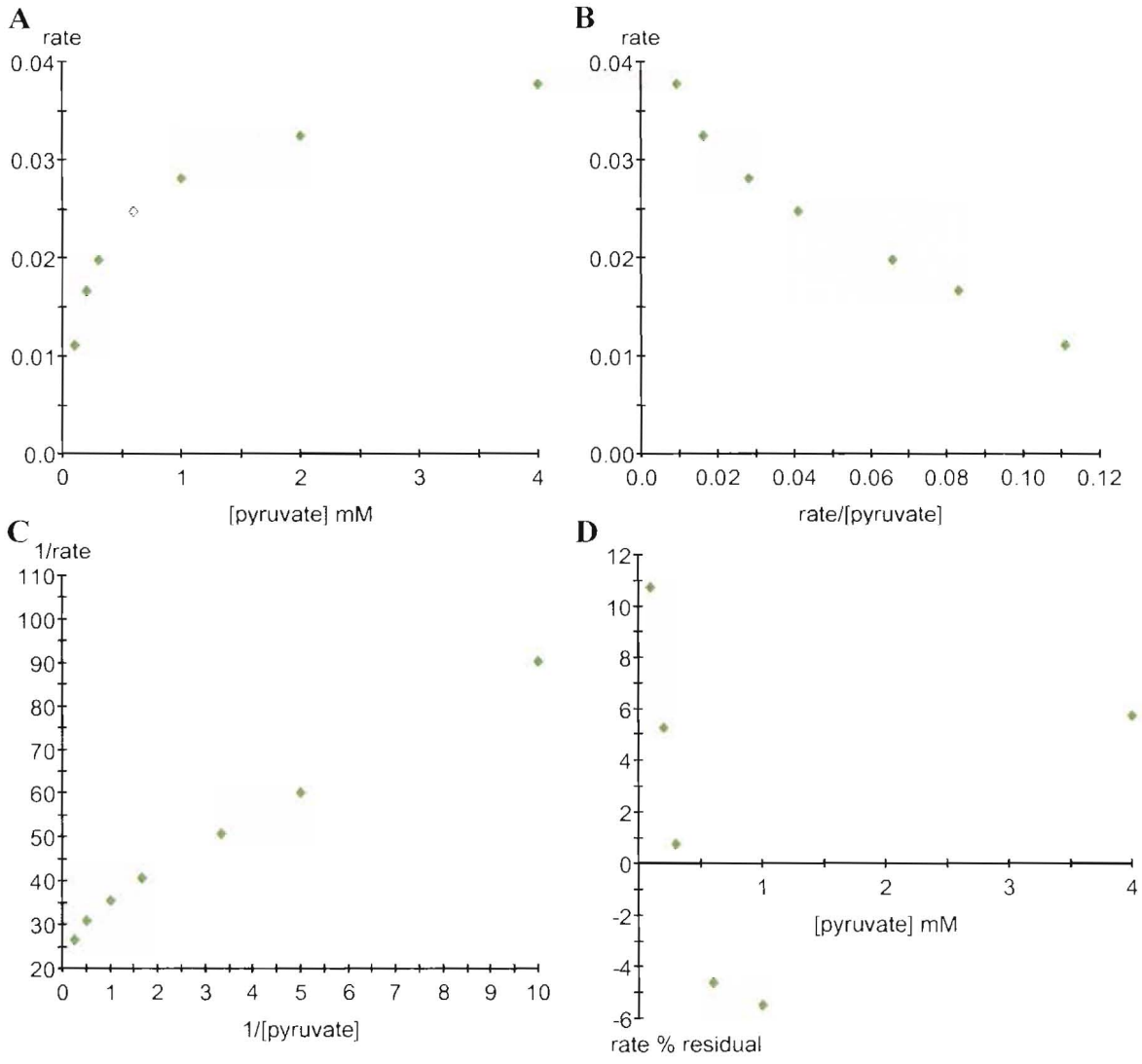

Figure 4.18 *Kinetic analysis of DHDPS-R138H with respect to (S)-ASA.* ***A*** *is a direct plot,* ***B*** *is the Eadie-Hofstee plot,* ***C*** *is the Lineweaver-Burk plot, and* ***D*** *is a percentage residual plot of the data* ($100\times(v_{obs}-v_{cal})/v_{cal}$). *Enzfitter generated all plots after non-linear regression of the data against the Michaelis-Menten model, Equation* ***10***. *The* $R^2 = 0.99$ *and* $p(F)<0.01$.

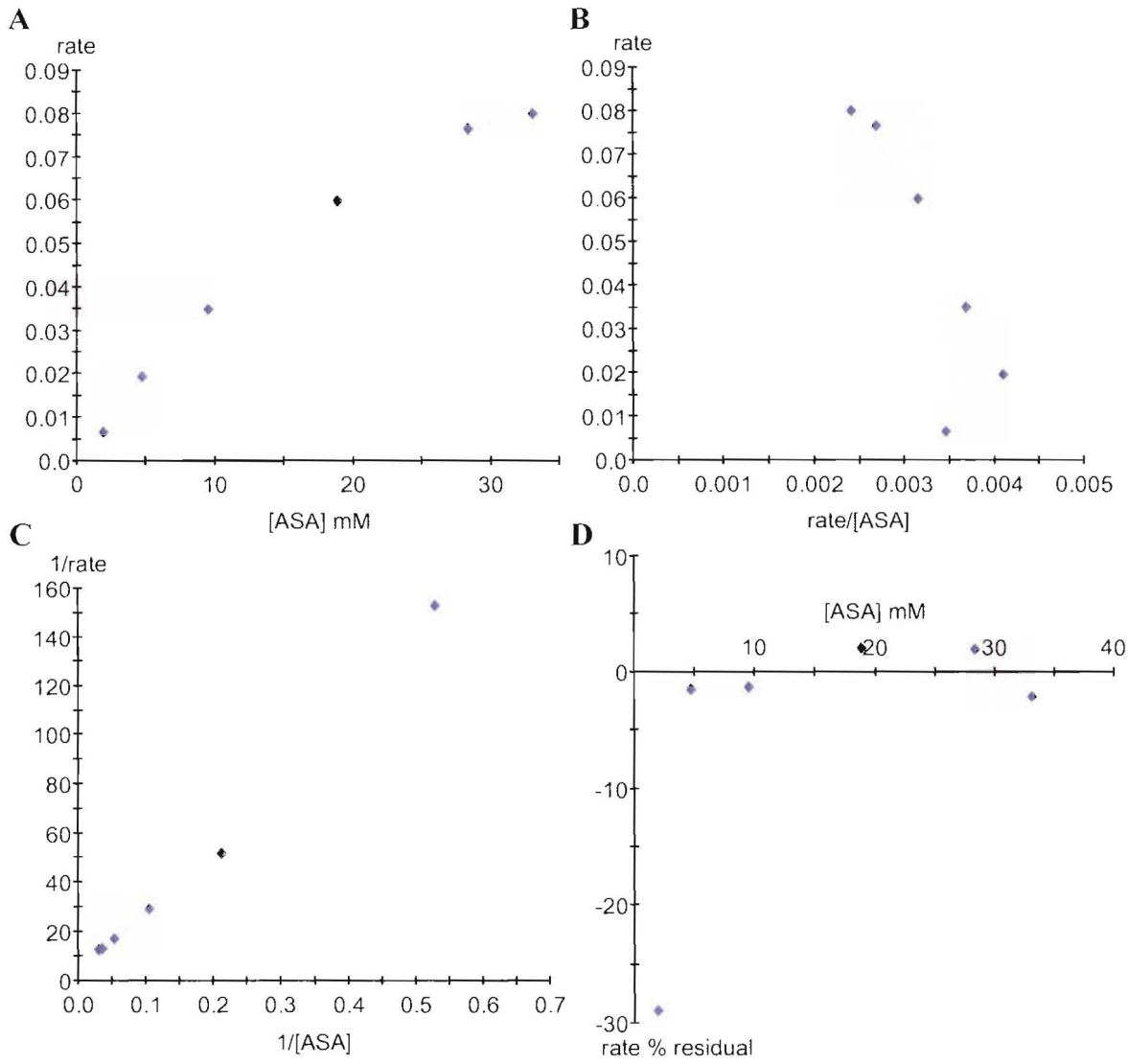

4.2.8 Trapping the covalent intermediate using sodium borohydride.

Shedlarski and Gilvarg,[23] and others,[16, 24] showed that the covalent intermediate formed when the free enzyme binds pyruvate, namely the Schiff base, could be observed by inactivation

inactivation (in the absence (*S*)-ASA) by reduction with sodium borohydride. For wild-type DHDPS, this has been used as evidence that pyruvate is the first substrate because (*S*)-ASA, when incubated with sodium borohydride, does not cause inactivation. Confirming these results, DHDPS activity was obliterated when incubated with pyruvate and sodium borohydride, but not (*S*)-ASA and sodium borohydride. The mutant enzymes also showed susceptibility to sodium borohydride in the presence of pyruvate, although they were also generally inactivated in the absence of substrates. This may reflect either the decreased stability under the conditions of the inactivation experiment or that part if the enzyme's population is in the form of the Schiff base with pyruvate. This can be seen in Table 4.5. DHDPS-Y133F was the only enzyme that showed sensitivity to sodium borohydride in the presence of (*S*)-ASA (45% inactivation) above that of the control reaction where neither substrate was added.

Table 4.5 *Activity of wild-type and mutant DHDPS after treatment with $NaBH_4$ in the absence and presence of substrates.*

	Enzymatic activity recovered (%)				
	Wild-type	**T44S**	**Y107F**	**T44V**	**Y133F**
Enzyme	100	100	100	100	100
Enzyme + $NaBH_4$	83	55	58	100	90
Enzyme + $NaBH_4$ + pyruvate	0.2	0.9	0.4	0	0
Enzyme + $NaBH_4$ + (*S*)-ASA	97	70	60	93	55

4.3 Discussion.

4.3.1 Mutations in the catalytic triad.

Y133 is considered central for DHDPS function.[4] The fact that it is positioned directly above K161 (the hydroxyl is 3.4–Å form the ε-nitrogen in the unbound wild-type structure[4]) suggests a role in both substrate binding and proton donation to the Schiff base hydroxyl (Figure 4.19: steps 1 and 2). The role of Y133 in enamine formation is uncertain due to its distance from the methyl carbon of the Schiff base (the back bone carbonyl of I203 has been implicated in this role because it is closer to the methyl group of the Schiff base[4]).

Mutation of Y133 to phenylalanine resulted in a marked loss of activity. Only 0.3% wild-type activity remained; a result consistent with the proposed role of this residue. A similar reduction of activity was seen when Y133 (*E. coli* numbering) of *N*-acetyl neuraminate lyase, whose role is proposed to be analogous during Schiff base formation,[25, 26] was mutated to phenylalanine.[25]

For each of the mutations in DHDPS, the specificity constant (k_{cat}/K_m) with respect to each substrate was markedly decreased, but particularly for DHDPS-Y133F. In the ping-pong model, the specificity constants reflect each half reaction because no individual rate constants are shared between the two Equations **3** and **4**. This was discussed in Chapter three, section 3.3.

$$k_{cat}/K_{mPyr} = k_1k_2 / (k_{-1} + k_2) \qquad \text{Equation (3)}$$

$$k_{cat}/K_{mASA} = k_3k_4 / (k_{-3} + k_4) \qquad \text{Equation (4)}$$

Given that the specificity constant with respect to pyruvate (k_{cat}/K_{mPyr}) is dramatically decreased (25000×) for DHDPS-Y133F compared to the wild-type, and its close proximity to the ε-nitrogen of K161, Y133 must play a crucial role in the first half reaction (Figure 4.19: steps 1a and 1b), probably in stabilisation of the Schiff base prior to enamine formation.

Besides the possible role of Y133 in Schiff base formation, it is also well placed to coordinate the hydrate of (*S*)-ASA, possibly donating a proton to the leaving hydroxyl group. Moreover, prior to cyclisation, Y133 may bridge the attacking amino group of ASA, which requires deprotonation to generate a lone pair of electrons necessary for attack (Figure 4.19: steps 5 and 6). That k_{cat}/K_{mASA} was also affected in DHDPS-Y133F, strongly indicates that this residue has some role in the binding of (*S*)-ASA and/or participates directly in the reaction, as hypothesised, by deprotonating the amine before cyclisation.

Unexpectedly, DHDPS-Y133F showed substrate inhibition with respect to both pyruvate (weakly) and (*S*)-ASA. For the ping-pong mechanism, substrate inhibition reflects the binding of the substrate to the alternative enzyme form producing a dead-end complex.[18, 21] For instance, in this case, (*S*)-ASA appears able to bind the unmodified E enzyme form (K_{ib} = 6.3 ± 3.1 mM) (refer to Chapter one, Figure 1.4). Presumably, the E form of Y133F is now able to accommodate (*S*)-ASA due to the space generated by the loss of the hydroxyl group.

Also unexpected, was that DHDPS-Y133F was more susceptible to sodium borohydride inactivation in the presence of (*S*)-ASA only, which together with its inhibition by (*S*)-ASA, may indicate that DHDPS-Y133F can covalently bind (*S*)-ASA.

Figure 4.19 *Proposed chemical mechanism of DHDPS.*

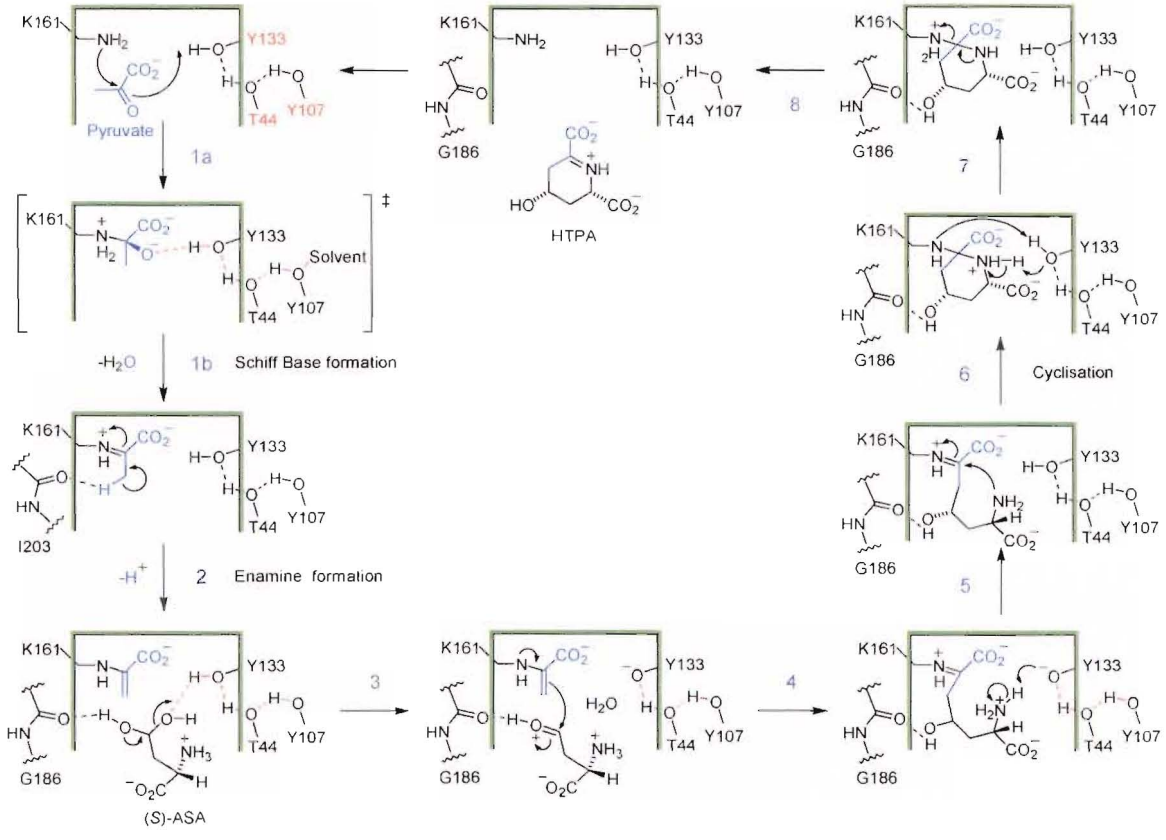

Although Y133 is clearly necessary in several steps of the reaction, it is unclear whether T44, which is hydrogen-bonded to both Y133 and Y107, modulates Y133. T44 is located opposite K161 at the C-terminal end of the $(\beta/\alpha)_8$-barrel. It is part of a conserved loop at the end of β-sheet 3 consisting of the sequence G_{43}-T_{44}-T_{45}-G_{46}-E_{47} (*E. coli* numbering). Blickling's structure of wild-type enzyme with bound pyruvate suggested that the role of T44 is not in substrate binding, rather its position in the hydrogen bonding network may play a role in Schiff base formation and cyclisation *via* the hydrogen bond to Y133.

Given the juxtaposition of T44, it was predicted that replacing its hydroxyl group with a methyl would result in the loss of the hydrogen bonding to Y107 and Y133 and, therefore, severe attenuation of the enzyme's function if this motif was important. As shown in Table

4.4, only 0.1% of wild-type activity remained. The specificity constants were also decreased (~500×), but to a lesser degree than seen in DHDPS-Y133. This may reflect the reduced ability of Y133 in DHDPS-T44V to function without the hydrogen-bonding network. Because k_{cat}/K_{mASA} decreased, the side chain of T44 must play some role in the mechanism of the second half reaction, probably in concert with Y133 given that they are connected by a hydrogen-bond. Little change is seen in the K_m values for either pyruvate or (*S*)-ASA, suggesting little change in substrate affinity, although the Michaelis-Menten constant for pyruvate is marginally lower than the wild-type.

When T44 was replaced with serine, activity, although lessened, was far greater than seen in DHDPS-T44V. The catalytic constant was measured at (10.4 ± 0.2) s^{-1}: this was 10-fold less than the wild-type but 100-fold greater than DHDPS-T44V. Thus, restoration of the hydrogen bonding system must, in part, play a catalytic role in the potency of DHDPS. The Michaelis-Menten constants for each substrate were similar to both the wild-type and DHDPS-T44V, suggesting similar substrate affinity for all three enzymes. These results provided additional evidence that the proton-relay is a functional moiety in wild-type DHDPS.

However, most surprising was that the kinetic mechanism of DHDPS-T44S appeared to fit the tertiary-complex mechanism (Equation **7**) better than the ping-pong model (Equation **1**). Karsten has also proposed the tertiary-complex mechanism for wild-type DHDPS but only at a pH of 5.7.[18] He concluded that the change in mechanism was because enamine formation was readily reversible at greater hydrogen ion concentrations: thus, the irreversible step no longer separates the two half reactions. Although probably not for the same reason, the irreversible step must also be absent in DHDPS-T44S. Herbert Fromm writes: "Implicit in all sequential mechanisms* is that all substrates must be present simultaneously at the enzyme's active site before product formation can occur".[27] In this case, unless (*S*)-ASA is present in the active site no reaction will occur, in contrast to the ping-pong model where Schiff base formation and enamine formation can occur in the absence of (*S*)-ASA. Consistent with this, it is suggested that the hydrate of (*S*)-ASA may assist in the generation of the enamine in a concerted way (Figure 4.20). Because serine lacks the methyl group

* Fromm defines a sequential mechanism as one which has an intersecting fit in the Lineweaver-Burk plot as seen in DHDPS-T44S (Figure 4.14).[26]

present in threonine, the active site of DHDPS-T44S may be able to accommodate (*S*)-ASA prior to Schiff base or enamine formation.

Figure 4.20 *Proposed mechanism of DHDPS-T44S.*

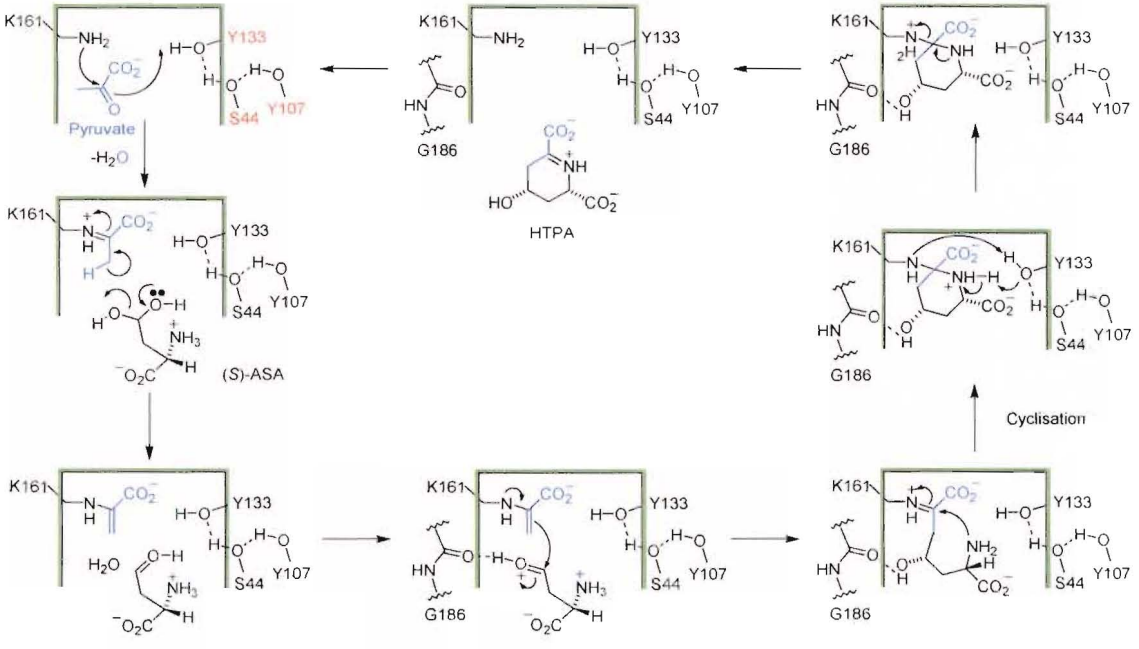

The tertiary complex mechanism can operate in an ordered or random fashion with respect to the order of substrate binding.[21] Given that the DHDPS-T44S is inactivated by sodium borohydride in the presence of pyruvate but not (*S*)-ASA, it is reasonable that pyruvate binding and Schiff base formation constitutes the first step. It is therefore proposed that DHDPS-T44S follows an ordered kinetic mechanism. This hypothesis can be tested by determining whether DHDPS-T44S is capable of exchanging protons from tritiated pyruvate to water in the absence of (*S*)-ASA; failure to do so would be consistent with the tertiary complex mechanism suggested in Figure 4.20.

An alignment of the sequences of DHDPS and *N*-acetyl neuraminate lyase (NAL) (both isolated from various sources) showed that T44 is exchanged by serine.[26] In NAL, serine is similarly juxtaposed with hydrogen bonds to Y133 and Y107 (*E. coli* DHDPS numbering), although no study to date has considered the importance of this motif in the mechanism of NAL.

The role of Y107 in the kinetic mechanism has been speculative. As discussed in the introduction, this residue contributes to the tight binding interface within each of the dimers of DHDPS, reaching into the active site of the other monomer, and forms an aromatic stack with Y106 of the opposing monomer. Moreover, the dihedral angles of Y107 fall in the disallowed region of the Ramachandran plot, suggesting some role in the enzyme's function.[4] Blickling *et al.* hypothesised that this residue was the third in a catalytic triad involved in shuttling protons between the active site and solvent. Mutation to phenylalanine at this position resulted in a 10-fold loss in activity. This, again, was consistent with the proton-relay mechanism, although the change in activity was not as great as in the previous mutations in the relay mentioned. Given that the hydroxyl is solvent accessible, and that space might be created by the loss of the hydroxyl, a water molecule could replace the hydroxyl in the mechanism, acting as a surrogate during the mechanism. This is explored further in Chapter five. The Michaelis-Menten constant for pyruvate was similar to the wild-type, while K_{mASA} was increased 5-fold.

4.3.2 The role of R138 in substrate binding.

R138 is situated at the entrance of the active site.[4] Blickling *et al.*[4] showed that the carboxyl groups of α-ketopimelic acid and succinate β-semialdehyde (in the presence of pyruvate) were both coordinated to R138. In addition, R138 is highly conserved among DHDPS isoenzymes, although replaced by valine in NAL.[28] In order to test the involvement of R138H in DHDPS, it was mutated to histidine. Following data collection and analysis, the results were compared with the wild-type and the other mutations. However, because of the extremely low activity of the mutant, the ping-pong model has been assumed but could not be tested.

The results, presented in Table 4.4, show that the k_{cat} was less than 0.1% that of the native. The K_{mASA} was increased to (37 ± 5) mM, and the k_{cat}/K_{mASA} has decreased nearly 500000-fold, suggestive that the binding affinity of (*S*)-ASA has decreased, and consistent with R138H being involved in substrate binding. However, k_{cat}/K_{mPyr} has also been severely decreased and this is more difficult to account for, although the value determined here is somewhat underestimated because only the apparent k_{cat} and K_{mPyr} can be determined. One explanation is that because of its position at the entrance of the active site, R138 may be

important in the initial binding of pyruvate prior to Schiff base formation, thus mutation to histidine may change k_{cat}/K_{mPyr}.

4.4 Summary.

In order to investigate the role of active site residues in DHDPS, mutations in the recombinant *dap*A gene have been made and their effect on the function of DHDPS assessed. In particular, the residues of the proton-relay, consisting of Y133, T44, and Y107, were examined as well as R138, thought to be involved in (*S*)-ASA binding. The mutants were over-expressed in an *E. coli* strain deficient in DHDPS activity and purified to apparent homogeneity as judged by SDS-PAGE with Coomassie Brilliant Blue staining.

Y133 is thought to be central in the catalytic mechanism, due to its conservation in all DHDPS isoenzymes and its position close to the active site lysine, K161, which covalently binds pyruvate. The results in this chapter suggest that the role of Y133 is to assist in Schiff base formation, the binding of the hydrate of (*S*)-ASA, and removing a proton from the amine prior to cyclisation. The kinetic characteristics of DHDPS-Y133F, compared to the wild-type, are entirely consistent with this proposal.

Mutations in T44 and Y107, both hydrogen-bonded to Y133, were examined to see if they too were important in the function of DHDPS *via* the proton-relay, and whether they modulated Y133 function. Again, mutations in both residues attenuated DHDPS activity, although the activity of DHDPS-Y107F was greater than expected. Moreover, when T44 was replaced with serine, DHDPS activity was partially recovered in comparison to DHDPS-T44V. Surprisingly, S44 appeared to have a different kinetic mechanism—the tertiay complex mechanism—whereby (*S*)-ASA must be bound to the active site before the reaction can proceed.

Finally, the role of R138 in (*S*)-ASA binding has been confirmed. Mutation to histidine results in 1000-fold loss in activity and 500000-fold decease in the specificity constant with respect to (*S*)-ASA.

4.5 References.

1. Fersht, A. (1998). *Structure and mechanism in protein science: a guide to enzyme catalysis and protein folding*, W.H. Freeman and Company, New York.

2. Plapp, B. V. (1995). Site-directed mutagenesis: a tool for studying enzyme catalysis. *Methods in Enzymology*, **249**, 91-119.

3. Peracchi, A. (2001). Enzyme catalysis: removing chemically 'essential' residues by site-directed mutagenesis. *Trends in Biochemical Sciences*, **26**, 497-503.

4. Blickling, S., Renner, C., Laber, B., Pohlenz, H., Holak, T. A. & Huber, R. (1997). Reaction mechanism of *Escherichia coli* dihydrodipicolinate synthase investigated by X-ray crystallography and NMR spectroscopy. *Biochemistry*, **36**, 24-33.

5. Kunkel, T. (1985). Rapid and efficient site-specific mutagenesis without phenotypic selection. *Proceedings of the National Academy of Sciences of the United States of America*, **82**, 488-492.

6. Stratagene. (1998). Quikchange site-directed mutagenesis kit: instruction manual.

7. Gerrard, J. A. (1992). Studies on dihydrodipicolinate synthase. D. Phil. thesis, Oxford University.

8. Coulter, C. V., Gerrard, J. A., Kraunsoe, J. A. E. & Pratt, A. J. (1999). *Escherichia coli* dihydrodipicolinate synthase and dihydrodipicolinate reductase: kinetic and inhibition studies of two putative herbicide targets. *Pesticide Science*, **55**, 887-895.

9. Yeh, P., Sicard, A. M. & Sinskey, A. J. (1988). General organization of the genes specifically involved in the diaminopimelate-lysine biosynthetic pathway of *Corynebacterium glutamicum*. *Molecular General Genetics*, **212**, 105-111.

10. Bukhari, A. I. & Taylor, A. L. (1971). Genetic analysis of diaminopimelic acid- and lysine-requiring mutants of *Escherichia coli*. *Journal of Bacteriology*, **105**, 844-854.

11. Vauterin, M., Frankard, V. & Jacobs, M. (2000). Functional rescue of a bacterial *dapA* auxotroph with a plant cDNA library selects for mutant clones encoding a feedback-insensitive dihydrodipicolinate synthase. *Plant Journal*, **21**, 239-248.

12. Yugari, Y. & Gilvarg, C. (1965). The condensation step in diaminopimelate synthesis. *Journal of Biological Chemistry*, **240**, 4710-4716.

13. Miller, J. (1992). *A short course in bacterial genetics; a lab manual and handbook for E. coli and related bacteria*, Cold Spring Harbour, New York.

14. Owttrim, G. W. & Coleman, J. R. (1987). Molecular cloning of a *recA*-like gene from the cyanobacterium *Anabaena variabilis*. *Journal of Bacteriology*, **169**, 1824-1829.

15. Bradford, M. (1976). A rapid and sensitive method for the quantitation of microgram quantities of protein utilizing the principle of protein-dye binding. *Analytical Biochemistry*, **72**, 248-254.

16. Borthwick, E. B., Connel, S. J., Tudor, D. W., Robins, D. J., Shneier, A., Abell, C. & Coggins, J. R. (1995). *Escherichia coli* dihydrodipicolinate synthase: characterisation of the imine intermediate and the product of bromopyruvate treatment by electrospray mass spectrometry. *Biochemical Journal*, **305**, 521-524.

17. Mirwaldt, C., Korndorfer, I. & Huber, R. (1995). The crystal structure of dihydrodipicolinate synthase from *Escherichia coli* at 2.5 Å resolution. *Journal of Molecular Biology*, **246**, 227-239.

18. Karsten, W. E. (1997). Dihydrodipicolinate synthase from *Escherichia coli*: pH dependent changes in the kinetic mechanism and kinetic mechanism of allosteric inhibition by L-lysine. *Biochemistry*,**36** , 1730-1739.

19. Selwyn, M. J. (1965). A simple test for the inactivation of an enzyme during assay. *Biochimica et Biophysica Acta*, **105**, 193-195.

20. Cleland, W. W. (1979). Statistical analysis of enzyme kinetic data. *Methods in Enzymology*, **63**, 103-138.

21. Cornish-Bowden, A. (1999). *Fundamentals of enzyme kinetics*. 2nd edit., Portland Press Ltd, London.

22. Cleland, W. W. (1979). Substrate inhibition. *Methods in Enzymology*, **63**, 500-513.

23. Shedlarski, J. G. & Gilvarg, C. (1970). The pyruvate-aspartic semialdehyde condensing enzyme of *Escherichia coli*. *Journal of Biological Chemistry*, **245**, 1362-1373.

24. Laber, B., Gomis-Ruth, F., Romao, M. & Huber, R. (1992). *Escherichia coli* dihydrodipicolinate synthase. Identification of the active site and crystallization. *Biochemical Journal*, **288**, 691-695.

25. Kruger, D., Schauer, R. & Traving, C. (2001). Characterization and mutagenesis of the recombinant *N*-acetylneuraminate lyase from *Clostridium perfringens*. *European Journal of Biochemistry*, **268**, 3831-3839.

26. Lawrence, M., Barbosa, J., Smith, B., Hall, N., Pilling, A., Ooi, H. & Marcuccio, S. (1997). Structure and mechanism of a sub-family of enzymes related to *N*-acetylneuraminate lyase. *Journal of Molecular Biology*, **266**, 381-399.

27. Fromm, H. J. (1979). Summary of kinetic reaction mechanisms. *Methods in Enzymology*, **63**, 42-53.

28. Joerger, A. C., Mayer, S. & Fersht, A. (2003). Mimicking natural evolution *in vitro*: an *N*-acetylneuraminate lyase mutant with an increased dihydrodipicolinate synthase activity. *Proceedings of the National Academy of Sciences of the United States of America*, **100**, 5694-5699.

Chapter Five.

The crystal structures of three site-directed mutants of *Escherichia coli* DHDPS: further evidence for a catalytic triad.

5.1 Introduction.

In Chapter four, it was demonstrated that mutations in the putative catalytic triad of wild-type DHDPS result in loss of activity. In light of these results, X-ray crystal structures of the catalytic triad mutants were sought in an effort to show that the mutations had not grossly altered the enzymes structure and to gain greater insight into the mechanism of DHDPS through the structure of these mutants. This work was performed in the lab of Professor Janos Hajdu (Uppsala, Sweden) with the help of Dr. Karin Valegård. Reported herein are the structures of DHDPS-Y133F, DHDPS-T44V, and DHDPS-Y107F.

Mirwaldt *et al.*[1] first published the structure of *E. coli* DHDPS, from which further structures were solved with bound ligands, such as pyruvate and various inhibitors.[2] These workers showed that the quaternary structure of DHDPS was homotetrameric and that the tertiary fold was that of the $(\beta/\alpha)_8$–barrel. When the structure of DHDPS with pyruvate bound to K161 was solved, the suspicions of Yugari and Gilvarg[3] that an active site lysine was involved in Schiff base formation were confirmed. Furthermore, Y133 was close to the ε-nitrogen of K161 and it was anticipated that the hydroxyl of Y133 would be involved in catalysis by acting as a general acid and base. As discussed in the previous chapter, the juxtaposition of Y133, T44, and Y107 lead to the formation of a hydrogen-bonding network between the side chains of these three residues—this is the catalytic triad.

This chapter explores the X-ray crystal structures of DHDPS-Y133F, DHDPS-T44V, and DHDPS-Y107F, in comparison to the wild-type structure determined previously.[1, 2] DHDPS-Y133F and DHDPS-T44V in particular, showed strong attenuation of catalytic function, so were of special interest. Furthermore, DHDPS-Y107F showed greater than

expected activity, which led to the hypothesis that a water molecule replaced the hydroxyl of Y107 in the catalytic mechanism. The structure of DHDPS-Y107F would test this hypothesis.

5.2 Results and discussion.

5.2.1 Crystallisation and refinement.

Crystallisation experiments were undertaken as described by Mirwaldt *et al.*[1] using the hanging drop-vapour diffusion method. Crystals were grown at either 4°C or 21°C. In both cases, crystals appeared after 3 to 4 days and grew up to 0.3 mm in the largest dimension (Figure 5.1 **A**). In addition to the hanging drop method, crystals were grown using the sitting drop technique and this afforded well formed, but very thin and delicate crystal sheets that were up to approximately 0.7 mm in their largest dimension (Figure 5.1 **B**). These, however, proved difficult to work with and data were not collected. For X-ray data collection, the crystals were soaked in cryo-protectant solution (K_2PO_4, 1.8 M, pH 10, 20% glycerol (v/v)) and flash-frozen in liquid nitrogen. A minor difference in the cell dimensions of the mutants and the wild-type was observed and this was attributed to the cryo-freezing of the crystals prior to data collection (*pers. comm.* Dr. Karin Valgård); data for wild-type DHDPS had previously been collected at 4°C.[1]

Figure 5.1 *Crystal forms of DHDPS-Y107F.* ***A****: Crystals grown using the hanging drop-vapour diffusion method. The large crystal is about 0.2 mm.* ***B****: Crystals grown using the sitting drop method. In its largest dimension, this crystal measures 0.5 mm. Image B was produced with a polarised light source.*

A

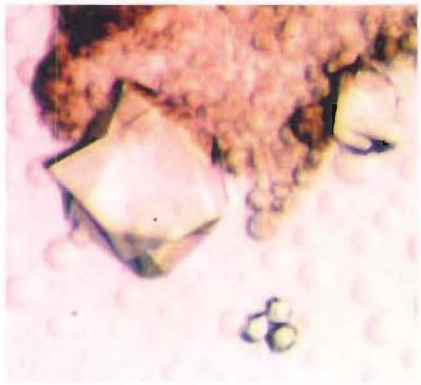

B

Crystals obtained by the hanging drop method diffracted to beyond 2.35–Å. Like the *E. coli* DHDPS structures previously reported, all of the mutant enzymes crystallised into the space group $P3_121$. They displayed catalytic activity, as judged by the coupled assay, even after one month if stored in their drops at 4°C. Diffraction data sets were processed and scaled using the programs DENZO[4] and SCALEPACK.[5]

Initial models for each mutant were obtained by rigid-body refinement using the structure of the wild-type enzyme (1DHP) obtained from the RCS Protein Data Bank, and were further refined using REFMAC5.[6] For this step, the 1DHP file was altered to place a glycine residue in the position of the mutation. The mutated residue was subsequently built and refined into the electron density. Manual model corrections were performed using the program O[7] and new models were refined with REFMAC5.[6] The final refinement rounds involved the placement of solvent molecules using the program ARP.[8] PROCHECK[9] was used as a guide for rebuilding at each refinement round and to check the quality of the final structures. Data collection and refinement statistics are summarized in Table 5.1.

Figure 5.2 *Ramachandran plot of both monomers in the asymmetric unit of DHDPS-Y107F generated by PROCHECK. The symbols are:* ▲ *= glycine;* ■ *= other residues;* ■ *= residues in disallowed regions. a, b, l, and p are allowed regions, while ~a, ~b, ~l, and ~p are generously allowed regions.*

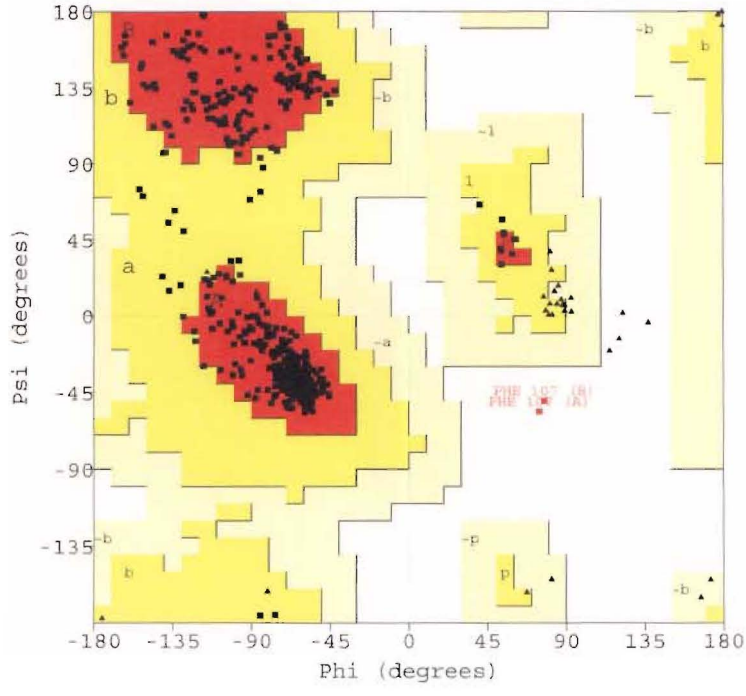

Table 5.1 *Data collection and refinement statistics.*

	DHDPS-Y133F	DHDPS-T44V	DHDPS-Y107F
Data Collection			
Number of images	151	171	120
Oscillation range (°)	0.5	0.5	0.5
Number of Crystals	1	2	1
Exposure Time (min)	60	60	45
Camera length (mm)	180	180, 200	180
Data Processing			
Resolution (outer shell)	2.32 (2.38–2.32)	2.30 (2.359–2.3)	2.35 (2.41–2.35)
Number of reflections (unique)	179116 (40716)	177303 (39811)	133787 (38813)
Completeness (outer shell)	99.7 (99.6)	94.3 (87.7)	98.6 (95.4)
Space Group	$P3_121$	$P3_121$	$P3_121$
Unit Cell[a] a,b,c (Å)	121.21, 121.21, 110.78	121.06, 121.06, 110.88	120.88, 120.88, 110.20
α,β,γ (°)	90, 90, 120	90, 90, 120	90, 90, 120
R_{merge}[b] (outer shell)	0.094 (0.318)	0.093 (0.32)	0.114 (0.285)
Refinement			
R_{Factor} (rigid-body)	0.445	0.453	0.497
R_{Free} (outer shell)[c]	0.2110 (0.25)	0.2134 (0.29)	0.2317 (0.24)
R_{Cryst} (outer shell)[d]	0.1781 (0.21)	0.1779 (0.22)	0.1970 (0.21)
Solvent molecules	270	322	231
Mean B-value	27.07	25.30	27.69
R.m.s. deviation			
Bond lengths (Å)	0.011	0.011	0.011
Bond angles (°)	1.318	1.38	1.313

[a] Wild-type space-group was $P3_121$ and cell dimensions were a = b = 122.41, c = 111.22.[1]
[b] R_{merge} = SUM (ABS(I – <I>)) / SUM (I).
[c] R_{free} based on 5% of the total reflections.
[d] $R_{cryst} = \sum\{|F_{obs}|-|F_{calc}|\} / \sum|F_{obs}|$.

The final models contained two chains in each asymmetric unit, where each chain had 292 amino acid residues. The tetramer was generated by crystallographic symmetry. The R_{Free} values were: 21.1% for DHDPS-Y133F, 21.3% for DHDPS-T44V, and 23.2% for DHDPS-Y107F. Upon examination of the Ramachandran plot[10] for each mutant, it was seen that all residues (aside from glycines) fell within the allowed regions, except for tyrosine or phenylalanine at position 107 (Figure 5.2). The mutant structures showed well-defined electron density about position 107 and the dihedral angles observed were similar to those of the wild-type structure.[1, 2] It has been proposed that the conformational strain at Y107 may be associated with function.[2]

The conformation of some residue side chains could not be resolved, either because there was no electron density to guide the rebuilding, or because the residues appeared to hold several different conformations—these side chains were deleted from the final PDB file. Without exception, the entire backbone of the proteins could be constructed from the carboxyl-terminal to the amino-terminal.

5.2.2 General features of the mutant DHDPS structures.

DHDPS from *E. coli* is a homotetramer[1] and the monomer is a $(\beta/\alpha)_8$-barrel with the active site situated deep within the centre of the β-barrel of each (Figures 1.5, 5.3 and 5.4). The quaternary structure reveals a dimer of dimers with strong connections between monomers A and D, in contrast to the weak connections between the dimers (Figure 5.3). Each monomer has two domains: an amino-terminal $(\beta/\alpha)_8$-barrel (residues 1–224) and a carboxyl-terminal α-helix domain (residues 225–292). None of the mutant structures showed any change in their quaternary or tertiary structures from that of the wild-type; this confirms that gross structural changes are not the cause of the attenuated function in each of the mutant enzymes. Elements of the tertiary structure are highlighted in Figure 5.4.

Figure 5.3 *Stereoplot showing the quaternary structure of DHDPS-Y133F. The monomers are labelled **A**, **B**, **C**, and **D**. **A/D** and **B/C** associate tightly to form dimers, which loosely associate to form the tetrameric structure of wild-type DHDPS. β-Sheets are coloured blue, α-helices are detailed in red and yellow, and the turns grey. This image was generated using MolMol[11] and the coordinates of DHDPS-Y133F.*

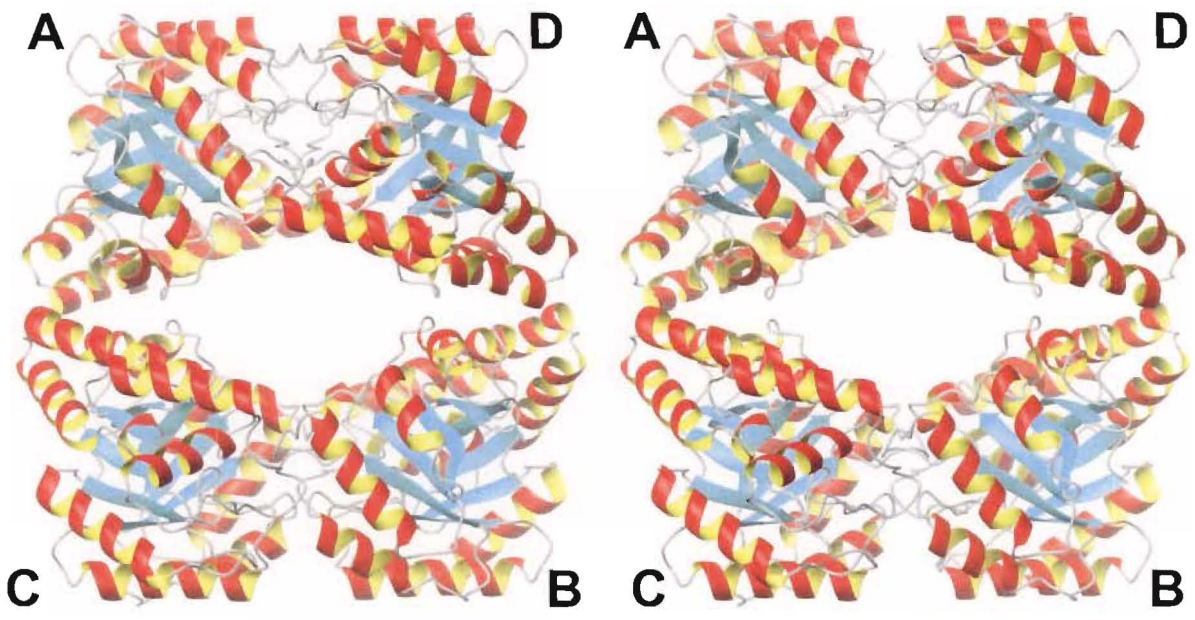

As described in earlier chapters, the active site of DHDPS, as defined by the position of K161, is situated within the β-barrel of each monomer (Figure 5.4). Y133 is positioned directly above this residue and T44 is hydrogen bonded to both Y133 and Y107. Y107 is supplied by the adjacent monomer in the dimer (**D**) to the active site of **A**. Each of these residues is highly conserved in all DHDPS enzymes known to date. Furthermore, Y133 is strictly conserved within the *N*-acetyl neuraminate lyase (NAL) subfamily of $(\beta/\alpha)_8$-proteins, of which DHDPS is a member. The NAL equivalent of residue Y133 in DHDPS is also proposed to play a central role in catalysis.[1, 12]

Figure 5.4 *Stereoplot describing the tertiary structure in the monomer. K161 (modelled in the CPK style) is seen in the centre of the barrel (light blue). The α-helices are coloured red and yellow and the turns are grey.*

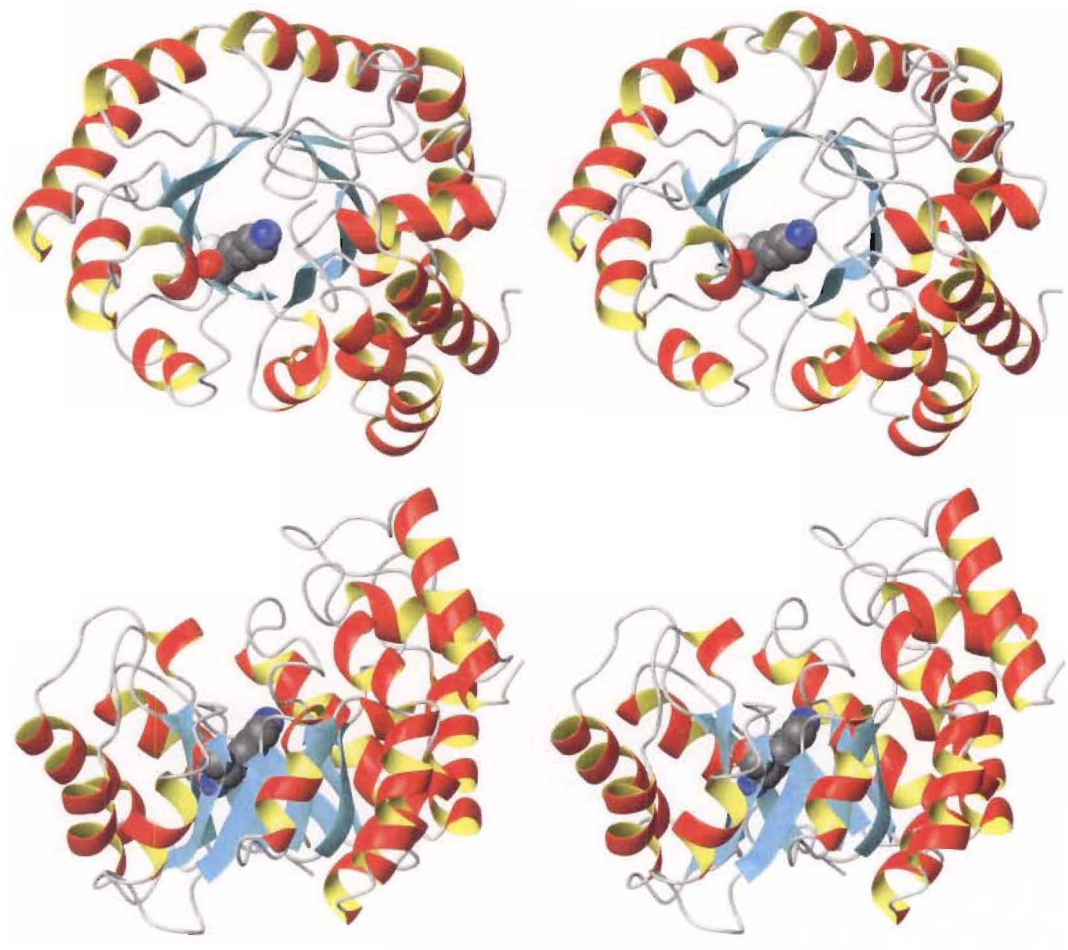

5.2.3 Structure/function relationships in the mutant DHDPS enzymes.

Y133F.

Y133 is considered central for DHDPS function because it is positioned adjacent to K161 which suggests a role in substrate binding and donation of a proton to the Schiff base hydroxyl (Table 5.2).[2] Its role in enamine formation is uncertain but it is well placed to coordinate the attacking amino group of (*S*)-ASA, which requires the loss of a proton subsequent to cyclisation.[2]

Table 5.2 *Comparison of key atomic distances within the proton-relay between the mutants and the wild-type.*

			Wild-type[a]	Y133F	T44V	Y107F
Protein distances (Å)	OH Y133	NT K161	3.4	-	3.7	3.8
	OH Y133	OH T44	3.6	-	-	2.7
	OH T44	OH Y107	2.7	2.7	-	-
	OH Y133	OH Y107	4.7	-	3.5	-

[a] As reported by Blickling *et al.*[2]

As presented in the last chapter, mutation of Y133 to a phenylalanine resulted in a marked loss of activity (Table 4.4)—consistent with the proposed role of this residue. A similar reduction of activity was seen when Y151 of *N*-acetyl neuraminate lyase (NAL) from *Clostridium perfringes*, whose role is proposed to be analogous to Y133 of DHDPS, was mutated to phenylalanine.[13] When the structure of DHDPS-Y133F was superimposed on the wild-type structure (r.m.s.d. = 0.274) there appeared little change in the active site (Figure 5.5 A). Whilst the main chain atoms of F133 are positioned similarly to the wild-type, the aromatic ring was twisted slightly. However, the hydroxyls of T44 and Y107 still appear to be hydrogen bonded, with a similar distance separating them compared to the wild-type (Table 5.2). The residual activity may result from surrogate activity of water, perhaps generated after Schiff base formation, or alternatively from the hydroxyl of T44, although this would require reorientation of the T44 side chain during catalysis. The structure of DHDPS-Y133F with bound substrates would be helpful in determining this.

Residue Y107 of DHDPS-Y133F still appears to be solvent accessible *via* a water channel exiting at the dimer interface (see below and Chapter six). However, unlike the wild-type, where a path of hydrogen bonds can be traced to the bulk solvent, the distance between the hydroxyl of Y107 and the nearest water is nearly 5–Å. If the proton-relay to bulk solvent does play an important part in catalysis then it appears that in DHDPS-Y133F the waters are disrupted in the channel.

In the *E. coli* NAL enzyme, the substrate carboxyl, which is in an analogous position to the carboxylate of the Schiff base in DHDPS, is thought to assist catalysis by acting as an active site base *via* Y151 (*E. coli* NAL numbering) to deprotonate a substrate hydroxyl during the

aldol cleavage.[14] It is unlikely that Y133 mediates an equivalent role in the catalytic reaction of DHDPS: unlike the analogous experiments with NAL, the crystal structures of DHDPS with substrate bound as a Schiff base do not show hydrogen-bonding between the carboxylate of the substrate and Y133.[2, 12, 15, 16] The structure of DHDPS-Y133F confirms the conclusions of Chapter four.

Furthermore, Y133 is well placed to bind the hydrate of (*S*)-ASA, donating a proton to the leaving hydroxyl. In later steps, the hydroxyl may bridge the acyclic adduct, after the aldol reaction, deprotonating the free amine, which allows subsequent attack to produce the cyclic product.

T44V.

All isoenzymes of DHDPS have a conserved loop at the end of β-sheet 3 consisting of the sequence G_{43}-T_{44}-T_{45}-G_{46}-E_{47} (*E. coli* numbering). This loop is located adjacent to K161 at the C-terminal end of the $(\beta/\alpha)_8$-barrel. Replacing the hydroxyl group of T44 with a methyl group resulted in severe attenuation of the enzyme's function. As shown in Chapter four, Table 4.4, only 0.1% maximal activity remained. Little change is seen in the K_m value of either pyruvate or (*S*)-ASA, which suggests no significant change in substrate binding, although the Michaelis-Menten constant for pyruvate is marginally lower than the wild-type.

The crystal structure of DHDPS-T44V showed that the side chain orientation of V44 is different to that of the wild-type (Figure 5.5 B). Whereas the hydroxyl of T44 can be seen to be hydrogen bonded to both tyrosine residues in the wild-type, the equivalent methyl group of V44 is orientated towards the active site. Overlaying the structures of DHDPS-T44V and wild-type showed that the conserved loop region, where V44 is situated, is not displaced. The r.m.s.d. for the overlay was 0.295. Intriguingly, Y133 is further away from the ε-nitrogen of K161 (3.7–Å) than seen in the wild-type (3.4–Å) and is closer to Y107 (3.5–Å) (Table 5.2). Apart from this movement, Y107 is orientated in the same manner as the wild-type.

For this mutation, the hydroxyl of Y107 was again accessible to bulk solvent through a number of hydrogen bonds to well ordered water molecules lining the channel leading to the lysine binding site (Figure 5.6). The distance between these waters is not more than 3–Å.

Figure 5.5 *Stereo view showing overlays of the active sites of wild-type (black) and mutant DHDPS structures (gold). Electron density covers the mutated residue in each image and is countered to 1σ. Shown from top to bottom: (A) DHDPS-Y133F; (B) DHDPS-T44V; (C) DHDPS-Y107F. These images were generated using O[7] and Molray.[17]*

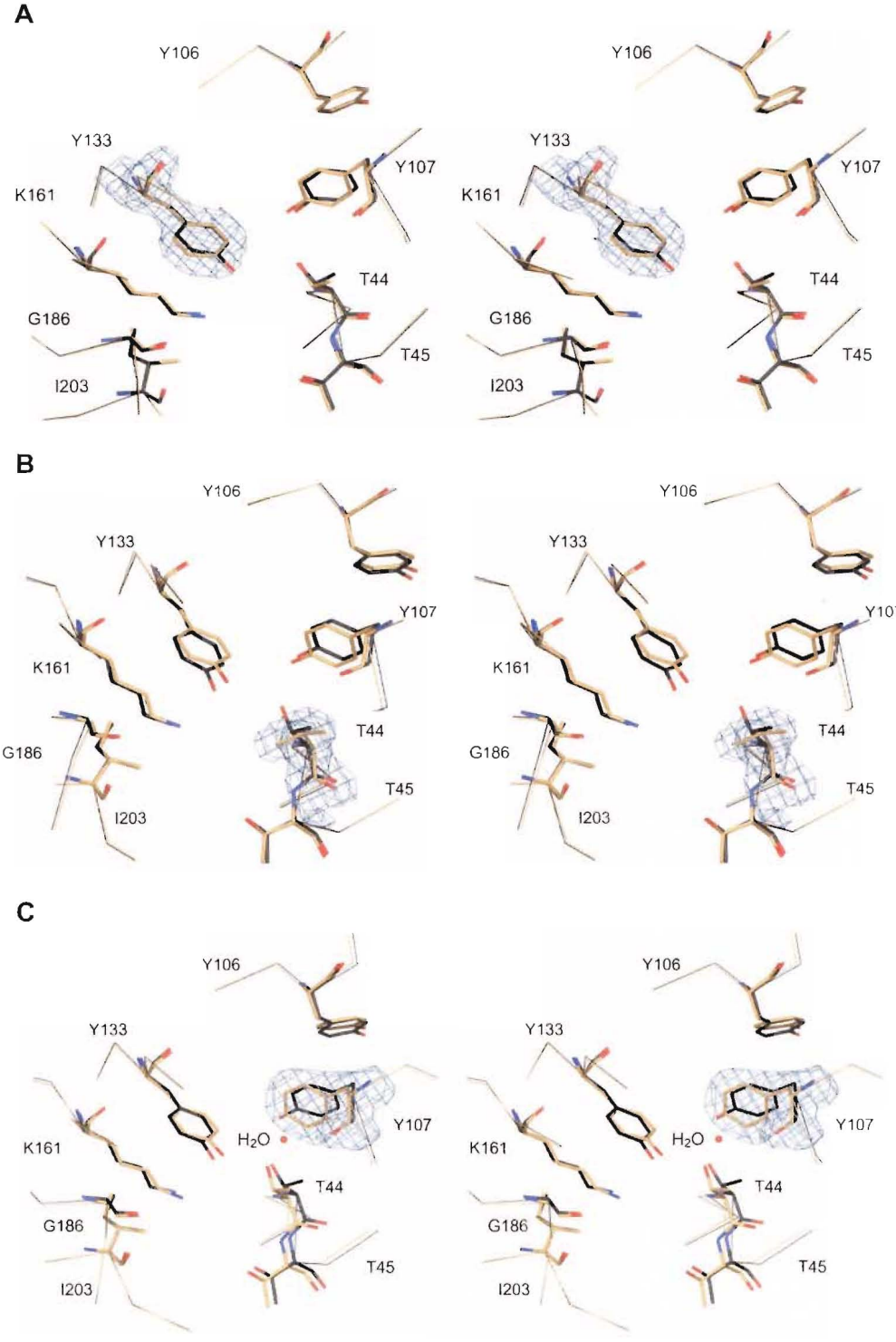

Figure 5.6 *Waters occupying the channel from the active site of DHDPS-T44V (as defined by K161 and Y133) leading to the lysine-binding site (as defined by Y106 and H53). The water molecules (red) are covered with electron density contoured to 1σ. The image was generated using O[7] and Molray.[17]*

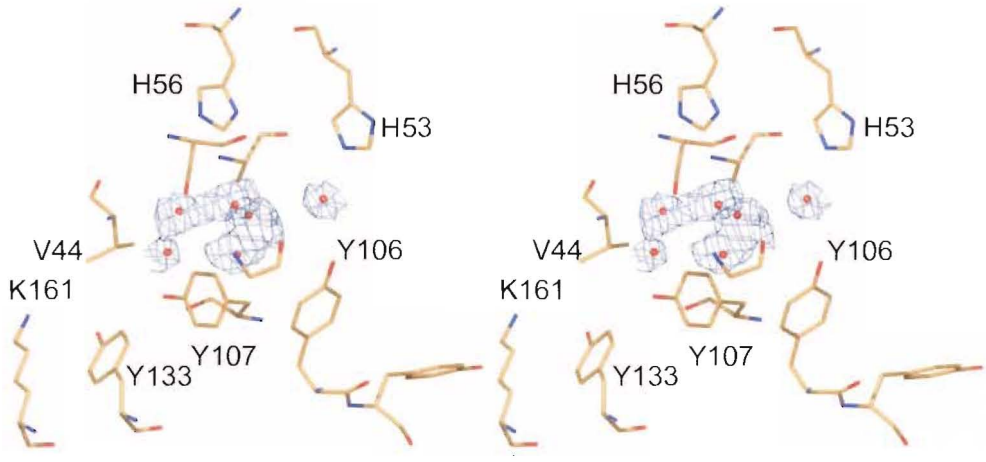

Y107F.

The role of Y107 in the kinetic mechanism has been speculative. As discussed above, this residue contributes to the tight binding interface within each of the dimers of DHDPS, reaching into the active site of the other monomer to form an aromatic stack with Y106 of the opposing monomer. Furthermore, the dihedral angles of Y107 fall into the disallowed region of the Ramachandran plot (Figure 5.2), suggesting some role in the enzyme's function.[2] Blickling *et al.*[2] hypothesised that this residue was the third in a catalytic triad involved in shuttling protons between the active site and bulk solvent.

Mutation to phenylalanine at this position resulted in a 10-fold loss of activity (Table 4.4). This, again, was consistent with the proton-relay mechanism, though the change in activity was not as great as in DHDPS-Y133F and DHDPS-T44V. It was hypothesised (Chapter four) that since the hydroxyl is solvent accessible, and that space might be created by its loss, a water molecule could replace the hydroxyl in the mechanism. When the crystal structure was examined it was found that a water molecule was indeed close to the hydroxyl of T44 (2.7–Å) and that it was in a position close to where the wild-type hydroxyl of Y107 would be (Figure 5.5 C). This may explain the greater than expected k_{cat} of DHDPS-Y107F when compared to the other mutations, because the active site of the mutant enzyme would still have access to solvent *via* the solvent channel (Figure 5.7). However, for DHDPS-Y107F,

it may be more difficult to shuttle protons to bulk solvent because the distances between some waters was greater than 3–Å and may explain the lower k_{cat} compared to the wild-type. The waters in the channel were well defined.

Figure 5.7 *Stereo view of waters occupying the channel from the active site (as defined by K161 and Y133) leading to the lysine-binding site of DHDPS-Y107F (as defined by Y106 and H53). The water molecules (red) are covered with electron density contoured to 1σ. The image was generated using O[7] and Molray.[17]*

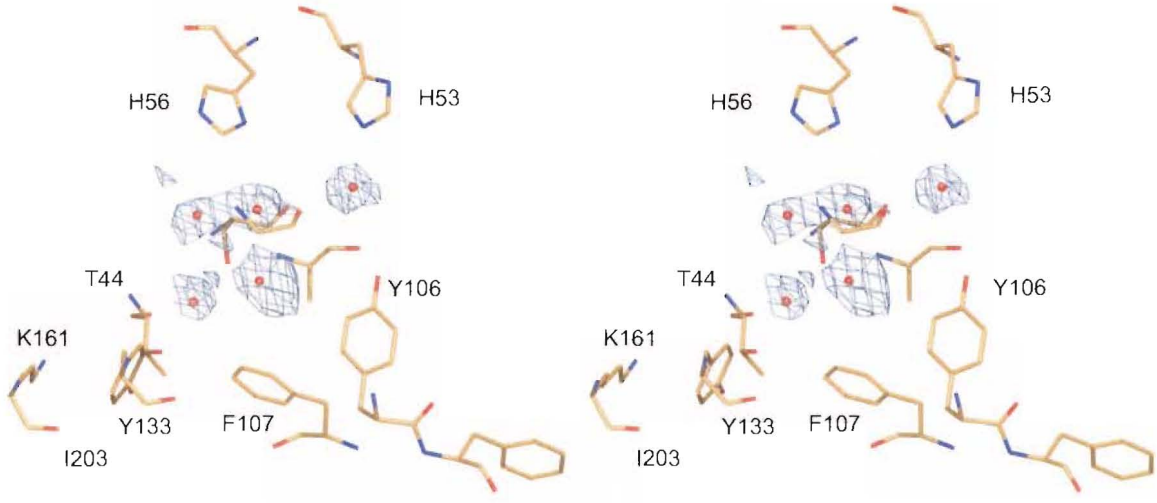

The structure of DHDPS-Y107F also showed that the phenylalanine at position 107 held a different orientation than the wild-type tyrosine (Figure 5.8). The aromatic ring of F107 in DHDPS-Y107F was twisted about 30° when overlaid with the wild-type Y107. This meant that the orientation in the aromatic stack (Y106 and Y107 in the wild-type[2]) also differed; the distance between the aromatic rings increased and their relative angle was twisted by about 23°. The loop between β-sheet 4 and helix 4, corresponding to residues 104 to 111, was in the same position as the wild-type. Nevertheless, the structure showed other subtle differences. The hydroxyl of Y133 was further from the ε-nitrogen of K161 (3.8–Å) due to its closer association with T44 (2.7–Å) (Table 5.2). The active site also contained some unexplained electron density bound to the active site lysine (Figure 5.9). The identity of this density is yet to be determined, but may explain the problematic mass spectral data.

Figure 5.8 *Image showing the difference in the aromatic stack of DHDPS-Y107F (gold) and wild-type (black). The electron density covers F107 of DHDPS-Y107F and is contoured to 1σ. The image was generated using O[7] and Molray.[17]*

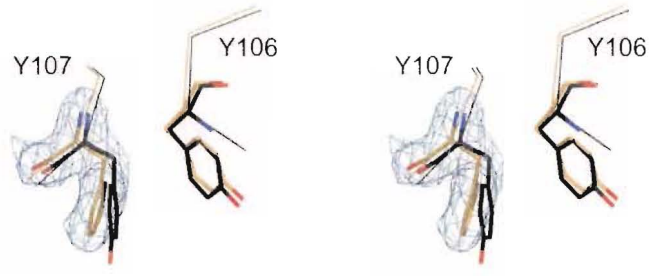

Figure 5.9 *Stereo image showing the unaccounted density in the active site of DHDPS-Y107F (purple). The density is contoured to 1σ. The image was generated using O[7] and Molray.[17]*

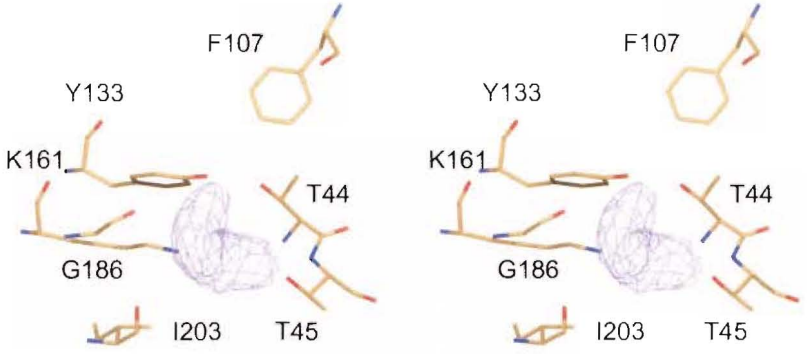

5.3 Summary.

The crystal structure for wild-type DHDPS has been published to 2.5–Å revealing a tetrameric molecule comprised of four $(\beta/\alpha)_8$-barrels, each containing one active site. Previous workers have hypothesized that the catalytic mechanism of the enzyme involves a catalytic triad of amino acid residues, which provide a proton shuttle to transport a proton from the active site to solvent. Site-directed mutagenesis was used to test this hypothesis by producing the mutants DHDPS-Y133F, DHDPS-T44V, and DHDPS-Y107F with subsequent analysis by steady state kinetics and X-ray crystallography. As shown in the last chapter, each mutant showed substantially reduced activity, consistent with the catalytic triad hypothesis.

The structure of each mutant was determined to at least 2.35–Å resolution, confirming the presence of the desired mutations. Despite the changes introduced into the enzyme, all the mutant enzymes crystallized in the same space group and with similar cell dimensions as the wild-type form. When compared to the wild-type enzyme, only minor differences in the structure are observed, meaning that the altered kinetic parameters seen in the mutants were not caused by gross structural changes.

The attenuated catalysis shown by DHDPS-Y133F is likely due to absence of an important active site general acid and base. These results suggest that the catalytic triad is indeed in operation in wild-type DHDPS.

5.4 Conclusions: tying together the kinetic and crystallographic experiments of the DHDPS mutants.

5.4.1 Schiff base and enamine formation: the first half reaction.

Pyruvate is the first substrate to bind to the active site. Two lines of evidence support this. Firstly, the Schiff base can be trapped by sodium borohydride[18]—in the absence of (*S*)-ASA—and observed by electrospray mass spectrometry[19] or X-ray crystallography.[2] Secondly, in the presence of DHDPS, proton exchange was observed between tritiated pyruvate and water, and that the rate of this process was dependant on the concentration of DHDPS.[20] However, Schiff base formation requires stabilisation of an oxyanion intermediate (Figure 5.10: step 1a), for which Y133 is suspected due to its proximity to the ε-nitrogen of K161.[2] A similar role is proposed for Y151 of *E. coli* NAL.[12, 13] For *E. coli* DHDPS, mutation of Y133 to phenylalanine attenuated catalytic function. The ensuing kinetic study showed that the specificity constant for pyruvate was nearly 25000 times decreased—consistent with the proposed role of this residue. Furthermore, the crystal structure of DHDPS-Y133F revealed, firstly, that the desired mutation was present, and secondly, that no significant changes in the arrangement of the active site had occurred. Thus, the dramatic decrease in k_{cat}/K_{mPyr} must be caused by the loss of the hydroxyl of Y133. This evidence builds a strong case for Y133 being an active site general acid/base. The involvement of Y133 in enamine formation (Figure 5.10: step 2), however, is tenuous because of the observed distance between the hydroxyl of Y133 and C3 of pyruvate in the Schiff base is large.[2]

T44 and Y107 are highly conserved in all DHDPS isoenzymes.[1] Furthermore, it has been shown that they are hydrogen-bonded to Y133. Blickling *et al.*[2] speculated that this motif was essential for the transfer of protons within the active site and to and from bulk solvent—a proton-relay. Before the mutagenesis study presented here, there was no evidence to suggest that such a motif was indeed in operation. The pathway for the later transfer is *via* a channel leading to the dimer interface. The mutation of T44 to valine and Y107 to phenylalanine, removing the hydroxyls, and thus the hydrogen bonds, resulted in marked decrease in activity—although the activity of DHDPS-Y107F was greater than expected. Moreover, mutation of T44 to serine resulted in only limited loss of function compared to the wild-type and DHDPS-T44V, presumably because the proton-relay was re-established.

Figure 5.10 *The proposed first half reaction of* E. coli *DHDPS.*

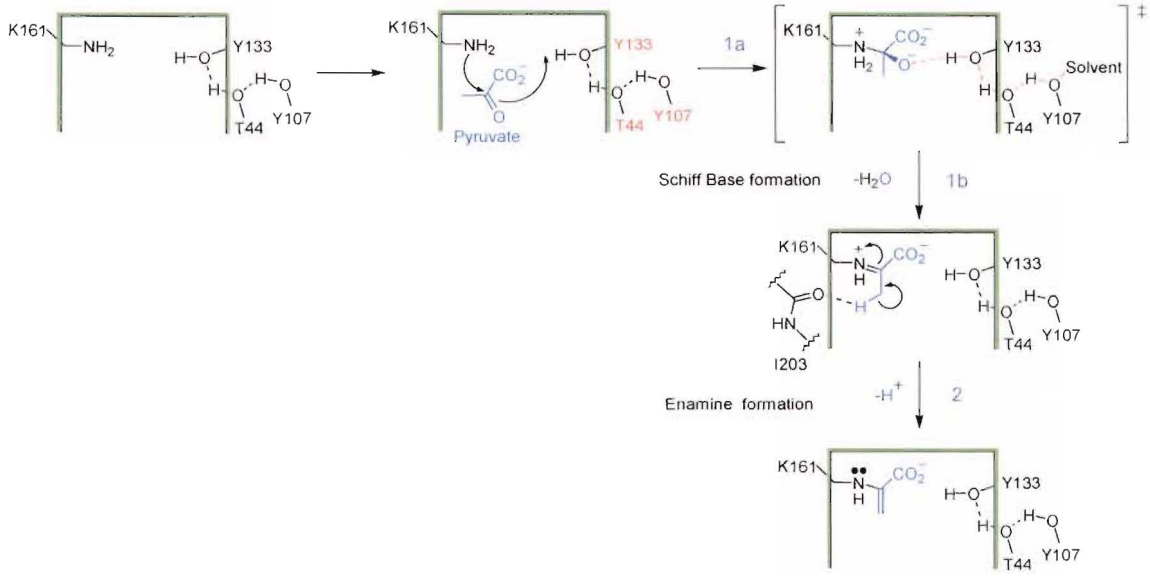

The crystal structure of DHDPS-T44V again showed that there was little change in the structure of the active site, although the side chain of V44 was reoriented, so the loss in activity is explained by the loss of the hydrogen bonding to Y133 and Y107. For the structure of DHDPS-Y107F, a water molecule was directly bonded to the hydroxyl of T44: thus, the high activity for this enzyme can be explained because the hydrogen-bonding link to bulk solvent was still connected. However, when examining the ordered waters in the channel of DHDPS-Y107F, it was observed that some water molecules were greater that 3–Å apart, which may explain the diminished activity compared to the wild-type. That the

specificity constant for pyruvate (k_{cat}/K_{mPyr}) was decreased in both DHDPS-Y107F and DHDPS-T44V suggests that both mutated residues are crucial in the first half reaction.

5.4.2 *Aldol reaction and cyclisation: the second half reaction.*

The second part of the reaction catalysed by DHDPS is the binding of (*S*)-ASA, followed by an aldol reaction, and cyclisation to release product (Figure 5.11). There is little evidence, beyond logic, to guide the exact determination of these steps—even the structure of (*S*)-ASA that binds to the enzyme is unknown (in Figure 5.11 it is assumed that the hydrate is the biologically relevant species).

Figure 5.11 *The proposed second half reaction of* E. coli *DHDPS.*

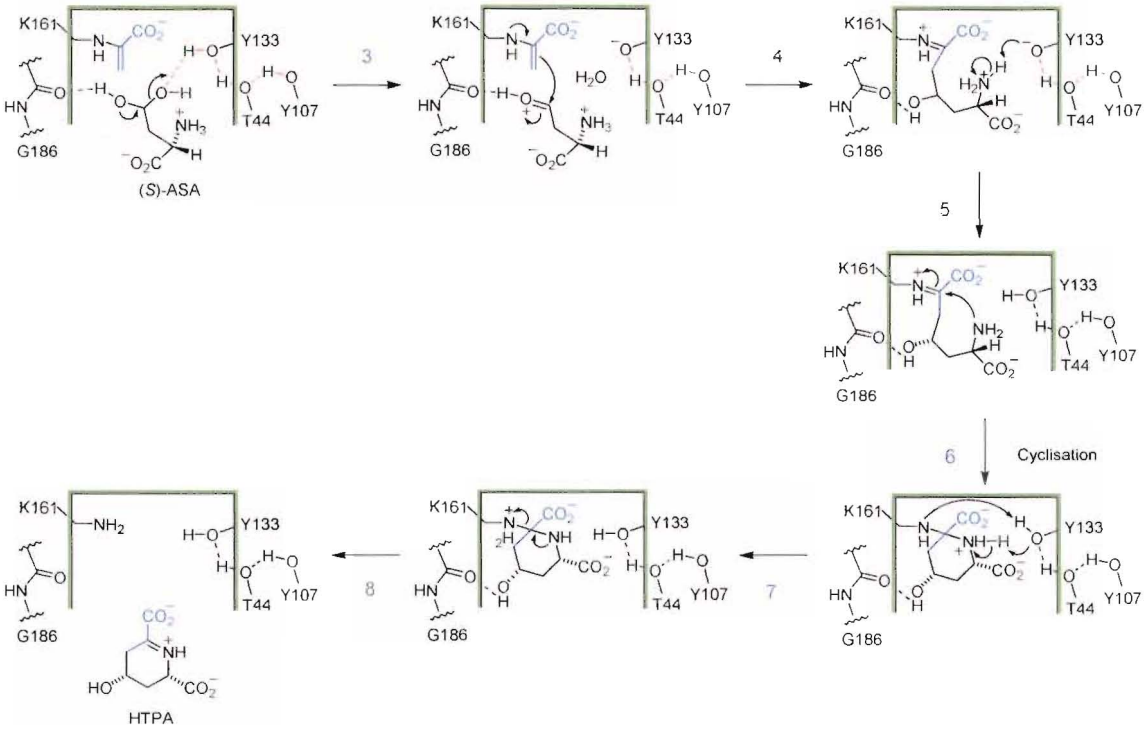

Blickling *et al.*[2] have described the structure of DHDPS with bound inhibitors that mimic the linear bound intermediate after the aldol reaction with (*S*)-ASA. The carboxyl of the (*S*)-ASA analogue was bound to R138, so this residue is likely to be involved in substrate binding. When R138 was mutated to histidine, DHDPS showed a large decrease in the specificity constant for (*S*)-ASA—this is consistent with a role in (*S*)-ASA binding. Mutations in the proton-relay also showed a decrease in this specificity constant so it must play some role in the second half reaction. Y133 is hypothesised to be involved in the

dehydration of the hydrate of (*S*)-ASA before the aldol reaction (Figure 5.11: steps 3 and 4), the abstraction of a proton from the amine prior to the cyclisation step (Figure 5.11: step 5), and finally acting as a proton shuttle within the active site to deprotonate amines as required (Figure 5.11: step 6).

In short, the mutagenic and crystallographic studies presented here suggest that a previously unrecognised motif, a proton shuttle, is necessary for the catalysis of the reaction mediated by DHDPS.

5.5 References.

1. Mirwaldt, C., Korndorfer, I. & Huber, R. (1995). The crystal structure of dihydrodipicolinate synthase from *Escherichia coli* at 2.5 Å resolution. *Journal of Molecular Biology*, **246**, 227-239.

2. Blickling, S., Renner, C., Laber, B., Pohlenz, H., Holak, T. A. & Huber, R. (1997). Reaction mechanism of *Escherichia coli* dihydrodipicolinate synthase investigated by X-ray crystallography and NMR spectroscopy. *Biochemistry*, **36**, 24-33.

3. Yugari, Y. & Gilvarg, C. (1965). The condensation step in diaminopimelate synthesis. *Journal of Biological Chemistry*, **240**, 4710-4716.

4. Murshudov, G., Vagin, A. & Dodson, E. (1997). Refinement of macromolecular structures by the maximum-likelihood method. *Acta Crystallographica Section D-Biological Crystallography*, **D53**, 240-255.

5. Otwinowski, Z. & Minor, W. (1997). Processing of X-ray diffraction data collected in oscillation mode. *Methods in Enzymology*, **276**, 307-326.

6. CCP4. (1994). The CCP4 suite: programs for protein crystallography. *Acta Crystallographica Section D-Biological Crystallography*, **D50**, 760-763.

7. Jones, T. & Kjeldgaard, M. (1997). Electron density map interpretation. *Methods in Enzymology*, **277**, 173-208.

8. Lamzin, V. S. & Wilson, K. S. (1997). Automated refinement for protein crystallography. *Methods in Enzymology*,**277** , 269-305.

9. Laskowsky, R., MacArthur, M., Moss, D. & Thornton, J. (1993). PROCHECK: a program to check the stereochemical quality of protein structures. *Journal of Applied Crystallography*, **26**, 283-291.

10. Ramachandran, G. & Sasisekharan, V. (1986). Conformation of polypeptides and proteins. *Advances in Protein Chemistry*, **23**, 283-437.

11. Koradi, R., Billeter, M. & Wüthrich, K. (1996). MOLMOL: a program for display and analysis of macromolecular structures. *Journal of Molecular Graphics*, **14**, 51-55.

12. Lawrence, M., Barbosa, J., Smith, B., Hall, N., Pilling, A., Ooi, H. & Marcuccio, S. (1997). Structure and mechanism of a sub-family of enzymes related to *N*-acetylneuraminate lyase. *Journal of Molecular Biology*, **266**, 381-399.

13. Kruger, D., Schauer, R. & Traving, C. (2001). Characterization and mutagenesis of the recombinant *N*-acetylneuraminate lyase from *Clostridium perfringens*. *European Journal of Biochemistry*, **268**, 3831-3839.

14. Smith, B. J., Lawrence, M. C. & Barbosa, J. A. R. G. (1999). Substrate-assisted catalysis in sialic acid aldolase. *Journal of Organic Chemistry*, **64**, 945-949.

15. Joerger, A. C., Mayer, S. & Fersht, A. (2003). Mimicking natural evolution *in vitro*: an *N*-acetylneuraminate lyase mutant with an increased dihydrodipicolinate synthase activity. *Proceedings of the National Academy of Sciences of the United States of America*, **100**, 5694-5699.

16. Blickling, S., Beisel, H., Bozic, D., Knablein, J., Laber, B. & Huber, R. (1998). Structure of dihydrodipicolinate synthase of *Nicotiana sylvestris* reveals novel quaternary structure. *Journal of Molecular Biology*, **274**, 608-621.

17. Harris, M. & Jones, T. A. (2001). Molray - a web interface between O and the POV-Ray ray tracer. *Acta Crystallographica Section D-Biological Crystallography*, **D57**, 1201-1203.

18. Shedlarski, J. (1970). The pyruvate-aspartic semialdehyde condensing enzyme of *Escherichia coli*. *Methods in Enzymology*, **17B**, 129-134.

19. Borthwick, E. B., Connel, S. J., Tudor, D. W., Robins, D. J., Shneier, A., Abell, C. & Coggins, J. R. (1995). *Escherichia coli* dihydrodipicolinate synthase: characterisation

of the imine intermediate and the product of bromopyruvate treatment by electrospray mass spectrometry. *Biochemical Journal*, **305**, 521-524.

20. Shedlarski, J. G. & Gilvarg, C. (1970). The pyruvate-aspartic semialdehyde condensing enzyme of *Escherichia coli*. *Journal of Biological Chemistry*, **245**, 1362-1373.

Chapter Six.

Investigating the mechanism of lysine inhibition in DHDPS.

6.1 Introduction.

DHDPS catalyses the committed step in (*S*)-lysine biosynthesis and is allosteric feedback regulated by (*S*)-lysine.[1] DHDPS isolated from plants is 20–100 times more sensitive to lysine inhibition compared to *E. coli*.[2] Mirwaldt *et al.*[3] divided DHDPS from different sources into three classes depending on their sensitivity with respect to lysine.

i Plant enzymes that are strongly inhibited by lysine (IC_{50} = 0.01–0.05 mM).[4-9]

ii Enzymes from Gram negative bacteria are only moderately inhibited, displaying an IC_{50} between 0.25 and 1.0 mM.[1, 10, 11]

iii DHDPS from Gram positive bacterial that appear weakly inhibited by lysine (IC_{50} > 10 mM).[12-17]

The mechanism by which lysine exerts regulatory control over DHDPS is unclear, although kinetic and structural studies support the proposal that lysine is an allosteric inhibitor.[1, 4, 12, 18-20] It was shown that two lysine molecules bind to the interface of the tight dimer of DHDPS (thus four lysines bind per tetramer) and that the lysine molecules interacted with each other, which may explain the observed cooperative binding.[19, 20] In *E. coli*, lysine binds in a bow conformation and makes numerous connections with residues of the monomer-monomer interface (Figure 6.1). The α-amino group hydrogen bonds to N80 and the backbone oxygen of A49, while the ε-amino group contacts H56, S48, and the main chain of G78. The carboxyl of lysine is bonded to the phenolic hydroxyl of Y106, which is twisted upon lysine binding.[19, 20]

Figure 6.1 *Stereoplot showing the lysine binding at the interface of wild-type DHDPS for the structures of Blickling* et al.[19] *This image was generated with O*[21] *and Molray,*[22] *using the coordinates of DHDPS determined by Blickling* et al.[19] *Lysine is coloured red.*

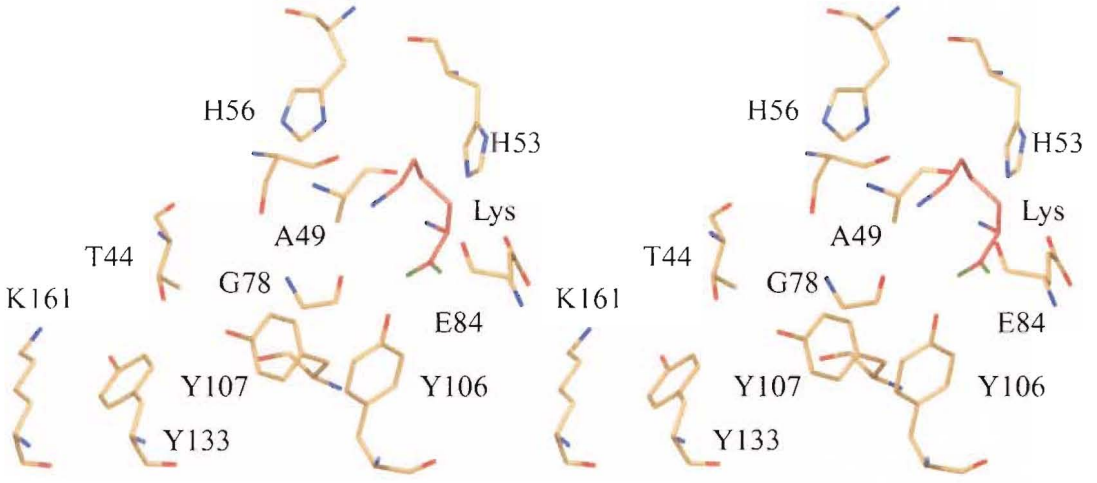

6.1.1 *The two proposed mechanisms of lysine inhibition.*

When the crystal structures of *E. coli* DHDPS with and without bound lysine were compared, there was surprisingly little difference.[19] One change noted was that the aromatic stack, comprising of Y106 and Y107, held an altered orientation when lysine was bound. Since Y107 formed part of the catalytic triad, and was reoriented when lysine was bound, it seemed that this might be one mechanism of inhibition.[19, 23] The second hypothesis was that Y107, upon reorientation, could affect the rigidity of R138, which binds the carboxyl of (*S*)-ASA. Blickling *et al.* argued that in the final steps of catalysis, cyclisation requires some flexibility in R138 in order to allow attack of the Schiff base.[19] Reduction in flexibility of R138 would, therefore, inhibit this step.

To understand the mechanism by which DHDPS is inhibited first requires an understanding of how the enzyme functions. Previous chapters have showed that the residues in the catalytic triad, and residue R138, are necessary for catalytic potency. These residues may also be important in lysine inhibition and the mutants designed in the last chapter were also analysed in the presence of (*S*)-lysine to probe their role in lysine inhibition of DHDPS.

Described herein are the results from kinetic studies of DHDPS-T44V, DHDPS-Y107F, DHDPS-Y133F, DHDPS-T44S, and DHDPS-R138H with respect to lysine inhibition. In addition, the crystal structure of DHDPS-T44V complexed with lysine has been solved and compared to the uncomplexed structure and the wild-type. A new mechanism of lysine inhibition is put forward.

6.2 Results.

Others have shown that (*S*)-lysine shows partial inhibition (approximately 80–90% inhibition) at very high (*S*)-lysine concentrations.[18, 24] The equations for the types of partial inhibition seen in the mutants and wild-type are shown in Equations **6** and **7** and Figures 6.2 and 6.3. These were discussed in Chapter three.

The initial rate data, again collected using the coupled assay, were analysed by Enzfitter to determine the correct model. The concentration of the other substrate was held constant at about its determined K_m. Data points were collected in duplicate or triplicate. As in Chapter four, the best fit was determined by the SIGMA value and standard error. The enzymes were purified as in Chapter four.

Figure 6.2 *Schematic representation of partial uncompetitive inhibition where* $V=k[E]_T$, $V'=k'[E]_T$, $K_i = k_3/k_{-3}$, *and* $K_s = k_1/k_{-1}$.[25, 26]

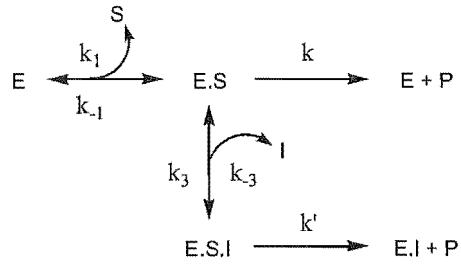

$$v = 1 / [1 / (VK_i + V'I)] [(I+K_i(1+K_s / S)] \qquad \text{Equation (6)}$$

Figure 6.3 *Schematic representation of partial non-competitive inhibition where* $V=k[E]_T$, $V'=k'[E]_T$, $K_i = k_4/k_{-4} = k_3/k_{-3}$, *and* $K_s = k_1/k_{-1} = k_2/k_{-2}$.[2, 5, 26]

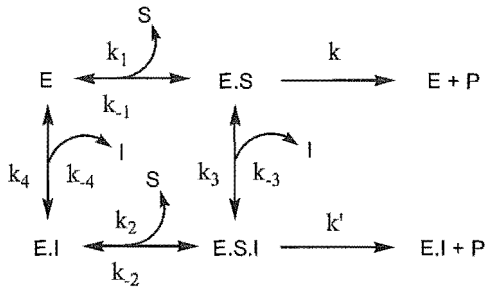

$$v = 1/\{[(K_i+I)/(VK_i+V'I)][1+K_s/S]\} \qquad \text{Equation (7)}$$

DHDPS-Y133F.

Because the mutation Y133F is not in the lysine-binding site, the K_i was expected to be unchanged. Although the K_i for lysine displayed by DHDPS-Y133F was similar to that of the wild-type, DHDPS-Y133F displayed different behaviour in regard to types of inhibition. With varying concentrations of (*S*)-ASA, DHDPS-Y133F exhibited partial non-competitive inhibition, the same type as shown by the wild-type. However, in contrast to the wild-type, when examined against varying pyruvate concentrations, DHDPS-Y133F also exhibited partial non-competitive inhibition. Table 6.1 shows the calculated parameters while the data and the fit are shown in Figures 6.4 and 6.5.

At saturating lysine concentrations, DHDPS-Y133F also behaved differently to the wild-type. As lysine approaches saturation, the wild-type was inhibited to 8% of the maximum rate in the absence of lysine. In Table 6.1 this is represented by α, which is the ratio of the maximal velocity in the absence of inhibitor (V) and the maximal velocity the presence of saturating inhibitor concentrations (V'). For DHDPS-Y133F, α approaches (63 ± 3)% (*vs.* pyruvate) and (73 ± 3)% (*vs.* (*S*)-ASA), reflecting the decreased affect of lysine on DHDPS-Y133F activity compared to the wild-type.

Table 6.1 *Inhibition of DHDPS mutant enzymes. In all cases the enzymes displayed partial inhibition with respect to lysine.*

	Wild-type [1]	Y133F	T44V	T44S	Y107F
Varied [Pyruvate]					
Inhibition Type	Uncompetitive	Non-competitive	Uncompetitive	Uncompetitive	Uncompetitive
V^{app} (units mg^{-1})[2, 3]	43 ± 2	0.35 ± 0.01	0.51 ± 0.01	11.7 ± 0.4	13 ± 0.3
V'^{app} (units mg^{-1})	3 ± 0.7	0.21 ± 0.01	0.14 ± 0.003	0.9 ± 0.1	0.6 ± 0.1
α (%)[4]	7 ± 2	63 ± 3	27 ± 1	8 ± 1	5 ± 1
K_{mPyr}^{app} (mM)	0.33 ± 0.03	6.5 ± 0.3	0.14 ± 0.1	0.5 ± 0.04	0.64 ± 0.04
K_i (mM)	0.22 ± 0.03	0.46 ± 0.09	0.17 ± 0.02	0.18 ± 0.02	0.13 ± 0.01
Varied [ASA]					
Inhibition Type	Non-competitive	Non-competitive	Non-competitive	Non-competitive	Non-competitive
V^{app} (units mg^{-1})	30 ± 1	0.45 ± 0.01	0.44 ± 0.01	14.4 ± 0.5	11 ± 0.3
V'^{app} (units mg^{-1})	2.3 ± 0.9	0.33 ± 0.01	0.16 ± 0.01	1.5 ± 0.2	0.9 ± 0.2
α (%)[4]	8 ± 3	73 ± 3	36 ± 2	10 ± 1	8 ± 2
K_{mASA}^{app} (mM)	0.10 ± 0.01	1.0 ± 0.05	0.06 ± 0.004	0.10 ± 0.01	0.09 ± 0.006
K_i (mM)	0.33 ± 0.05	0.17 ± 0.04	0.29 ± 0.04	0.3 ± 0.02	0.17 ± 0.01

[1] As determined in Chapter three.

[2] One unit is equal to 1 mM_{NADPH} min^{-1}.

[3] The protein concentration was determined using the method of Bradford.

[4] α is defined as the ratio of V, the maximal velocity in the absence of inhibitor, and V', the maximal velocity at saturating inhibitor concentration.

Figure 6.4 *Inhibition of DHDPS-Y133F by lysine with respect to pyruvate. DHDPS-Y133F showed partial non-competitive inhibition* vs. *pyruvate.* ***A*** *is a direct plot,* ***B*** *is the Eadie-Hofstee plot,* ***C*** *is the Lineweaver-Burk plot, and* ***D*** *is a percentage residual plot of the data* ($100\times(v_{obs}-v_{cal})/v_{cal}$). *Enzfitter generated all plots after non-linear regression of the data against the partial non-competitive model, Equation 7. The* R^2 *for the fit was 0.99 and p(F) was* $<<0.01$.

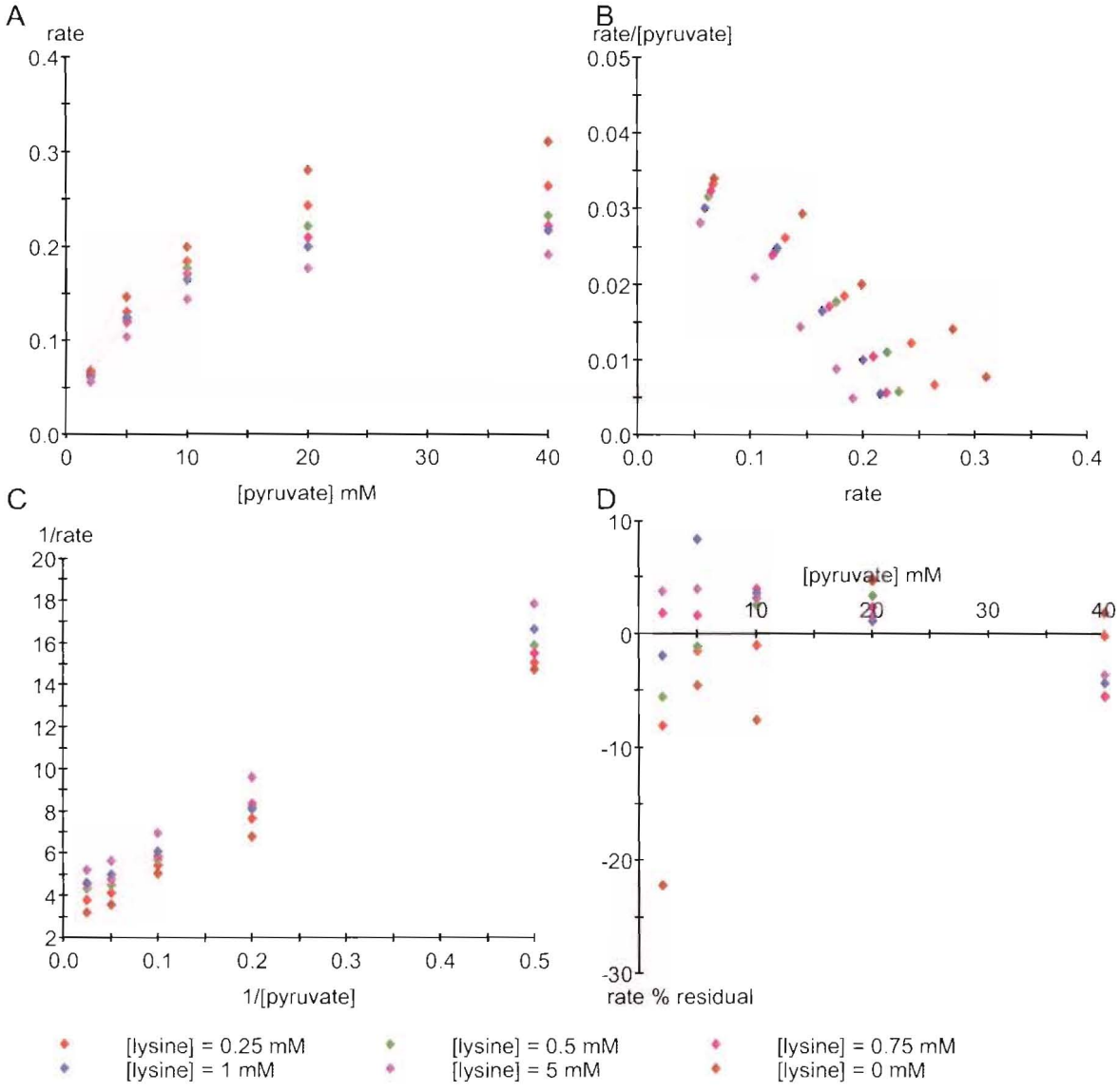

Figure 6.5 *Inhibition of DHDPS-Y133F by lysine with respect to (S)-ASA. DHDPS-Y133F showed partial non-competitive type of inhibition.* ***A*** *is a direct plot,* ***B*** *is the Eadie-Hofstee plot,* ***C*** *is the Lineweaver-Burk plot, and* ***D*** *is a percentage residual plot of the data* ($100\times(v_{obs}-v_{cal})/v_{cal}$). *Enzfitter generated all plots after non-linear regression of the data against the partial non-competitive model, Equation 7. The* R^2 *for the fit was 0.99 and p(F) was* $<<0.01$.

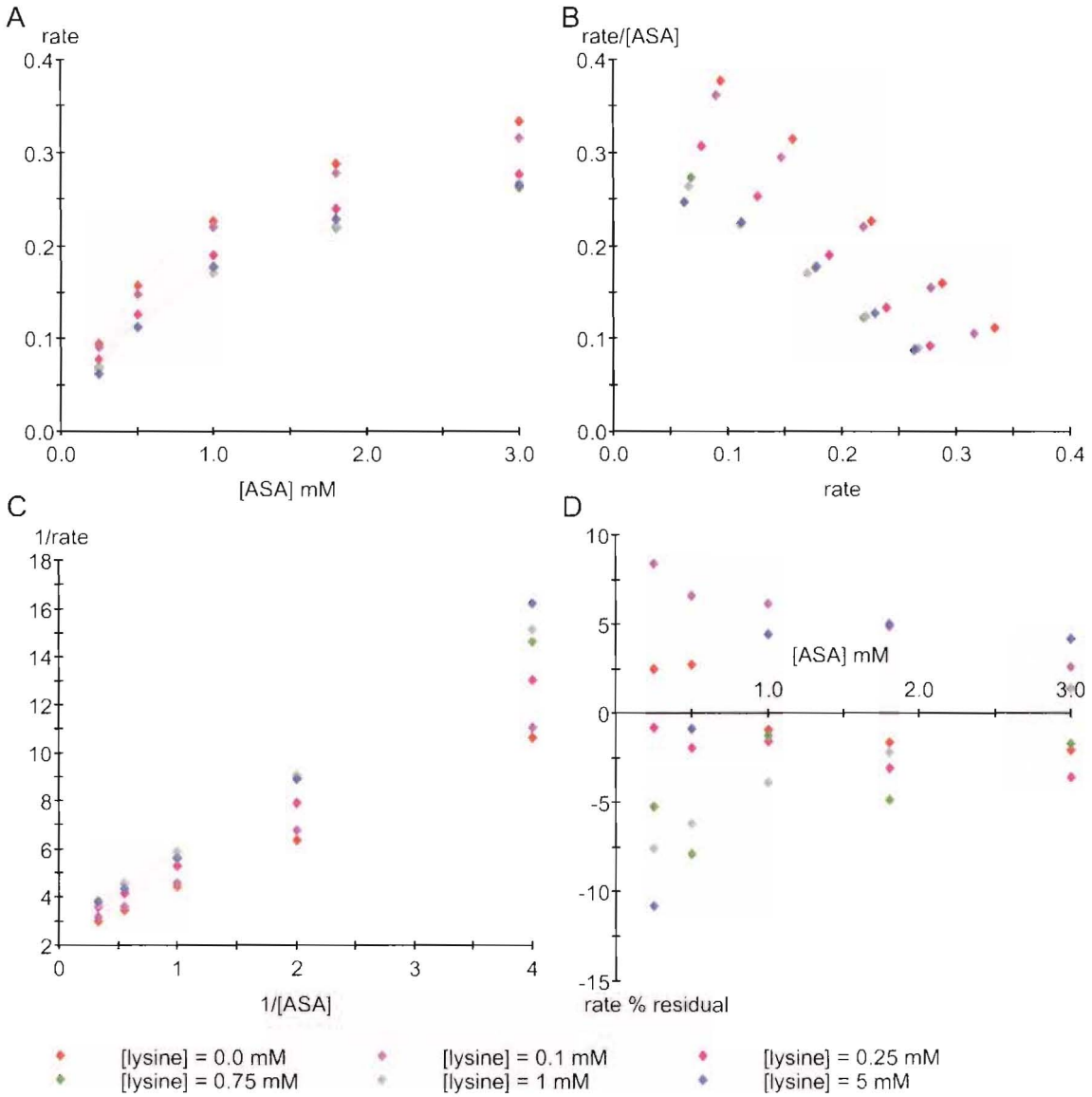

DHDPS-T44V.

In contrast to DHDPS-Y133F, DHDPS-T44V showed the same types of inhibition as the wild-type with respect to each substrate (Figures 6.6 and 6.7): when pyruvate was varied, partial uncompetitive inhibition was observed and when (*S*)-ASA was varied, partial non-competitive inhibition was observed. The K_i for lysine was (0.17 ± 0.09) mM with respect to pyruvate and (0.29 ± 0.04) mM with respect to (*S*)-ASA (Table 6.1). However, DHDPS-T44V showed an altered response when considering the degree of lysine inhibition. At saturating lysine concentrations DHDPS-T44V still showed DHDPS activity at 35% of maximal velocity. Thus, although the K_i was similar to DHDPS-Y133F and the wild-type, the affect of lysine was lessened.

In an effort to further examine the effect of lysine on this mutant, the crystal structure of DHDPS-T44V with bound lysine was solved. Crystals were grown by the hanging drop method as described in Chapter seven before being soaked with lysine (100 mM for 5 days at 21°C). Although the diffraction of many crystals was tested, none diffracted beyond 2.8–Å; this compares unfavourably with the same unligated crystals of DHDPS-T44V, which diffracted beyond 2.30–Å. The structure was solved using the same methods outlined in Chapter six but using the coordinates of DHDPS-T44V to initially solve the structure by rigid-body refinement. This yielded an R_{Factor} of 0.44, which minimised to a R_{Cryst} of 0.197 by alternate modification in O[21] and refinement with REFMAC5.[27] The final R_{Free} was 0.232. The final structure was checked with PROCHECK, which showed that, except for Y107, all residues lay in the allowed region of the Ramachandran plot. Table 6.2 summarises the data collection and refinement statistics.

Figure 6.6 *Inhibition of DHDPS-T44V by lysine with respect to pyruvate. DHDPS-T44V showed partial uncompetitive type of inhibition* vs. *pyruvate.* ***A*** *is a direct plot,* ***B*** *is the Eadie-Hofstee plot,* ***C*** *is the Lineweaver-Burk plot, and* ***D*** *is a percentage residual plot of the data* ($100\times(v_{obs}-v_{cal})/v_{cal}$). *Enzfitter generated all plots after non-linear regression of the data against the partial uncompetitive model, Equation* ***6***. *The* R^2 *for the fit was 0.99 and p(F) was* < 0.01.

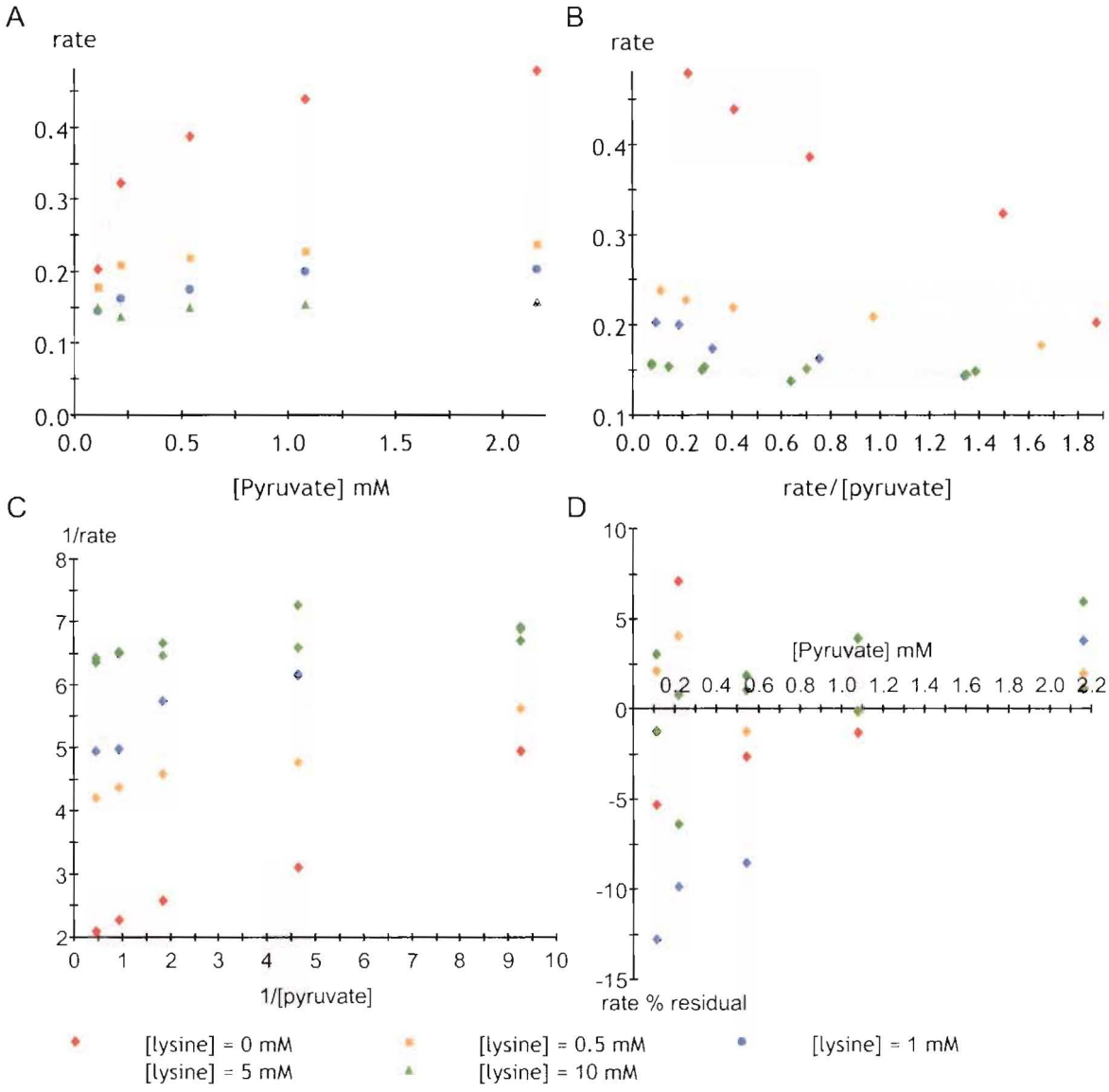

Figure 6.7 *Inhibition of DHDPS-T44V by lysine with respect to (S)-ASA. DHDPS-T44V showed partial non-competitive inhibition* vs. *(S)-ASA.* ***A*** *is a direct plot,* ***B*** *is the Eadie-Hofstee plot,* ***C*** *is the Lineweaver-Burk plot, and* ***D*** *is a percentage residual plot of the data* $(100\times(v_{obs}-v_{cal})/v_{cal})$. *Enzfitter generated all plots after non-linear regression of the data against the partial non-competitive model, Equation 7. The* R^2 *for the fit was 0.99 and p(F) was <<0.01.*

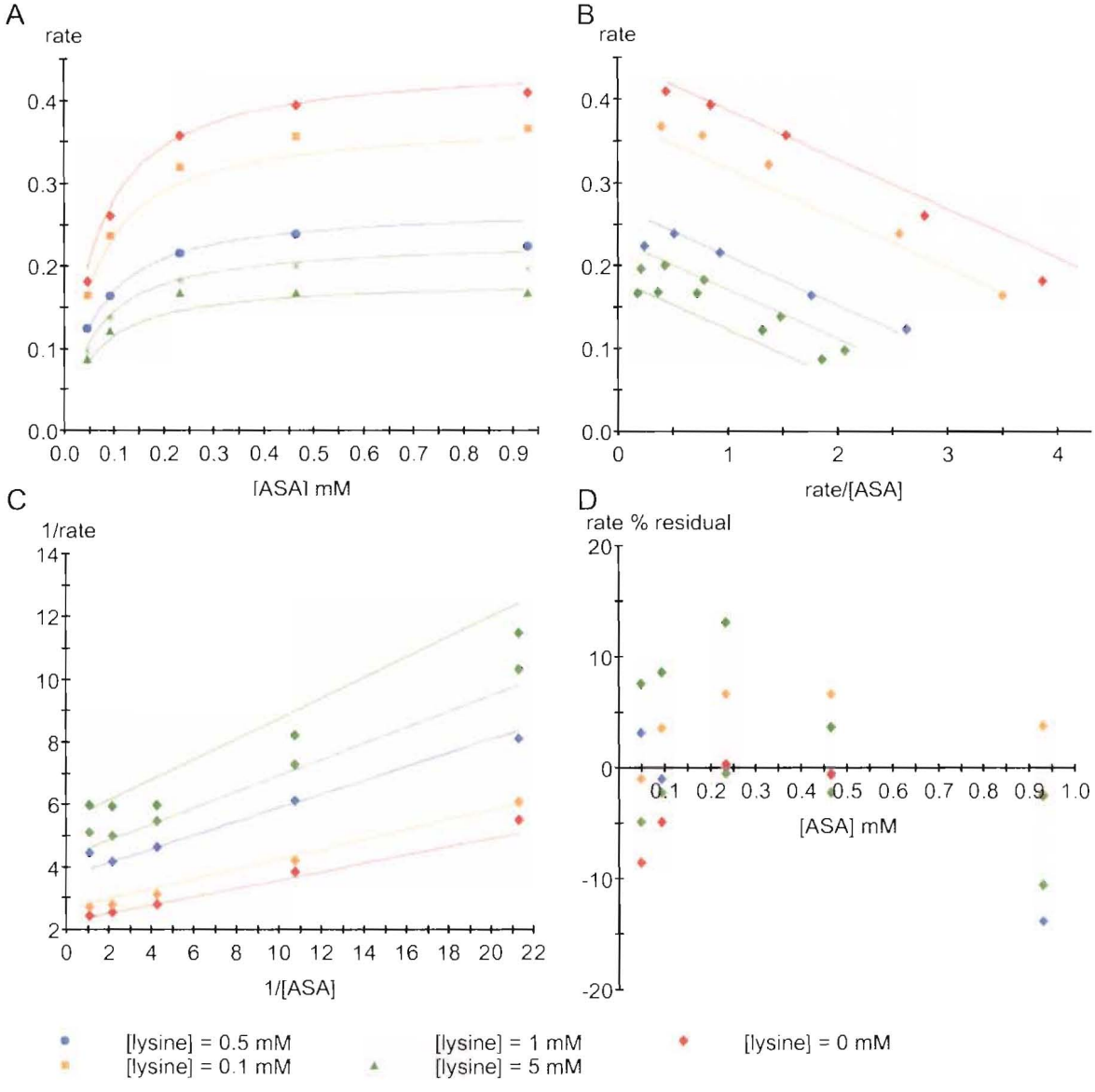

Table 6.2 *Crystal structure statistics for the DHDPS-T44V, complexed with lysine.*

	DHDPS-T44V + lysine
Data collection	
Number of images	124
Oscillation range (°)	0.5
Number of Crystals	1
Exposure Time (min)	60
Camera length (mm)	250
Data processing	
Resolution (outer shell)	2.8 (2.87–2.8)
Number of reflections (Unique)	48460 (19271)
Completeness (outer shell)	0.829 (0.504)
Space group	$P3_121$
Unit cell a,b,c (Å)	121.092, 121. 092, 109.441
α,β,γ (°)	90, 90, 120
R_{merge}[1] (outer shell)	0.082 (0.27)
Refinement	
R_{Fact} (rigid-body)	0.44
R_{Free} (outer shell)[2]	0.2316
R_{Cryst} (outer shell)[3]	0.1975
Solvent molecules	65
Mean B value (Å^2)	32.93
r.m.s. deviation	
Bond lengths (Å)	0.013
Bond angles (°)	1.421

[1] R_{Merge} = SUM (ABS(I – <I>)) / SUM (I).
[2] R_{Free} based on 5% of the total refections.
[3] $R_{Cryst} = \Sigma\{|F_{obs}|-|F_{calc}|\} / \Sigma|F_{obs}|$.

As with the wild-type complexed with lysine, positive electron density was observed at the interface of the monomers in the tight dimer, indicating that lysine was indeed bound.[19] (*S*)-Lysine was found to have a similar orientation when compared to the structure of wild-type DHDPS complexed with (*S*)-lysine and makes the same connections within the lysine-binding pocket, except that the ε-nitrogen was orientated differently and contacted the main chain oxygen of S48 instead of H53 in the wild-type. This can be seen in Figure 6.8 and Table 6.3. In the unligated structure of DHDPS-T44V, the side chain of N80 was partially removed because its conformation could not be determined from the electron density. However, in the structure with complexed lysine, N80 was easily determined and found to contact the α-amino group of lysine (Figure 6.8).

Figure 6.8 *An overlay of the lysine-binding pocket of DHDPS-T44V with (gold) and without (black) bound lysine. The r.m.s.d. for the overlay of the α-carbon trace for the monomers was 0.207. The electron density covers the complexed lysine and is contoured to a level of 1σ. This image was generated with O*[21] *and Molray.*[22] *using the coordinates of DHDPS-T44V with and without bound lysine*

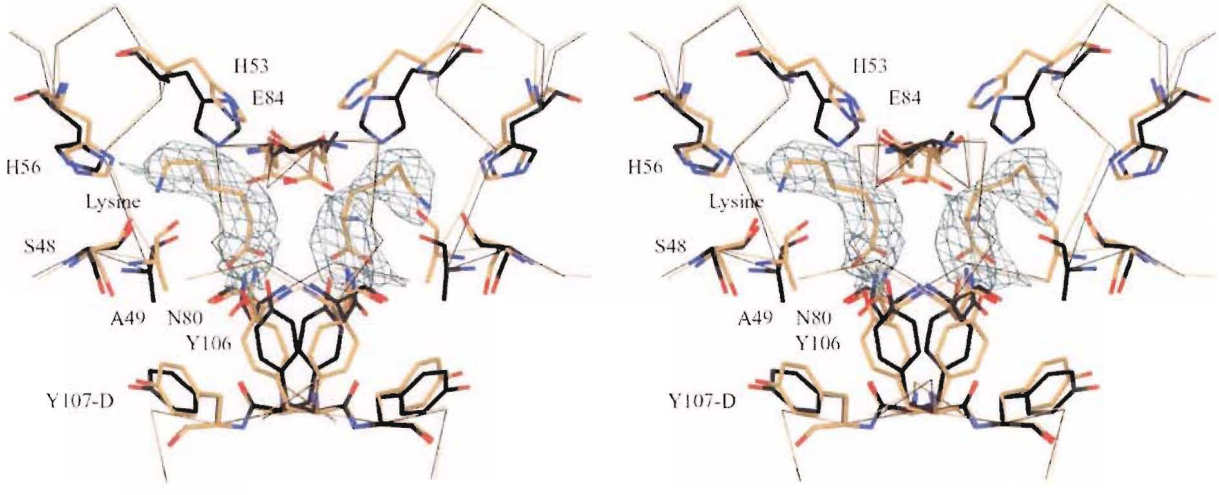

Overall, the refined structure with lysine was very similar to that of DHDPS-T44V, although there were some changes. When lysine binds, Y106 moves towards the carboxyl of lysine and thus the aromatic stack, comprising Y106 and Y107, holds an altered conformation.

These same movements are seen in comparisons between the wild-type complexed with and without lysine. The connections that lysine makes to the interface are shown in Table 6.3. R138, which in the wild-type becomes rigid upon the binding of lysine, shows the opposite effect in DHDPS-T44V: the B-factor for this residue is noticeably increased indicating that it is now more flexible when lysine is bound. Moreover, R138 in each of the mutant structures is bonded differently to the strained main chain of Y107. In Blickling's structures, the δ-nitrogen is bound to the main chain oxygen of Y107, but in the mutant structures discussed here, and in Chapter five, the ε-nitrogen is bound to the main chain of Y107. Electron density was well resolved about this residue.

Table 6.3 *Connections and distances between (S)-lysine and DHDPS-T44V*

(*S*)-lysine	Residue	Distance (Å)
α-carboxyl 1	–OH Y106	2.45
α -carboxyl 2	$-NH_2$ N80 (monomer D)‡	2.84
α -NH_2	main =O A49	2.86
α -NH_2	=O N80	2.92
α -NH_2	=O E84	2.46
ε- NH_2	–NH H56	3.62
ε - NH_2	main =O S48	2.63

‡ N80 cross-links the monomers in the dimer *via* the lysine inhibitor.

Most changes in the DHDPS-T44V structure were observed in the lysine-binding site, although there were some differences in the active site of DHDPS-T44V (Figure 6.8). Notably, the hydroxyl of Y133 moved closer to the ε-nitrogen of K161 (from 3.7–Å in the wild-type to 3.5–Å in DHDPS-T44V) and, consequently, the distance between the hydroxyl of Y107 and Y133 increased from 3.5–Å to 4.8–Å. The side chain of V44 was also slightly twisted. Other residues in the active site showed little or no observable change (Figure 6.9).

Figure 6.9 *An overlay of the active site of DHDPS-T44V with (gold) and without (black) lysine. The thin trace in both images is the α-carbon trace about the displayed residues. This was included to highlight movement about these residues. The image was generated with O*[21] *and Molray*[22] *using the coordinates of DHDPS-T44V with and without lysine.*

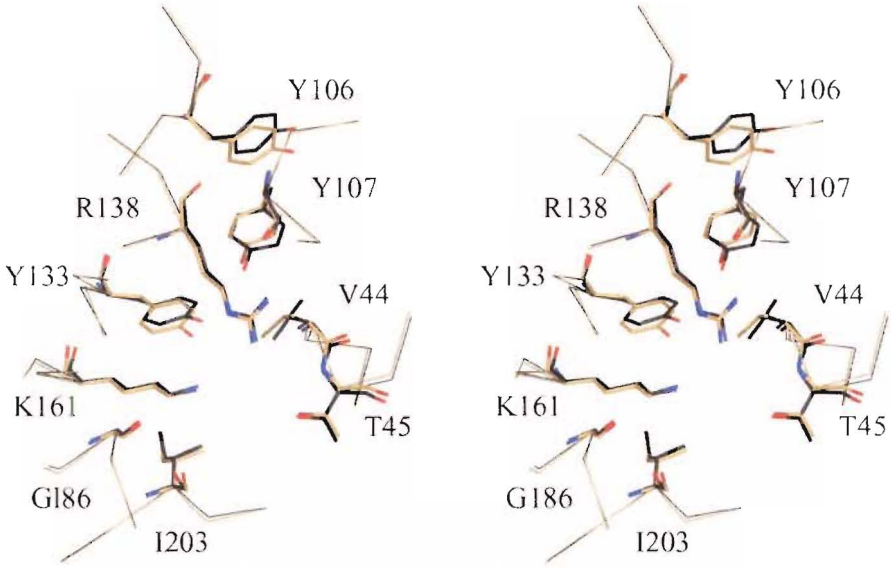

In order to see if lysine binding induces changes in the conformation of the tetramer, monomer A of DHDPS-T44V with and without lysine was overlaid (Figure 6.10). If the quaternary structure had changed then monomer C, across from monomer A, should be visibly displaced. The r.m.s.d. for the overlay was 0.203–Å. It can be seen in Figure 6.10 that monomer C is displaced but when the distances were determined, the α-carbons were less than 1–Å apart. Thus, no significant quaternary change had occurred.

Figure 6.10 *An overlay of monomer A in DHDPS-T44V with and without lysine. DHDPS-T44V with bound lysine is shown in gold and without lysine in black. The image was generated with O*[21] *and Molray*[22] *using the coordinates of DHDPS-T44V with and without lysine*

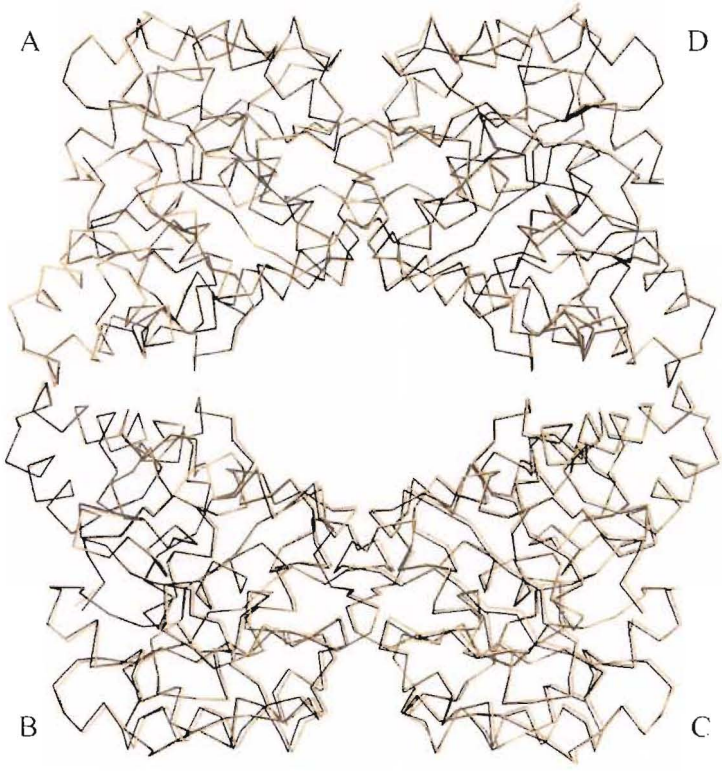

DHDPS-T44S.

When DHDPS-T44S was tested for lysine inhibition it was found that it behaved in an entirely analogous fashion to the wild-type. Not only were the same types of inhibition displayed, at saturating inhibitor levels, DHDPS-T44S was about 91% inhibited, as with the wild-type (Table 6.1). The K_m values were consistent with those calculated for DHDPS-T44S in the last chapter (K_{mASA}^{app} was (0.1 ± 0.01) mM and the K_{mPyr}^{app} was (0.5 ± 0.04) mM) and the K_i values were also unchanged with the wild type. The data and fits can be viewed in Figures 6.11 and 6.12.

Figure 6.11 *Inhibition of DHDPS-T44S by lysine with respect to pyruvate. DHDPS-T44S showed partial uncompetitive inhibition* vs. *pyruvate.* ***A*** *is a direct plot,* ***B*** *is the Eadie-Hofstee plot,* ***C*** *is the Lineweaver-Burk plot, and* ***D*** *is a percentage residual plot of the data* ($100\times(v_{obs}-v_{cal})/v_{cal}$). *Enzfitter generated all plots after non-linear regression of the data against the partial uncompetitive model, Equation* ***6***. *The* R^2 *for the fit was 0.99 and p(F) was* $<<0.01$.

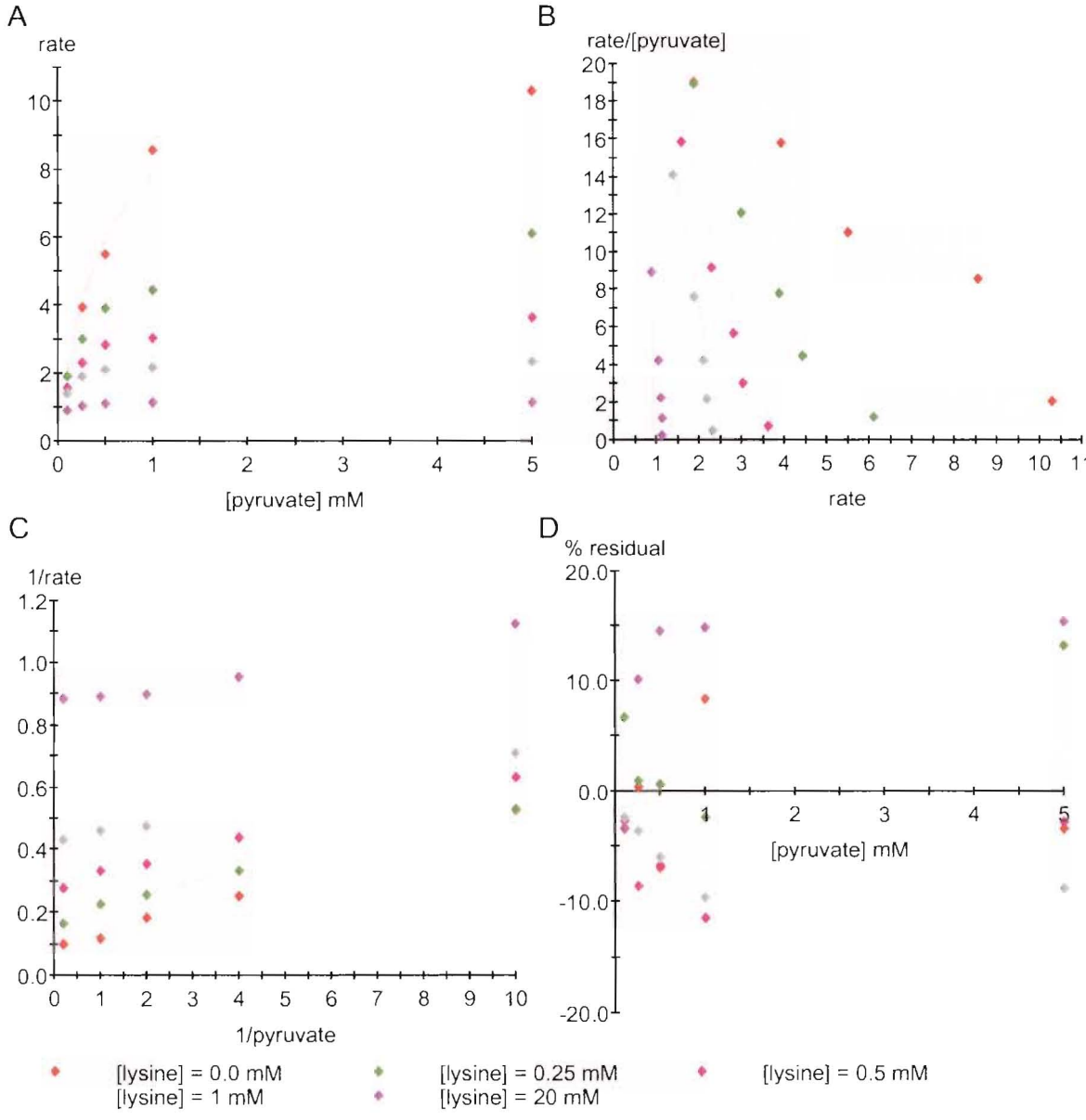

Figure 6.12 *Inhibition of DHDPS-T44S by lysine with respect to (S)-ASA. DHDPS-T44S showed partial non-competitive inhibition* vs. *(S)-ASA.* ***A*** *is a direct plot,* ***B*** *is the Eadie-Hofstee plot,* ***C*** *is the Lineweaver-Burk plot, and* ***D*** *is a percentage residual plot of the data* $(100\times(v_{obs}-v_{cal})/v_{cal})$. *Enzfitter generated all plots after non-linear regression of the data against the partial non-competitive model, Equation 7. The* R^2 *for the fit was 0.99 and p(F) was* $<<0.01$.

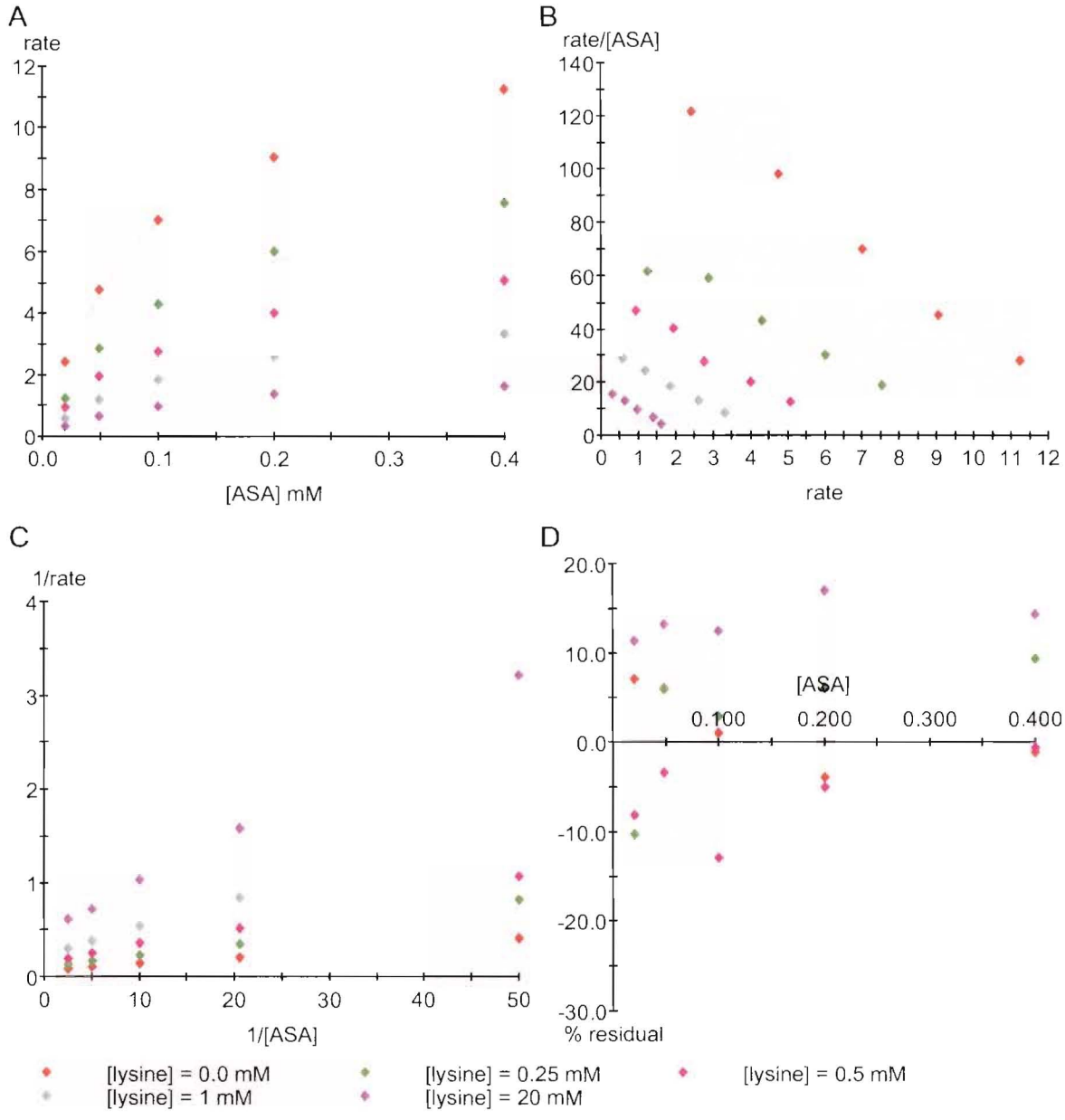

DHDPS-Y107F.

In the presence of lysine, DHDPS-Y107F also showed identical behaviour to the wild-type with respect to each substrate. The K_i was the marginally lower to that the wild-type with respect to both (*S*)-ASA and pyruvate, while α approached the same values (within error) to the wild-type. Thus, even though DHDPS-Y107F showed decreased activity, this mutation exhibits the same inhibitory properties as the wild-type (Figures 6.13 and 6.14).

Figure 6.13 *Inhibition of DHDPS-Y107F by lysine with respect to pyruvate. DHDPS-Y107F showed partial uncompetitive inhibition* vs. *pyruvate.* ***A*** *is a direct plot,* ***B*** *is the Eadie-Hofstee plot,* ***C*** *is the Lineweaver-Burk plot, and* ***D*** *is a percentage residual plot of the data* ($100\times(v_{obs}-v_{cal})/v_{cal}$). *Enzfitter generated all plots after non-linear regression of the data against the partial uncompetitive model, Equation* ***6***. *The* R^2 *for the fit was 0.99 and p(F) was* $<<0.01$.

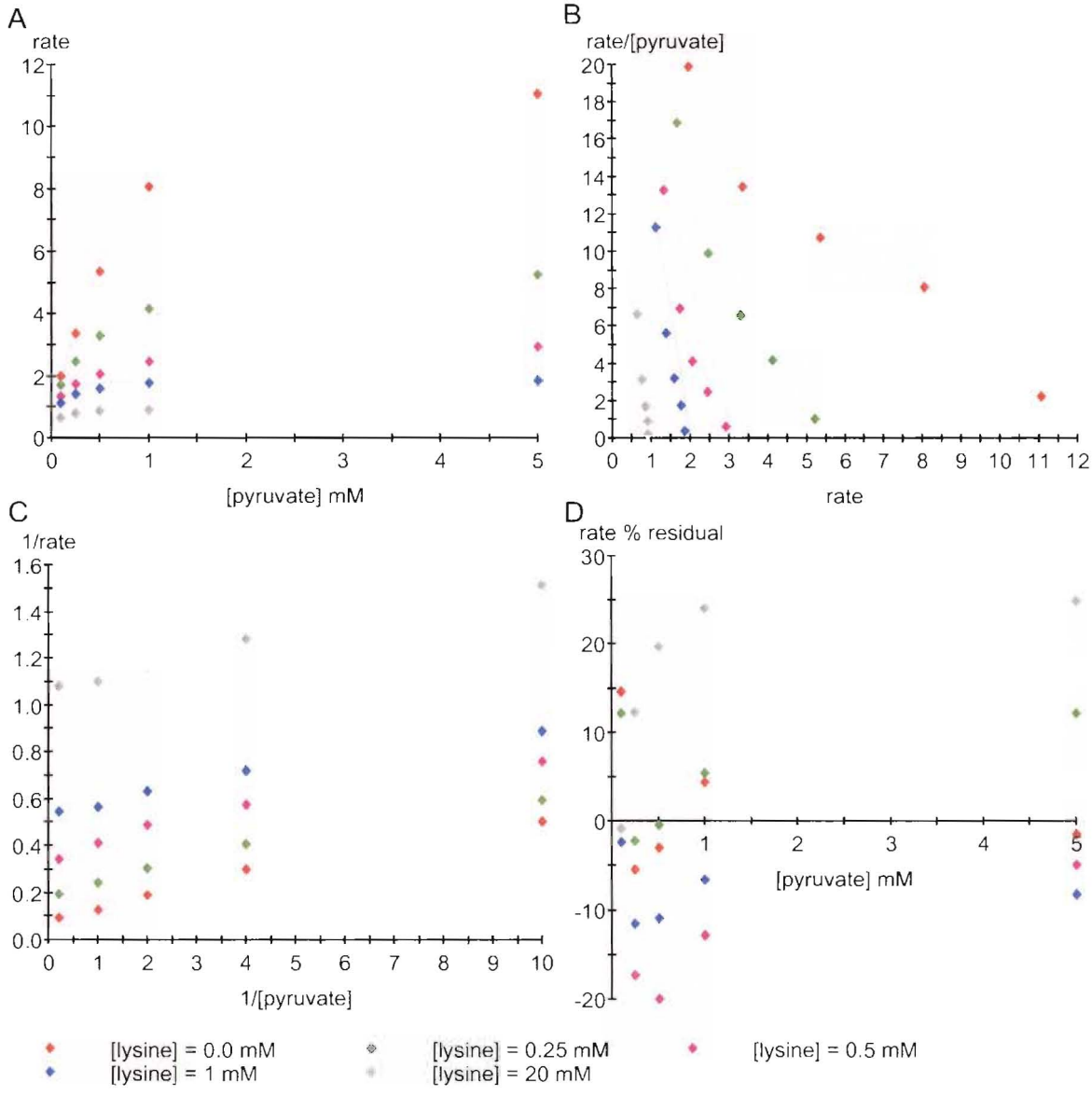

Figure 6.14 *Inhibition of DHDPS-Y107F by lysine with respect to (S)-ASA. DHDPS-Y1707F showed partial non-competitive inhibition* vs. *(S)-ASA.* ***A*** *is a direct plot,* ***B*** *is the Eadie-Hofstee plot,* ***C*** *is the Lineweaver-Burk plot, and* ***D*** *is a percentage residual plot of the data* ($100\times(v_{obs}-v_{cal})/v_{cal}$). *Enzfitter generated all plots after non-linear regression of the data against the partial non-competitive model, Equation 7. The* R^2 *for the fit was 0.99 and p(F) was* $<<0.01$.

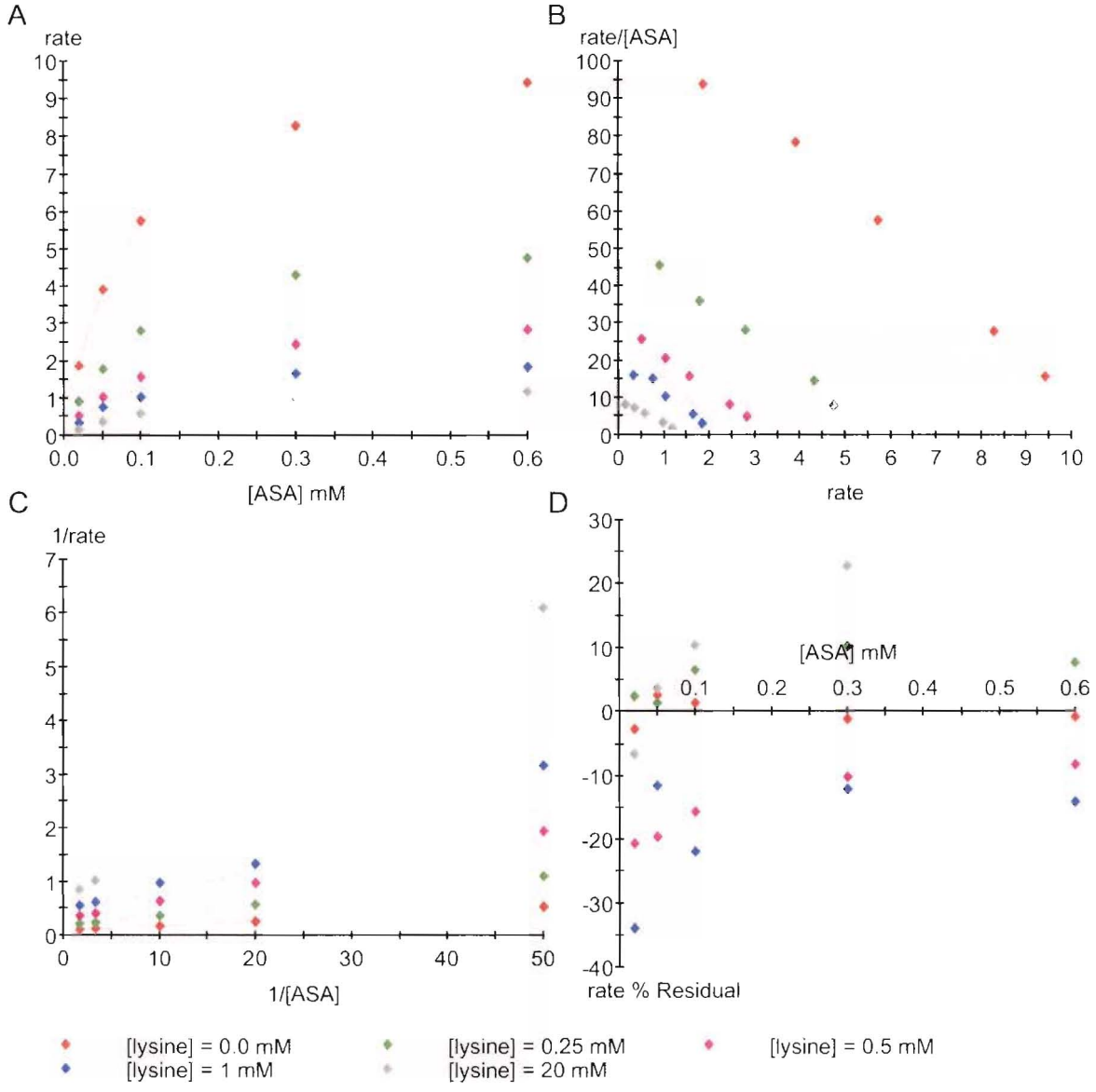

DHDPS-R138H.

Unlike the mutations discussed previously, DHDPS-R138H was not analysed in detail due to its extremely low activity. However, an approximate IC_{50} was obtained when measuring initial rate with increasing lysine concentrations, while keeping constant the substrate and DHDPS-R138H concentrations (Figure 6.15). This data suggests that as lysine increased, the activity of DHDPS-R138H approached 30% of maximal rate. That is, lysine inhibits DHDPS-R138H to approximately 30% maximal velocity as opposed to 15% in the wild-type. The data also suggest that, under the conditions of the experiment, the K_i for lysine is similar or lower to the wild-type.

Figure 6.15 *Inhibition of DHDPS-R138H (red) and wild-type (blue) by (S)-lysine. For DHDPS-R138H the substrate concentrations were 11.3 mM and 4 mM for (S)-ASA and pyruvate respectively. For the wild-type, the substrate concentrations were 0.12 mM and 0.4 mM for (S)-ASA and pyruvate respectively. Initial rates were determined using the coupled assay and data points were duplicated. The error bars are generated from the standard deviation. Normalised rate refers to the percentage inhibition a varying lysine concentrations compared to the rate in the absence of lysine.*

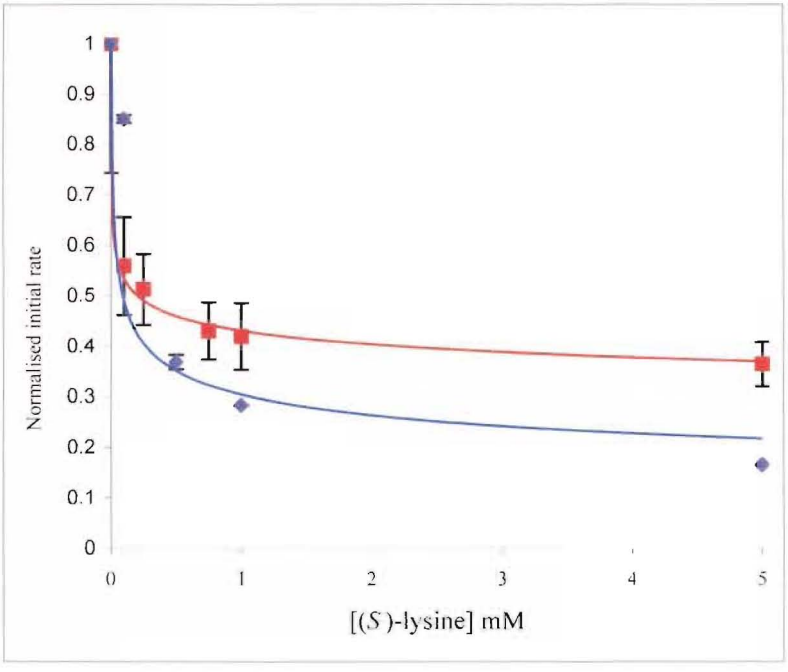

6.3 Discussion.

6.3.1 Is the effect of lysine to inhibit the function of the proton-relay?

Chapter five presented results supporting the hypothesis that the proton-relay assists in the catalysis of DHDPS. If important for catalysis, the functioning of this motif may be attenuated by lysine binding to inhibit the function of DHDPS. Four mutations were made in the proton-relay, two of which severely affected the catalytic function of DHDPS—these were Y133F and T44V. Because none of mutations were in the lysine-binding site, the K_i was expected to be similar and this was the case for all mutations where the K_i was determined.

Consistent with the hypothesis that Y133 and T44 are also important in the inhibitory mechanism of lysine, both showed reduced inhibition by lysine. Karsten[24] argues that because lysine shows uncompetitive inhibition *vs.* pyruvate and non-competitive inhibition *vs.* (*S*)-ASA in the wild-type enzyme, the inhibitory effect of lysine must be downstream of the first half reaction (Schiff base and enamine formation with pyruvate). Given that mutations in Y133 and T44, which disrupt the hydrogen-bonding network, also show reduced inhibition by lysine, the effect of lysine may be, at least in part, through some interaction with these residues. If, as Karsten points out, the effect is downstream, then according to the catalytic mechanism proposed in the previous chapter, the inhibitory effect may be to attenuate the bridging of the amine originating from (*S*)-ASA (Figure 5.11, step 5) and its subsequent deprotonation to allow cyclisation (Figure 5.11, step 6).

Unexpectedly, DHDPS-Y133F showed non-competitive inhibition *vs.* both substrates indicating that in this mutant there is also some effect during Schiff base and enamine formation. Since the hydroxyl of Y133 is missing, the effect is elusive, but may reflect repositioning of T44. If this same effect is present in the wild-type, then it must have a minor contribution.

The proposal that lysine inhibits the function of the proton-relay is supported by the observation that DHDPS-T44S, which to some extent restores the hydrogen-bonding system, shows identical inhibition properties to the wild-type. This is because the proton-relay is

operative in DHDPS-T44S, and since Blickling's hypothesised inhibition mechanism *via* Y107 is downstream of S44, the level of inhibition would be expected to be the same.

However, this predicts that mutation of Y107 to phenylanine should have similar effect on inhibition to that of DHDPS-Y133F and DHDPS-T44V. Contrary to what was expected, DHDPS-Y107F exhibited identical inhibitory properties to the wild-type—the K_i was about 0.15 mM and the α value approached 6%. However, as shown in the structure of DHDPS-Y107F in Chapter five, water may act as a surrogate in place of the hydroxyl of Y107 during proton transfer steps. Therefore, changes in that aromatic stack could influence the position and function of this water, thus showing the same inhibition as the wild-type. Otherwise, the normal inhibition pattern shown by DHDPS-Y107F may reflect the prospect that the hydroxyl of Y107 plays little (or no) role in the inhibitory mechanism. In order to distinguish between the two, the crystal structure of DHDPS-Y107F complexed with lysine would be very helpful.

6.3.2 Is the effect of lysine to inhibit the function of R138?

Structural studies have suggested that the function of R138 is to bind the carboxyl of (*S*)-ASA.[19] It is also proposed that one mode of inhibition by lysine may be to influence either (*S*)-ASA binding or cyclisation. The weakened inhibition of DHDPS-R138H with respect to lysine appears consistent with this hypothesis. However, the experimental design meant that the K_i could not be determined, although, as shown in Figure 6.15, this mutation is similarly sensitive to increased lysine concentration but the degree of inhibition is weaker.

In the wild-type DHDPS structures determined thus far, R138 is connected to the backbone oxygen of Y107 by the δ-nitrogen of R138.[19] In contrast, each of the DHDPS mutant structures determined here showed an alternate conformation of R138, whereby the ε-nitrogen of R138 is bound to the backbone of Y107. This is interesting since the ε-nitrogen of R138 is proposed to be involved in binding the carboxyl of (*S*)-ASA.[19] Although well defined in all the structures, higher resolution structures may be required to distinguish between the two conformations and the exact nature of the interaction between R138 and Y107.

Because mutations in the proton-relay show some inhibition by lysine, it is proposed that the effect on R138H is not the only mechanism of inhibition. The structure of DHDPS-T44V complexed with lysine was solved in an effort to investigate if other mechanisms may be in operation. It was expected that when the structures of DHDPS-T44V with and without bound lysine were compared, R138 would show similar changes to those observed when the analogous experiment was performed for the wild-type[19]—that is, when lysine is bound, R138 would become rigid, thus explaining the observed inhibition in DHDPS-T44V. This is because there is no obvious way of connecting a mutation at T44 to the flexibility of R138. Surprisingly, the opposite occurred: R138 became more flexible when lysine was bound to DHDPS-T44V. This seemingly contradicts the hypothesis of Blickling *et al.* and suggests that R138 does not function as proposed by Blickling *et al.* in the inhibition of DHDPS-T44V.

Clearly, R138 is involved in lysine inhibition because mutation of R138 to histidine reduces the effect of lysine on DHDPS, yet R138 appears not to play any role in DHDPS-T44V where it might be expected. How are these contradictory conclusions reconciled? One possibility is that when lysine binds DHDPS-T44V, the increased flexibility at R138 partially inhibits the binding of (*S*)-ASA. Thus, DHDPS-T44V shows inhibition from a mechanism not seen in the wild-type. This conclusion could be tested by a more detailed kinetic examination, such as that by Karsten[24] for the wild-type enzyme, whereby the inhibitor (lysine) is treated as a pseudo-reactant and the kinetic constants are examined with increasing inhibitor concentration. If the effect of lysine in DHDPS-T44V is solely on (*S*)-ASA binding, then as the lysine concentration increases, V and V/K_{mPyr} would be unchanged, while V/K_{mASA} would decrease. This is because the only microscopic rate constants not shared between V and V/K_{mASA} are those that reflect (*S*)-ASA binding (k_3 and k_{-3} in the equations below).

$$V/K_{mPyr} = k_1k_2 / k_{-1} + k_2$$

$$V/K_{mASA} = k_3k_4 / k_{-3} + k_4$$

$$V = k_2k_4 [E]_T / k_2 + k_4$$

6.3.3 *An alternative theory for lysine inhibition.*

Prompted by the observation that DHDPS-Y107F showed identical inhibitory properties to the wild-type (also, because it was difficult to see how movements in F107 might influence activity) it was decided to re-examine the conclusions of Blickling *et al.*[19] concerning lysine inhibition. Underpinning the idea of the proton-relay is that Y107 is solvent accessible. Inspection of the crystal structure of the wild-type shows that ordered water molecules line a channel starting from Y107 and exiting at the dimer interface. The channel is approximately 13–Å in length and 7–Å wide at it narrowest point. The waters in the channel can be connected to the bulk solvent by a series of hydrogen-bonds not more than 3–Å long. This can be seen in Figure 6.16. If a proton moves to bulk solvent from Y107, then it would need to be shuttled by this chain. A similar (although much longer) chain has been proposed for alcohol dehydrogenase from *Drosophila*.[28]

Lysine, when bound to the interface, all but covers this channel (Figure 6.16, 6.17 and 6.18). It is proposed that lysine inhibits DHDPS by blocking the proton shuttle through the channel. The ε-nitrogen of lysine is positioned approximately where a water molecule is found in the unbound structure. A chain can still be made to the solvent but this requires an alternative path *via* the backbone of A78. However, the waters connected to the backbone carbonyl of A78 are also connected to the ε-nitrogen of the lysine inhibitor, which, at pH 8, is likely to be protonated. Additionally, a water molecule accessible to bulk solvent is also connected to the carboxyl of lysine (2.85–Å) (Figure 6.17); thus, the propensity of proton transfer *via* this route may be questionable. The presence of another shuttle pathway might explain why DHDPS exhibits partial inhibition: when lysine is bound, the direct route to solvent is blocked but the alternate route may still be effective, albeit at a slower rate.

Figure 6.16 *A slab view of the proposed proton-relay connecting the active site and the lysine-binding site of wild-type DHDPS. The waters lining the channel are shown as red spheres. This image was generated with O*[21] *and Molray,*[22] *using the coordinates of DHDPS determined by Mirwaldt* et al.[3]

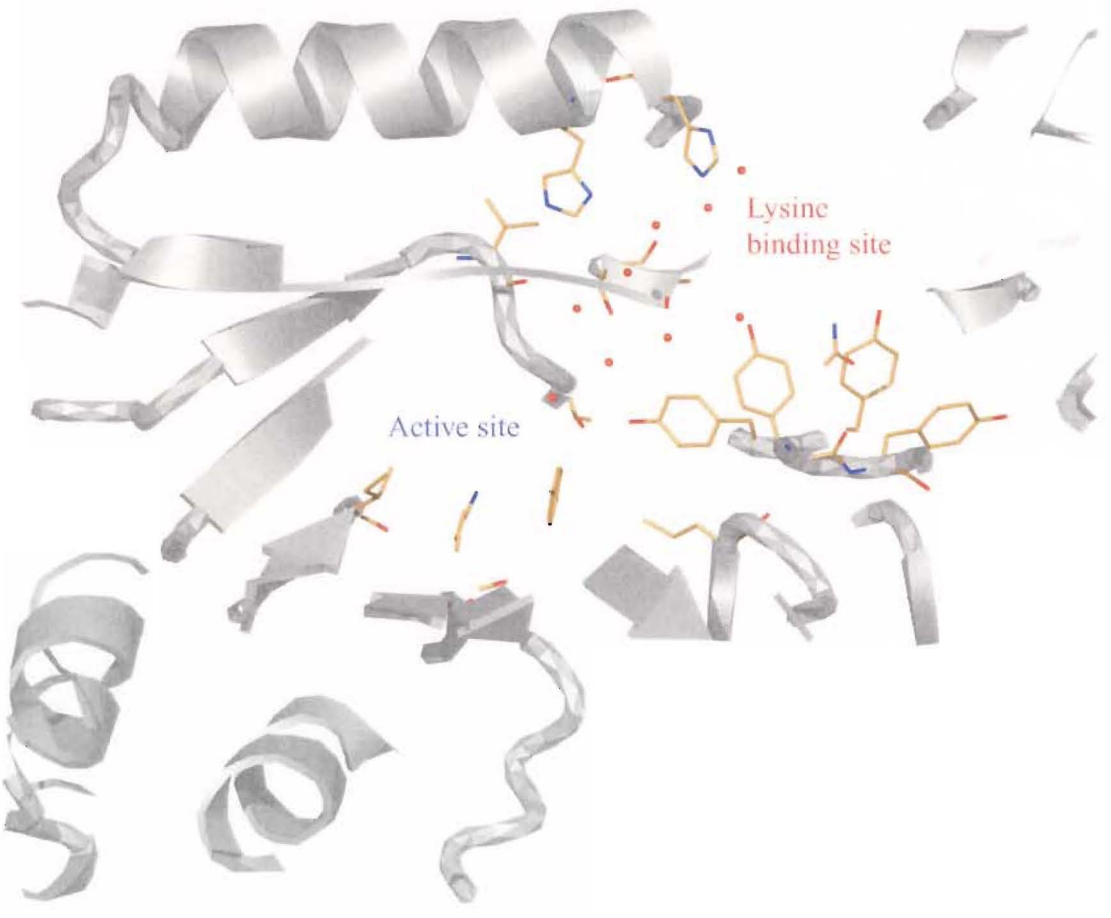

Figure 6.17 *This image was generated by an overlay of wild-type DHDPS without lysine and wild-type DHDPS with bound lysine. The waters (green) and (S)-lysine at the interface are from the structure solved by Blickling et al.*[19] *Those in red are from the structure without bound lysine solved by Mirwaldt et al.*[3] *The secondary structure (grey) is from unbound DHDPS.*[3] *This image was generated with O*[21] *and Molray.*[22]

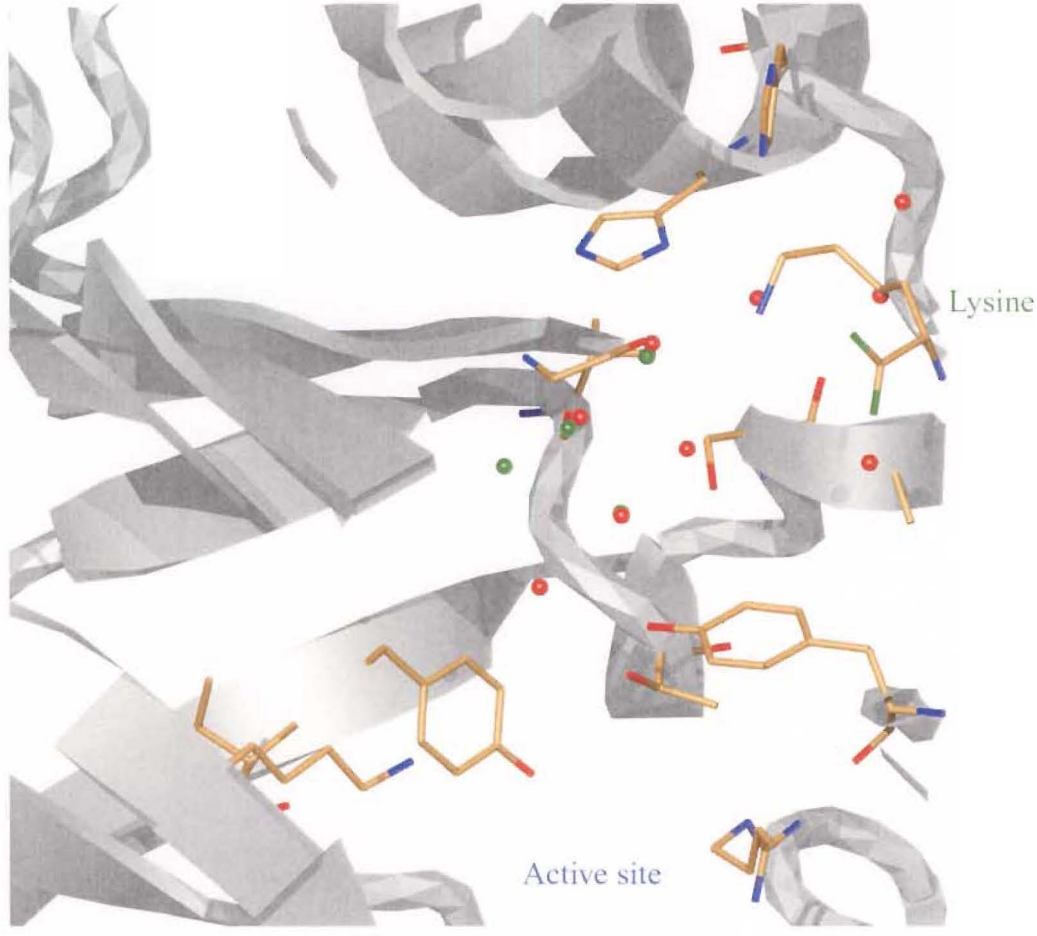

Figure 6.18 *Stereo view of the lysine (CPK) at the lysine-binding site. This image was generated to show the extent of space filled by (S)-lysine when covering the channel and attempts to portray the blocking of the channel. It was produced with O*[21] *and Molray,*[22] *using the coordinates of wild-type DHDPS determined by Mirwaldt* et al.[3] *and Blickling* et al.[19]

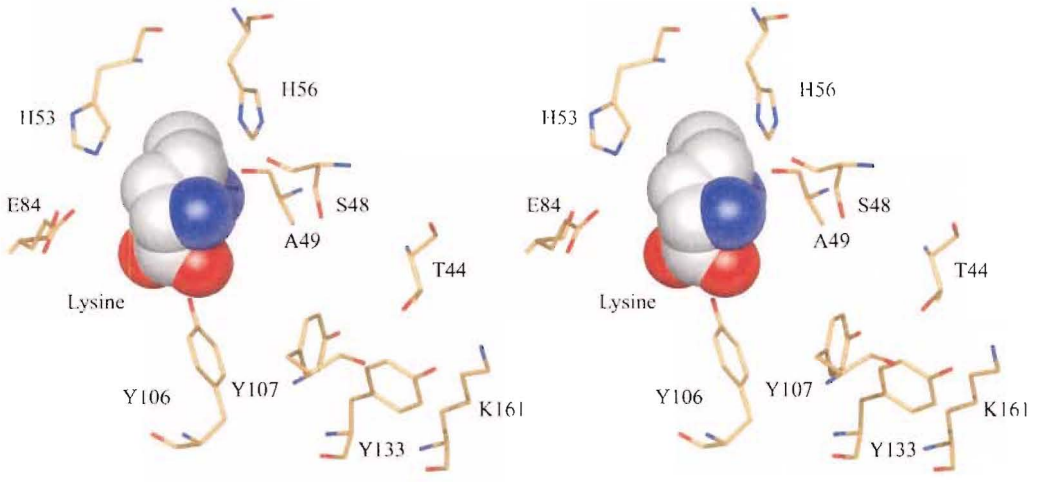

This hypothesis is consistent with the types of inhibition observed, as the proton ferried through the channel is probably that removed from the amine of (*S*)-ASA prior to cyclisation. This is mediated by Y133, transferred to Y107 *via* the hydroxyl of T44 and then through the channel to bulk solvent. As discussed above, partial uncompetitive inhibition with respect to pyruvate and partial non-competitive inhibition *vs.* (*S*)-ASA would be expected because this step is downstream of Schiff base and enamine formation. Moreover, this model also explains why DHDPS-Y107F displays the same inhibitory properties as the wild-type, while mutations at T44 and Y133 show attenuated inhibition. For DHDPS-Y107F, the proton, once removed by Y133 is transferred *via* T44 directly to a water (positioned near to where the hydroxyl of Y107 was positioned) from where it may be transferred to bulk solvent through the channel as with the wild-type.[≈] Blocking the channel with lysine would therefore have the same effect in DHDPS-Y107F as in the wild-type. However, weaker inhibition would be expected for DHDPS-T44V and DHDPS-Y133F because the pathway is

[≈] The waters in the channel of DHDPS-Y107F are not positioned in the same way as in the wild-type. The chain may be slightly disrupted due to the length of one hydrogen bond being elongated to 3.8–Å. This may explain the lower activity observed in this mutant.

already attenuated by the mutations in T44 and Y133; the structures of DHDPS-Y133F and DHDPS-T44V show no plausible routes *via* the channel to bulk solvent at the lysine-binding site. As predicted, DHDPS-T44S showed the same level of inhibition as the wild-type, presumably because the proton-relay is re-established.

6.4 Summary.

The mechanism of lysine inhibition in DHDPS appears complex. The mutations generated in Chapter five were tested for lysine inhibition and compared to the wild-type. The results showed that mutations in the proton-relay also attenuated lysine inhibition, but not completely. The crystal structure of DHDPS-T44V with bound lysine was solved and showed that the flexibility of R138 had increased, in contrast to the situation of the wild-type. Furthermore, there was no change in the kinetics of lysine inhibition with respect to DHDPS-Y107F, suggesting that lysine-binding, and the concomitant movements in the aromatic stack, either similarly effect the surrogate water found near the same position as the hydroxyl of DHDPS-Y107F, or that the hydroxyl of Y107 is not involved in lysine inhibition at all.

To reconcile these results, a new mechanism of inhibition is proposed. Lysine-binding affects catalysis, at least in part, by blocking the channel connecting the active site and the bulk solvent, thus, protons may no longer be removed from the active site, which inhibits key points in the reaction. Consistent with the idea that lysine affects DHDPS in the second half reaction, it is proposed the proton removed form the amino group of (*S*)-ASA is blocked, inhibiting cyclisation and catalysis.

6.5 References.

1. Yugari, Y. & Gilvarg, C. (1965). The condensation step in diaminopimelate synthesis. *Journal of Biological Chemistry*, **240**, 4710-4716.

2. Galili, G. (1995). Regulation of lysine and threonine synthesis. *Plant Cell*, **7**, 899-906.

3. Mirwaldt, C., Korndorfer, I. & Huber, R. (1995). The crystal structure of dihydrodipicolinate synthase from *Escherichia coli* at 2.5 Å resolution. *Journal of Molecular Biology*, **246**, 227-239.

4. Kumpaisal, R., Hashimoto, T. & Yamada, Y. (1989). Inactivation of wheat dihydrodipicolinate synthase by 3-bromopyruvate. *Agricultural and Biological Chemistry*,**53** , 355-359.

5. Mathews, B. & Widholm, J. (1978). Regulation of lysine and threonine synthesis in carrot cell suspension cultures and whole carrot roots. *Planta*, **141**, 315-321.

6. Wallsgrove, R. M. & Mazelis, M. (1981). Spinach leaf dihydrodipicolinate synthase: partial purification and characterization. *Biochemistry*, **20**, 2651-2655.

7. Ghislain, M., Frankard, V. & Jacobs, M. (1990). Dihydrodipicolinate synthase of *Nicotiana sylvestris*,a chloroplast-localized enzyme of the lysine pathway. *Planta*, **180**, 480-486.

8. Frisch, D. A., Gengenbach, B. G., Tommey, A. M., Sellner, J. M., Somers, D. A. & Myers, D. E. (1991). Isolation and characterization of dihydrodipicolinate synthase from maize. *Plant Physiology*, **96**, 444-452.

9. Dereppe, C., Bold, G., Ghisalba, O., Ebert, E. & Hans-Peter, S. (1992). Purification and characterization of dihydrodipicolinate synthase from pea. *Plant Physiology*, **98**, 813-821.

10. Bartlett, A. & White, P. (1986). Regulation of the enzymes of lysine biosynthesis in *Brevibacterium lactofermentum* NCTC 9602 during vegetative growth. *Journal of General Microbiology*, **132**, 3169-3177.

11. Bakhiet, N., Forney, F., Stahly, D. & Daniels, L. (1984). Lysine biosynthesis in *Methanobacterium thermoautotropicum* is by the diaminopimelic acid pathway. *Current Microbiology*,**10** , 195-198.

12. Stahly, D. (1969). Dihydrodipicolinate synthase of *Bacillus licheniformis*. *Biochimica et Biophysica Acta*, **191**, 439-451.

13. Webster, F. & Lechowich, R. (1970). Partial purification and characterization of dihydrodipicolinate synthase from sporulating *Bacillus megaterium*. *Journal of Bacteriology*, **101**, 118-126.

14. Yamakura, F., Ikeda, Y., Kimura, K. & Sasakawa, T. (1974). Partial purification and some properties of pyruvate-aspartic semialdehyde condensing enzyme from sporulating *Bacillus subtilis*. *Journal of Biochemistry*,**76** , 611-621.

15. Cremer, J., Eggeling, L. & Sahm, H. (1990). Cloning the *dapA dapB* cluster of the lysine-secreting bacterium *Corynebacterium glutamicum*. *Molecular General Genetics*, **229**, 478-480.

16. Hoganson, D. & Stahly, D. (1975). Regulation of dihydrodipicolinate synthase during growth and sporulation of *Bacillus cereus*. *Journal of Bacteriology*, **124**, 1344-1350.

17. Tosaka, O. & Takinami, K. (1978). Pathway and regulation of lysine biosynthesis in *Brevibacterium lactofermentum*. *Agricultural Biological Chemistry*, **42**, 95-100.

18. Laber, B., Gomis-Ruth, F., Romao, M. & Huber, R. (1992). *Escherichia coli* dihydrodipicolinate synthase. Identification of the active site and crystallization. *Biochemical Journal*, **288**, 691-695.

19. Blickling, S., Renner, C., Laber, B., Pohlenz, H., Holak, T. A. & Huber, R. (1997). Reaction mechanism of *Escherichia coli* dihydrodipicolinate synthase investigated by X-ray crystallography and NMR spectroscopy. *Biochemistry*, **36**, 24-33.

20. Blickling, S., Beisel, H., Bozic, D., Knablein, J., Laber, B. & Huber, R. (1998). Structure of dihydrodipicolinate synthase of *Nicotiana sylvestris* reveals novel quaternary structure. *Journal of Molecular Biology*, **274**, 608-621.

21. Jones, T. & Kjeldgaard, M. (1997). Electron density map interpretation. *Methods in Enzymology*, **277**, 173-208.

22. Harris, M. & Jones, T. A. (2001). Molray - a web interface between O and the POV-Ray ray tracer. *Acta Crystallographica Section D-Biological Crystallography*, **D57**, 1201-1203.

23. Blickling, S. & Knablein, J. (1997). Feedback inhibition of dihydrodipicolinate synthase enzymes by L-lysine. *Biological Chemistry*, **378**, 207-210.

24. Karsten, W. E. (1997). Dihydrodipicolinate synthase from *Escherichia coli*: pH dependent changes in the kinetic mechanism and kinetic mechanism of allosteric inhibition by L-lysine. *Biochemistry*,**36** , 1730-1739.

25. Engel, P. C. (1996). Enzyme kinetics. In *Enzymology* (Engel, P. C., ed.). BIOS Scientific, San Diego.

26. Keleti, T. (1986). *Basic enzyme kinetics*. 1st edit. Trans. Freidrich, P. & Kramer, M., Akademiai Kiado, Budapest.

27. CCP4. (1994). The CCP4 suite: programs for protein crystallography. *Acta Crystallographica Section D-Biological Crystallography*, **D50**, 760-763.

28. Koumanov, A., Benach, J., Atrian, S., Gonzàlez-Duarte, R., Karshikoff, A. & Ladenstein, R. (2003). The catalytic mechanism of Drosophila alcohol dehydrogenase: Evidence for a proton relay modulated by the coupled ionization of the active site Lysine/Tyrosine pair and a NAD+ ribose OH switch. *Proteins-Structure Function and Genetics*, **51**, 289-298.

Chapter Seven.

Experimental.

7.1 Introduction.

This thesis utilises a wide variety of techniques from different disciplines—chemical synthesis to the phage infection of bacteria; PCR to X-ray crystallography. Many of the techniques have already been described by Coulter, who initially developed the enzyme purification and early synthetic procedures in our lab.[1] The laboratory texts authored by Maniatis *et al.*[2] and Miller[3] were invaluable for routine manipulation of bacterial strains and DNA. "Fundamentals in Enzyme Kinetics" by Cornish-Bowden[4] is an excellent text for evaluating a wide range of kinetic phenomena and was used as a guide for designing kinetic experiments and evaluating data. Also used was the LabFax manual "Enzymology".[5]

7.2 Materials and Equipment.

Unless otherwise stated, chemicals were purchased from Aldrich Chemicals or Sigma Chemical Company Ltd (Castle Hill, Australia). Media for bacterial cultures was purchased from Invitrogen (Christchurch, New Zealand). SDS-PAGE gels were provided from Gradipore Ltd (Frenchs Forest, Australia). Restriction enzymes were supplied by Roche (Christchurch, New Zealand). Bio-Rad protein assay kit and DNA ladders were purchased from Bio-Rad Laboratories (Auckland, New Zealand). Column chromatography media were purchased from Amersham Pharmacia Biotech (Auckland, New Zealand) as Hi-Trap pre-packed columns or as a loose gel, which was later packed in Pharmacia XK type columns of various sizes.

pH measurements were made using a standard pH meter fitted with a Russell Combination (Tris compatible) Electrode type number TR/CMAW711/TB.

Centrifugation was performed in an Eppendorf Centrifuge 5430, on a small scale (< 1.5 mL) at up to 15000 rpm using a 16 F24-11 rotor, and on a large scale (< 50 mL) at up to 5250 rpm using a 16A4-44 rotor at 4°C.

Columns were run using Gilson Minipuls M312 peristaltic pumps with Gilson Model 740 system control software and a Gilson FC-203B fraction collector.

Polyacrylamide gel electrophoresis (PAGE) was routinely run on a Hoefer Sturdier Slab Gel Electrophoresis Unit SE 400, using a Bio-Rad 300 power pack.

Ultraviolet (UV) spectroscopy was performed on a Hewlett Packard 8452A Diode Array Spectrophotometer with a circulating water bath to maintain a constant temperature.

Protein crystallisation was performed with equipment supplied by Hampton Research. All solutions were made with Millipore purified water and filtered through a 0.44 μm Millipore filter. Diffraction data were collected at 110 K using a MAR Research image plate detector and an in-house Rikagu rotating anode generator operating at 50 kV and 100 mA.

Unless otherwise stated, all synthetic reactions were performed in dry glassware under an atmosphere of oxygen free nitrogen or argon. All organic extracts were washed with brine and dried over anhydrous magnesium sulfate. After filtration of solutions to remove drying agents, the solvents were removed under reduced pressure on a Büchi rotary evaporator.

^{1}H NMR spectra were recorded on either a Varian Unity 300 or Varian Inova 500 spectrometer, operating at 300 and 500 MHz respectively. ^{13}C NMR spectra were obtained on either a Varian Unity 300 or Varian Inova 500 spectrometer, operating at 75 and 126 MHz respectively. For ^{1}H NMR, chemical shifts are reported relative to tetramethylsilane (TMS) if run in deuterated chloroform ($CDCl_3$). For samples run in deuterium oxide (D_2O) the spectra were referenced to the residual protonated solvent at 4.7 ppm, and for samples run in deuterated methanol (CD_3OD) the spectra were referenced to the residual protonated solvent peak at 3.3 ppm. For ^{13}C spectra run in deuterated chloroform ($CDCl_3$), the spectra were referenced to the residual protonated solvent at 77 ppm, and for samples run in deuterated methanol (CD_3OD), the spectra were referenced to the residual protonated solvent at 49.3 ppm.

Thin layer chromatography (TLC) was conducted on aluminium-backed Merck Kieselgel KG60F254 silica plates. The developed plates were analysed under short-wave UV light and stained with a potassium permanganate or phosphomolybdic acid dip. Unless otherwise stated, flash chromatography was performed on Merck Silica 60.

Solvents and reagents were purified according to well-established procedures. In particular, dichloromethane, pyridine, and *N,N*-diisopropylamine were freshly distilled from calcium hydride before use. Diethyl ether and tetrahydrofuran were freshly distilled from sodium/benzophenone ketyl before use. The petroleum ether used had a boiling range of 50–70°C. Methanol and ethanol were distilled from the appropriate magnesium alkoxide and stored under dry nitrogen over 4–Å molecular sieves.

7.3 Methods in molecular biology and microbiology.

7.3.1 Bacterial strains.

All the bacterial strains used in this thesis are summarised in the following table:

***E. coli* Strain**	**Relevant genotype**	**Source**
XL-1 Blue	recA1, endA1, gyrA96, thi-1, hsdR17, supE44, relA1, lac [F' proAB lacI ZΔM15 Tn10(Tet^r)]	Obtained from Stratagene as part of the Quikchange site-directed mutagenesis kit.[6]
AT997	relA1, spoT1, dapA15, thi-1, λ-	This strain was a gift from the *E. coli* genetic stock centre, Yale University (CGSC# 4547). The strain was originally characterised as a *dap*C mutant[7] but recharacterised as a *dap*A mutant after showing that the *dap*A gene, if in trans, rescued the strain when grown on minimal media.[8]
AT997r$^-$	relA1, spoT1, dapA15, thi-1, λ-, recA-	This study.
W3110	relA1, spoT1, dapA15, thi-1, λ-	Was a gift from Assoc. Prof. Khris Mahanty.
JB377	recA ΔTn10(Tet^r), spoT1, dapA15, thi-1, λ-	Was a gift from Assoc. Prof. Jack Heinemann.[9]

7.3.2 Plasmids.

All the plasmids used in this work were based on the vector pBluescript KS+.[6] The genes *dap*A and *dap*B encode dihydrodipicolinate synthase and dihydrodipicolinate reductase respectively, and have been previously cloned into pBluescript KS+ by others.[1, 10, 11]

Plasmids	Relevant genotype	Source
pJG001	::*dap*A, Amp^r	Gerrard[10]
pJK001	::*dap*B, Amp^r	Kraunsoe[11]
pRD-T44V	::*dap*A-thr44val, Amp^r	This work
pRD-T44S	::*dap*A-thr44ser, Amp^r	This work
pRD-R138H	::*dap*A-arg138his, Amp^r	This work
pRD-Y107F	::*dap*A-tyr107phe, Amp^r	This work
pRD-Y133F	::*dap*A-tyr133phe, Amp^r	This work

7.3.3 Bacterial cultures.

All cultures were grown under sterile conditions. All media and equipment were either autoclaved at 121°C for 20 min, filtered through a 0.2 micron acrodisc (Gellman Sciences), or purchased sterile. Solutions were made up in sterile deionised or double distilled water. During the transfer of cultures all equipment was flamed and manipulations were carried out in a laminar flow hood and/or near a naked flame. Each experiment was accompanied by an appropriate control to monitor for contamination.

7.3.4 Media.

For making LB or minimal media plates 15 g/L agar or agarose were included.

Luria-Bertani medium (LB)—LB base was supplied by Gibco BRL in a ready to use powdered form. 20g of LB base was added to a litre of water, the pH adjusted to 7 by addition of NaOH, and the resulting media autoclaved.

Minimal Media—Minimal media (10.6 g), supplied by Gibco BRL, was added to 1 L of deionised water. This was autoclaved (121°C for 15 min) followed by the addition of 10% glucose (filter-sterilised prior to addition) (10 mL L^{-1}).

NZY+ broth—NZ amine (10 g), yeast extract (5 g), and NaCl (5 g) was added to ddH_2O (1 L). The pH was adjusted to 7 with the addition of NaOH before the media was sterilised by autoclave, following which $MgCl_2$ (1 M, 12.5 mL), $MgSO_4$ (1 M, 12.5 mL), and glucose (20%, 20 mL) were added (all were filter-sterilised prior to addition).

SOC—To dH_2O was added (to a final concentration): bacto-tryptone (2% w/v), yeast extract (0.5% w/v), NaCl (10 mM), KCl (2.5 mM), $MgCl_2$ (10 mM), $MgSO_4$ (10 mM), and glucose (0.36% w/v). This was then sterilised by autoclave (121°C, for 15 min).

H-Top Agar—Bacto-tryptone (1 g), NaCl (0.8 g), and agar (0.8 g), were added to distilled water (100 mL), mixed, and aliquots (5 mL) were added to test tubes. These were sterilised by autoclave (121°C, for 15 min).

7.3.5 Antibiotics and nutritional supplements.

Stock solutions of antibiotics and supplements (1000×) were sterilised by filtration, where required, and stored at –20°C. The following final concentrations were used for selection:

Supplement	**[Stock]** mg mL^{-1}	**[Working]** μg mL^{-1}
Ampicillin	100	100
Tetracycline	25	25
meso-Diaminopimelate	10	50

7.3.6 Plate preparation.

Molten agar (LB or minimal media) at ~50°C was supplemented with the appropriate antibiotics, and poured directly into sterile petri dishes in a laminar flow hood and/or close to a flame. Minimal media plates were prepared with agarose, which had been autoclaved separately (2× strength) from the salt solution (2× strength) and mixed immediately prior to pouring the plate. Glucose (10 mL of a pre-sterilised 10% glucose solution) was also added at this point. Any bubbles were removed by flaming the surface before the plates

had hardened. The plates were allowed to set overnight before use and could be stored for several weeks if sealed and kept at 4°C. After the plates were dried, IPTG (8 μL, 100 mg mL^{-1}) and X-gal (40 μL, 20 mg mL^{-1}) were spread onto the surface. The DMSO, which is used to dissolve the IPTG, was removed by incubation at 37°C for 2 hours.

7.3.7 Colony growth.

Agar plates were streaked with *E. coli* (from a glycerol freeze, an overnight culture, or a single colony on an agar plate) using a flamed sterilised nichrome wire. The plates were incubated overnight at 37°C. Individual colonies were selected and used to inoculate liquid medium (usually 5 mL). Starter cultures were grown overnight in a shaker incubator (37°C, 180 rpm) and subsequently used to inoculate larger quantities of media. Single colonies remained viable on an agar plate for approximately one week if sealed and stored at 4°C.

7.3.8 Preparation of glycerol freeze stocks for storage.

An aliquot (750 μL) from an overnight culture (3 mL) was centrifuged (5000 g for 5 min) in a screw top cryo-storage tube and the supernatant aspirated. Another aliquot of culture (750 μL), followed by glycerol (sterile 50% v/v, 750 μL), was added and vortexed before being frozen and stored at –80°C.

7.3.9 Competent cell preparation and transformation by electroporation.

This procedure was adapted from the methods used by the Genetics Laboratory of Assoc. Prof. Khris Mahanty, University of Canterbury. An overnight culture (5 mL), with appropriate supplements and antibiotics, was inoculated with bacteria from an agar or agarose plate, and the culture was grown overnight. This inoculum was used to seed 1 L of media, which was grown (37°C, 180 rpm) until $A_{600} = 0.8$. The cells were chilled on ice for 15 min, and then harvested by centrifugation (4000 *g* at 4°C for 10 min). The cell pellet was washed with cold sterilised water (1 L) and centrifuged as before. The cell pellet was then washed with cold water (0.5 L) and centrifuged again; this step was repeated once more. A final wash was performed with glycerol/water (20 mL, sterile, 10% v/v) and the cells were collected by centrifugation as before. This final cell pellet was re-suspended

in 3 mL of ice-cold glycerol/water (10% v/v), from which 40 μL aliquots were stored at –80°C.

When required, competent cells were removed from the –80°C freezer and defrosted on ice 15 min prior to electroporation. Plasmid DNA (usually 1 μL and dissolved in either dH_2O or low ionic strength buffer) was added to the cells before being transferred to a pre-chilled electroporation cuvette (0.2 cm gap).

Electroporation was performed on a Bio-Rad Gene Pulser set to 2.5 kV at 25 μF with the pulse controller set at 200 Ω. After delivery of a single pulse, the cells were immediately re-suspended in 1 mL of SOC medium, transferred to an Eppendorf, and incubated (37°C) with gentle shaking (100 rpm for 1–2 hours). Transformants were spread on LB agar plates, with the appropriate selection and supplements, and incubated overnight.

7.3.10 Competent cell preparation and transformation by the calcium chloride method.

Competent cell preparation.

A culture (50 mL) was grown overnight with the appropriate controls, antibiotics, and supplements. After cooling on ice for 10 min the cells were gently centrifuged (4000 *g* for 5 min). The supernatant was removed and replaced with a quarter volume of ice cold $CaCl_2$ (10 mM), then centrifuged as before, and the supernatant removed. The cells were washed in one-tenth volume of ice cold $CaCl_2$ (100 mM) and again centrifuged. The cells were finally re-suspended in a one fifteenth volume of ice cold $CaCl_2$ (100 mM) and aliquots (100 μL) were stored on ice overnight before transformation.

Transformation.

2 μL of DNA was added to an aliquot of competent cells and incubated on ice (30 min). Although normal procedures use a heat shock at 42°C,[2] for *E. coli* AT997, this was not used.

7.3.11 Transforming Epicurean coli *XL-1 Blue supercompetent cells.*

Epicurean coli XL-1 Blue competent cells were gently thawed on ice and aliquots (50 μL) transferred to pre-chilled Falcon 2059 polypropylene tubes. DNA (1 μL) was added to separate aliquots, mixed gently by pipetting and incubated on ice (30 min). The transformation reaction was heat pulsed for 45 seconds at 42°C, and then placed on ice for 2 min. NZY+ broth (0.5 mL, preheated to 42°C) was added and incubated (37°C for 1 hour) with shaking at 225–250 rpm.

7.3.12 Phage transduction and recombination using P_{1vir}.

Preparation of the *E. coli* JB377 P_{1vir} lysate.

$CaCl_2$ was added to an overnight culture of *E. coli* JB377 (5 mL) to give a final concentration of 10 mM, and the culture was shaken at 37°C for a further 10 min. The cell suspension (1 mL) was transferred to a sterile Eppendorf tube along with of P_{1vir} stock (100 μL), kindly provided by Assoc. Prof. Khris Mahanty, University of Canterbury. The stock had been initially grown on *E. coli* W3110. The phage were allowed to absorb (stationary) for 10 min at 37°C. One drop of $CaCl_2$ (1 M) and 2 drops of glucose were added, and the mixture was added to an overlay (see below). This was incubated overnight (37°C). Because of the small size of the P_{1vir} plaques, a control containing no phage was also included.

Overlays—H-Top agar (5 mL) was melted in boiling water and left until the temperature was ~42°C. The sacrificial strain (1 mL) was added, along with the phage stock (100 μL), and this was immediately poured onto a pre-warmed agar plate (55°C oven for 10 min). The molten agar was allowed to set before incubation overnight (37°C).

P_{1vir} Transduction of *E. coli* AT997.

From an overnight culture of *E. coli* AT997, grown in the presence of DAP (50 μg mL^{-1}) and with a DAP minus control plate that was clear, an aliquot (1.5 mL) was taken, centrifuged, and the pellet re-suspended in 1 mL of MC buffer ($MgSO_4$, 10 mM; $CaCl_2$, 5 mM), again supplemented with DAP. This was transferred to a sterile flask and shaken for 10 min. This culture was added to three Eppendorfs, along with 0, 10, and 100 μL of the P_{1vir} lysate prepared above. The phage were allowed to absorb without shaking

(20 min at 37°C) and the cells were added to LB (3 mL) supplemented with sodium citrate (100 mM) and DAP (50 μg mL^{-1}). They were shaken for 2 hours at 37°C, after which an aliquot from each (200 μL) was spread onto LB agar plates that contained tetracycline, sodium citrate (100 mM), and DAP (50 μg mL^{-1}). The remaining infected culture was centrifuged, re-suspended in LB (100 μL), and spread onto another LB agar plate with the same supplements as above.

Assaying for *rec*A function.

There were two methods used in this study to test for *rec*A function. The first involved the growth of bacteria following exposure to UV radiation and the second involved growth of bacteria on agar plates in the presence of MMS (methyl methane sulfonate). Both cause mutagenesis of the bacterial chromosome that can be repaired by the error prone SOS response regulated by *rec*A protein. Failure to grow after mutagenesis suggests that the *rec*A SOS response is not functioning. Strains that were *rec*A^- or *rec*A^+, but otherwise isogeneic, were also subject to mutagenesis as controls for sensitivity to UV and MMS.

UV mutagenesis—Immediately after spreading bacteria, the plates were subject to UV irradiation by placing them 50 cm from a Philips TUV 30W/630T8 lamp for 13 s.

MMS mutagenesis—MMS (3 μL) was added to LB broth (100 μL) and spread onto LB agar plates (50 mL).

7.3.13 Standard plasmid preparation by alkaline lysis.[2, 3]

Solution one—glucose (50 mM), EDTA (10 mM), Tris.HCl (25 mM, pH 8.0)

Solution two—sodium hydroxide (0.2 M), 1% SDS (made fresh at r.t.)

Solution three—sodium acetate (3 M, pH 4.8)

A single bacterial colony was used to inoculate LB broth (10 mL) containing appropriate antibiotics and incubated overnight (37°C, 180 rpm). An aliquot of culture (1.5 mL) was then transferred to an Eppendorf and centrifuged (5000 *g*, 2 min at 4°C). The supernatant was removed by aspiration and the pellet re-suspended in ice-cold solution one (100 μL) and chilled on ice (10 min). Freshly prepared solution two (200 μL) was added, mixed by gentle inversion, and chilled on ice (5 min). Ice-cold solution three (150 μL) was added

with gentle mixing until a white precipitate formed and was incubated on ice for 20 min. The tube was centrifuged (12000 *g*, 5 min) and the supernatant decanted into a fresh tube. Ethanol (95%, 250 μL) was added to the supernatant, mixed, and incubated on ice for 5 min. The tube was centrifuged (12000 *g*, 5 min) and the supernatant was carefully removed. The DNA pellet was rinsed with ethanol (70%, 1 mL at 4°C), centrifuged (12000 *g*, 1 min) and the supernatant again aspirated. The pellet was dissolved in 200 μL of 3 M sodium acetate and vortexed briefly. Ethanol (100%, 400 μL, ice-cold) was added, mixed, and the solution stored on ice for 10 min. The tube was finally centrifuged (12000 *g*, 5 min) and supernatant was aspirated. The pellet was dried in a 37°C incubator and if no further purification was required, dissolved in $T_{10}E_1$ buffer or dH_2O (10 μL).

Extra steps were included when the DNA was required for sequencing or PCR mutagenesis. Lithium chloride and RNase were included to remove RNA, followed by a phenol:chloroform step to remove protein.

Following on from the procedure above, the dried pellet was re-dissolved in cold $T_{10}E_1$ (100 μL) and incubated on ice (30 min). Following incubation, cold lithium chloride (3 M, 100 μL) was added, and the resultant solution incubated on ice (10–30 min). The solution was centrifuged (11000 *g*, 10 min at r.t.) and the supernatant was poured into a fresh centrifuge tube containing isopropanol (0.54 volumes). The solution was incubated on ice for 10 min and centrifuged (11000 *g* for 10 min at 4°C). The pellet was washed, centrifuged, and dried as previously mentioned. The pellet from the RNA precipitation step was re-suspended in $T_{10}E_1$ (200 μL) and RNase (0.5 μL) was added; the solution was incubated (37°C, 30 min). After incubation, phenol (200 μL) and chloroform:isopropanol (1:1 200 μL) was added, the solution gently mixed, and centrifuged (13000 *g*, 5 min at r.t.). After centrifugation, the top layer was transferred into a new Eppendorf containing phenol (200 μL) and chloroform:isopropanol (200 μL). Again the solution was mixed and centrifuged (13000 *g*, 5 min at r.t.). The top layer was again removed and added to potassium acetate (2 M, 0.125 volume) in cold ethanol (100%, 2 volumes). This resultant solution was gently mixed, incubated on ice (10 min), and centrifuged (13,000 *g*, 10 min at 4°C). The DNA pellet was rinsed with ice-cold ethanol, briefly centrifuged, and dried as outlined above. The dried pellet was re-suspended in $T_{10}E_1$ or ddH_2O (10 μL).

Restriction digests.

If required, RNAse was added to a final concentration of 10 μg mL^{-1}. Restriction digests were performed in 10 μL volumes. A typical protocol is illustrated with the double digest of pJG001 with the restriction enzymes *Bam*HI and *Xho*I. The reaction mixture contained: dH_2O (7 μL), DNA solution (1 μL), 10× reaction buffer (1 μL), *Xho*1 (5 Units, 0.5 μL), and *Bam*HI (5 Units, 0.5 μL). This was incubated for 2 hours at 37°C before electrophoresis.

Agarose gel electrophoresis.

Restriction fragments were typically mapped on a 1% (w/v) agarose gel against a 1 kb and/or a 100 bp ladder. When the fragments to be viewed were small (<500 bp) a 1.5% agarose gel was used. The 1% agarose gel (TAE buffer 30 mL, agarose 0.3 g) was cooled to ~50°C, poured into a gel casting tray, and the well comb inserted. The gel was allowed to set completely (~30 min) before the comb was removed. The casting tray was then transferred into a gel tank containing electrophoresis TAE buffer. The gel was loaded with the digested DNA (10 μL) or uncut DNA (~1 μL) from above, which had been mixed with loading buffer (1 μL), along with a DNA ladder. The gel was run at 60 V for two to three hours or until the bromophenol blue band was nearing the end of the gel. The gel was stained with ethidium bromide (0.5 mg mL^{-1}, 20 min) and the DNA fragments were visualised under UV radiation (302 nm).

Loading dye—glycerol (30% v/v), bromophenol blue (0.25% w/v), and xylene cyanol (0.25% w/v).

7.3.14 PCR site-directed mutagenesis.

This method was carried out as described in the Stratagene Quikchange site-directed mutagenesis manual[6] with minor changes in the PCR cycling parameters.

Primer Design.

Mutagenic primers introduce specific alterations into each strand of the template DNA by being incorporated into the plasmid during the PCR step.[6] The following considerations were made when designing the primers. Firstly, both primers contained the desired mutation and annealed to the same sequence on opposite strands of the plasmid. The primers were between 25 and 45 bases in length and had a calculated melting temperature

(T_m) > 78°C. The following formula was used to determine the melting temperature: {T_m = 81.5 + 0.41(%GC) – 675/N – % mismatch}, where N is the primer length in base pairs. The base changes were in the middle of the primer with at least 10–15 bases of correct flanking sequence. Finally, the primers had a minimum GC content of 40% and terminated in one or more CG bases. As an example, the threonine to valine mutation is illustrated. The *dap*A sequence, either side of T44 (highlighted in red), is shown below.

$^{5'}$GCG ATC GTT TCT GTT GGC ACC ACT GGC GAG TCC GCT ACC TTA$^{3'}$
T44

The generation of the amino acid change threonine to valine required a double mutation from ACC to GTC (blue). Thus the primers were:

Primer 1 (RD1)

$^{5'}$ CG ATC GTT TCT GTT GGC GTC ACT GGC GAG TCC GC $^{3'}$
(17) V44 (15)

Primer 2 (RD2)

$^{3'}$ GC TAG CAA AGA CAA CCG CAG TGA CCG CTC AGG CG $^{5'}$
(17) V44 (15)

Primers were purified by Gibco BRL using polyacrylamide gel electrophoresis (PAGE).

PCR Reaction conditions.

Four PCR reactions were set up with increasing amounts of template DNA: 5, 10, 20, and 50 ng. A diagnostic control for this step was the reversion mutation of pWhitescript with mutagenic primers, which were supplied with the mutagenesis kit. The pWhitescript plasmid has a point mutation in the *lacZ'* gene (β-galactosidase) generating a stop codon at the ninth position of the coding region. Mutagenic primers replace the stop codon with a glutamine codon restoring activity to the enzyme and allowing the determination of mutational efficiency by the proportion of blue/white colonies on IPTG/X-Gal plates.

The sample reactions used pJG001, which had been isolated from *E. coli* XL-1 Blue (pJG001) by alkaline lysis. The DNA was quantified spectrophotometerically and the reactions where set up in thin walled PCR tubes as follows:

	[Initial]	**Volume** (μL)	**Amount** (ng)
10× reaction buffer		5	
Template dsDNA 4.1-kb plasmid	18.5 ng μL^{-1}	2.7	50
RD1 GT 34-mer	9.41 ng μL^{-1}	13.28	125
RD2 CA 34-mer	7.21 ng μL^{-1}	17.17	125
dNTP mix		1	
double-distilled water (ddH_2O)		9.85	
Pfu Turbo DNA polymerase	2.5 Units μL^{-1}	1	

The control reaction was set up as follows:

	[Initial]	**Volume** (μL)	**Amount** (ng)
10× reaction buffer		5	
pWhitescript 4.5-kb control plasmid	5 ng μL^{-1}	2	10
oligonucleotide control primer#1 34-mer	100 ng μL^{-1}	1.25	125
oligonucleotide control primer#2 34-mer	100 ng μL^{-1}	1.25	125
dNTP mix		1	
Double-distilled water (ddH_2O)		37.5	
Pfu Turbo DNA polymerase	2.5 Units μL^{-1}	1	

Each reaction was overlaid with mineral oil to prevent evaporation and the PCR reaction carried out in a thermocycler equipped with a "hot bonnet", which also helped to prevent evaporation.

PCR Cycling Parameters:

Control Reaction			**Sample reaction**		
step	Temperature (°C)	Time (min)	step	Temperature (°C)	Time (min)
1	95	0.5	1	95	0.5
2	95	0.5	2	95	0.5
3	55	1	3	50	1
4	68	12	4	68	8.2
5	steps 2–4 eleven times		5	steps 2–4 eleven times	

At this point, agarose gel electrophoresis was used to check for amplification of the parent plasmid using the equivalent amount of starting template as a control.

Template Digestion.

Endonuclease enzyme, *Dpn*I (1 μL, 10 Units μL^{-1}), was added to each of the amplification reactions below the mineral oil. *Dpn*I is a methylated and hemimethylated specific enzyme, which digests the parent template DNA, leaving the mutation-containing newly synthesised DNA intact. The reaction mixture was gently, but thoroughly mixed, centrifuged, and incubated at 37°C for 1 hour to digest the parental (non-mutated) supercoiled dsDNA.

DNA sequencing.

DNA sequencing reactions were performed at either the Auckland Genomics Facility or the Waikato Sequencing Facility. Plasmids to be sequenced were prepared to the highest quality, quantified spectrophotomectrically,[2] and sequenced using the dideoxynucleic acid chain termination method,[12] using the IR-labelled primers T3 and T7.

7.4 Techniques in Biochemistry.

Unless otherwise stated, enzymes were manipulated on ice or at 4°C to reduce denaturation. All enzymes were routinely stored in 20 mM Tris.HCl pH 8 at 4°C (buffer A) at –20°C in 1 mL aliquots.

7.4.1 Standard Bradford assay for determining protein concentration.[13]

The protein solution (800 μL) was added to the Bradford reagent (200 μL) and mixed thoroughly. The solution was allowed to stand for exactly 10 min before the absorbance was measured at 595 nm against a blank solution (800 μL of sample buffer and 200 μL of Bradford reagent). Protein concentrations were obtained from the calibration curve generated with BSA obtained from Sigma). All measurements were taken in duplicate.

7.4.2 Sodium dodecyl sulfate polyacrylamide gel electrophoresis (SDS-PAGE).

For routine analysis of protein samples, pre-cast 8–16% gradient gels were used. Samples to be loaded were diluted with buffer to allow the loading of ~20 μg of total protein, and then mixed with an equal volume of 2× treatment buffer.

Treatment Buffer (2×)—Tris.HCl (0.125 M, pH 8.6), SDS (4%), glycerol (20%), 2-mercaptoethanol (10%), bromophenol blue (0.25%), and stored at –20°C.

Samples were boiled for 2 min then briefly centrifuged before loading into the wells of the gel. The gel was electrophoresed at 4°C at constant voltage (150 V) until the bromophenol blue had run from the bottom of the resolving gel. The gel was then stained with Coomassie brilliant blue for 30 min followed by de-staining in a solution of glacial acetic acid (10%) and methanol (5%) in water overnight.

7.4.3 Preparation of dialysis tubing.

Dialysis tubing was boiled for 10 min in a solution of sodium bicarbonate (2% w/v) and EDTA (0.05% w/v). Care had to be taken to ensure the tubing remained submerged at all times. The tubing was then boiled for a further 10 min in deionised water, and this step was then repeated. The solution was cooled and the tubing stored at r.t. in sodium azide (0.1% w/v) for up to three months.

7.4.4 Over-expression and purification of wild-type and mutant DHDPS enzymes.

Growth of *E. coli* XL-1 Blue(pJG001) and *E. coli* AT997(pRDmutants).

E. coli XL-1 Blue(pJG001) and *E. coli* AT997r⁻(pRDmutant) cultures were streaked out on LB agar plates with the appropriate selection and supplements and grown overnight (37°C). A single colony was selected, re-streaked as before, and incubated overnight (37°C). A single colony was then selected and used to inoculate LB broth (10 mL) containing antibiotics and supplements, and incubated overnight with shaking (37°C, 180 rpm). From this culture, 1 mL was used to inoculate 1 L of LB broth under the same conditions and incubated overnight as above. The cells were chilled on ice for 30 min and harvested by centrifugation (5000 *g*, 10 min). One litre of inoculated LB broth gave ~4 g of wet cells.

Preparation of a crude cell free extract.

Harvested cells were washed by re-suspending in an equal culture volume of buffer A with gentle pipetting. The cell suspension was centrifuged (5000 *g*, 10 min). The supernatant was discarded and the cell pellet was re-suspended in an equal volume of buffer A. The sample was then flash frozen in liquid nitrogen and gently thawed by incubation on ice overnight. At this point, two methods were used to isolate the crude extract of DHDPS.

The first followed the methods of Coulter[1] and Gerrard.[10] This involved a further six freeze thaw cycles as above. The crude extract was then obtained by centrifugation (5000 *g*, 20 min) to remove cell debris. The supernatant, containing DHDPS, was collected for the next step. An alternative method was to subject the cells to 5 min of ultrasonication, in 3 second bursts, and with a 10 second pause in-between to ensure the temperature stayed below 4°C. The supernatant was collected after centrifugation (5000 *g*, 20 min), the remaining pellet was re-suspended in buffer A and the sonication process repeated. The second sonication step routinely increased the yield by up to 30%.

Purification.

Heat Shock.

Aliquots of the crude extract (1 mL) were added to sterile Eppendorf tubes, incubated for 2 min at 70°C, immediately cooled on ice, and finally centrifuged (20000 *g*, 10 min). The supernatant was collected and pooled.

Ion exchange chromatography.

The pooled sample from the heat shock, or the crude extract from the freeze thaw method, was loaded on to a Q-Sepharose ion exchange column (bed volume 60 mL, 13 × 2.6 cm) that had been pre-equilibrated with three bed volumes of buffer A. The column was then washed with five bed volumes of buffer A and the enzyme was then eluted with a NaCl gradient (0–1 M) in buffer A. The column was then washed with three bed volumes of regeneration buffer (1 M NaCl in buffer A). The eluted fractions were tested for DHDPS activity using the *o*-aminobenzaldehyde micro assay described in the following table:

	[Initial] (mM)	**Volume** (μL)	**[Final]** (mM)
Tris.HCl (pH 8 at 25°C), pyruvate	200, 40	150	166, 33
o-aminobenzaldehyde (in ethanol)	400	5	10
DHDPS test solution		5	
(*S*)-ASA	40	15	1.2
Total volume		175	

The assay mixture was incubated (30°C, 30 min), after which the reaction was quenched by the addition of TFA (10%, 100 μL). Active fractions showed purple coloration and were pooled. Control reactions without enzyme or substrate were also included to ensure the integrity of the assay.

Hydrophobic interaction chromatography (HIC).

Ammonium sulfate was added to the pooled fractions from the ion exchange step to a concentration of 0.5 M. This was then loaded onto a Phenyl-Sepharose column (bed volume 25 mL, 7 × 2.6 cm) that had been pre-equilibrated with at least five bed volumes of 0.5 M ammonium sulfate in buffer A. The column was then washed with five bed volumes of the start buffer (0.5 M ammonium sulfate, buffer A) and the enzyme was eluted with an ammonium sulfate gradient (0.5–0 M) in buffer A. The column was washed with three bed volumes of buffer A. The eluted fractions were tested for enzyme activity using the *o*-aminobenzaldehyde micro assay above. Active fractions eluted between 0.2 and 0.1 M ammonium sulfate and were pooled.

Hi-trap ion exchange.

Where required, active fractions from the phenyl-sepharose column were loaded onto a Hi-Trap Q-Sepharose column (bed volume 1 mL) that had been pre-equilibrated with three bed volumes of buffer A. The column was washed with five bed volumes of the buffer A and the enzyme eluted with a NaCl salt gradient (0–1 M) in buffer A. The column was washed with three bed volumes of regeneration buffer (1 M NaCl in buffer A). The eluted fractions were tested for DHDPS activity using the *o*-aminobenzaldehyde micro assay above. As with the first ion exchange column, active fractions eluted between 0.4 and 0.6 M NaCl and were pooled.

Dialysis.

Before the purified enzyme was used for crystallography, kinetic studies, or other purposes, the pooled fractions were dialysed overnight at 4°C. Dialysis buffer included: buffer A with EDTA (1 mM), 2-mercaptoethanol (1 mM), and ammonium sulfate (1%).

7.4.5 Over-expression and purification of DHDPR.

Growth of *E. coli* XL-1 Blue (pJK001).

E. coli XL-1 Blue(pJK001) was streaked out on LB agar and incubated overnight (37°C). A single colony was selected and re-streaked on LB agar, containing both ampicillin and tetracycline, incubated overnight at 37°C. A single colony was, again, selected and used to inoculate LB broth (10 mL) containing both ampicillin and tetracycline, and incubated overnight (37°C, 180 rpm). 1 mL of overnight culture was used to inoculate 1 L of LB broth containing antibiotics, and incubated as above. The culture was chilled on ice (30 min) before cells were harvested by centrifugation (5000 *g*, 10 min).

Preparation of a crude cell free extract.

Cells were harvested and washed as with DHDPS. The cell pellet was re-suspended in an equal volume of buffer A, flash frozen in liquid nitrogen, and thawed slowly on ice overnight. To obtain the crude extract the frozen cells were slowly thawed on ice at 4°C overnight. The suspension was then ultrasonicated on ice for 4 min, in 3 second bursts with 10 seconds between each burst. The supernatant was then collected by centrifugation (10000 *g*, 10 min). As with DHDPS, the remaining pellet was re-suspended in buffer A and subjected to sonication a second time.

Purification.

Heat shock.

The supernatant was heat shocked in 1 mL aliquots within Eppendorf tubes at 70°C for two min, followed immediately by cooling on ice. Precipitated proteins were removed by centrifugation (10000 *g*, 10 min), and the supernatant was collected.

Ion exchange.

The sample was loaded onto a Q-Sepharose ion exchange column (bed volume 65 mL, 13× 2.6 cm) that had been pre-equilibrated with three bed volumes of buffer A. The column was washed with five bed volumes of buffer A and the DHDPR was eluted with a NaCl salt gradient (0–1 M) in buffer A. The column was then washed with three bed volumes of regeneration buffer (1 M NaCl, buffer A). The eluted fractions were tested for DHDPR activity using the coupled assay below. Active fractions eluted between 0.6 and 0.9 M NaCl, and were pooled. The assays were set up as follows:

	[Initial] mM	**Volume (μL)**	**[Final] mM**
HEPES (pH 8), pyruvate	200, 80	500	100, 40
NADPH	5.4	30	0.162
DHDPR test sample	-	10	-
DHDPS (in excess)	-	50	-
(*S*)-ASA	40	30	1.2
dH_2O	-	380	-
Total		1000	

The reaction mixture, excluding the DHDPR test sample, was incubated in the preheated auto-sampler of the diode array for exactly 15 min to allow the temperature to reach 30°C and for the generation of the substrate of DHDPR, which is catalysed by DHDPS. Catalysis was initiated by the addition of the DHDPR sample (typically 10 μL) and the initial rate recorded. Water was used as a blank.

Hi-Trap Blue Chromatography.

Active fractions from the ion-exchange column were then loaded onto a Hi-Trap Blue column (bed volume 1 mL) that had been pre-equilibrated with three bed volumes of buffer A. The column was then washed with five bed volumes of buffer A and the enzyme was eluted with a NaCl salt gradient (0–1 M) in buffer A. The column was washed with three bed volumes of regeneration buffer (1 M NaCl in buffer A). The eluted fractions were again tested for enzyme activity using the coupled assay as above.

7.4.6 LC-MS.

Samples for protein electrospray mass spectroscopy were first purified on a Waters LC2790 liquid chromatography apparatus. The sample (5 μL) was loaded onto a C5 column (150 mm × 2 mm) with two C5 guard columns. Fractions (200 μL) were eluted with a water to acetonitrile linear gradient over 25 min. DHDPS, and its mutant forms, were typically eluted after 13 min. From each fraction, 20 μL was injected into the mass spectrometer, while the remaining (180 μL) was sent to a diode array for UV/Visible spectral analysis.

J. Healy and B. Clark performed electrospray mass spectrometry on a Micromass LCT mass spectrometer operating with electrospray ionisation and using the Micromass time of flight technique. The sample collected from the LC was injected and scanned over a mass range of 10–40 kD. The sample cone was 50, the desolvation temperature was 150°C, and a 250 R_f lens used. The machine was calibrated with horse heart myoglobin.

7.4.7 Kinetic studies of DHDPS and DHDPS mutants.

In order to determine the kinetic constants of DHDPS and its mutants, two-substrate steady state kinetics was used. DHDPS activity was measured using a coupled assay to DHDPR, as previously described.[14]

Coupled assay to measure DHDPS activity.

Because the K_m values for the mutants were unknown, apparent K_m values (K_m^{app}) were initially determined using a range of substrate concentrations as wide as practically possible. Determination of the true kinetic constants (K_m and k_{cat}) was then accomplished using an approximate 10× range above and below these values. Initial velocities were usually reproducible within 10%.

Reactions conditions used to determine kinetic constants for wild-type DHDPS.

Assays were performed in HEPES buffer (100 mM at pH 8) at 30°C, which was kept constant using a circulating water bath. Water was used as a blank. Care was taken to ensure that enzymes and substrates were stable over the course of the assay (usually 2 min). The stability of the mutants was examined using Selwyn's test.[15] This involved directly plotting the change in absorbance of a reaction multiplied by the volume of enzyme against time (see Appendix 1). This was done for several different enzyme concentrations. If the enzyme is stable, the resulting progress curves, when over-laid, do not deviate from one another. The low activity of the mutants necessitated the addition of greater quantities of enzyme to the assay. In all cases, it was ensured that enzyme concentration was proportional to initial rate.

Care was also taken to ensure an excess of DHDPR; about 30 μg (specific activity = 1.7 units mg^{-1}) was used per assay. The reaction was therefore initiated with (*S*)-ASA, after the cuvette had pre-incubated at 30°C for 10 min.

The table below is the experimental design to determine the kinetic constants for wild-type DHDPS. At least 25 data points were collected for a data series and in some cases this was increased (36 data points) to improve the data. The data was reproduced in duplicate or triplicate. The assay conditions were:

	[Initial] mM	**Volume (µL)**	**[Final] mM**
HEPES (pH 8 at 25°C)	200	500	100
NADPH	5.4	30	0.162
DHDPR	(in excess)†	100	
DHDPS wild-type	*	5	
(*S*)-ASA	0.6–30	50	0.03–1.5
Pyruvate	1–40	50	0.05–2
dH_2O		265	
Total		1000	

† "In excess" refers to the amount of DHDPR required such that additional amounts of DHDPR do not alter the initial reaction rate. In the case of the assay design above, ~30 µg of purified DHDPR was added to each assay.
* The amount of purified wild-type DHDPS used was ~1 µg per assay (specific activity = 1.5 units mg^{-1}).

To evaluate the effect of lysine on the catalytic potency of DHDPS, the kinetic experiments were designed differently, as outlined in the following table. Here, the concentration of one substrate was kept constant (close to its K_m), and the other substrate concentration was varied at varying lysine concentrations. Thus, $K_m^{apparent}$ and $k_{cat}^{apparent}$ constants were determined (distinguished from the true constants, K_m and k_{cat}), as well as K_i.

The assay conditions were as follows:

	[Initial] mM	Volume (μL)	[Final] mM
HEPES (pH 8 at 25°C)	200	500	100
NADPH	5.4	30	0.162
DHDPR	(in excess)†	100	
DHDPS	*	5	
(*S*)-ASA	0.6–30	50	0.03–1.5
pyruvate	10	50	0.2
lysine	0, 2, 10, 10, 100	50	0, 0.1, 0.5, 1, 5
dH_2O		215	
Total		1000	

† "In excess" refers to the amount of DHDPR required such that additional amounts of DHDPR do not alter the initial reaction rate. In the case of the assay design above, ~30 μg of purified DHDPR was added to each assay.
* The amount of purified wild-type DHDPS used was ~1 μg per assay (specific activity = 1.5 units mg^{-1}).

The reaction mixture was incubated in the preheated auto-sampler of the diode array to 30°C. Catalysis was initiated by the addition of (*S*)-ASA. Water was used as a blank.

Data analysis.

Initial rate data were analysed using the Enzfitter programme available from Biosoft (Cambridge, UK). Data were fitted to the appropriate models as judged by SIGMA values and the lowest standard error associated with the kinetic constants.

7.4.8 Sodium borohydride inactivation.

Enzyme samples (0.3–1 mg mL^{-1}) were incubated (30 min, at r.t.) in the presence of either pyruvate (20 mM) or (*S*)-ASA (5 mM). The reactions were buffered with Tris.HCl (200 mM, pH 8, at 4°C). As a control, water was used instead of substrate and sodium borohydride. Following incubation (r.t.), samples were placed on ice. Sodium borohydride (25 μL, 100 mM made up with Tris.HCl (200 mM, pH 8, at 4°C)) was added over 15 min, after which the samples were incubated (on ice) for a further 30 min. Samples were then

dialysed against 100 volumes of buffer A for two hours. The buffer was replaced and the samples again dialysed. DHDPS activity was assessed using the coupled assay.

7.4.9 Crystallisation Experiments.

Crystallisation and X-ray data collection.

The crystallisation experiments were undertaken as described by Mirwaldt *et al.*[16, 17] using the hanging drop-vapour diffusion method at either 4°C or 21°C. Drops contained: DHDPS solution (3 μL, ~10 mg mL^{-1}); K_2PO_4 (1.2 μL, 1.8 M, pH 10); *N*-octyl-β-*R*-glucopyrandoside (0.6 μL, 6% w/v). The reservoir contained K_2PO_4 solution (2 mL, 1.8 M, pH 10). Crystals appeared after one to three days and grew to dimensions of up to 0.3 mm. In addition, crystals were grown with the sitting drop technique using the same conditions as for the hanging drop method. However, data were not collected from these crystals. For X-ray data collection, the crystals were soaked in cryo-protectant solution (30% glycerol in mother liquor) and directly flash-frozen in liquid nitrogen and the data was collected at –110°C, kept constant by a stream of nitrogen. The crystals belong to space group $P3_121$ and diffracted to beyond 2.35–Å resolution. When the crystals obtained by the hanging drop method were soaked in lysine (100 mM, 5 days), a lesser resolution was achieved (2.8–Å). Diffraction data sets were processed and scaled using the programs DENZO[18] and SCALEPACK.[19]

Structure determination and refinement

Preliminary models for each mutant were obtained by rigid-body refinement using the structure of the wild-type enzyme (1DHP) obtained from the RCS Protein Data Bank, and were then further refined using REFMAC5.[20] The PDB file was initially altered to place a glycine in the position of the mutation and the side chain was built into the electron density during successive rounds of modelling and refinement. Manual model corrections were performed using the program O,[21] and the new models were again refined with REFMAC5.[20] In some cases the residue side chains showed little or ambiguous electron density after 6–8 rounds of refinement and these portions were removed from the PDB file. The final refinement rounds involved the placement of solvent molecules using the program ARP.[22] Waters with a B-factor of 50 or greater were removed. The quality of the final structures was checked using the program PROCHECK.[23]

7.5 Chemistry

This section outlines the synthesis of just one molecule, (*S*)-aspartate β-semialdehyde ((*S*)-ASA). Three methods are outlined. The first method was a single step synthesis reported by Black and Wright.[24] The second was that developed by Coulter,[14] which has minor changes in some solvents or purification. The third was developed during the course of this study in collaboration with Sarah Roberts and is reported in Roberts *et. al.*[25] The compounds synthesised in this section were from known methods, with some minor modifications in some reactions. As such, only ^{1}H NMR data has been reported in some sections. NMR data reported here are consistent with the literature data.[14, 26]

7.5.1 Synthesis of (S)-ASA via ozonolysis.[24]

A solution of (*S*)-allylglycine (1.0 g, 9.3 mmol), dissolved in HCl (1 M, 25 mL), was cooled in an ice bath, and O_3 bubbled through for 3 hours. The yield was 83% as judged by the coupled assay (see section 7.5.4). ^{1}H NMR (300 MHz D_2O)—δ_H 1.97–2.21 (2H, m, -CH_2CHNH_2-), 4.01–4.05 (1H, m, -CHNH_2), 5.21 (1H, t, -CH(OH)$_2$). ^{1}H NMR were consistent with the formation of a mixture of compounds, one of which corresponded to (*S*)-ASA.[26]

7.5.2 Synthesis of (S)-ASA via the Lemiex-Johnson reaction.

Potassium (*S*)-*N*-*tert*-butoxycarbonylallylglycine.[26]

To a solution of (*S*)-allylglycine (497 mg, 4.32 mmol) in water (12.5 mL) was added dioxane (5.9 mL), $KHCO_3$ (475 mg, 4.75 mmol) and di-*tert*-butyl pyrocarbonate (941 mg, 4.31 mmol) with continuous stirring at r.t. for 24 hours. The solvents were removed by azeotroping with ethanol (60 mL) *in vacuo,* yielding a white oily solid. The solid was washed with methanol (10 mL), which was removed *in vacuo* to yield the product as a white powdery solid. The yield of the potassium (*S*)-*N*-tert-butoxycarbonylallylglycine was 998 mg (3.98 mmol)—92%. Mp = 230–235°C. ^{1}H NMR (300 MHz, D_2O)—δ_H 1.35 (9H, s, 3× -CH_3), 2.31–2.41 (2H, m, -CH=CH_2), 3.91 (1H, m, $CHCH_2CH=CH_2$), 5.04–5.23 (2H, m, =CH_2), 5.66–5.75 (1H, m, -CH=CH_2) ppm. The melting point and ^{1}H were consistent with the literature.[1, 26]

(*S*)-*N*-*tert*-Butoxycarbonylallylglycine p-methoxybenzyl ester.[1]

To a solution of potassium (*S*)-*N*-*tert*-butoxycarbonylallylglycine (998 mg, 3.98 mmol) in DMF (6.7 mL) was added *p*-methoxybenzyl chloride (1.04 ×, 555 μL, 4.09 mmol). The mixture was stirred continuously for 48 hours, after which the solvent was removed by azeotroping with xylene *in vacuo*. The crude product was partitioned between Na_2SO_4 saturated water and CH_2Cl_2 followed by washing with water (2 × 20 mL water). The solvent was removed *in vacuo* and resulted in a clear yellow oil that was analysed by TLC (pet ether:diethyl ether, R_f 0.4 = product, 0.7 = starting material). The crude product was purified by column chromatography using silica and the solvent was pet ether:diethyl ether. (*S*)-*N*-*tert*-Butoxycarbonylallylglycine *p*-methoxybenzyl ester was obtained as a colourless oil. The yield was 1.217 g (3.63 mmol, 92.1%). ^{1}H NMR (300MHz, $CDCl_3$)—δ_H 1.44 (9H, s, 3× $-CH_3$), 2.46–2.50 (2H, m, $-CH_2CH{=}CH_2$), 3.82 (3H, s, $-OCH_3$), 4.38–4.42 (1H, m, $-CHCH_2CH{=}CH_2$), 5.05–5.17 (5H, m, $=CH_2$-, $-CH_2$- aryl, -NH-), 5.60–5.69 (1H, m, $-CH{=}CH_2$), 6.87–6.91 and 7.26–7.31 (4H, m, aryl) ppm. The ^{1}H NMR data were consistent with those in the literature.[1, 26]

(*S*)-*N*-*tert*-Butoxycarbonylaspartate β-semialdehyde *p*-methoxybenzyl ester.[1]

(*S*)-*N*-*tert*-Butoxycarbonyl allylglycine *p*-methoxybenzyl ester (1.21 g, 3.63 mmol) was dissolved in water and dioxan (1:2, 105 mL). A catalytic amount of osmium tetroxide (~1 mg) was added to this mixture and was stirred at r.t. for 1 hour, during which time a blue-black colour appeared. Sodium periodate (3.7 ×, 2.87 g, 13.44 mmol) was slowly added over 30 min and the reaction was stirred for a further 16 hours. The mixture was partitioned between ethyl acetate (85 mL) and water (85 mL). The organic layer was again washed with water (2 × 85 mL), and then evaporated *in vacuo* to yield a yellow black oil. The yellow-black product was dissolved in diethyl ether and passed through a silica plug to remove any last traces of osmium tetroxide (TLC diethyl ether and pet ether 3:1, R_f 0.76 = starting material, 0.40 = product). The product was purified by column chromatography (diethylether 3:1 pet ether). The solvent was removed *in vacuo* to yield the (*S*)-*N*-*tert*-butoxycarbonylaspartate β-semialdehyde *p*-methoxybenzyl ester as a clear and yellow oil. The yield was 671 mg (1.99 mmol, 54%), % conversion = 71%. ^{1}H NMR (300 MHz, $CDCl_3$)—δ_H 1.42 (9H, s, 3× $-CH_3$), 3.02–3.06 (2H, m, $-CH_2$-CHO), 3.81 (3H, s, $-OCH_3$), 4.57–4.63 (1H, m, $-CHCH_2CHO$), 5.11 (2H, s, $-CH_2$ aryl), 5.42 (1H, bd, -NH), 6.89

and 7.26 (4H, m, aryl), 9.71 (1H, s, -CHO) ppm. The ^{1}H NMR data were consistent with those in the literature.[1, 26]

(*S*)-Aspartate β-semialdehyde hydrate trifluoroacetate.[26]

(*S*)-*N*-*tert*-Butoxycarbonylaspartate β-semialdehyde *p*-methoxybenzyl ester (1.30 mg, 3.86 mmol) was dissolved in dry dichloromethane (24 mL). The reaction was stirred under nitrogen and trifluoroacetic acid (24 mL) was added *via* a syringe. The reaction was stirred for two hours until a deep red colour developed. The solvent was then removed *in vacuo* to give a brown oily residue, which was partitioned between water (120 mL) and ethyl acetate (3 × 120 mL). The aqueous layer was then concentrated under high vacuum to yield (*S*)-aspartate β-semialdehyde hydrate trifluoroacetate as a pale yellow solid/oil. The overall yield for this synthesis was 51%. The yield of (*S*)-aspartate β-semialdehyde hydrate trifluoroacetate was 814 mg (3.27 mmol, 85%). ^{1}H NMR (300 MHz D_2O)—δ_H 1.97–2.21 (2H, m, $-CH_2CHNH_2-$), 4.01–4.05 (1H, m, $-CHNH_2$), 5.21 (1H, t, $-CH(OH)_2$). ^{13}C NMR (75 MHz D_2O)—δ_c 36.2 ($-CH_2CHNH_2$), 49.7 ($-CHNH_2-$), 87.7 ($-CH(OH)_2$), 118.0 ($-CCF_3$), 162 ($-CCF_3$), 171.2 (-C=O). The ^{1}H and ^{13}C NMR data were consistent with those in the literature.[1, 26]

7.5.3 (S)-ASA via a Wienreb amide.

***N*-*tert*-BOC-(*S*)-Aspartic acid 1-(*tert*-Butyl ester) *N*-Methoxy-*N*-Methylamide.**[27]

(Benzotriazol-1-yloxy) tris(dimethylamino)phosphonium hexafluorophosphate (BOP.PF_6) (163 mg, 0.380 mmol) was added to a stirred solution of *N*-*tert*-BOC-(*S*)-aspartic acid 1-(*tert*-butyl ester) (100 mg, 0.346 mmol) and triethylamine (54 μL, 0.385 mmol) in dichloromethane (3.5 mL) at r.t. After 5 min of stirring, *O*,*N*-dimethylhydroxyamine hydrochloride (40 mg, 0.397 mmol) was added, followed by triethylamine (54 μL, 0.385 mmol). All solid material dissolved within 10 min and the mixture was stirred for 2 hours at r.t. The reaction mixture was washed with 1 M HCl solution (3× 1 mL), H_2O (1 × 1 mL), 1 M $NaHCO_3$ solution (2 × 1 mL) and H_2O (2 × 1 mL). The solvent was removed *in vacuo* to give a clear yellow oily product, which was purified by flash chromatography on silica, using 30% ethyl acetate/petroleum ether as the eluant, to give *N*-*tert*-BOC-*S*-aspartic acid 1-(*tert*-butyl ester) *N*-methoxy-*N*-methylamide as a colourless oil (100 mg, 86%). ^{1}H NMR (300 MHz, DMSO)—δ_H 1.38 (18H, s, 2 × $-C(CH_3)_3$), 2.8 (2H, m, $-CH_2-$), 3.06 (3H, s,

-CH_3), 3.7 (3H, s, -CH_3), 4.23 (1H, m, -CHNH-), 6.98 (1H, m, -NH-). The ^{1}H NMR data were consistent with those in the literature.[27]

1-*tert*-Butyl (*S*)-2-(*tert*-BOC-amino)-4-oxobutanoate.[27]

A solution of diisobutylaluminum hydride (DIBAL) in hexane (1 M, 0.55 mL, 0.55 mmol) was added dropwise over 20 min to a stirred solution of *N*-*tert*-BOC-(*S*)-aspartic acid 1-(*tert*-butyl ester) *N*-methoxy-*N*-methylamide (110 mg, 0.36 mmol) in anhydrous THF (1.8 mL) at –78°C . The mixture was allowed to stir at –78 °C for 2 hours. The reaction mixture was partitioned between 0.35 M aqueous $NaHSO_4$solut ion (3.6 mL) and diethyl ether (5.5 mL). After separation, the aqueous layer was extracted with diethyl ether (3 × 2 mL). The combined ethereal layers were washed with 1 M HCl solution (3× 1 mL), 1 M $NaHCO_3$ solution (3× 1 mL), and brine (3× 1 mL). Concentration *in vacuo* gave 1-*tert*-butyl (*S*)-2-(*tert*-BOC-amino)-4-oxobutanoate as a colourless oil (92 mg, 95%), which solidified on standing at r.t. ^{1}H NMR (300 MHz, $CDCl_3$)—δ_H 1.43 (9H, s, -$C(CH_3)_3$), 1.44 (9H, s, -$C(CH_3)_3$), 2.98 (2H, m, -CH_2-), 4.45 (1H, m, -CH), 5.38 (1H, m, -NH-), 9.75 (1H, s, -CHO). The ^{1}H NMR data were consistent with those in the literature.[27] (*S*)-ASA was afforded using the deprotection method above.

7.5.4 Assessing the purity of ASA via the coupled assay.

To determine the purity of ASA, the coupled assay was used to quantify the (*S*)-ASA concentration and this was compared to the calculated concentration. This method utilised the next enzyme in the lysine biosynthetic pathway, DHDPR. The reaction was followed by a change in the absorbance at 340 nm with the loss of NADPH. The method assumes the reactions are irreversible and that (*R*)-ASA, when present, does not influence the reaction. Fresh solutions of ASA and NADPH were prepared in ddH_2O.

The reaction was set up as follows:

	[Initial] mM	**Volume** (μL)	**[Final]** mM
HEPES (pH 8 at 25°C)	200	500	100
NADPH	5.4	30	0.162
DHDPR		100	
DHDPS		10	
(*S*)-ASA		50	> 0.15
Pyruvate	100	50	20
dH_2O		265	
Total		1000	

Under these conditions, the limiting substrate was (*S*)-ASA. This was confirmed by the addition of more NADPH or pyruvate, after the reaction had reached a plateau, did not restart the reaction. Thus the total turnover of NADPH was equivalent to the turnover of (*S*)-ASA.

7.6 References.

1. Coulter, C. V. (1997). Studies in lysine biosynthesis. PhD thesis, University of Canterbury.

2. Maniatis, T., Fritsch, E. & Sanbrook, J. (1990). *Molecular cloning: A laboratory Manual*. 2nd edit., Cold Spring Harbor Press, Cold Spring Harbor, New York.

3. Miller, J. (1992). *A short course in bacterial genetics; a lab manual and handbook for E. coli and related bacteria*, Cold Spring Harbour, New York.

4. Cornish-Bowden, A. (1999). *Fundamentals of enzyme kinetics*. 2nd edit., Portland Press Ltd, London.

5. Engel, P. C. (1996). Enzyme kinetics. In *Enzymology* (Engel, P. C., ed.). BIOS Scientific, San Diego.

6. Stratagene. (1998). Quikchange site-directed mutagenesis kit: instruction manual.

7. Bukhari, A. I. & Taylor, A. L. (1971). Genetic analysis of diaminopimelic acid- and lysine-requiring mutants of *Escherichia coli*. *Journal of Bacteriology*, **105**, 844-854.

8. Yeh, P., Sicard, A. M. & Sinskey, A. J. (1988). General organization of the genes specifically involved in the diaminopimelate-lysine biosynthetic pathway of *Corynebacterium glutamicum*. *Molecular General Genetics*, **212**, 105-111.

9. Heinemann, J. & Ankenbauer, R. (1993). Retrotransfer in *Escherichia coli* conjugation: bidirectional change or *de novo* mating? *Journal of Bacteriology*, **175**, 583-588.

10. Gerrard, J. A. (1992). Studies on dihydrodipicolinate synthase. D. Phil. thesis, Oxford University.

11. Kraunsoe, J. A. E. (1992). Studies in lysine biosynthesis. BSc. Hons. Part II, Corpus Christi College.

12. Sanger, F., Nicklen, S. & Coulson, A. R. (1977). DNA sequencing with chain-terminating inhibitors. *Proceedings of the National Academy of Sciences of the United States of America*, **74**, 5463-5467.

13. Bradford, M. (1976). A rapid and sensitive method for the quantitation of microgram quantities of protein utilizing the principle of protein-dye binding. *Analytical Biochemistry*, **72**, 248-254.

14. Coulter, C. V., Gerrard, J. A., Kraunsoe, J. A. E. & Pratt, A. J. (1996). *(S)*-Aspartate semi-aldehyde: synthetic and structural studies. *Tetrahedron*, **52**, 7127-7136.

15. Selwyn, M. J. (1965). A simple test for the inactivation of an enzyme during assay. *Biochimica et Biophysica Acta*, **105**, 193-195.

16. Mirwaldt, C., Korndorfer, I. & Huber, R. (1995). The crystal structure of dihydrodipicolinate synthase from *Escherichia coli* at 2.5 Å resolution. *Journal of Molecular Biology*, **246**, 227-239.

17. Laber, B., Gomis-Ruth, F., Romao, M. & Huber, R. (1992). *Escherichia coli* dihydrodipicolinate synthase. Identification of the active site and crystallization. *Biochemical Journal*, **288**, 691-695.

18. Murshudov, G., Vagin, A. & Dodson, E. (1997). Refinement of macromolecular structures by the maximum-likelihood method. *Acta Crystallographica Section D-Biological Crystallography*, **D53**, 240-255.

19. Otwinowski, Z. & Minor, W. (1997). Processing of X-ray diffraction data collected in oscillation mode. *Methods in Enzymology*, **276**, 307-326.

20. CCP4. (1994). The CCP4 suite: programs for protein crystallography. *Acta Crystallographica Section D-Biological Crystallography*, **D50**, 760-763.

21. Jones, T. & Kjeldgaard, M. (1997). Electron density map interpretation. *Methods in Enzymology*, **277**, 173-208.

22. Lamzin, V. S. & Wilson, K. S. (1997). Automated refinement for protein crystallography. *Methods in Enzymology*,**277** , 269-305.

23. Laskowsky, R., MacArthur, M., Moss, D. & Thornton, J. (1993). PROCHECK: a program to check the stereochemical quality of protein structures. *Journal of Applied Crystallography*, **26**, 283-291.

24. Black, S. & Wright, N. G. (1954). Aspartic β-semialdehyde dehydrogenase and aspartic β-semialdehyde. *Journal of Biological Chemistry*, **213**, 39-50.

25. Roberts, S. J., Morris, J. C., Dobson, R. C. J. & Gerrard, J. A. (2003). The preparation of (*S*)-aspartate semi-aldehyde appropriate for use in biochemical studies. *Bioorganic and Medicinal Chemistry Letters*, **13**, 265-267.

26. Tudor, D. W., Lewis, T. & Robins, D. J. (1993). Synthesis of the trifluoroacetate salt of aspartic acid β-semialdehyde, an intermediate in the biosynthesis of L-lysine, L-threonine, and L-methionine. *Synthesis*, **11**, 1061-1062.

27. Wernic, D., Dimaio, J. & Adams, J. (1989). Enantiospecific synthesis of L-α-aminosuberic acid. Synthetic applications in preparation of atril natriuretic factor analogues. *Journal of Organic Chemistry*, **54**, 4224-4228.

Appendix one.

Selwyn's test for enzyme inactivation.

Selwyn devised this simple test in 1965 in order to examine the stability of an enzyme during the course of its assay.[1] The procedure involved monitoring the reaction curve over a given time at different concentrations of enzyme. If the enzyme is unstable, then at various enzyme concentrations, the plot of enzyme concentration multiplied by time *vs.* absorbance, will not overlay. Selwyn's test was used to examine the stability of the attenuated DHDPS mutants—DHDPS-T44V, DHDPS-Y133F, DHDPS-R138H, DHDPS-Y107F, and DHDPS-T44S; the results of which are shown below (Figure A1.1). In all cases, the stability during the enzyme assay was confirmed.

1. Selwyn, M. J. (1965). A simple test for the inactivation of an enzyme during assay. *Biochimica et Biophysica Acta*, **105**, 193-195.

Figure A1.1 *Selwyn's test for enzyme stability. The plots are:* ***A****, wild-type DHDPS;* ***B****, DHDPS-R138H;* ***C****, DHDPS-Y133F;* ***D****, DHDPS-T44V;* ***E****, DHDPS-T44S;* ***F****, DHDPS-Y107F.*

A **B**

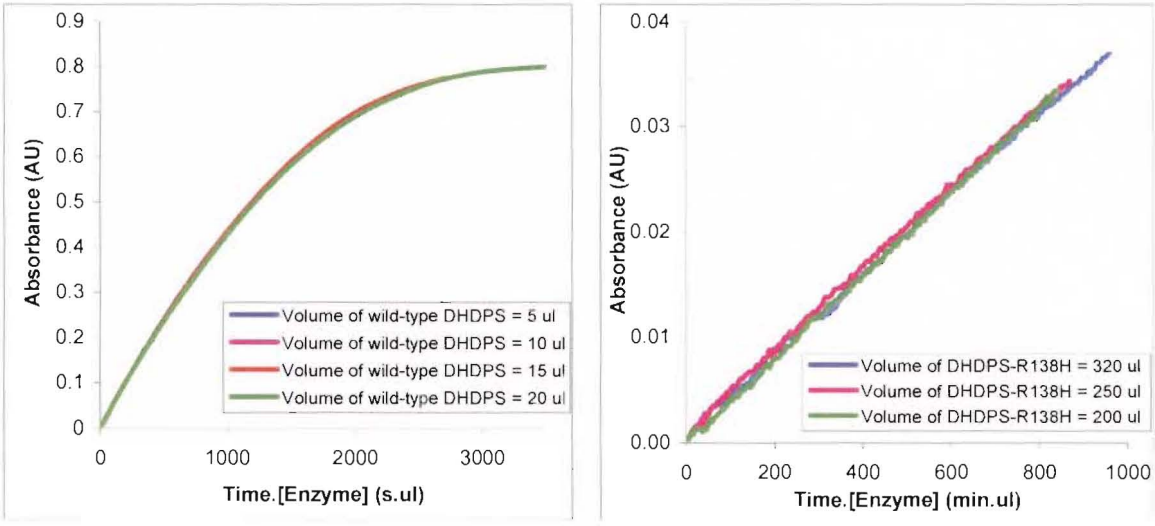

C

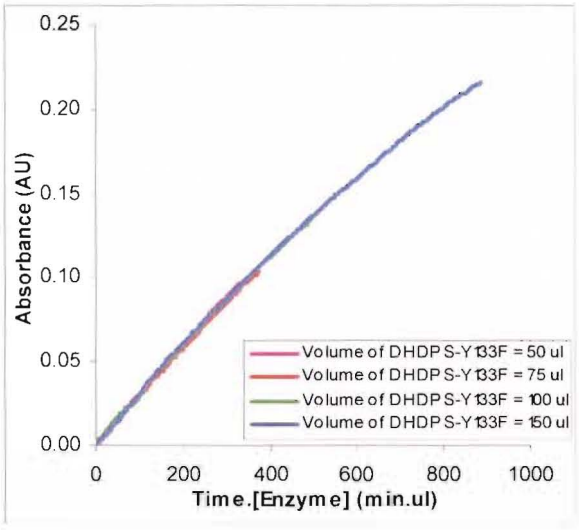
0.25
0.20
0.15
0.10
0.05
0.00
Absorbance (AU)
0
200
400
600
800
1000
Time.[Enzyme] (min.ul)
Volume of DHDPS-Y133F = 50 ul
Volume of DHDPS-Y133F = 75 ul
Volume of DHDPS-Y133F = 100 ul
Volume of DHDPS-Y133F = 150 ul

D

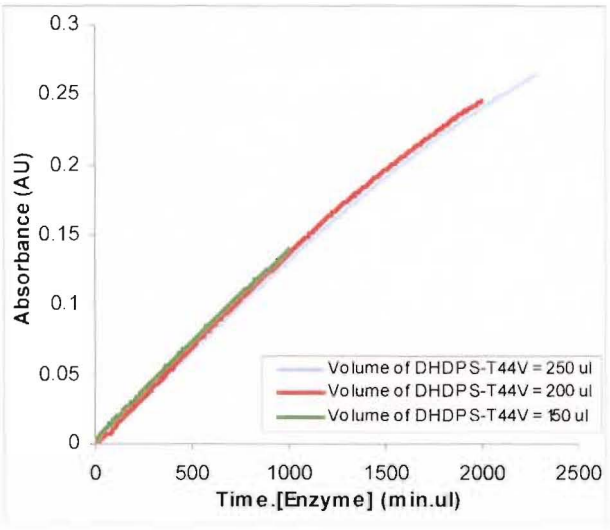
0.3
0.25
0.2
0.15
0.1
0.05
0
Absorbance (AU)
0
500
1000
1500
2000
2500
Time.[Enzyme] (min.ul)
Volume of DHDPS-T44V = 250 ul
Volume of DHDPS-T44V = 200 ul
Volume of DHDPS-T44V = 150 ul

E

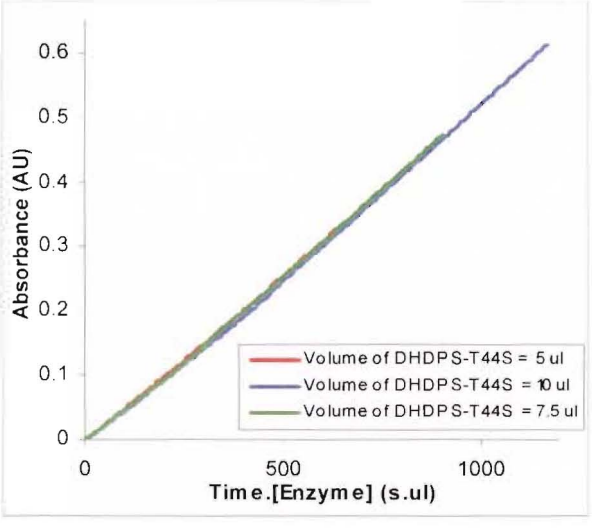
0.6
0.5
0.4
0.3
0.2
0.1
0
Absorbance (AU)
0
500
1000
Time.[Enzyme] (s.ul)
Volume of DHDPS-T44S = 5 ul
Volume of DHDPS-T44S = 10 ul
Volume of DHDPS-T44S = 7.5 ul

F

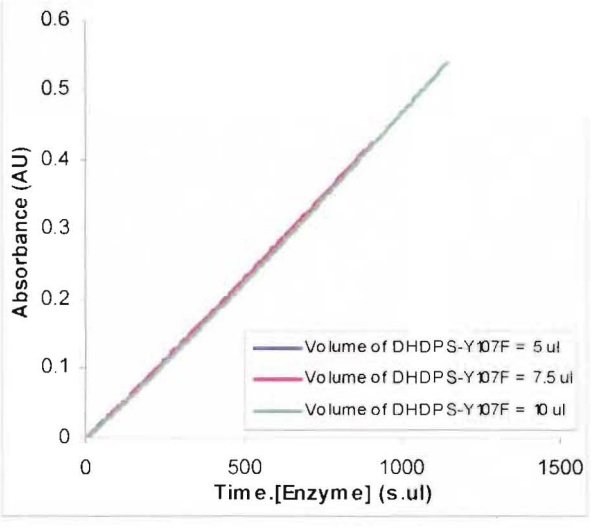
0.6
0.5
0.4
0.3
0.2
0.1
0
Absorbance (AU)
0
500
1000
1500
Time.[Enzyme] (s.ul)
Volume of DHDPS-Y107F = 5 ul
Volume of DHDPS-Y107F = 7.5 ul
Volume of DHDPS-Y107F = 10 ul